Department of Applied Geology

Thermal History and Deep Overpressure Modelling in the Northern Carnarvon Basin, North West Shelf, Australia

ACKNOWLEDGEMENTS

I wish to extend my gratitude to the following people and organisations for their assistance and support during the course of this study.

– Professor Mike F. Middleton, my principal supervisor, for his supervision and supporting my study at the Centre of Excellence in Petroleum Geology (CEPG), Department of Applied Geology, Curtin University of Technology, for giving me the benefit of numerous discussions and guidance throughout this doctoral program, providing invaluable assistance and feedback, correcting paper drafts, reading all chapters including detailed comments and providing funding for my stipend and capital expenses for hardware and software costs, attendance of academic activities and thesis preparation costs.

– Professor Robert Alexander, my previous supervisor, who encouraged me to apply for an International Postgraduate Research Scholarship (IPRS) and a Curtin University of Technology Scholarship (CUTS), for supporting my study at the Centre for Petroleum and Environmental Organic Geochemistry (CPEOG), Department of Applied Chemistry, Curtin University of Technology, and for his guidance in various aspects of petroleum organic geochemistry and financial support.

– Associate Professor Lindsay Collins, my co-supervisor, who encouraged me to undertake the course and for his guidance and assistance, and kindness to me through my research study.

– Professor Robert I. Kagi who encouraged me to apply for IPRS and CUTS, supported and guided my organic geochemical laboratory work.

– Associate Professor Alan M. Tait for his discussions, suggestions, reviewed papers, corrected all chapters of my thesis and English language assistance.

– Dr. Alex R. Kaiko who took a kind interest in my work, provided some technical advice, assisted in sampling and reviewed papers.

– Dr. Chunqing Jiang for his geochemical analyses of source rock samples and for many useful discussions.

– Dr. Trever Bastow for his analysis of GC-MS of a source rock sample.

– Mr. Garrie Meddings for assistance in thin section preparations of claystone, and Mr. Dale Longman for free use of the CSIRO Chemical Laboratory facilities.

– The Department of Employment, Education and Training of the Australian government who awarded me an IPRS covering my tuition fees and health cover for my family.

– Curtin University of Technology who awarded me a CUTS providing a living allowance.

– China University of Geosciences for supporting my studies in Australia.

– The American Association of Petroleum Geologists who awarded me a grant-in aid of the AAPG Foundation (1999) to assist in my study of source rocks.

– The Department of Minerals and Energy of Western Australia who provided me with great help in collecting open-file data.

– Platte River Associates, Inc. for their support on providing the academic loan of the BasinMod software package for basin modelling, for frequent answering questions and providing technical assistance.

– The Australian Geological Survey Organization for their help in supplying about 1600 km interpreted deep seismic data, some velocity data and some digital well-log data.

– The Geological Survey of Canada, Calgary who provided free geochemical analyses of Rock-Eval, GC and GC-MS for 17 source rock samples.

– BHP Petroleum Pty. Ltd. for supplying 5 interpreted seismic lines.

– CSIRO Petroleum who supplied the Eq VR (FAMM) data in 8 wells to support this study.

I wish to extend my thanks to all those who assisted me during this study, particularly, Professor Richard R. Hillis, Dr. Nancy Hunter, Dr. Maowen Li, Dr. Samuelsson, J., Dr. Peter R. Tingate, Dr. John Kennard, Dr. Daniel M. Jarvie, Ms. Rosie Emms, Ms. Henrietta Wong, Dr Lila W. Gurba and Mr. Ken Whitbread.

My grateful thanks are also extended to all staff of CEPG and Department of Applied Geology at Curtin for their benevolence and help, particularly, Associate Professor Peter A. Cawood, Professor Simon A. Wilde, Professor Krishna K Sappal, Dr. Zhongrong Zhu, Mrs. Annette Labrooy and Mr. Peter Glover, and to Ph.D. students: Mr. Marcus Sweetapple, Mr. Tingguang Song, Mr. Xiao'ou Zhang, Mrs. Min Xu, Mr. Matthew Great and Mr. Annamalai Mahizhnan.

Likewise, I wish to record my appreciation for help from all members of CPEOG and Department of Applied Chemistry at Curtin, particularly, Mr. Geoff Chidlow, Mr. Ian Sills, Dr. Ben van Aarssen, Dr. Michale Audino and Mrs. Joyce Wong.

Finally, I wish to thank my wife, Juan Liu, and my son, Chen He, for their unwavering support, encouragement and patience that also made this study possible. I would also like to thank my parents and sisters for their encouragement and great support through this study.

ABSTRACT

The Northern Carnarvon Basin is the richest petroleum province in Australia. About 50 gas/condensate and oil fields, associated mainly with Jurassic source rocks, have been discovered in the sub-basins and on the Rankin Platform since 1964. The basin is located at the southern end of the North West Shelf of Australia. It can be mainly subdivided into the Exmouth, Barrow, Dampier and Beagle Sub-basins, the Rankin Platform and Exmouth Plateau. The sub-basins are rift-related grabens and half-grabens developed during the Jurassic to the earliest Cretaceous and contain over 10 kilometres of Mesozoic and Cainozoic sedimentary rocks, among which are several thousand meters of Jurassic rocks. The formations of the Jurassic and the lower part of the Barrow Group of Early Cretaceous age in the sub-basins of the Northern Carnarvon Basin were found to be overpressured with excess pressures of 5-29 MPa at depths of 2900-3600 m indicated by repeat formation tests (RFTs) and drill stem tests (DSTs). The characteristics of organic matter, thermal history and thermal maturity, pressure seal and overpressure evolution in the sub-basins are crucial to a proper understanding of the nature and dynamic processes of hydrocarbon generation and migration in the basin.

Based on organic geochemical data, the important source rocks in the basin are Jurassic organic-rich fine-grained rocks including the Murat Siltstone, the rift-related Athol Formation and Dingo Claystone. The Mungaroo Formation of the Middle-Upper Triassic contains gas-generating source rocks. These formations are recognised to be organic rich based on 1256 values of the total organic carbon content (TOC, %) from 17 wells. Average TOC values (calculated from samples with TOC < 15 %) are about 2.19 % in the Mungaroo Formation, about 2.09 % in the Murat Siltstone and about 1.74 % in the Athol Formation and Dingo Claystone. Data from kerogen element analysis, Rock-Eval pyrolysis, visual kerogen composition and some biomarkers have been used to evaluate the kerogen type in the basin. It appears that type III kerogen is the dominant organic-matter type in the Triassic and Jurassic source rocks, while the Dingo Claystone may contain some oil-prone organic matter.

The vitrinite reflectance (R_o) data in some wells of the Northern Carnarvon Basin are anomalously low. As a major thermal maturity indicator, the anomalously low R_o data seriously hinder the assessment of thermal maturity in the basin. This study differs from other studies in that it has paid more attention to Rock-Eval T_{max} data. Therefore, problems affecting T_{max} data in evaluating thermal maturity were investigated. A case study of contaminated Rock-Eval data in Bambra-2 and thermal modelling using T_{max} data in 16 wells from different tectonic subdivisions were carried out. The major problems for using T_{max} data were found to be contamination by drilling-mud additives, natural bitumen and suppression due to hydrogen index (HI) > 150 in some wells. Although the data reveal uncertainties and there is about !3-10 % error for thermal modelling by using the proposed relationship of R_o and T_{max}, the "reliable" T_{max} data are found to be important, and useful to assess thermal maturity and reduce the influence of unexpectedly low R_o data.

This study analyzed the characteristics of deep overpressured zones and top pressure seals, in detail, in 7 wells based on the observed fluid pressure data and petrophysical data. The deep overpressured system (depth greater than 2650-3000 m) in the Jurassic formations and the lower part of the Barrow Group is shown by the measured fluid pressure data including RFTs, DSTs and mud weights. The highly overpressured Jurassic fine-grained rocks also exhibit well-log responses of high sonic transit times and low formation resistivities. The deep overpressured zone, however, may not necessarily be caused by anomalously high porosities due to undercompaction. The porosities in the deep overpressured Jurassic rocks may be significantly less than the well-log derived porosities, which may indicate that the sonic-log and resistivity-log also directly respond to the overpressuring in the deep overpressured fine-grained rocks of the sub-basins. Based on the profiles of fluid pressure and well-log data in 5 wells of the Barrow Sub-basin, a top pressure seal was interpreted to be consistent with the transitional pressure zone in the Barrow Sub-basin. This top pressure seal was observed to consist of a rock layer of 60-80 % claystone and siltstone. The depths of the rock layer range from 2650 m to 3300 m with thicknesses of 300-500 m and temperatures of 110-135 ^{o}C. Based on the well-log data, measured porosity and sandstone diagenesis, the rock layer seems to be

well compacted and cemented with a porosity range of about 2-5 % and calculated permeabilities of about 10^{-19}-10^{-22} m^2.

This study performed thermal history and maturity modelling in 14 wells using the BasinMod 1D software. It was found that the thermal maturity data in 4 wells are consistent with the maturity curves predicted by the rifting heat flow history associated with the tectonic regime of this basin. The maximum heat flows during the rift event of the Jurassic and earliest Cretaceous possibly ranged from 60-70 mW/m^2 along the sub-basins and 70-80 mW/m^2 on the southern and central Exmouth Plateau. This study also carried out two case studies of thermal maturity and thermal modelling within the deep overpressured system in the Barrow and Bambra wells of the Barrow Sub-basin. These case studies were aimed at understanding whether overpressure has a determinable influence on thermal maturation in this region. It was found that there is no evidence for overpressure-related retardation of thermal maturity in the deep overpressured system, based on the measured maturity, biomarker maturity parameters and 1D thermal modelling. Therefore, based on the data analysed, overpressure is an insignificant factor in thermal maturity and hydrocarbon generation in this basin.

Three seismic lines in the Exmouth, Barrow and Dampier Sub-basins were selected and converted to depth cross-sections, and then 2D geological models were created for overpressure evolution modelling. A major object of these 2D geological models was to define the critical faults. A top pressure seal was also detected based on the 2D model of the Barrow Sub-basin. Two-dimensional overpressure modelling was performed using the BasinMod 2D software. The mathematical 2D model takes into consideration compaction, fluid thermal expansion, pressure produced by hydrocarbon generation and quartz cementation. The sealed overpressured conditions can be modelled with fault sealing, bottom pressure seal (permeabilities of 10^{-23}-10^{-25} m^2) and top pressure seal (permeabilities of 10^{-19}-10^{-22} m^2). The modelling supports the development of a top pressure seal with quartz cementation. The 2D modelling suggests the rapid sedimentation rates can cause compaction disequilibrium in the fine-grained rocks, which may be a mechanism for overpressure generation during the Jurassic to the Early Cretaceous.

The data suggest that the present-day deep overpressure is not associated with the porosity anomaly due to compaction disequilibrium and that compaction may be much less important than recurrent pressure charges because most of the porosity in the Jurassic source rocks has been lost through compaction and deposition rates have been very slow since the beginning of the Cainozoic.

Three simple 1D models were developed and applied to estimate how rapidly the overpressure dissipates. The results suggest that the present day overpressure would be almost dissipated after 2 million years with a pressure seal with an average permeability of 10^{-22} m^2 (10^{-7} md). On the basis of numerous accumulations of oil and gas to be expelled from the overpressured Jurassic source rocks in the basin and the pressure seal modelling, it seems that the top pressure seal with permeabilities of 10^{-19}-10^{-22} m^2 (10^{-4}-10^{-7} md) is not enough to retain the deep overpressure for tens of millions of years without pressure recharging. Only if the permeabilities were 10^{-23} m^2 (10^{-8} md) or less, would a long-lived overpressured system be preserved. This study suggests that hydrocarbon generation, especially gas generation and thermal expansion, within sealed conditions of low-permeability is a likely major cause for maintaining the deep overpressure over the past tens of millions of years.

Keywords: Thermal history; Deep overpressure; Type III kerogen; Rock-Eval T_{max}; Thermal maturity; Palaeoheatflow modelling; Pressure seal; 2D deep overpressure modelling; Pressure behaviour modelling; Overpressure generation; Northern Carnarvon Basin

TABLE OF CONTENTS

LIST OF TABLES

Table **Page**

LIST OF FIGURES

Figure **Page**

Sheng HE

This thesis is presented for the Degree of

Doctor of Philosophy of

Curtin University of Technology

June 2002

Part I

Introduction and Regional Geology

CHAPTER 1 INTRODUCTION

1.1 Previous work and background of this study

1.1.1 Previous work

The Northern Carnarvon Basin, the most important gas and oil province in Australia, is located at the southern end of the North West Shelf, Western Australia. Petroleum exploration in the basin commenced in 1924 (Hocking et al., 1987). In 1953 the first exploration well, Rough Range-1, was drilled by WAPET (Western Australian Petroleum Pty. Ltd.) on the Rough Range Anticline in the Exmouth Sub-basin and it brought the first flowing oil in Australian history (Hocking et al., 1987). The Barrow Island Anticline in the Barrow Sub-basin had been found in 1954 and a well, Barrow-1, was drilled by WAPET in 1964 on the Anticline. This was the first commercial oilfield in the Northern Carnarvon Basin associated with Upper Jurassic sandstone reservoirs (Campbell et al., 1984). Production started in 1966 (Baillie and Jacobson, 1997). The first offshore well, Legendre-1 in Western Australian waters was drilled by Woodside (Woodside Offshore Petroleum Pty. Ltd.) in 1968 in the Dampier Sub-basin and obtained oil flow to the surface at a rate of 160 m^3/day from Lower Cretaceous sandstones (Vincent and Tilbury, 1988). In 1971, Woodsite made the first discovery on the Rankin Platform, the large North Rankin gas field with sandstone reservoirs of Late Triassic to Early Jurassic age (Beston, 1986; Cockbain, 1989). The large Goodwyn gas and condensate field (reservoir in the Mungaroo Formation) was also discovered in 1971 by Woodside (Vincent and Tilbury, 1988). The West Tryal Rocks gas field (reservoir in the Mungaroo Formation) was discovered in 1972 by WAPET (McClure et al., 1988) and the large Gorgon gas field with reservoirs in the Late Triassic and earliest Cretaceous, was discovered in 1981 by WAPET (Campbell and Smith, 1982; McClure et al., 1988). From the early 1970s to the 1990s, intensive petroleum exploration has led to a series of discoveries of gas, gas/condensate and oil fields. Up to 1999, approximately 50 gas, gas/condensate and oil fields had been discovered in the Northern Carnarvon Basin (Fig. 1-1) (Hocking et al., 1987; Kopsen, 1994; le Poidevin and Lowden, 1994; Baillie and Jacobson, 1997; Petroleum Division of the

Department of Minerals and Energy, Western Australia, 1999), while some gas and/or oil accumulations still wait to be developed.

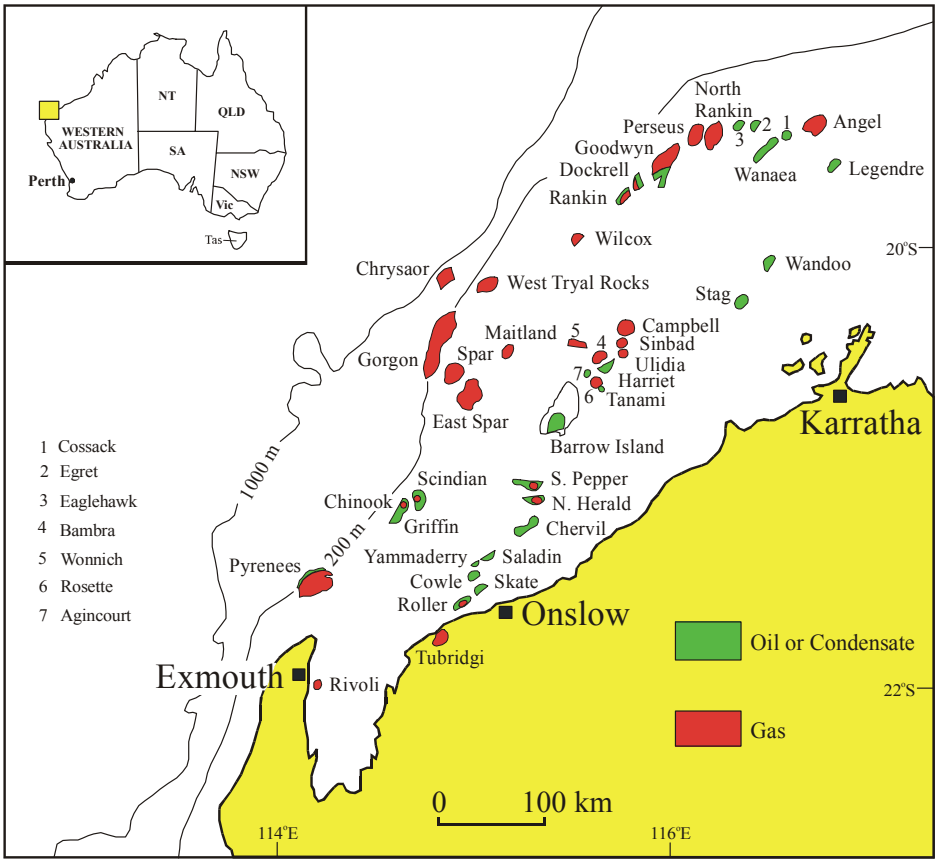

Fig. 1-1 Gas, gas/condensate and oil fields in the Carnarvon Basin prior to 1997 (after Hocking et al., 1987; Baillie and Jacobson, 1997; Petroleum Division of the Department of Minerals and Energy, Western Australia, 1999).

With petroleum exploration and discovery in the Northern Carnarvon Basin, the regional geology, origin and evolution of the basin and petroleum geology have been extensively studied and research papers, concerning several aspects of organic geochemistry of oils and source rocks, organic-matter maturity, basin modelling of thermal history and overpressure evolution, have been published. Some significant publications, research reports and theses related to the above topics in the Northern Carnarvon Basin are listed below:

1. Petroleum organic geochemistry and geochemical correlation (Powell and McKirdy, 1972, 1973a, 1973b; Brikké, 1982; Volkman et al., 1983; van Aarssen et al., 1996; Pitchford et al., 1999; van Aarssen et al., 1999).

2. Source rocks and organic matter (Scott, 1992, 1994; Gorter, 1994; Teerman, 1994).

3. Thermal maturation and suppression of vitrinite reflectance (R_o) (Cook and Kantsler, 1980; Volkman et al., 1983; Alexander et al., 1988; Wilkins et al., 1992a, 1992b, 1995; Kaiko and Tingate, 1996; Kaiko, 1998; Samuelsson and Middleton, 1998).

4. Overpressure (Horstman, 1988; Zaunbrecher, 1994; Yassir, 1996; Swarbrick and Hillis, 1999; van Ruth et al., 2000; Tingate et al., 2001)

5. Thermal and maturity modelling (Swift et al., 1988; Alexander et al., 1990; Wilkins et al., 1994; Ghori, 1995; Kaiko and Tingate, 1996; Kaiko, 1998; 2000; Samuelsson and Middleton, 1998; Tindale et al., 1998)

6. Two-dimensional modelling of petroleum system (Vear, 1998) and two-dimensional overpressure modelling (Bekele et al., 2001).

1.1.2 Background of this study

The Northern Carnarvon Basin can be subdivided into the Exmouth, Barrow, Dampier and Beagle Sub-basins, the Rankin Platform and the Exmouth Plateau (e.g. Hocking et al., 1994). These tectonic subdivisions were developed by rifting during the Jurassic-Early Cretaceous on the Pre-Triassic basement (e.g. Barber, 1982; Hocking et al., 1987; Westphal and Aigner, 1997). Although different tectonic models for the evolution of the Northern Carnarvon Basin were proposed by Stagg and Colwell (1994), and Daim and Lennox (1998), the conceptual model for this study is based on a rift tectonic setting and thermal regime (e.g. McKenzie, 1978; Middleton and Hunt, 1989). Direct evidence of thermal maturity experienced during rifting in most sub-basin wells may have been removed by burial in a later sag-phase

deposition in the Barrow-Dampier Sub-basins (Kaiko and Tingate, 1996). However, there is still an absence of studies for evidence of rift heat flow in the Northern Carnarvon Basin.

According to well-drilling records and interpretations of seismic data, the sedimentary rocks associated with the syn-rift phase in the sub-basins are up to 7000 m thick. The Jurassic rift-related sequence is dominated by organic-rich claystones and siltstones which are recognized as the most important source rocks in the sub-basins (e.g. McClure et al., 1988; Parry and Smith, 1988; Baillie and Jacobson, 1997; Ellis et al., 1999). However, the richness, type and maturity of organic matter in the Jurassic source rocks have not been well understood.

On the basis of studies of maturity and thermal modelling (e.g. Wilkins et al., 1992a; Kaiko and Tingate, 1996; Samuelsson and Middleton, 1998), vitrinite reflectance (R_o), as a major maturity indicator, in some wells is considered to be significantly suppressed by perhydrous effects through marine influenced suppression and/or inaccurate identification of vitrinite, and shows an anomalously small increase with depth. So far, Rock-Eval T_{max} values, as a maturity indicator, have not been well studied in this basin. It could be useful to constrain the anomalously low vitrinite reflectance and to assess thermal maturity.

The anomalously low R_o profiles in the Barrow and Bambra wells occur within the overpressured Jurassic sequence (Kopsen and McGann, 1985). Swarbrick and Hillis (1999) suggest that the overpressure may retard the thermal maturation of the Jurassic source rocks and delay the petroleum generation and charging time predicated by basin modelling. Therefore, whether thermal maturity and hydrocarbon generation in the sealed overpressured compartments are retarded by the overpressuring has remained a question. Further study is indicated.

Overpressure in the Northern Carnarvon Basin has been studied by Horstman (1988), Zaunbrecher (1994), van Ruth et al. (2000) and Tingate et al. (2001). Its presence in the Jurassic section and the lower part of the Barrow Group of the earliest Cretaceous is confirmed by the measured fluid pressure data. Tingate et al. (2001) stated that all overpressure occurrences are accompanied by an increase in

sonic transit time and that disequilibrium compaction is the dominant mechanism for the overpressure. Recently, Bekele et al. (2001) have carried out numerical 2D basin modelling to reconstruct the overpressure generation in the Barrow Sub-basin. They proposed that compaction disequilibrium and the permeability of shale layers are dominant controls on overpressures, while the contribution to the maximum pressure anomaly by organic maturation is approximately 15 %. However, the features and formation of pressure seal, interpretation of well-log data for the deep overpressured system and top pressure seal, and the processes of deep overpressure generation and maintenance in the Jurassic sequence with varying major mechanisms are still poorly understood.

1.2 Aims and objectives

1.2.1 Aims

The heat flow history and overpressure build-up in the Jurassic sequence are intrinsically related to the dynamic processes (extension, rapid subsidence and sedimentation, thermal input and fluid flow) of the basin. Geotemperature and fluid overpressure are recognized as essential agents for hydrocarbon generation and migration, which interact with the basin evolution. Based on the discussion above, the studies of thermal history modelling and overpressure evolution in the rift-related basin aim at significantly increasing understanding of (1) palaeoheatflow and thermal maturity, (2) thermal maturity and petroleum generation in the Jurassic overpressured system, and (3) the origins and processes of development and preservation of the deep overpressured system.

1.2.2 Objectives

This research has been carried out with the following objectives.

1. Collection of data on total organic carbon content of source rocks, type and maturity of organic matter, especially in the Jurassic source rocks.

2. Assessment of Rock-Eval T_{max} data for thermal maturity study and thermal modelling.

3. Analyses of the characteristics of the deep overpressured system and top pressure seal.

4. Interpretation of well-log data for the deep overpressured system and top pressure seal.

5. One-dimensional modelling for thermal history associated with the rift heat flow (McKenzie, 1978; Jarvis and McKenzie, 1980) in some selected wells.

6. Studies of thermal maturity and thermal modelling in the Jurassic sealed overpressured system.

7. Seismic data interpretation and depth conversion for 2D geological models.

8. Two-dimensional overpressure modelling for three cross-sections in the Exmouth, Barrow and Dampier Sub-basins, and one-dimensional pressure behavior modelling in low-permeability (10^{-18}-10^{-22} m^2) environments.

1.3 Methodology

Heat-flow and fluid pressure are the principal agents in sedimentary basin evolution. In the processes of basin development, the most significant geochemical and geophysical phenomena of self-organization are petroleum generation, migration and accumulation, which are closely related to geothermal and geopressure histories. Organic-matter maturation and hydrocarbon generation are controlled by chemical reaction kinetics which are primarily temperature and time dependent (e.g. Hunt, 1979, 1991, 1996; Waples, 1980; Middleton, 1982; Tissot and Welte, 1984; Burnham and Sweeney, 1989; Sweeney and Burnham, 1990; Barker, 1996; Cranganu and Deming, 1996; Schenk et al, 1997). It is well-known that petroleum migration is governed by physical and physiochemical processes in relation to

sedimentation, compaction, fluid pressure, pore, microfracture and faults, and the properties of rocks and pore fluids (e.g. Hubbert, 1953; McAuliffe, 1979; Schowalter, 1979; Aydin, 2000), while fluid pressure is the most important factor for oil and gas migration in an overpressure environment called the pressure-driven process (Hunt, 1990; Schegg et al., 1999). The heat-flow history is a geodynamic process associated with basin origin (e.g. Middleton and Hunt, 1989; Allen and Allen, 1990). The history of fluid pressure is of solid-fluid interactive processes related to sedimentation, compaction, temperature, diagenesis, hydrocarbon generation and expulsion. Numerical basin models can synthesize the geological, geophysical and geochemical data to describe the complex phenomena and integrate the process in temporal order and spatial limit (e.g. Ungerer et al., 1990; Waples et al., 1992a, 1992b; Barker, 1996). Also calculated results by basin modelling can be calibrated and optimized by the observed data. Swarbrick (1995) pointed out that the results based on the present data matched in basin modelling still give limited information to test the validity of the models to simulate practical conditions in the geological past. However, it is undoubted that basin modelling is a very useful tool to understand geological processes. This study integrates geological, geochemical and geophysical data and emphasizes geological models in combination with the numerical modelling approach. The generalized ideal and work processes of basin modelling for these studies are shown in Fig. 1-2.

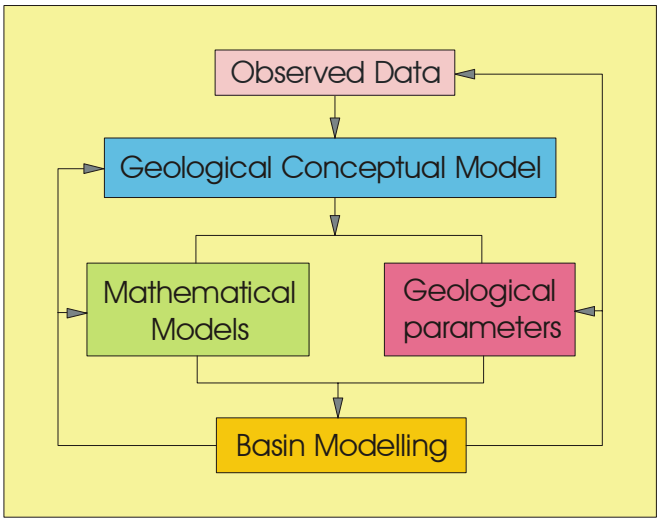

Fig. 1-2 Generalised ideal and work process of basin modelling for the thermal history and overpressure modelling in this study.

1.3.1 Geological method

The geological method aims at creating a conceptual geological model of the basin evolution on the basis of previous works and using geological, geochemical and geophysical data collected from various sources, selecting and studying geological variables as well as their relationships.

(1) Basic geological processes: tectonic, subsidence, deposition, uplift and erosion.

(2) The present thermal state including the present temperatures and heat-flows.

(3) The measured fluid pressure, formation compaction, the properties of the boundaries and the distribution of faults etc.

(4) Organic-matter parameters including total organic carbon, kerogen type and thermal maturity.

(5) Characteristics of measured porosity and well-log-derived porosity from claystone, and porosity and permeability from sandstones.

1.3.2 Basin modelling

Basin modelling is the study of dynamic and interactive geological processes using the BasinMod 1D and 2D software package. The software used in this study aims at applying a mathematical method to describe and calculate sedimentation, compaction, cementation, heat transfer, hydrocarbon generation, fluid pressure evolution and fluid flow through geological time.

Mathematical method

(1) The equations of backstripping (decompaction) and tectonic subsidence were used to reconstruct burial history or geohistory and subsidence.

(2) The kinetic model of quartz cementation and porosity loss (Walderhaug, 1996) was applied to calculate porosity associated with the cementation in the rock layer of the top pressure seal in 2D modelling

(3) The kinetic model of the Arrhenius first-order parallel-reaction (Burnham, 1989) and the chemical kinetic model of vitrinite reflectance (Sweeney and Burnham, 1990) were selected to describe the temperature and time dependence, and to calculate thermal maturity and hydrocarbon generation.

(4) The volumetric change model of organic matter during thermal evolution of solid kerogen into gas, oil and residue was used to calculate generation pressure.

(5) The pressure-controlled model (Düppenbecker et al., 1991) was selected for calculation of hydrocarbon expulsion in 2D overpressure modelling.

(6) The transient heat flow equation (governing equation) was used to describe thermal conduction and convection.

(7) The pressure equation (governing equation) was used to calculate fluid pressure (overpressure generation and preservation) as a function of formation compaction, temperature (fluid thermal expansion) and hydraulic conductivity.

(8) Multiphase fluid flow equations (governing equation) were used to model the processes of compaction-driven water flow direction.

Numerical modelling

Numerical modelling was carried out for thermal history reconstruction and overpressure evolution. The modelled results were correlated with the observed data for the calibration and optimization of geological parameters so that acceptable results were produced including the histories of burial, subsidence, heat flow, temperature, thermal maturity, hydrocarbon generation, and overpressure generation and maintenance.

The numerical modelling was performed using the BasinMod 1D software (version 7.06) and 2D software (version 4.61) by Platte River Associates, Inc. Parameters and models used in the BasinMod software package can be selected or modified by users. The theory, methodology and default parameters in the BasinMod software are given in the BasinMod reference manuals (Platte River Associates, Inc., 1996, 1998a, 1998b).

1.4 Data sources and sets

1.4.1 Data sources

The data used for this study were collected from different sources including open files, research reports and published literature. Most well data, including well completion reports, geochemical data, formation temperatures, pore fluid pressures and well logs, were taken from open files at the Department of Minerals and Energy of Western Australia (DMEWA). Seismic data (3100 km) were collected from open files at either the Australian Geological Survey Organisation (AGSO) or the DMEWA. Velocity data of 101R/09 and 110/11 deep seismic lines were supplied by AGSO. Five cross-sections of interpreted seismic lines in the Exmouth Sub-basin and the Exmouth Plateau were also provided by BHP Petroleum. Some default values, including initial porosity, matrix density, grain size, matrix thermal conductivity, fluid conductivity, matrix heat capacity, kerogen kinetic parameters etc., were provided by the BasinMod 1D and 2D softwares.

Additionally, experimental analyses in this study include: Rock-Eval pyrolysis, gas chromatography (GC), gas chromatography-mass spectrometry (GC-MS) and claystone density measurements for samples from a conventional core, side-wall cores and cuttings in the Bambra-2 well (Table 1-1). The Rock-Eval pyrolysis was carried out at the Geological Survey of Canada, Calgary. The GC and GC-MS were analyzed at the Geological Survey of Canada, Calgary and Curtin University of Technology. The claystone density was measured at Curtin University of Technology.

Table 1-1 Samples from the Bambra-2 well for geochemical analyses

Depth (m)	Type of Sample	Analysis
2012.5	Side Wall Core	Rock-Eval Pyrolysis
2172.5	Side Wall Core	Rock-Eval Pyrolysis
2313.5	Side Wall Core	Rock-Eval Pyrolysis
3795	Side Wall Core	Rock-Eval Pyrolysis
3795	Side Wall Core	Rock-Eval Pyrolysis (Extracted)
3906	Side Wall Core	Rock-Eval Pyrolysis
3906	Side Wall Core	Rock-Eval Pyrolysis (Extracted)
4225	Side Wall Core	Rock-Eval Pyrolysis
4225	Side Wall Core	Rock-Eval Pyrolysis (Extracted)
4225	Side Wall Core	Gas Chromatography
4274	Conventional Core	Rock-Eval Pyrolysis
4274	Conventional Core	Gas chromatography-mass spectrometry
4283	Conventional Core	Rock-Eval Pyrolysis
4283	Conventional Core	Gas Chromatography
4283	Conventional Core	Gas chromatography-mass spectrometry
4301	Side Wall Core	Rock-Eval Pyrolysis
4301	Side Wall Core	Rock-Eval Pyrolysis (Extracted)
4301	Side Wall Core	Gas Chromatography
4406	Side Wall Core	Rock-Eval Pyrolysis
4406	Side Wall Core	Rock-Eval Pyrolysis (Extracted)
2660-2665	Cuttings	Rock-Eval Pyrolysis
2660-2665	Cuttings	Rock-Eval Pyrolysis (Extracted)
2660-2665	Cuttings	Gas Chromatography
3090-3095	Cuttings	Rock-Eval Pyrolysis
3090-3095	Cuttings	Rock-Eval Pyrolysis (Extracted)
3440-3445	Cuttings	Rock-Eval Pyrolysis
3530-3535	Cuttings	Rock-Eval Pyrolysis
3970-3975	Cuttings	Rock-Eval Pyrolysis
3970-3975	Cuttings	Rock-Eval Pyrolysis (Extracted)
3970-3975	Cuttings	Gas Chromatography
4115-4120	Cuttings	Rock-Eval Pyrolysis
4280-4285	Cuttings	Rock-Eval Pyrolysis
4274	Conventional Core	Density
4279	Conventional Core	Density
4283	Conventional Core	Density

Rock-Eval 6 pyrolysis for 17 samples were carried out at the Geological Survey of Canada, Calgary (2000).
Extraction and Rock-Eval 6 pyrolysis for 8 samples were carried out at the Geological Survey of Canada, Calgary (2000).
Gas Chromatography analysis for 5 samples was performed at the Geological Survey of Canada, Calgary (2000).
Gas chromatography-mass spectrometry analysis for two samples was performed at the Geological Survey of Canada, Calgary (2000) and the School of Applied Chemistry of Curtin University of Technology (2001).
Density measurements for three claystone samples were completed at the CSIRO Chemical Laboratory (2001).

1.4.2 Data sets

A total of 67 exploration well completion reports were reviewed with 41 wells being further studied for heat flow histories. The data sets of 14 wells from their well completion reports were available for 1D modelling of the heat flow histories using the BasinMod 1D software. The data sets of 8 wells from their well completion reports (among them, 3 wells used for 1D modelling) were used in 2D modelling. These wells used in the modelling were drilled in different tectonic subdivisions between 1964 and 1984 by various companies (Fig. 1-3 and Table 1-2).

1600 km of interpreted migrated deep seismic data from AGSO (Fig. 1-3), acquired between 1990 and 1992, were reviewed. 1500 km of migrated seismic lines, with a time record of 5 to 6 seconds TWT, were also reviewed. These seismic lines had been acquired between 1978 and 1991, and were collected from DMEWA and AGSO (Fig. 1-3). Three seismic lines, 110/11, 101R/09 and A-B were selected for 2D modelling. Line A-B, in the Barrow Sub-basin, was assembled from eight lines shown in table 1-3 and is about 120 km long. Lone 110/11 is in the Exmouth Sub-basin and about 150 km long. Line 101R/09 is in the Dampier Sub-basin and about 135 km long. These seismic lines were converted from time to depth cross-sections based on well velocity surveys and seismic velocity data for two-dimensional overpressure modelling.

The data sets of organic-matter richness, type and maturity were derived from 17 exploration wells in the basin. The values of porosity and permeability were collected from 59 wells in the basin.

Table 1-2 The data from 23 wells in the Northern Carnarvon Basin for the modelling

Well Name	SD	T. D. (m)	R.T.-MSL (m)	W. D. (m)	Age of T. D.	Year Completed	Operator
Jurabi-1[a]	EB	3712.00	17.4	60.0	Late Triassic	1982	ESSO
Novara-1[b]		2753.00	8.0	372.0	Early Cretaceous	1983	ESSO
Outtrim-1[b]		1725.00	30.5	91.0	Late Jurassic	1984	ESSO
Zeewulf-1[a, b]		3500.00	10.4	1194.2	Late Triassic	1979	ESSO
Anchor-1[a]	BB	3049.00	24.5	18.0	Middle Jurassic	1969	WAPET
Bambra-1		3666.00	31.75	24.51	Late Jurassic	1983	AOPL
Bambra-2[a, b]		4591.00	26.0	26.0	Middle Jurassic	1983	AOPL
Barrow-1[a]		2982.47	3.35*	0	Late Jurassic	1964	WAPET
Barrow Deep-1[a]		4650.00	7.92*	0	Middle Jurassic	1973	WAPET
Bowers-1[a]		4300.00	25.0	133.3	Late Triassic	1982	WAPET
West Barrow-1/1A		3520.00	10.3	98.0	Early Cretaceous	1982	OONL
West Barrow-2		3437.00	8.3	98.0	Early Cretaceous	1985	BHP
Dampier-1	DB	4141.62	9.14	76.2	Late Jurassic	1969	Woodside
Hampton-1[b]		2584.00	30.0	53.0	Early Triassic	1974	Woodside
Madeleine-1[a]		4427.53	9.14	68.9	Middle Jurassic	1969	Woodside
Rosemary-1[a, b]		3909.06	9.5	64.9	Middle Jurassic	1973	Woodside
Depuch-1[a]	BS	4300.00	10.0	143.0	Early Jurassic	1974	Woodside
Goodwyn-7[b]	RP	3446.00	17.0	134.0	Late Triassic	1985	Woodside
North Gorgon-1[a]		4500.00	25.0	215.0	Late Triassic	1983	WAPET
North Rankin-1[a]		3534.00	30.2	122.2	Late Triassic	1971	Woodside
West Tryal Rocks-1[b]		3866.39	12.2	137.8	Late Triassic	1973	WAPET
Investigator-1[a]	EP	3745.60	10.4	841.2	Late Triassic	1979	ESSO
Jupiter-1[a]		4946.00	9.5	959.8	Middle-Late Triassic	1979	Phillips

SD: Subdivision; T. D.: Total depth; R. T.: Rotary table; MSL: Mean sea level; W. D.: Water depth; EB: Exmouth Sub-basin; BB: Barrow Sub-basin; DB: Dampier Sub-basin; BS: Beagle Sub-basin; RP: Rankin Platform; EP: Exmouth Plateau. * R. T. - G. L. (ground level). a: Wells for 1D thermal modelling; b: Wells for 2D modelling.

AOPL - Australian Occidental Pty. Ltd.

BHP - BHP Petroleum Pty Ltd.

ESSO - ESSO Exploration and Production Australia Ltd.

Lasmo - Lasmo Oil (Australia) Limited.

OONL - Offshore Oil N.L.

Phillips - Phillips Australian Oil Company

WAPET - West Australian Petroleum Pty. Ltd.

Woodside - Woodside Offshore Petroleum Pty. Ltd.

Table 1-3 Seismic lines used in this study collected from the Department of Minerals and Energy of Western Australia

Line	Shot Point	Operator	Line	Shot Point	Operator
82-53	1-1310	AOPL	86A-3106/A	1-1563	Woodside
82-53A	1204-1370	AOPL	CD88-B32	1001-2105	CPNL
82-52A	1-155	AOPL	86B-3175/A	1-558	Woodside
82-133	1-380	AOPL	G86-122	101-1003	ARCO
83-388	1-779	AOPL	G86-140	952-101	ARCO
83-405	1-361	AOPL	HM88A-197	1426-927	BHP
B85T-649	63-426	BCPL	X78A-933	2260-1952	GSI
81-65 (stack)	1-1732	WOPL	X79B-1203	2000-2835	GSI
K91-13	101-1345	WOPL	C81B-145	4757-3272	BHP
K91-36	1-1177	WOPL	C81B-145B	3271-1929	BHP
J89-23	1-1560	WMC	LC89-29	440-1832	LOL
B82-01M	125-629	WAPET	LC89-058	63-470	LOL

AOPL - Australian Occidental Pty. Ltd.

BCPL - Bond Corporation Pty. Ltd.

WOPL - Wesminco Oil Pty. Ltd.

WMC - Western Mining Corporation.

WAPET - West Australian Petroleum Pty. Ltd.

Woodside - Woodside Offshore Petroleum Pty. Ltd.

CPNL - Command Petroleum N. L.

ARCO - ARCO International

BHP - BHP Petroleum Pty. Ltd.

GSI - Geophysical Service International

LOL - Lasmo Oil Ltd.

CHAPTER 2 REGIONAL GEOLOGY

2.1 Location of study area

The Northern Carnarvon Basin is one of a series of extensional basins that form the North West Shelf of Australia. It is located at the southern end of the North West Shelf (Fig. 2-1). Geologically, it belongs to the Westralian Superbasin which is composed of the Perth, Northern Carnarvon, Offshore Canning, Browse and Northern Bonaparte basins (Yeates et al., 1987). It stretches from the Precambrian Craton in the east to a continental-oceanic crustal boundary in the north, west and the southwest, with, respectively, the Argo, Gascoyne and Cuvier Abyssal Plains (Hocking, et al., 1987; AGSO North West Shelf Study Group, 1994) (Fig. 2-2). The basin is transitional towards the Canning Basin in the northeast, and the Southern Carnarvon Basin in the south (Figures 2-1 and 2-2). The main tectonic subdivisions of the Northern Carnarvon Basin (Fig. 2-2) are the Exmouth, Barrow, Dampier and Beagle sub-basins, the Rankin Platform and the Exmouth Plateau (Hocking, 1988). These subdivisions are commonly referred to as the Mesozoic-Cainozoic basin over the pre-Triassic basement. Sediments usually extend to the continental-oceanic crust boundary.

2.2 Stratigraphy

The Northern Carnarvon Basin contains thick Mesozoic and Cainozoic sedimentary rocks overlying the pre-Triassic basement. The sub-basins contain up to 12 km of Mesozoic-Cainozoic sediments. The generalized stratigraphic column of the Mesozoic and Cainozoic in the Northern Carnarvon Basin, especially for the sub-basins, based on Barber (1994), Labutis (1994), Stagg and Colwell (1994) and Polomka et al. (1999), is shown in Fig. 2-3. There are thinner (non-existent in places) Middle-Upper Jurassic syn-rift sedimentary rocks on the Rankin Platform and the Exmouth Plateau.

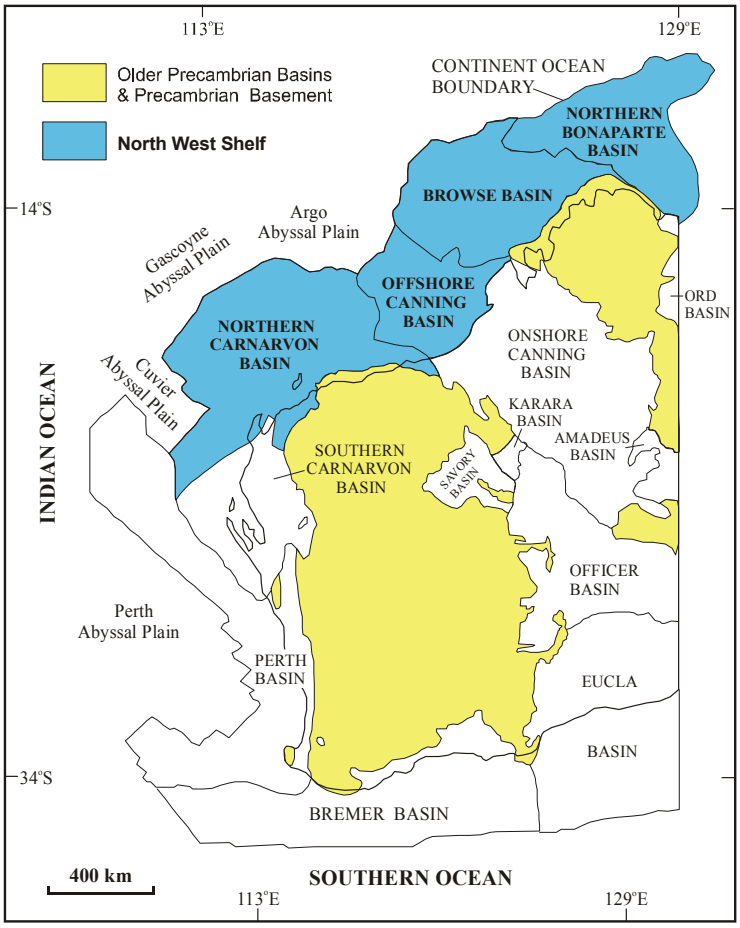

Fig. 2-1 Sedimentary basins of Western Australia (after Trendall and Cockbain, 1990; Hocking et al., 1994; Purcell and Purcell, 1994).

2.2.1 Triassic

The Triassic sequence represents a series of northeast-trending depocentres in the Northern Carnarvon Basin (Hocking, 1988). The boundary between the Permian and Triassic in the Barrow-Dampier Sub-basins is an angular unconformity in places (Westphal and Aigner, 1997). This sequence is a several kilometers blanket over most areas of the basin and can be divided into two parts (Cook et al., 1985; Hocking, 1988). The lower part of the Triassic sequence, the Locker Shale, is dominated by shale and siltstone but contains minor intercalated limestone and sandstone with low-energy marine conditions. The upper part, called the Mungaroo Formation, is mostly fluvio-deltaic sedimentary rocks involving sandstone, siltstone,

mudstone with thin coals, and minor conglomerates. Deposition of the overlying Mungaroo Formation extended into the Rhaetian in most areas in the basin (Hocking, 1988).

2.2.2 Jurassic

The bottom of the Jurassic is the Brigadier Formation, a sequence of thinly interbedded sandstone and shale, which overlies the Mungaroo Formation, and extends into the Rhaetian-Middle Hettangian in most areas of the basin margin (Crostella and Barter, 1980; Parry and Smith, 1988). The Jurassic section overlying the Brigadier Formation is separated mainly into three formations which are the Murat Formation, the Athol Formation and the Dingo Claystone.

The lower part of the Jurassic between the Upper Hettangian and the Pliensbachian is the Murat Formation with paralic environments, dominated by land-organic-rich siltstone and claystone in the Exmouth, Barrow and Dampier Sub-basins (Hocking, 1988). The equivalent of the Murat Formation (the lower Legendre Formation) in the Beagle Sub-basin consists of shallow-marine and fluvial-deltaic sandstone, siltstone and shale with thin coals (Blevin et al., 1994).

The middle part of the Jurassic, between the Toarcian and the Callovian, is the Athol Formation, a syn-rift graben deposit dominated by organic-rich claystone and siltstone. The formation is up to several thousand meters thick in the depocentres of the rift grabens or half-grabens, and gradually thins on the graben flanks. The depositional environment for the Athol Formation in the Exmouth, Barrow and Dampier Sub-basins is a low-energy, restricted marine environment (Kopsen and McGann, 1985; Hocking, 1988; Parry and Smith, 1988; Woodside Offshore Petroleum, 1988; Baillie and Jacobson, 1997). The equivalent of the Athol Formation (the upper part of the Legendre Formation) in the Beagle Sub-basin consists of fluvial sandstone, siltstone and claystone with minor coal (Blevin et al., 1994).

The upper part of the Jurassic is the marine Dingo Claystone, composed of fine-grained rocks with minor sandstone over the Exmouth, Barrow and Dampier Sub-basins, and thin to missing in the Beagle Sub-basin. The upper part of the Upper Jurassic is the Dupuy Formation. It developed as submarine-fan sediments in the Exmouth Sub-basin, as turbidite sandstones and debris flows in the Barrow Sub-basin, and as turbidite sandstones (Angel Formation) in the Dampier Sub-basin (Kopsen and McGann, 1985; Tait, 1985; Hocking, 1988; Parry and Smith, 1988; Woodside Offshore Petroleum, 1988; Baillie and Jacobson, 1997).

2.2.3 Cretaceous

The Barrow Group was deposited during the Berriasian to Valanginian, and is considered to be a syn-rift sequence of sandstone and shale in the Exmouth and Barrow Sub-basins, and on the southern margin of the Exmouth Plateau (Tindale et al., 1998; Polomka et al., 1999). This group was formed by a prograding delta. The delta's bottomsets are submarine fan, turbidite and deepwater facies and its topsets are fluvial to shallow marine deposition (Kopsen and McGann, 1985; Tait, 1985). The Barrow Group is two coarsening up sequences composed of interbedded sandstone, siltstone and claystone in the lower part of the group, and sandstone with minor siltstone in the upper part of the group (Hocking, 1988). The group has a maximum thickness of 1600 m (Baillie and Jacobson, 1997) and is an excellent reservoir unit over the underlying basin structures and some uplift blocks (McClure et al., 1988). The Forestier Claystone between Berriasian and middle Valanginian in the Beagle Sub-basin is a marine claystone over the sub-basin and can act as a seal (Blevin et al., 1994).

After the breakup of Australia from Greater India in the Valanginian, the Mardie Greensand and Birdrong Sandstone were deposited along the shoreface-nearshore areas and in the offshore with higher energy conditions. The Muderong Shale formed a widespread transgressive marine shale and siltstone with minor sandstone and blanketed most of the Northern Carnarvon Basin until the late Aptian (Kopsen and McGann, 1985; Hocking, 1988; Blevin et al., 1994). This formation is recognised to be an effective regional top seal to the underlying Barrow Group sandstone, and Jurassic and older reservoirs on some structurally high elements in

the sub-basins (McClure et al., 1988; Parry and Smith, 1988; Baillie and Jacobson, 1997). The Windalia Sandstone is considered to be a member of the Muderong Shale and interpreted as a storm-generated shelf sand deposited below normal wave base (Campbell et al., 1984). The Windalia Radiolarite, Gearle Siltstone and Haycock Marl were deposited under a general deepening of depositional environments and continued till approximately the Turonian (Apthorpe, 1979), with inferred water depths in excess of 200 m (Kopsen and McGann, 1985).

A basin-wide change of lithology from siliciclastic to calcareous deposition commenced in the Santonian (Hocking, 1988). Because of the lack of terrigenous clastic supply, marl, calcarenite and limestone were the principal lithologies from the Santonian to the Cainozoic (Barber, 1982). The Toolonga Calcilutite is widespread in the Northern Carnarvon Basin. Korojon Calcarenite deposition occurred locally, in shallower areas where energy levels were higher. The Withnell Formation is an offshore equivalent of the Korojon Calcarenite in the Beagle Sub-basin. The Miria Marl also has a wide deposition in the Northern Carnarvon Basin (Hocking, 1988).

2.2.4 Cainozoic

During the Cainozoic, carbonate-dominated sequences were deposited with moderate to low energy shelf to slope environments (Hocking, 1988). Four sedimentation cycles were recognised by Quilty (1977) and Hocking (1988). Cycle 1 was the Late Paleocene to the Early Eocene associated with Cardabia Calcarenite deposition. Cycle 2 occurred in the Middle-Late Eocene corresponding to the Giralia Calcarenite. This formation was deposited in environments ranging from nearshore and inner marine shelf to outer shelf and slope with various lithologies of calcilutite, calcisiltite, calcarenite, calcareous siltstone and siliciclastic sediments. Cycle 3 was from the Late Oligocene to Middle Miocene. During this period the Cape Range Group, including the Mandu Limestone, Tulki Limestone and Trealla Limestone, was deposited as carbonate-dominated lithologies of calcilutite and calcareous marl in environments which deepened from shallow marine and inner shelf to outer shelf, slope and deep marine. This sequence is a northwards-thickening sheet of sediment

over the continental shelf. Siliciclastic deposition occurred only in the Middle Miocene on the western flank of Cape Range and in the northeast along parts of the Rankin Platform. Cycle 4 ranged from the Late Miocene to the Holocene. The Delambre Formation with fine calcisiltite and calcilutite was deposited mainly in a low energy, marine shelf to slope environment. This sequence ranges in thickness from several hundred meters to more than one thousand meters.

2.3 Tectonic subdivisions, structures and faults

2.3.1 Tectonic subdivisions

Based on the studies of Hill (1994), Hocking et al. (1994), and Stagg and Colwell (1994), a tectonic subdivision map for the Northern Carnarvon Basin is shown in Fig. 2-4. From southeast to northwest, the Northern Carnarvon Basin comprises the Peedamullah and Lambert Shelves flanked by the Enderby Terrace, a series of four northeast-trending grabens and half-grabens which are the Exmouth, Barrow, Dampier and Beagle Sub-basins, the Rankin Platform and its southerly extension, the Alpha Arch, and the Exmouth Plateau.

2.3.2 Structures and faults

The depocentres of the Jurassic and Early Cretaceous are bounded by a series of horsts to the west and by the Peedamullah and Lambert Shelves to the east. The Exmouth and Barrow Sub-basins are separated by the Alpha Arch. The Dampier and Beagle Sub-basins are separated by the De Grey Nose. The Exmouth Plateau can be divided into two parts, the central and southern plateau, and the northern plateau, on the basis of fault features. The central and southern Exmouth Plateau is dominated by north-trending or north-northeast-trending faults at the Upper Triassic to Middle Jurassic or Early Cretaceous. The principal fault trends on the northern Exmouth Plateau are east-northeast. The northeast- and north-northeast-trending normal faults predominate in the areas of the sub-basins and the Rankin Platform. These faults are associated with the extension of the lithosphere during the rift phase until the

breakup of Gondwana. There are several fault systems, including the Rankin Fault System, the Flinders Fault System and the Rosemary Fault System. The Flinders and Rosemary Fault Systems extend along the east flanks of the Barrow and Dampier Sub-basins and consist of high-angle faults that may be antithetic to the Rankin Fault System. There are several anticlines, structural arches and noses along the eastern margin of the basin.

2.4 Geological evolution

The geological evolution of the Northern Carnarvon Basin, as a part of the Northwest Shelf, commenced in the Late Palaeozoic. During this time the North West Shelf belonged to the eastern part of Gondwana and formed part of the southern Tethyan continental margin (Exon and Colwell, 1994; Westphal and Aigner, 1997). Falvey and Mutter (1981) believed that the subsidence of the continental margin occurred as an intracratonic phase, which started in the Permian and resulted in the Westralian Superbasin on the southern margin of Tethys (Yeates et al., 1987). A previous extension of the superbasin terminated in the Late Permian. Thus, the geological evolution of the Northern Carnarvon Basin from the Triassic can be divided into three major phases: (1) a pre-rift phase which occurred during the Triassic, (2) a syn-rift phase which occurred during the Early Jurassic until a complete continental breakup of Gondwana in the earliest Cretaceous, and (3) a post-rift phase as a passive continental margin from the Early Cretaceous to the Cainozoic when the basin experienced various short episodes of compression due to the convergence between the Australian and Asian plates.

2.4.1 Pre-rift phase

The Triassic section shows little, or no evidence, of syn-depositional extensional faulting along the entire North West Shelf (Etheridge and O'Brien, 1994; Westphal and Aigner, 1997) and, thus, a tectonically calm period is thought to have taken place in the Triassic (Falvey and Mutter, 1981; Barber, 1982; Westphal and Aigner, 1997). Based on seismic data, Barber (1982) and the AGSO North West Shelf Study Group (1994) interpreted the presence of several kilometres of Triassic sedimentary

rocks nearly everywhere on the continental margin. The lower part of the Triassic sequence is composed of the marine Locker Shale (Barber, 1982). The Mungaroo Formation, the upper part of the Triassic rocks, is mostly of fluvio-deltaic origin. The top of the Mungaroo Formation consists of shallow-marine siliciclastics and shallow-marine carbonates on the Exmouth Plateau (Barber, 1982; Cook et al., 1985; Colwell et al., 1994; Exon and Colwell, 1994). The Murat Siltstone of the Lower Jurassic is a pre-rift shallow marine succession deposited over the sub-basin area. Several hundred meters of this sequence were probably deposited on the Exmouth Plateau and eroded during the Middle Jurassic (Barber, 1982).

2.4.2 Syn-rift phase

The early rift is interpreted to have commenced in the Latest Triassic to the earliest Jurassic based on K/Ar ages from three volcanic samples on the Wombat Plateau dated from 213 to 192 Ma (von Stackelberg et al., 1980; Exon and Colwell, 1994; Westphal and Aigner, 1997). Hocking et al. (1987) considered that the rifting recommenced in either the latest Triassic or the earliest Jurassic. Boyd et al. (1993) considered that the rift occurred from Hettangian to Callovian, and a second rift and final breakup took place between Callovian and Hauterivian. The extension in the sub-basins of the Northern Carnarvon Basin began in the Early Jurassic (about 190 Ma), until the continental breakup of Gondwana in the Late Jurassic and Valanginian (Barber, 1982; Westphal and Aigner, 1997; Tindale et al., 1998; Polomka et al., 1999). The extension finally caused the separation of Australia from Greater India in the Callovian-Valanginian (Exon and Colwell, 1994; Westphal and Aigner, 1997). The rifting led to a series of four NE-SW to NNE-SSW-trending rift grabens and half-grabens (sub-basins) with rapid subsidence and deposition, numerous parallel normal faults and the block-faulted structures of the Rankin Platform (Barber, 1982). Differential subsidence occurred due to the extension resulting in the accumulation of thick fine-grained sequences in the sub-basins, whereas several hundred metres to 2500 metres of sediments were eroded on the shoulders of rift grabens along the Rankin Platform, the Peedamullah and Lambert Shelves (Barber, 1982; Kopsen and McGann, 1985; Hocking, 1988; Westphal and Aigner, 1997; Crostella et al., 2000). Tindale et al. (1998) considered that the Jurassic syn-rift sequence is either absent or highly condensed across the Exmouth

Plateau. Based on regional deep seismic data interpreted by AGSO on the Exmouth Plateau, a number of small-scale faulted half-grabens developed during rifting. The faults controlled deposition, and up to one thousand metres of Jurassic syn-rift sequence were deposited on the downthrown sides of these faults, while syn-rift sediments are thin, or absent, on the upthrown side of the faults. Erosion of several hundred metres has been interpreted on the structural highs of the Exmouth Plateau as a result of rifting (Barber, 1982).

The earliest continental breakup of Gondwana occurred at about 160 Ma (Veevers and Li, 1991), or at about 155 Ma (Ludden, 1992), to the north of the basin where the Argo Abyssal Plain formed the earliest part of the Indian Ocean. Seafloor spreading (further extension) has been proposed to have begun in the Valanginian, ca. 136 Ma (Müller et al., 1998), or 132.5 Ma (Veevers and Li, 1991), associated with separation of Australia and Greater India, and the formation of the Gascoyne and Cuvier Abyssal Plains to the west and southwest of the basin. The breakup times were widely accompanied by volcanism along the outer Western Australian margin (Exon and Colwell, 1994). The actual continental breakup is commonly dated as being concomitant with an unconformity, called the "main unconformity" in the Northern Carnarvon Basin. As a result of the breakup, the main unconformity in the Beagle Sub-basin is the contact between the Callovian and the Oxfordian sequences (Blevin et al., 1994). The main unconformity in the Dampier Sub-basin is within the Oxfordian sequence (Vincent and Tilbury, 1988; Barber, 1994). An important unconformity in the Exmouth and Barrow Sub-basins is the boundary between the Barrow Group and the Winning Group (Valanginian to early Late Cretaceous) (Westphal and Aigner, 1997; Tindale et al., 1998; Polomka et al., 1999). The thickness of the Upper Jurassic to the lowest Cretaceous sedimentary rocks varies considerably in the Northern Carnarvon Basin. During this period, the sequences are considered to be syn-rift deposits in the Exmouth and Barrow Sub-basins (Tindale et al., 1998). On the Exmouth Plateau, the Oxfordian to Tithonian interval is a thin sequence (condensed sedimentary section). During the Late Jurassic, the Rankin Platform remained a positive area above sea-level (Barber, 1982). In the earliest Cretaceous before the Valanginian breakup, a syn-rift sequence (Barrow Group) was deposited in the Exmouth and Barrow Sub-basins, and over the southern margin of the Exmouth Plateau, while several localised Triassic fault blocks of the Rankin

Platform still remained elevated above sea-level (Barber, 1982). The marginal areas of the basin were subjected to erosion (Hocking, 1988).

2.4.3 Post-rift phase

Following the breakup of Australia from Greater India, the basin developed as a passive continental margin and underwent a thermal subsidence phase as a result of cooling in the lithosphere. Thermal subsidence commenced in the north of the basin and progressively shifted to the south. During the Cretaceous, several periods of minor uplift and erosion (structural inversion) occurred in the basin (Tindale et al., 1998). From the Santonian, calcilutite, calcarenite and marl became the prime lithologies due to peneplanation of the continental provenance areas (Barber, 1982). During the Cainozoic, northwest Australia experienced various short and localised episodes of compression during the Cainozoic which have been interpreted as a result of tectonic stresses generated from the convergence of Australian and Asian plates (Westphal and Aigner, 1997). This compression caused localised structural deformation and strike-slip faulting throughout the North West Shelf (Kopsen and McGann, 1985; Cockbain, 1989; Tindale et al., 1998). However, the effects of these tectonic events on the entire Northern Carnarvon Basin are considered to be small and of brief duration (Westphal and Aigner, 1997; Keep et al., 1998). The carbonate-dominated Cainozoic sequence with minor siliciclastic sediments was deposited over the basin (Hocking, 1988).

Part II

Source Rocks, Rock-Eval T_{max} and Deep Overpressure

CHAPTER 3 SOURCE ROCKS AND ORGANIC MATTER

3.1 Source rocks

The potential source rocks and characteristics of the organic matter in the Triassic, Jurassic and Lower Cretaceous in the Northern Carnarvon Basin have been studied by Scott (1992, 1994), and discussed by a number of researchers (e.g. Powell and McKirdy, 1973a; Volkman et al., 1983; Cook et al., 1985; Kopsen and McGann, 1985; Parry and Smith, 1988; Woodside Offshore Petroleum, 1988).

The Triassic source rocks can be separated into two parts. The lower part (Locker Shale) appears to contain oil-potential organic matter deposited in a marine environment (Barber, 1982; Scott, 1992, 1994). The upper part (Mungaroo Formation) is composed of a coaly sequence of fluvio-deltaic facies, and sources gas and condensate. However, the very top of the Mungaroo Formation had some marine influence (Cook et al., 1985).

The Jurassic sequences, including the Murat Siltstone, Athol Formation and Dingo Claystone, are the most important source rocks in the sub-basins of the Northern Carnarvon Basin (McClure et al., 1988; Parry and Smith, 1988; Baillie and Jacobson, 1997). The Lower-Middle Jurassic rocks in the sub-basins are composed of paralic-marginal marine lithofacies containing a large amount of woody, land-derived organic matter and are thus considered to form predominately gas/condensate-prone source rocks (Scott, 1992). The Dingo Claystone of the Upper Jurassic contains mixed terrestrial and marine organic matter (gas and oil-prone source) deposited in a near-shore environment (Powell and McKirdy, 1973a; Volkman et al., 1983), with somewhat less terrestrial input than the Lower-Middle Jurassic (Kopsen and McGann, 1985; Parry and Smith, 1988; van Aarssen et al., 1996). Geochemical evidence reveals a general similarity in the compositions of the condensates and oils from the Triassic, Jurassic and Cretaceous reservoirs in the Dampier Sub-basin and on the Rankin Platform, and also suggests that the hydrocarbons have been generated from these Jurassic source rocks with the mixed

nonmarine and marine organic matter (Powell and McKirdy, 1973a). Volkman et al. (1983) and van Aarssen et al. (1996) proposed that the Upper Jurassic source rock is the most important oil source in the Barrow Sub-basin, based on the oil-source rock correlation. Furthermore, van Aarssen et al. (1996) suggested that these oils and condensates from the Barrow Sub-basin, correlated with samples from the Koolinda-1 well, were sourced from an interval of the source rocks of Middle-Upper Oxfordian age. It is recognized that the kerogen of the Upper Jurassic from wells drilled on structural highs, and basin margins, is mainly derived from terrestrial higher plants (Kopsen and McGann, 1985; Parry and Smith, 1988). Kopsen and McGann (1985) stated that the Lower Cretaceous has some oil-prone source rocks within the Barrow Group and the lower part of the marine Muderong Shale in the Barrow-Dampier Sub-basins.

3.2 Richness of organic matter

The organic matter richness of source rocks is estimated usually using the total organic carbon content (TOC, %), although the TOC is residual TOC when dealing with mature source rocks as the overall converting efficiency of organic carbon is generally less than 15 wt.% (Hunt, 1979). Quantity of organic matter in source rocks can be calculated using a universal conversion factor of 1.22 (Barker, 1996). The study has collected 1256 values of TOC from 17 wells in the various tectonic subdivisions of the Northern Carnarvon Basin (see Table 3-1 and Fig. 3-1). The distributions of TOC at different intervals of the potential source rocks are shown in histograms (Figures 3-2 to 3-6).

Figure 3-2 shows that 206 TOC values in the Cretaceous Gearle Siltstone, Windalia Radioarite and Muderong Shale mainly range from 0.5 % to 3 %, and that values between 1 and 2 % cover more than 50 % of the shale samples. About 80 % of the samples have more than 1 % TOC. Figure 3-3 and Table 3-1 show that most TOC values in the Barrow Group range from 0.1 to 3.7 %. About 60 % of the samples in this group are higher than 1.0 % TOC, but about 40 % are lower than 1.0 % TOC. An average TOC value in the Barrow Group is 1.30 %.

Figure 3-4 shows that 582 TOC values in the Dupuy Formation, Dingo Claystone and Athol Formation of the syn-rift Jurassic mostly range from 0.5 % to 3.5 %. The

values between 1 % and 2.5 % cover about 80 % of the samples. The TOC values in the Murat Siltstone of the pre-rift Jurassic principally vary from 0.5 to 6 %, whereas the TOC values of about 70 % of the samples are higher than 1 % (Fig. 3-5). In the Beagle Sub-basin, the coal-bearing sequence of the Jurassic source rocks has higher TOC, and most values of greater than 10 % TOC in Figures 3-4 and 3-5 occur in the Beagle Sub-basin. In general, the Jurassic rocks can be considered to be rich in total organic matter. An average TOC value in the Dupuy Formation, Dingo Claystone and Athol Formation is 1.74 % and in the Murat Siltstone is 2.09 %.

The Mungaroo Formation of the Middle-Upper Triassic is a coaly interval rich in organic matter. TOC values in this formation are from 0.1 to 35.9 % with an average TOC value of 2.19 %. The TOC values range from 0.5 to 14 % for 80 % of the samples. The TOC values in approximately 65 % of the samples are greater than 1 % (Fig. 3-6). TOC values in the Locker Shale of the Lower-Middle Triassic are between 0.6 and 1.94 % from the limited data (Table 3-1).

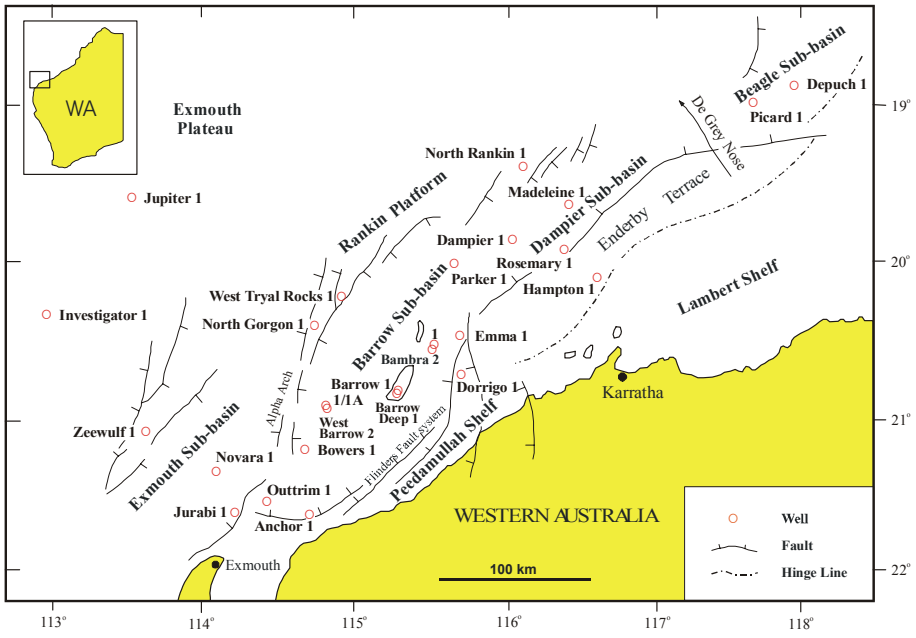

Fig. 3-1 A map shows well locations and the tectonic subdivisions in the Northern Carnarvon Basin (after Woodside Offshore Petroleum, 1988; Scott, 1992).

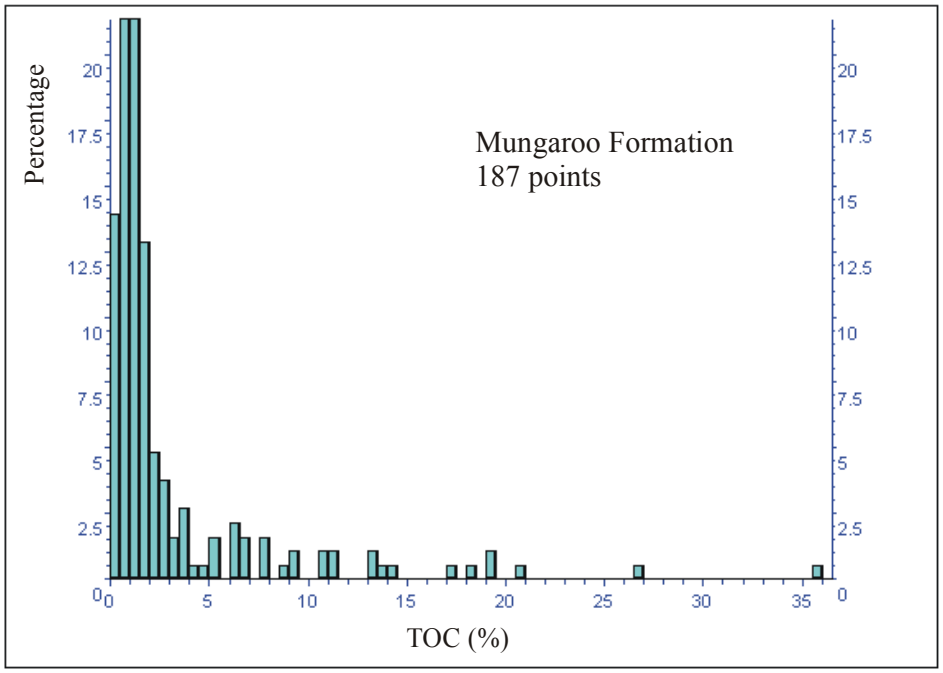

Fig. 3-6 Histogram of total organic matter for the Mungaroo Formation in the Northern Carnarvon Basin.

Barker (1996) considered that a TOC value of 1.0 % is the lower limit for an effective source rock because a source rock with less than 1.0 % will never generate enough oil to initiate primary migration. Peters (1986) mentioned that a TOC between 0.5 and 1.0 % indicates a fair source-rock generative potential, TOC values ranging from 1.0 % to 2.0 % a good generative potential, and TOC values greater than 2.0 % a very good generative potential. According to this criterion, 60 to 80 % of the TOC values from the samples of the Triassic, Jurassic and Cretaceous in this basin belong to the good or very good source-rock generative-potential categories. Baillie and Jacobson (1997) pointed out that TOC values typically range from 1 to 6 % in the Dingo Claystone, Athol Formation and Murat Siltstone. The range and the calculated average values of the total organic carbon in the five intervals mentioned above in 17 wells are shown in Table 3-1. The values of TOC >15 % are not included in Table 3-1.

3.3 Type of organic matter

Organic matter type is an important factor in evaluating source rock potential and has an important influence on the nature of hydrocarbon products (Hunt, 1979; Tissot and Welte, 1984; Barker, 1996). Jones (1984) studied generative potential of oil and gas from different organic facies with R_o of about 0.5 %. He pointed out that gas-prone organic facies have a hydrogen index (HI=S_2%100/TOC) of less than 200; mixed oil-gas-prone facies have a HI between 200 and 350; oil-prone facies have a HI ranging from 350 to more than 1000. Peters (1986) proposed that for immature source rocks, the HI for gas-prone organic matter is less than 150; gas-oil-prone organic matter is between 150-300; oil-prone organic matter is more than 300. The organic matter type within the Triassic, Jurassic and Cretaceous in this basin has been reviewed on the basis of kerogen element analysis and Rock-Eval pyrolysis for bulk geochemical properties, and organic petrographic analysis for visual kerogen compositions and some biomarker data.

The atomic H/C (hydrogen/carbon ratio) and atomic O/C (oxygen/carbon ratio) from elemental analyses of kerogen for three wells in the Exmouth Sub-basin are shown in the van Krevelen diagrams (Fig. 3-7). Their evolution paths with maturation indicate that the bulk geochemical properties of kerogen in the Jurassic and Early Cretaceous are mainly those of type III kerogen. The organic matter in the upper part of the Jurassic sequence in the Jurabi-1 well of the Exmouth Sub-basin appears to have relatively high HI ranging from 200 to 315 (Fig. 3-7). The plot of HI against T_{max} values in Fig. 3-8 for six wells in the Barrow and Dampier Sub-basins indicates that the organic matter is dominated by type III kerogen. Figure 3-9 shows organic matter of the Jurassic source rock samples in the Depuch-1 well of the Beagle Sub-basin. Some coaly samples of the Jurassic source rocks in this well have relatively high HI values ranging from 241 to 389. Rock-Eval data of the Upper Triassic rocks (Mungaroo Formation) from the North Gorgon-1, Investigator-1 and Jupiter-1 wells (Fig. 3-10) show that the organic matter belongs to type III kerogen in accordance with the coal-bearing nature of the Upper Triassic sequence. Consequently, from the bulk geochemical data, the organic matter within the Upper Triassic, Jurassic and Lower Cretaceous in these well sites is mainly type III kerogen.

The relative percentages of visual kerogen compositions based on organic petrographic analysis in seven wells in the Barrow Sub-basin by Teerman (1994) are given in Table 3-2. The organic matter in the Upper and Middle Jurassic rocks consists of various mixtures of amorphous II and III, structured liptinite, vitrinite and inertinite. Structured liptinite in the Athol Formation of the Middle Jurassic consists of relatively more terrestrial sources, including pollen, spores and cuticle, compared to a higher proportion of marine algal source in the Dingo Claystone of the Upper Jurassic (Teerman, 1994). The kerogen composition data listed in Table 3-2 indicate that the maximum percentages of vitrinite and inertinite in the Athol Formation are 70 % and 25 %, respectively, while the maximum percentages of vitrinite and inertinite in the Dingo Claystone are 45 % and 20 %, respectively. Although the analyses from certain wells may not accurately represent the entire organic matter assemblage in the basin, the organic matter in the Jurassic is of a mixed marine and terrigenous source with more land materials in the Middle Jurassic rocks and more marine input in the Upper Jurassic rocks. The organic matter in the Upper Triassic Mungaroo Formation in the West Tryal Rocks-1 well is composed of amorphous III, structured liptinite, vitrinite and inertinite, which is oxidized organic matter and humic materials (Teerman, 1994).

Table 3-2 Visual compositions of organic matter (%) from organic petrographic analyses (Teerman, 1994)

Well	Formation	[1]Amorphous II	[2]Amorphous III	Structured Liptinite	Vitrinite	Inertinite	Solid Bitumen
Bambra-1	Dupuy	35-40	0	15-20	25-30	15-20	
	Dingo	25-50	0-5	10	30-45	10-15	
Barrow Deep-1	Athol	20-50	10-25?	<5-5	20-50	5-10	Trace-5
Bowers-1	Athol	30-40	0?	5	40-50	10-20	Trace
Dorrigo-1	Dingo	50	0	10	35	10	
	Athol	30-50	0	10	30-60	10-25	
Emma-1	Dingo	30-45	0	10-25	20-35	10-20	
	Athol	30-50	0-55	5-10	30-45	10-15	
Parker-1	Athol	Trace-20	10-40	5-10	40-70	5-15	
West Tryal Rocks-1	Mungaroo		35-50	5-15	25-40	10-20	

1: Amorphous II is chemically equivalent to end member type II kerogen that primarily originates from algal and bacterial precursors.

2: Amorphous III is generally equivalent to type III kerogen that derives from hydrogen-poor humic precursors or a product of poor preservation.

See Fig. 3-1 for well locations.

Several molecular parameters for assessment of the source from the relative abundances of C_{27} and C_{29} steranes, and pristane and phytane in oils and rocks in the Barrow Sub-basin are listed in Table 3-3. The C_{29} steranes originate from the precursor C_{29} sterols that predominate in higher plants (Huang and Meinshein, 1979; Volkman et al., 1983). Thus, the proportion of C_{27} and C_{29} steranes in oils and rocks can serve as an indicator for the source of land-plant organic matter (Volkman et al., 1983). The geochemical correlation indicates that the crude oils in the Barrow Sub-basin had a source in the Dingo Claystone of the Upper Jurassic and that the ratios of C_{27} and C_{29} steranes in oils and source rocks in the Dingo Claystone (A and B; Table 3-3) are consistent with a mixed marine and terrigenous source (Volkman et al., 1983). The pristane/phytane ratios in the oils are also consistent with their formation (C; Table 3-3) from the mixed marine and nonmarine organic matter deposited in a marginal marine (near-shore) environment (Powell and McKirdy, 1973a; Volkman et al., 1983). Moreover, the oils in the Jurassic rocks have a high wax content which suggests that the terrestrial source is a significant contributor to the hydrocarbon potential in the basin (Powell and McKirdy, 1973a).

Parry and Smith (1988) stated that sampling from wells drilled on structural highs or basin margins for source rock analysis is obviously limited. They believed that there is sufficient source rock of the oil-prone type in the Barrow Sub-basin. Scott (1992) suggested that the Rock-Eval method is underestimating the oil potential of the Jurassic source rocks in both marine and continental sequences. Ellis et al. (1999) considered that the organic matter in the Dingo Claystone is mixed marine and terrestrial material, and the Athol Formation may have contributed some oil in the Barrow Sub-basin. Tissot and Welte (1984) pointed out that type III kerogen occurs quite frequently in thick sequences of clastic sediments along continental margins, and microbial degradation of the terrestrial plant and vegetal debris in these basins is usually limited due to depositional environment and rapid burial. The discussion of type III kerogen mentioned above is not incompatible with the major accumulations of gas and oil discovered in the sub-basins and on the Rankin Platform. Based on the viewpoint of Peters (1986) and the geochemical data of samples from these wells, most of the organic matter within the Lower-Middle Jurassic in the areas of well locations on the structural highs and basin margins have the potential to generate mixtures of gas and oil, but mainly gas (Parry and Smith, 1988), while the partial

organic matter in the Upper Jurassic source rocks from the organic facies in the depocentres of the Barrow-Dampier Sub-basins is likely to be more oil-prone. The kerogen within the Upper Triassic coaly sequence is primarily gas-prone organic matter.

Table 3-3 Molecular parameters of organic source for paraffinic oils and rocks in the Barrow Sub-basin

Well	Sample	Depth (m)	Formation	A	B	C
Barrow[a]	Oil	1890	Dupuy (SS)	0.80	1.70	3.10
Barrow[a]	Oil	2010	Dupuy (SS)	0.94	1.20	2.80
Bambra-1[b]	Condensate (RFT)	2051	Barrow (SS)	1.25	0.81	3.46
Bambra-1[b]	Oil	2053.25	Barrow (SS)	1.41	0.88	2.81
Bambra-1[b]	Oil (RFT)	3640.5	Dingo (SS)	0.60	0.56	2.54
Bambra-2[b]	Oil (DST)	2032-2033.5	Barrow (SS)	0.86	1.27	2.39
Bambra-2[b]	Oil (DST)	2037-2038.5	Barrow (SS)	0.88	1.09	1.90
Barrow-1[a]	Core 10	1036	Barrow (ST)	0.54	0.90	2.50
Barrow-1[a]	Core 34	2402	Dingo (ST)	1.00	1.20	2.40
Barrow-1[a]	Core 37	2835	Dingo (CS)	1.30	1.50	2.30
Bambra-1[b]	Core	2715.5	Dupuy (CS)	0.66	0.47	2.40
Bambra-1[b]	Core	2727.8	Dupuy (CS)	0.76	0.82	2.79
Bambra-1[b]	Cuttings	3610	Dingo (CS)	1.00	0.55	2.53
Bambra-2[c]	Core	4274	Athol (CS)	0.79	0.53	1.85
Bambra-2[d]	Core	4283	Athol (CS)	0.93	1.11	3.16

RFT: Repeat formation test; DST: Drill stem test; SS: Sandstone; ST: Siltstone; CS: Claystone.
A: C_{27} (20R)-5α(H), 14α(H), 17α(H)-sterane / C_{29} (20R)-5α(H), 14α(H), 17α(H)-sterane
B: C_{27} (20R)-13β(H), 17α(H)-diasterane / C_{29} (20R)-13β(H), 17α(H)-diasterane
C: Pristane / Phytane
a: Data were taken from Volkman et al. (1983).
b: Data were collected from well-completion reports.
c: Data were analyzed at Curtin University of Technology (2001).
d: Date were analyzed at the Geological Survey of Canada, Calgary (2001).
See Fig. 3-1 for well locations.

Figures 3-11, 3-12 and 3-13 are three typical geochemical profiles of the Jurassic source rocks from the Rock-Eval pyrolysis data for Jurabi-1 in the Exmouth Sub-basin, Barrow Deep-1/ Barrow-1 in the Barrow Sub-basin and Depuch-1 in the Beagle Sub-basin.

3.4 Summary

The most important source rocks in the basin are the Jurassic claystone and siltstone rocks. The rift-related Dingo Claystone and Athol Formation of the Jurassic generally contain 0.2 to 4 % TOC with an average value of about 1.74 %. TOC values from about 80 % of the samples in these formations range from 1 % to 4 %. TOC values in the Murat Siltstone of the Lower Jurassic are primarily between 0.5 and 6 % with an average value of about 2.1 %. TOC values in the coaly Mungaroo Formation of the Middle-Upper Triassic are between 0.1 and 35.9 % with an average value of about 2.2 % (calculated from samples with TOC < 15 %).

The organic matter in the Middle-Upper Triassic is mainly derived from land materials, which is dominated by the type III kerogen with gas potential. The organic matter in the Lower-Middle Jurassic consists of a mixture of more terrestrial and less marine input giving a gas and oil-prone source but mainly a gas source. The organic matter in the Upper Jurassic is mixed marine and terrigenous materials, but it seems to have less terrestrial input than in the Lower-Middle Jurassic source rocks, and may contain a significant source of oil-prone organic matter within the Barrow-Dampier Sub-basins. It should be noted that there are not enough data to evaluate the type of organic matter in the Murat Siltstone of the Lower Jurassic in these sub-basins.

Table 3-1 Statistics of total organic matter (TOC, %) in 17 wells from various tectonic subdivisions in the Northern Carnarvon Basin

	Cretaceous				**Jurassic**				
Well	Gearle	*Windalia	Muderong	Barrow	Dupuy	Dingo	Athol	Murat	
Jurabi-1	1.28-3.68 2.14 (4)	1.06-1.80 1.43 (2)	1.26			0.34-4.12 1.70 (82)		0.50-1.16 0.77 (13)	
Novara-1	0.55-1.82 1.40 (10)	0.19-1.52 0.96 (5)	1.23-2.42 1.80 (4)	0.14-1.67 1.01 (10)					
Outtrim-1	1.27-3.17 2.09 (13)	1.05-1.96 1.63 (5)	0.87-2.51 1.64 (9)	0.10-2.54 1.30 (22)	0.35-2.74 0.96 (6)				
Zeewulf-1				0.27-0.53 0.44 (3)					
Anchor-1			1.55-2.27 1.88 (5)	0.75-1.93 1.47 (9)	0.66-1.37 1.00 (3)	0.48-2.47 1.41 (80)			
Barrow-1 Barrow Deep-1	2.08-8.43 3.87 (24)	1.66-3.24 2.45 (2)	1.28-3.78 2.17 (18)	0.10-3.68 1.38 (22)	0.37-1.49 1.12 (7)	0.35-3.68 1.90 (110)	0.92-2.56 1.54 (70)		
Dampier-1	0.25-3.13 1.12 (9)			0.36-3.70 1.84 (21)	0.35-3.31 1.63 (91)				
Hampton-1	1.18-1.54 1.36 (2)					0.23-1.89 0.80 (8)		0.70-3.81 1.32 (23)	
Madeleine-1	0.21-2.74 1.12 (16)			0.21-2.35 1.15 (33)	0.39-3.31 1.75 (83)		0.16-2.19 1.19 (17)		
Rosemary-1						0.57-2.16 1.72 (12)	0.55-4.64 2.11 (13)		
Depuch-1	0.46-2.22 1.33 (8)						1.77-12.81 6.40 (11)	3.06-10.65 5.16 (9)	
Picard-1	0.25-3.37 1.45 (23)						0.19-4.88 2.31 (13)	0.37-5.92 2.26 (40)	
North Gorgon-1	0.60-1.82 1.13 (17)	1.00-1.12 1.06 (2)	1.10-2.84 1.65 (28)	0.24-2.00 1.41 (10)					
North Rankin-1									
Investigator-1				0.15-1.41 0.94 (15)					
Jupiter-1									

Range/average value (total samples). * Windalia: Windalia Radiolarite. See Fig. 3-1 for well locations. The data were collected from well completion reports. The values of TOC > 15 % are not included in this table.

CHAPTER 4 ASSESSMENT OF ROCK-EVAL T_{MAX} DATA IN THE BAMBRA-2 WELL: A CASE STUDY OF THE CONTAMINATED ROCK-EVAL DATA

4.1 Introduction

Rock-Eval T_{max} (^{o}C) is the temperature at which the S_2 (mg HC/g rock) peak reaches its maximum amount of hydrocarbon generation during Rock-Eval pyrolysis (e.g. Espitalié et al., 1984; Peters, 1986; Tissot et al., 1987). When reliable values are obtained, Rock-Eval T_{max} increases progressively with thermal maturity (e.g. Espitalié et al., 1984; Tissot and Welte, 1984; Waples, 1985; Peters, 1986). Tissot and Welte (1984), Peters (1986), and Hunt (1996) have also recognized factors that influence T_{max} values, such as organic matter types, contamination, and the mineral matrix. Peters (1986) stressed that many maturity parameters, especially T_{max}, depend on the type of organic matter from which they are derived. Tissot et al. (1987) proposed that T_{max} is a good maturation indicator between 420 and 460 ^{o}C in type II kerogen, and between 400 and 600 ^{o}C in terrestrially derived type III kerogen. It has also been shown that T_{max} values can be correlated to vitrinite reflectance for humic coal and type III kerogen (Teichmüller and Durand, 1983; Espitalié et al., 1984; Waples, 1985; Tissot et al., 1987).

Hunt (1996) and Peters (1986) pointed out that contaminants, such as drilling-mud additives and natural bitumen, can raise or lower T_{max} values depending on their composition and the relative kerogen concentration. Hunt (1996) reported that heavy hydrocarbons can cause multiple S_2 peaks. He also reported that T_{max} values of about 365 to 375 ^{o}C within an interval of 600 metres in a well offshore Louisiana (Gulf Coast) were derived from cuttings contaminated with cetane ($C_{16}H_{34}$) due to the presence of diesel in the mud. Bordenave et al. (1993) reported an example showing that the T_{max} has no meaning when the total organic carbon (TOC) is lower than 0.3 % and S_2 lower than 0.5 mg HC/g rock, especially if an oil base mud is used. Peters (1986) reported T_{max} values for drilling-mud additives, such as walnut hulls which have a T_{max} value of 425 ^{o}C. A recent study by Daniel M. Jarvie

indicates that walnut hulls will give a T_{max} value of about 335 to 360 ^{o}C (personal communication, 2001). Clementz (1979) reported that solid bitumen and the heavy-end fraction of petroleum produce a measurable response in the S_2 temperature range from 350 to 450 ^{o}C. Kruge (1983) also stated that heavy bitumen can affect the S_2 peak causing abnormal T_{max} values. Vandenbroucke et al. (1993) showed that the T_{max} values measured on kerogen in the overpressured zone of the Handil field, Mahakam Delta, Indonesia, are significantly lower than the values measured on the coal samples, because the organic matter contains a significant percentage of pyrobitumen. Snowdon (1995) pointed out that T_{max} might be suppressed about 1 ^{o}C for each 50 hydrogen index ($HI=S_2\times100/TOC$) increment, when it is above 100 to 150 for typical type III organic matter. Peters (1986) noted that samples dominated by recycled organic matter with equivalent low maturity (R_o < 0.6 %) show variations in T_{max} up to about 10^{o} C.

It has been shown, however, that the use of solvent extraction techniques prior to Rock-Eval pyrolysis may produce more accurate T_{max} values (Clementz, 1979; Kruge, 1983; Peters, 1986; Tissot et al., 1987). Solvent extraction removes extraneous and indigenous hydrocarbons that both elute in the S_1 (free hydrocarbons, mg HC/g rock) peak and sometimes carry over into the S_2 peak (Clementz, 1979). Extraction provides a relatively "clean" sample for Rock-Eval pyrolysis and increased accuracy in T_{max} measurements.

This study demonstrates that the cuttings below about 3300 metres in the Bambra-2 well are strongly contaminated, possibly by drilling-mud additives, yielding T_{max} values much lower than those from conventional core and some side-wall core samples. It also demonstrates that some side-wall cores are also contaminated by drilling-mud additives such as diesel. Since the measured vitrinite reflectance values for the Upper-Middle Jurassic source rocks in the Bambra-2 well are anomalously low (e.g. Kopsen and McGann, 1985; Kaiko and Tingate, 1996) and the Jurassic sequence is highly overpressured (e.g. Kopsen and McGann, 1985; Tingate et al., 2001), the case study for the reliability of Rock-Eval T_{max} data is significant for evaluation of the thermal maturity in this well.

4.2 Sources of Rock-Eval data

The Bambra-2 well is located in the Barrow Sub-basin of the Northern Carnarvon Basin, North West Shelf of Western Australia (Fig. 3-1). The well was drilled to a total depth of 4591 metres (RT) within Middle Jurassic rocks (Fig. 4-1). The Jurassic sediments are considered to be major source rocks dominated by land-derived organic matter (e.g. Kopsen and McGann, 1985; Scott, 1992). Rock-Eval data from 280 cuttings, 21 side-wall cores and 2 conventional core samples, and 4 gas chromatograms (GC) of saturated hydrocarbon fractions were obtained from the Bambra-2 well. The majority of the Rock-Eval data were measured using standard methods by the Australian Mineral Development Laboratories (AMDEL) in 1983. In addition four side-wall core samples, two conventional core samples, and four cuttings samples, were analyzed with Rock-Eval 6 pyrolysis, using standard methods at the Geological Survey of Canada, Calgary (GSCC) in 2000. The four side-wall core samples and three of the cuttings samples were also extracted in a Soxhlet extraction apparatus using an azeotropic mixture of chloroform:methanol (87:13) for 24 hours to remove soluble organic matter (both diesel contaminants and indigenous) in order to examine the effect of the additives on T_{max} values. The Rock-Eval data are shown in Fig. 4-1, Table 4-1 (Rock-Eval data from the conventional core and the side-wall core samples) and Table 4-2 (Rock-Eval data from the cuttings samples).

4.3 Gas Chromatography (GC) Analysis

Based on the Bambra-2 Well Completion Report, 5 % and 6 % (by volume) of diesel was added to the drilling mud at 2424 and 4486 metres respectively (Fig. 4-1). It was also noted in the well completion report that diesel was present in trace amounts in the mud system during the drilling from about 3100 to 4485 metres. Figure 4-2 shows the distinct characteristics of the saturated hydrocarbon fractions from GC analysis for two conventional core samples (uncontaminated) and from three examples of side-wall core samples and one cuttings sample. Based on the distribution of saturated hydrocarbons in Fig. 4-2, these traces indicate that the SWC and cuttings samples were both contaminated by diesel in the drilling mud. The

Table 4-1 Rock-Eval pyrolysis results for Jurassic core samples from Bambra-2 in the Barrow Sub-basin

Depth (m)	T_{max} (°C)	S_1	S_2	S_3	TOC (wt. %)	HI	OI	PI	Type of Sample	Evaluation for T_{max}
2616[b]	438	0.46	0.78	1.29	0.74	105	174	0.37	SWC (CS)	Acceptable
2734[b]	436	1.09	0.62	1.42	0.69	89	205	0.64	SWC (ASST)	Low
2803[b]	438	0.61	1.05	1.16	0.93	112	124	0.37	SWC (CS)	Acceptable
2955[b]	438	0.77	0.84	1.21	0.81	103	149	0.48	SWC (CS)	Low
3056.5[b]	439	1.24	0.55	1.23	0.63	87	195	0.69	SWC (CS)	Low
3195[b]	445	0.51	1.76	1.45	1.11	158	130	0.22	SWC (STS)	Acceptable
3250[b]	441	0.53	1.08	0.79	0.83	130	95	0.33	SWC (STS)	Low
3430[b]	446	1.05	2.12	5.49	1.43	148	383	0.33	SWC (CS)	Acceptable
3650[b]	454	0.57	0.83	1.38	1.16	71	118	0.41	SWC (CS)	Acceptable
3676[b]	451	3.21	1.81	1.46	1.66	109	87	0.64	SWC (CS)	Low
3782[b]	455	1.70	1.39	1.89	1.67	83	113	0.55	SWC (CS	Low
3795[b]	444	6.52	1.20	2.62	1.57	76	167	0.84	SWC (CS)	Low
3795[a]	453	1.81	3.51	4.81	2.53	139	190	0.34	SWC (CS)	Low
3795[a]	461	0.05	1.67	3.57	1.95	86	183	0.03	Extracted	Normal
3824[b]	454	3.02	1.56	3.21	1.67	93	192	0.66	SWC (CS)	Low
3851[b]	451	4.45	1.09	3.87	1.56	69	248	0.80	SWC (CS)	Low
3906[a]	457	1.27	2.34	2.44	2.05	114	119	0.35	SWC (CS)	Low
3906[a]	462	0.05	1.04	2.48	1.63	65	152	0.04	Extracted	Normal
3980[b]	457	1.55	0.84	1.41	0.90	93	156	0.65	SWC (STS)	Low
4090[b]	462	2.39	1.03	0.96	0.86	119	111	0.70	SWC (SCS)	Low
4225[a]	335	1.04	1.32	0.92	1.42	93	65	0.44	SWC (CS)	Abnormal
4225[a]	485	0.03	0.53	0.68	1.11	48	61	0.05	Extracted	Normal
4274[a]	484	0.11	0.34	0.10	0.74	46	14	0.25	CC (CS)	Normal
4279[b]	484	0.30	0.31	2.74	0.86	36	318	0.49	CC (CS)	Normal
4282.9[b]	487	0.20	0.25	0.71	0.76	32	93	0.44	CC (CS)	Normal
4283[a]	490	0.13	0.39	0.03	0.97	40	3	0.24	CC (CS)	Normal
4295[b]	410	3.85	0.81	3.99	1.19	68	335	0.83	SWC (CS)	Abnormal
4301[a]	337	0.53	0.95	1.16	0.99	96	117	0.37	SWC (CS)	Abnormal
4301[a]	488	0.03	0.35	0.86	0.77	45	112	0.07	Extracted	Normal
4353[b]	389	3.00	0.55	2.28	0.85	64	268	0.85	SWC (STS)	Abnormal
4445.5[b]	412	1.29	0.42	1.25	0.60	70	208	0.75	SWC (STS)	Abnormal

a: Rock-Eval data were measured with Rock-Eval 6 by the Geological Survey of Canada, Calgary (GSCC) (2000).
b: Rock-Eval data were measured by the Australian Mineral Development Laboratories (AMDEL) (1983).

CC-conventional core; SWC-side-wall core; CS-claystone; STS-siltstone; ASST-argillaceous sandstone; SCS-sandy claystone.

T_{max}: Temperature of the top of S_2 peak; S_1: Free hydrocarbons (mg HC/g rock); S_2: Pyrolysable hydrocarbons (mg HC/g rock); S_3: CO_2 from pyrolysis (mg CO_2/g rock); TOC: Total organic carbon (wt. %); HI: Hydrogen index (S_2 % 100/TOC); OI: Oxygen index (S_3 % 100/TOC); PI: Production index (S_1/S_1+S_2).

contaminants mainly contain C_{14}-C_{18} hydrocarbons (diesel) and C_{19}-C_{25} hydrocarbons (heavy gas oil), with boiling points of about 250 to 400 °C (Tissot and Welte, 1984; Hunt, 1996). Furthermore, an obvious difference from the GC characteristics of saturated hydrocarbon fractions is the much higher relative intensities of pristane and phytane in the SWC and the cuttings samples compared

with the conventional core samples at similar depths. This increased pristane to phytane ratio may represent a characteristic feature of the diesel in the drilling-mud additives. The extractable organic matter (EOM, mg/g TOC) from the side-wall core samples is also noted to be much higher than those in the conventional core samples (Fig. 4-2 A and B).

Table 4-2 Rock-Eval pyrolysis results for the Jurassic drill cuttings (claystone) from Bambra-2 in the Barrow Sub-basin

Depth (m)	T_{max} (°C)	S_1	S_2	S_3	TOC (wt.%)	HI	OI	PI	Washed	Picked	Extracted
2660-2665	431	0.14	0.43	0.06	0.35	123	16	0.25	√		
2660-2665	432	0.00	0.23	0.48	0.25	92	192	0.01	√		√
3090-3095	433	0.65	3.75	1.83	1.54	244	119	0.15	√		
3090-3095	435	0.08	1.44	2.16	1.00	145	216	0.05	√		√
3440-3445	442	0.14	0.65	3.55	1.12	59	397	0.17	√	√	
3970-3975	430	0.14	0.85	1.75	1.43	60	122	0.14	√		
3970-3975	442	0.04	0.49	2.99	1.21	41	247	0.07	√		√
3970-3975	442	0.04	0.49	2.95	1.23	41	240	0.07	√		√ repeat
3970-3975	450	0.12	0.27	1.08	0.60	47	180	0.30	√	√	

The Rock-Eval data were measured with Rock-Eval 6 at the Geological Survey of Canada.

4.4 Discussion

Figure 4-1 illustrates the results from the Rock-Eval analysis for Bambra-2. Note that the T_{max} values from all the samples show two distinct trends. One trend shows progressive increase in values with depth and consists of results from core samples, extracted SWC samples and SWC samples with S_1 values between 0.46 and 1.05 (Table 4-1). The other trend is defined by the data from cuttings samples. This trend is noted to have very little increase in value with depth and a slight decrease at depths greater than approximately 3600 metres. It should be also noted that the T_{max} values from the side-wall core samples with S_1 values generally between 1.09 and 6.52 (Table 4-1 and Fig. 4-1, SWC (2)) exhibit relatively lower, or significantly lower, values than the higher value T_{max} trend defined by the data from the conventional core samples, extracted SWC samples and SWC samples with S_1 values between 0.46 and 1.05, which is considered to be that of normal and acceptable T_{max} data. Clementz (1979) proposed that data from a sample should be treated with caution if S_1 is more than 1. The presence of free hydrocarbons (S_1>1 or 2) is likely to affect the S_2 peak, and extraction is necessary prior to pyrolysis to

avoid misinterpretation of the Rock-Eval data (Kruge, 1983). The extracted samples can generally give more reliable T_{max} values (Clementz, 1979; Kruge, 1983; Peters, 1986; Tissot et al., 1987). T_{max} values for some unextracted side-wall core samples with relatively low S_1 values are considered acceptable, based on the increasing T_{max} trend (Fig. 4-1). The relatively low and abnormally low T_{max} values (< approximately 415 ^{o}C) from the side-wall cores, especially those with S_1 values more than 1 and anomalously high PI (production indices=S_1/S_1+S_2) (Table 4-1), are thought to be caused by the diesel added to the mud at 2424 and 4486 metres. The observation of bitumen in thin- sections of the source rocks suggests that the difference of S_2 values between the extracted and unextracted SWC samples (the lower T_{max} values in SWC) may be influenced by natural heavy bitumen to some extent. This problem may be overcome by solvent extraction prior to pyrolysis (e.g. Clementz, 1979; Kruge, 1983). In fact, if the S_2 peak is shifted and/or altered by any additive, the T_{max} value may be dramatically affected.

Comparisons of the Rock-Eval data from the cuttings, the side-wall cores and the conventional core samples indicate that total organic carbon and hydrogen indices in the cuttings and the side-wall cores are likely to be increased by organic contaminants such as the diesel (Fig. 4-1 and Table 4-1). Anomalously high PI in the cuttings between 2424 and 3076 metres, and from 4486 metres to total depth, are related to the diesel contaminated drilling mud. This is reflected in the low T_{max} values from the cuttings samples, especially from about 3300 metres to total depth which are much lower than those from the T_{max} trend defined by the conventional core samples, extracted SWC samples and SWC samples with S_1 values between 0.46 and 1.05 (Table 4-1; Fig. 4-1). The T_{max} values from the cuttings samples, between 2424 and 3100 metres, generally range from 430 ^{o}C to 439 ^{o}C. Between about 3100 and 4430 metres, they generally range from 415 ^{o}C to 439 ^{o}C with the lowest value being 334 ^{o}C. In the depth interval from about 4430 to 4500 metres, the T_{max} values from the cuttings samples range from 436 ^{o}C to 468 ^{o}C, which is significantly higher than the shallower T_{max} values but these values are still also obviously lower than those from the conventional core samples and extracted SWC samples. From 4500 metres to total depth, the cuttings samples are considered to be heavily contaminated by the diesel. This is indicated by the anomalously low T_{max} values of 383 to 401 ^{o}C (Fig. 4-1).

Four cuttings samples were washed and air-dried for Rock-Eval 6 pyrolysis, and a duplicate sample for three of them was also extracted for additional Rock-Eval 6 pyrolysis. Table 4-2 shows that the T_{max} values for the washed cuttings range from 430 ^{o}C to 433 ^{o}C. The values for the washed and extracted cuttings range from 432 ^{o}C to 442 ^{o}C. Two cuttings samples at 3440-3445 metres and 3970-3975 metres were also picked free of contaminants after being water-washed and air-dried, and the two T_{max} values of 442 ^{o}C and 450 ^{o}C obtained from Rock-Eval 6 pyrolysis (Table 4-2), which are significantly higher than the previous trend from cuttings (Fig.4-1). It should be noted that although these values are still lower than those indicated by the conventional core and extracted SWC trend, it does indicate a marked increase from the samples that had not been picked. The results from picked and extracted samples strongly suggest that at least part of the difference in T_{max} values between the cuttings samples and the core samples may have been caused by the contamination by the diesel and other drilling-mud additives. It also indicates that even when dealing with extracted cuttings samples other factors may influence the results, therefore, care should be taken in the final interpretation of the results. Additionally, for the cuttings samples, between approximately 4500 and 4591 metres, it would seem that contamination by the diesel is likely to be the major cause for the higher S_1 and PI with correspondingly low T_{max} values ranging between 383 and 410 ^{o}C (Fig. 4-1).

Based on the analysis of migrated hydrocarbon in the Barrow Group from the well completion report, the T_{max} values over the upper part of the group between 2000 and 2300 metres (Fig. 4-1) may be suppressed by 2 to 10 ^{o}C by the natural hydrocarbon compared to the T_{max} trend from the core samples which increase regularly with depth. The T_{max} values in the top part of the Barrow Group and the Muderong Shale between 1630 and 2000 metres (Fig. 4-1) may be related to recycled organic matter to some extent, which may cause the T_{max} values to rise by up to several degrees compared to the "normal" T_{max} trend. Although depositional environment and organic facies may also influence the T_{max} values, the influence should be minor in the present T_{max} data, because of the type III kerogen and clastic lithologies in this well.

Hunt (1996) proposed that T_{max} values should be rejected if HI is less than 50 mg HC/g TOC or if S_2 is less than 0.2 mg HC/g rock. However, T_{max} values from the conventional core samples from 4274 to 4283 metres in Table 4-1 are 484 to 490 ^{o}C

with HI ranging from 32 to 46 and S_2 ranging from 0.25 to 0.39. These T_{max} values should be considered normal results for three reasons. Firstly, two examples of gas chromatograms of saturated fractions from the conventional core samples at 4274.2 and 4282.9 metres in Fig. 4-2 show that the organic matter is obviously mature (e.g. Allan and Douglas, 1977). Thus, thermal maturity is the major cause of the low HI. Secondly, the T_{max} from the solvent extracted side-wall cores at 4225 and 4301 metres give similar T_{max} values to the conventional core samples (Table 4-1), and the T_{max} values of 485 ^{o}C and 488 ^{o}C indicate a high maturity level. Finally, average vitrinite reflectance values of 1.45 % to 1.74 % were measured in the conventional core sample at 4274 metres by Dr. L.W. Gurba (University of New South Wales) and Dr. Alex Kaiko (Curtin University of Technology), corresponding to T_{max} values of 470 to 490 ^{o}C (Teichmüller and Durand, 1983; Espitalié et al., 1984; Tissot et al., 1987). Obviously, the T_{max} values of the conventional core samples are in agreement with the higher maturity assessment from the vitrinite reflectance measurements.

4.5 Summary

In this study, it was found that the main problems to affect T_{max} data in the Bambra-2 well included (1) contamination by drilling mud additives, (2) natural hydrocarbons, and (3) recycled organic matter. The cuttings samples in the Barrow Group may be contaminated by natural hydrocarbons, resulting in their T_{max} values being 2 to 10 ^{o}C lower than the regularly increasing T_{max} trend from core samples. The T_{max} values in the cuttings in the Jurassic section, especially from about 3300 metres to total depth, within the higher maturity interval, in the Bambra-2 well, were significantly lowered by contamination by drilling-mud additives, including diesel. The GC analysis indicates that the use of diesel in drilling mud is considered to be the major cause for the abnormal and low T_{max} values in the side-wall cores. Generally, the T_{max} values, from the SWC with S_1<1, the solvent extracted SWC and the conventional core samples, provide a relatively reliable maturity trend in this well. This study indicates that higher quality Rock-Eval T_{max} results are obtained from the conventional core samples and the relatively cleaned samples. The study also suggests that samples with a HI between 30 and 50 in higher maturity zones should provide valid T_{max} values in this case.

CHAPTER 5 DEEP OVERPRESSURED SYSTEM AND TOP PRESSURE SEAL

5.1 Introduction

Overpressure distribution in the Northern Carnarvon Basin has been investigated by Horstman (1988), Zaunbrecher (1994), Yassir (1996), van Ruth et al. (2000) and Tingate et al. (2001). Overpressure in the Northern Carnarvon Basin is observed in the Early Cretaceous Muderong Shale and Barrow Group, the Jurassic sequences and the Mungaroo Formation of Triassic age (Zaunbrecher, 1994; Tingate et al., 2001). This study focuses on the fluid pressure modelling in the deep overpressured system in the Jurassic section in the sub-basins of the Northern Carnarvon Basin. The deep overpressured system is evidenced by the measured fluid pressure data, including repeat formation tests (RFT) and drill stem tests (DST), and is also confirmed by mud weights and well-log responses associated with high sonic transit times and low resistivity values in the Jurassic fine-grained rocks.

A pressure seal within a rock layer is defined as capable of confining anomalous pressure over geological time (e.g. Hunt, 1990; Deming, 1994). Hunt (1990) stated that the tops of many compartment seals in clastic rocks appear to consist of multiple bands of calcite mineralization along a thermocline where temperatures range from 90 ^{o}C to 100 ^{o}C. The pressure seal is a cement diagenetic layer (Weedman et al., 1996), and the cementation process causes the precipitation of minerals in the pore space (Wangen, 2000). Weedman et al. (1996) noted that most of the cement diagenesis occurred before the pressure seal became effective as a permeability barrier. Quartz overgrowth precipitation forms at 80-110 ^{o}C (Bjørlykke and Egeberg, 1993; Walderhaug, 1996; Weedman et al., 1996), and the calcite cement precipitation forms at about 100-135 ^{o}C (Weedman et al., 1996).

5.2 Overpressure and petrophysical data

Relevant data from eight wells are used in this study. The wells in the Barrow Sub-basin are clustered in three groups (1) “Barrow Island” (Barrow-1 and Barrow

Deep-1, which is a deeper well close to Barrow-1), (2) the "Bambra location" (Bambra-1 and Bambra-2), and (3) the "West Barrow location" (West Barrow-1/1A and West Barrow-2). The selected Jurabi-1 well is in the Exmouth Sub-basin and the Dampier-1 well is in the Dampier Sub-basin. Figure 3-1 shows the locations of these wells. Pressure data from Barrow Deep-1 have been used in a previously published studied by Tingate et al. (2001).

5.2.1 Measured fluid pressure data for overpressure

Overpressure is the condition when pore-fluid pressure exceeds hydrostatic pressure (a static column of water or brine) for a given depth (Dickinson, 1953; Bradley, 1975). The hydrostatic pressure gradient of a fresh water column is 0.0098 MPa/m (0.43 psi/ft) (Hunt, 1990). Hunt (1990) pointed out that the pressure/depth gradient of a saturated salt solution is 0.012 MPa/m (0.53 psi/ft), and any pressures outside this limit are considered to exhibit abnormally high fluid pressure (overpressure).

Usually the fluid pressures are measured by repeat formation tests (RFT) and drill stem tests (DST) at specific depths in permeable formations, and these are valuable control points for fluid pressures in a pressure profile from an individual well. The RFT is specifically designed to evaluate formation pressures (Swarbrick, 1995). Mud weight can act as a rough approximation for the trend of fluid pressure within a well because it is used to overbalance pore fluid pressures by a small amount during drilling. It is important to distinguish and discard data that reflect a significantly overbalanced drilling condition. Horstman (1988) indicated that on the North West Shelf a formation is considered to be overpressured if a mud weight of 0.0125 MPa/m (1.25 g/cm^3 Specific Gravity) is encountered. van Ruth et al. (2000) considered that the mud pressure is a fairly reliable indicator of pore pressure in permeable formations of the North West Shelf. They also proposed that the mud weight gradient of 0.0125 MPa/m demarcates the boundary between the overpressured and normally pressured regimes in the North West Shelf basins. However, it must be remembered that mud weight is often only the "best guess" of the drilling engineers as to where the overpressured formations are situated.

Plots of pressure versus depth for the various wells are shown in Figures 5-1 to 5-7. The observed pressure data are annotated with respect to their source: either RFT or DST. All three separate locations in the Barrow Sub-basin (Barrow Island, Bambra location and West Barrow location) show a deep overpressured zone. The observed overpressure and excess pressure, above the hydrostatic pressure (hydrostatic pressure gradient assumed to be 0.0103 MPa/m), for 4 wells are listed in Table 5-1.

Table 5-1 Measured high fluid pressures in four studied wells in the Northern Carnarvon Basin

Depth (m)	**Fluid Pressure (MPa)**	**Excess Pressure (MPa)**	**Type of Data**	**Formation**	**Well**
3130	56.39	23.84	RFT	Dingo Claystone	Bambra-1
3640.5	66.52	28.66	RFT		
3231	58.95	25.35	DST		Barrow Deep-1
3307	61.36	26.97	DST		
3411	63.43	27.96	DST		
3459	64.40	28.43	DST		
2929	38.95	8.49	DST		Dampier-1
3037	36.89	5.30	DST		
3650	42.47	4.51	DST		
3306	60.63	26.25	RFT	Barrow Group	West Barrow-2
3423	63.85	28.25	RFT		

The measured pressure data were collected from well-completion reports. The calculation of excess pressure is based on the hydrostatic pressure gradient of 0.0103 MPa/m. RFT: Repeat formation test; DST: Drill stem test.

5.2.2 Well-log data for overpressure

Sonic-log and resistivity-log data from the seven wells used in this study, are plotted in Figures 5-1 to 5-7. Note that Barrow-1 and Barrow Deep-1 are combined into a single plot. Also, porosity and permeability data were extracted from well completion reports (Tables 5-2, 5-3 and 5-4) where available and mainly based on well-log interpretation with few laboratory measurements of porosity and permeability available.

Table 5-2 Measured total porosity and horizontal permeability values from the conventional core (claystone) in Bambra-2

Depth (m)	Porosity (%)	Horizontal Permeability (md)	Depth (m)	Porosity (%)	Horizontal Permeability (md)
4274	5.6	0.01	4279	5.0	0.02
4275	5.5	0.01	4280	5.1	< 0.01
4276	5.6	< 0.01	4281	5.7	0.01
4277	6.6	0.02	4282	5.1	< 0.01
4278	5.5	0.01	4283	4.9	< 0.01

Data were collected from the well-completion report.

Table 5-3 Measured porosity and permeability values for the conventional core samples (sandstone) in the Bambra-1 well

Depth (m)	Porosity (%)		Horizontal Permeability (md)		Vertical Permeability (md)	
	Range	Average	Range	Average	Range	Average
2713.05-2728.7	4.2-19.8	16.62	0.02-16	6.41	0.02-12	4.45

$1md = 10^{-15}\ m^2$

Data were collected from the well completion report.

Table 5-4 Porosity evaluations based on density and neutron log data for sandstones of the Barrow Group in West Barrow-2

Depth Interval (m)	Range of Porosity (%)	Average Porosity (%)
2520-2834	3-20	11.5
2882-2922	3-12	8
3291-3319	2-10	4.5
3366-3437	1-12.5	4.5

Data were collected from the well-completion report.

The fluid pressure in low-permeability rocks, such as shales, is rarely determinable. It may be inferred from adjacent permeable rocks, or from the interpreted well-log porosity, such as sonic and density logs (Swarbrick and Osborne, 1998). Trends showing high sonic transit times versus depth in shale, which deviate from a normal compaction trend, are often interpreted to be a product of undercompaction. These high-sonic trends, in turn, are often interpreted to reflect a high fluid pressure regime (e.g. Magara, 1978). Typical shale resistivity is observed to increase with depth, as a

complex function of decrease of saline-, bound- and pore-water volume versus a relative increase of electrically conductive clay minerals. However, in many overpressured zones, shale resistivity has been observed to decrease with depth (e.g. Bigelow, 1994a; Hermanrud et al. 1998).

Hermanrud et al. (1998) proposed that both sonic and resistivity logs may also be influenced by textural changes induced by overpressuring in shales without abnormally high porosities from wells on Haltenbanken, offshore Mid-Norway. They suggested that resistivity logs might respond directly to fluid overpressuring because of increase fluid connectivity in the microfractures of the overpressured shales rather than "indirectly" to anomalous shale porosity, as predicted by the undercompaction mechanism. They also suggested that the sonic-log produces a higher transit time (lower formation velocity), because of reduced transport capacity in the matrix of the overpressured rocks.

In evaluating porosity and permeability of the fine-grained (clay-dominated) rocks for the studied wells in the Barrow and Exmouth Sub-basins, intervals with gamma-ray values greater than 80 API units in Cretaceous formations and greater than 90 API units in Jurassic sequences were selected. These gamma-ray values reflect typical "shale-base-lines" for these sequences. The resistivity analysis was based on the deep induction log (R_{ILD}). Induction logs can be run in all types of drilling mud (Bigelow, 1994a). It was assumed that the deep induction log records relatively accurate formation resistivity values in thick (> 1.5 m), resistive zones with true formation resistivity values less than 100 ohm/meters (Asquith and Gibson, 1983). The lithologies in the Jurassic overpressured system are dominated by massive organic-rich claystones and siltstones. Tingate et al. (2001) stated that all overpressure occurrences are accompanied by an increase in sonic transit time. These well-log data, in combination with the measured high fluid pressures in the Jurassic sandstones, can be explained by overpressuring in the Jurassic fine-grained rocks.

In the Barrow Sub-basin, on the basis of the available density-log data at 2800-3660 metres in Bambra-1 (Fig. 5-3), the bulk density-log readings in the Jurassic overpressured sequence are about 2.57-2.63 kg/m^3 without any abnormal trend.

Thus, the density-log-derived porosities could be smaller than 6 % in the observed overpressured compartment, which are significantly less than the calculated sonic-derived porosities of 13 to 18 % and resistivity-derived porosities of 9 to 11 % in the compartment of this well. The measurements of total porosity from a conventional core (claystone) between 4274 and 4283 metres in the overpressured system in Bambra-2 range from 4.9 % to 6.6 % (Table 5-2). The ranges of the measured bulk density and matrix density for the core are 2.55 and 2.56 kg/m^3 and 2.63 to 2.64 kg/m^3, respectively. However, the calculated sonic-derived and resistivity-derived porosities are 13.5 to 17.6 % (sonic transit times: 279 to 295 ③s/m) and 11.6 to12.5 % (resistivity values: 2.31 to 2.71 ohmm), respectively, at this specific depth interval in this well. Again, the overpressured zone of the lower part of the Barrow Group in the West Barrow wells is also associated with high sonic transit times and low resistivity values in mudstones (Figures 5-6 and 5-7). However, the average bulk density-log readings for the fine-grained rocks are about 2.55 to 2.65 kg/m^3, and do not exhibit a density (or porosity) anomaly within the overpressured zone (3000 metres to a total depth of 3520 metres) in West Barrow-1/1A (Fig. 5-6).

In the Exmouth Sub-basin, the density-log from 3200 to 3550 metres within the major Jurassic overpressured zone in Jurabi-1 (Fig. 5-4) indicates that the bulk density values range from 2.60 kg/m^3 to 2.65 kg/m^3, which in turn suggest that the porosities in the overpressured interval could be lower than 4 %. However, the sonic-derived and resistivity-derived porosities are estimated to be 6 to 12 % from the sonic transit times of 250 to 275 ③s/m and 7.8 to 9.6 % from resistivity values of 3.9 to 5.9 ohmm, respectively. The results illustrate that the porosities in situ in the main overpressured zone are also lower than the calculated porosities based on the sonic-log and resistivity-log data in the fine-grained rocks.

The correlation of the acoustic, electric, density well-log data and the measured porosities in the claystone and siltstone-dominated highly overpressured zone suggests that the actual porosity values are likely to be significantly lower than the sonic-log and resistivity-log-derived porosities in these cases. This also suggests that the present-day Jurassic overpressured source rocks do not have a significant porosity anomaly due to underpressure. In other words, it seems that most of the porosity in the overpressured source section has been lost through compaction. This

appears to be consistent with the finding by Hermanrud et al. (1998) and Teige et al. (1999), who proposed that the sonic and resistivity logs also respond anomalously, due to overpressuring in shales.

5.2.3 Petrophysical expression of the deep overpressured zone

The characteristics of the overpressure from the pressure profiles in the Jurassic section and the Barrow Group are explained based on the RFT, DST, mud weight and well-log data (Figures 5-1 to 5-7).

5.2.3.1 Jurassic overpressure in the Barrow Sub-basin

As shown in Fig. 5-1, the resistivity-log values in fine-grained rocks appear to decline at about 2650 metres in the combined Barrow Deep-1/Barrow-1 well, which is approximately consistent with the top of the interpreted Jurassic overpressured zone in the well studied by Zaunbrecher (1994). In this well, four measured pressure values in sandstones (Table 5-1) from DST, high mud weights of 0.0128-0.0203 MPa/m used from 2743 to 4650 metres (total depth) and sonic-log and resistivity-log data in claystones confirm that the Jurassic fine-grained section is highly overpressured. The excess pressures underlying the transitional pressure zone range from about 20 MPa to 30 MPa, if 0.0103 MPa/m is used as a hydrostatic pressure gradient with a water salinity of 30 g/l NaCl equivalent.

Figures 5-2 and 5-3 indicate that an increase of sonic transit times and decrease of resistivity values in the Jurassic shaley sequence begin about 2800 metres in Bambra-1 and 2900 metres in Bambra-2, which are approximately coincident with the tops of the Jurassic overpressured zone. In Bambra-1, high mud weights of 0.0124 to 0.0185 MPa/m took place from 2853 metres to a total depth of 3666 metres. In Bambra-2, high mud weights of 0.0124 to 0.0193 MPa/m were used from 2821 metres to a total depth of 4591 metres. The mud weight in this well was progressively increased from about 3000 metres to the total depth in the Jurassic sequence, which was usually accompanied with high gas reading, as an indication of pore pressure, based on the well completion report. In combination with two RFT pressure values in sandstones (Table 5-1) in Bambra-1, well-log data and high mud weights indicate that there is an anomalously high fluid pressure regime in the

Jurassic sequence. According to the well completion reports, water salinity in the Upper Jurassic section is approximately 20 to 45 g/l NaCl equivalent. Thus, the hydrostatic pressure gradient is about 0.0102 to 0.0104 MPa/m, and the estimated excess pressure in the Jurassic overpressured compartment of the Bambra-2 well may be in the range of 20 to 30 MPa. Based on a kick condition in Bambra-1 (Tingate et al., 2001), the kick occurred at 3169.4 metres with a kill mud weight of 1.82 S.G. (Specific Gravity), indicating that the mud weight pressure was about 58.76 MPa and that the formation pressure may be 57 to 58 MPa with a excess pressure of 25 to 26 MPa, which is consistent with the measured data in this well (Table 5-1).

5.2.3.2 Jurassic overpressure in the Exmouth Sub-basin

On the basis of acoustic and electric well-log profiles and mud weight pressure data in Jurabi-1 (Fig. 5-4), the top of the deep overpressured system appears to be about 2900 metres. The pressure/depth gradient of mud weight between 2900 metres and the total depth of 3712 metres (R.T.) ranges from about 0.0125 MPa/m to 0.0169 MPa/m and the expected excess pressure can be up to 20 MPa in the Jurassic section in this well. It was found that the sonic-log and resistivity-log data reveal that the Jurassic rocks between 2385 and 2950 metres have abnormalities from the normal trends. However, there are relatively low density-log values in the interval 2385 to 2950 metres. It suggests that these well-logs respond to anomalously high porosities owing to undercompaction but the zone is only slightly overpressured based on the mud weights.

5.2.3.3 Jurassic overpressure in the Dampier Sub-basin

There are no suitable well-log data for Dampier-1. Based on the measured pressure data in Fig. 5-5, the Jurassic (slightly) overpressured zone is likely to occur in the upper part of the Upper Jurassic sequence (> 2900 m) in this well. The DST data indicate that the excess pressures may range from 4 MPa to 8 MPa between 2900 and 3700 metres. Based on the study by Tingate et al. (2001), the top of the overpressure zone in the well occurs at 3643 metres. Perhaps an obvious increase in the overpressure starts at 3805 metres because the pressure/depth gradient of the

mud weight changes from 0.0125 MPa/m at 3753 metres to 0.0144 MPa/m at this depth, indicating that the excess pressure may reach 15 to 20 MPa in the Jurassic shaley sequence from 3805 metres to a total depth of 4142 metres (R.T.). The fluid pressure profile in Fig. 5-5 confirms that the Jurassic deep overpressured system has also been developed and preserved in the Dampier Sub-basin.

5.2.3.4 Overpressure in the Barrow Group of the Barrow Sub-basin

Figures 5-6 and 5-7 show that the observed overpressured zones in the lower part of the Barrow Group in the West Barrow-1/1A and West Barrow-2 wells are indicated by RFT pressures (Table 5-1), mud weights and well-log data with excess pressures of about 10 to 30 MPa. The top of the overpressured zone appears to be consistent with sonic and resistivity log responses at about 3000 metres. The mud weight used in West Barrow-1/1A increased from 2990 to 3142 metres with mud weight gradients from 0.011 MPa/m to 0.013 MPa/m and then gradually increased to a total depth of 3520 metres with a mud weight gradient of 0.0173 MPa/m. The mud weight used in the Barrow Group in West Barrow-2 began to increase at 2969 metres with a mud weight gradient of 0.0127 MPa/m and continued to increase to a total depth of 3437 metres with a mud weight gradient of 0.0192 MPa/m. Based on the well-completion report of Tryal Rocks-1 in this sub-basin, the overpressure may also occur in the Barrow Group as indicated by mud weight records with 0.0152 to 0.0168 MPa/m from 2866 metres to a total depth of 3695 metres. In addition, based on the sonic-logs in these two West Barrow wells (Figures 5-6 and 5-7) and the density log in West Barrow 1/1A (Fig. 5-6), the sonic-log response has been interpreted to reflect undercompaction with slight overpressuring in the Muderong Shale between about 2200 and 2500 metres. The mud weights are less than 1.23 S.G. in West Barrow 1/1A and less than 1.35 S.G. in West Barrow 2. There are, however, no measured data to confirm the abnormal porosities and overpressured status.

Table 5-5 shows the tops of the Jurassic overpressured zones in five wells as recorded by Zaunbrecher (1994) and Tingate et al. (2001). Table 5-6 shows temperatures at the top of the deep overpressured zone in the studied wells.

Table 5-5 Tops of the Jurassic overpressured zone in five wells in three sub-basins

Well	Top of Overpressure (m) (Zaunbrecher, 1994)	Top of Overpressure (m) (Tingate et al., 2001)	Sub-basin
Bambra-1	2725	2900	Barrow
Bambra-2	2725		
Barrow Deep-1	2650	2603	
Dampier-1		3643	Dampier
Jurabi-1	2400	2383	Exmouth

Table 5-6 Temperatures at the top of the deep overpressured zone in seven wells in three sub-basins

Well	Top of Overpressure (m)	Temperature (^{o}C)	Sub-basin
Bambra-1	2800	115	Barrow Sub-basin
Bambra-2	2900	118	
Barrow Deep-1	2650	110	
West Barrow-1A	3000	125	
West Barrow-2	3000	125	
Dampier-1	2900 ?	110 ?	Dampier Sub-basin
Jurabi-1	2900	125	Exmouth Sub-basin

5.3 Top pressure seal in the Barrow Sub-basin

The data for explaining top pressure seals are available from the wells in the Barrow Sub-basin. In general, top pressure seals are coincident with the pressure transition zone (Hunt, 1990). The depths of the top pressure seal for the deep overpressured system in the five wells range from about 2650 m to 3300 m and the temperatures range from about 110 ^{o}C to 135 ^{o}C.

The proposed top pressure seal within the Jurassic overpressured system ranges from about 2650 to 3150 metres in Barrow Deep-1, about 2800 to 3100 metres in Bambra-1 and about 2900 to 3200 metres in Bambra-2 (Figures 5-1, 5-2 and 5-3), with temperatures ranging from about 110 ^{o}C to 130 ^{o}C. The top pressure seal in the three wells consists of a rock layer of thick claystone and siltstone with interbedded

sandstone and thin limestone. The rock layer contains about 60 to 80 % claystone and siltstone and its thickness varies from about 300 to 500 metres.

Figures 5-6 and 5-7 show that the top pressure seal in the Barrow Group of West Barrow-1/1A and West Barrow-2 may range from 3000 to 3300 metres with temperatures between 125-135 ^{o}C. The rock layer of the pressure seal contains about 80 % claystone and siltstone with thin sandstone and its thickness is about 300 metres.

The sandstones inside or near the deep overpressured system appear to have extensive cementation, which in turn leads to a significant decrease in porosity and permeability in the sandstones. Wulff (1991) studied the cementation of sandstone in a conventional core at 2713 to 2730 m just overlying the interpreted pressure seal in Bambra-1. The main mineral compositions of the sandstones collected from Wulff (1991) and the well completion report are shown in Table 5-7. This Upper Jurassic fine sandstone is cemented with moderately abundant authigenic quartz overgrowths, siderite and calcite/dolomite, resulting in quite low permeability compared with porosity as listed in Table 5-3.

Based on the well-completion report of West Barrow-2, the ranges of well-log-derived porosities in the sandstones from the Barrow Group are given in Table 5-4. Secondary silica cement and interstitial detrital clay has severely reduced the primary porosity in the sandstones between 2882 and 3319 metres in comparison to the sandstones at 2520 to 2834 metres. Extensive silica and clay cementation has filled in almost all pore voids, resulting in negligible effective porosity in the sandstones from the interval 3366 to 3437 metres in this well. The claystone and silty claystone in the rock layer of the top pressure seal were strongly compacted according to the density-log data (Figures 5-2 and 5-6). The density values in the top pressure seal are 2.57 to 2.63 kg/m^3 in Bambra-1 and 2.55 to 2.63 kg/m^3 in West Barrrow-1/1A. Based on the density-log data in the interval of the top pressure seals and the measured matrix density (2.63-2.64 kg/m^3) for the Jurassic claystone core (4274-4283 m) in Bambra-2 (Appendix 1), the claystone porosities within the top pressure seal can be assessed to be □ 5 %, thus the permeability values are

calculated to be 10^{-19} m^2 or lower using the modified Kozeny-Carman equation (Ungerer et al., 1990):

$$\kappa = \frac{20\phi_*^{\ 5}}{S_0^{\ 2}(1-\phi_*)^2}, \qquad 0 < \phi_* < 10\%, \tag{5-1}$$

where k is permeability (m^2), S_0 is specific surface area of rock matrix (m^2/ m^3); ϕ_* is effective porosity, ϕ_* = □ - 3.1 % 10^{-10} % S_0, □ is porosity. The equation 5-1 describes the very low permeabilities of compacted shales with S_0 about 1.51%10^7 (m^2/ m^3), based on a shale grain size of about 4%10^{-7} m. Therefore, 3.1 % 10^{-10} % S_0 is about 0.0047.

Table 5-7 Average compositions of minerals from the conventional core samples (sandstone) in the Bambra-1 well

Minerial	2716 m	2716.75 m	2720 m	2721.19 m	2722.05 m	2723.05 m	2725 m
Quartz (%)	53	55	55	30	60	60	60
Feldspar (%)	16	5	17	5	10	10	15
Calcite/dolomite Cement (%)	NA	15	NA	2	5	Trace	NA
Siderite (%)	21			10	10	2	1
Argillaceous matrix (%)	NA	10	NA	40	5	10	NA

Data from the samples at 2716.75 m, 2721.19 m, 2722.05 m and 2723.05 m were analyzed by Wulff (1991). Data from samples at 2716 m, 2720 m and 2725 m were collected from the well completion report. NA: Not available.

Deming (1994) demonstrated that three factors are necessary to define a pressure seal; time (t, Ma), thickness (z, m) and permeability (k, m^2) and gave the equation (5-2) (derived from a diffusion equation):

$$t = \frac{z^2 \alpha \mu}{4\kappa}, \tag{5-2}$$

where ș is rock compressibility ($10^{-10} < ș > 10^{-8}$ Pa^{-1}) (Neuzil, 1986; Ge and Garven, 1992), ȥ is dynamic viscosity of pure water (about 3.0 % 10^{-4} Pa∃s at 95 ^{o}C). If the compressibility value for shale is 10^{-9} Pa^{-1}, then,

$$t = (\frac{z^2}{\kappa}) \times 2.4 \times 10^{-27}, \qquad (5\text{-}3)$$

As described by the equation, the time over which a seal may confine a pressure transient is directly proportional to the square of the seal thickness (z) and inversely proportional to the seal permeability (k). If the time span required for the pressure seal unit (about 300 to 500 metres thick) to confine the overpressure in the Jurassic sequence is considered to be 1 to 100 Ma, the calculated permeabilities range from about 10^{-22} m^2 to 10^{-24} m^2. An error as large as a factor of 10 could occur due to uncertainties in the values used for rock compressibility (Deming, 1994). Based on the calculation of Deming (1994), without pressure recharge, a 500-m-thick pressure seal unit with permeability of 10^{-22} m^2 can maintain overpressure for several million years at best.

5.4 Summary

The Jurassic sequence in the sub-basins of the Northern Carnarvon Basin is highly overpressured with excess pressure between about 10-30 MPa as indicated by DSTs, RFTs and mud weights. A deep overpressured system commonly has associated high sonic transit times and low resistivity values in the fine-grained rocks. The response of the sonic-log and resistivity-log to the fine-grained rocks in the study area further supports the overpressured regime in the Jurassic source rocks. The overpressure is also found in specific zones in the Barrow Group of the Barrow Sub-basin.

This study suggests that the sonic and resistivity logs may respond anomalously to the overpressuring in the thick claystone and siltstone in these sub-basins, and also suggests that the deep overpressured system is not associated with high porosities that could be derived from the sonic-log and resistivity-log data by conventional

interpretation procedures. It seems that the deep overpressured zone at present is related to relatively high density, and that the porosity is likely to be less than 6 !1 % based on the density-log and measured claystone porosities.

The top pressure seals, associated with pressure transition zones, consist of a rock layer with 60 to 80 % claystone and siltstone, 20 to 40 % sandstone, and thin carbonate units within the Barrow Group and Upper Jurassic strata in the Barrow Sub-basin. The rock layer appears to be well compacted and cemented by quartz overgrowths and calcite which have relatively high density values. The top of the deep overpressured system can vary from about 2650 to 3000 metres with temperatures between 110 ^{o}C and 125 ^{o}C. The thickness of the rock layer varies from about 300 to 500 metres in the Barrow Sub-basin. The estimated porosities in the claystone of the rock layer are 2 to 5 % based on well-log data and some measured porosity values, and thus the calculated permeability may range from about 10^{-19} m^2 to 10^{-22} m^2.

Part III

One-dimensional Thermal History Modelling

CHAPTER 6 ONE-DIMENSIONAL MODELS AND DATA SETS

6.1 One-dimensional models

One-dimensional modelling aims at reconstructing thermal and maturity histories in this study. The primary models and calculations include geohistory/burial history, heat flow, temperature and thermal maturity (Platte River Associates, Inc., 1996).

6.1.1 Geohistory/burial history

The quantitative analysis of geohistory/burial history through time is used to reconstruct thermal and maturity histories. This analysis aims at producing time-depth histories and sedimentation rates. The correction of decompaction needs to be carried out for geohistory/burial history analysis. The reconstruction of geohistory also needs the data of palaeobathymetry and sea level fluctuations. Decompaction (backstripping) is based on the skeletal (solid grain) volume being constant, while the rock volume is changed with depth of burial due to the loss of porosity (Allen and Allen, 1990). Thus, the integrated equation is given:

$$\int_{z_1}^{z_2} \left[1-\phi(z)\right]\, dz = \int_{z_3}^{z_4} \left[1-\phi(z)\right]\, dz, \qquad (6\text{-}1)$$

where z_1 and z_2 are the top and bottom depths of a rock layer at a given time, z_3 and z_4 are new depths of the rock layer at another time, ϕ is porosity that is a function of depth (z).

6.1.2 Tectonic subsidence

A tectonic subsidence curve is useful in explaining the basin-forming mechanism. Tectonic subsidence can be obtained after the removal of the subsidence due to the sediment load and corrections for variations in water depth and eustatic sea-level changes. It reflects the lithospheric isostatic processes which cause basins to form

and is considered as the subsidence by tectonic effects, which backstrips (removes) the sediment load and replaces its load only by a column of water (Lerche, 1990; Joy, 1992). Tectonic subsidence is calculated using the equation of Steckler and Watts (1978):

$$T_s = H\left(\frac{\rho_m - \rho_s}{\rho_m - \rho_w}\right) + \left(W_d - \Delta SL\right) - \Delta SL\left(\frac{\rho_w}{\rho_m - \rho_w}\right), \qquad (6\text{-}2)$$

where T_s is the tectonic subsidence, H is the sedimentary layer thickness of the column corrected for compaction, W_d is the palaeo-water depth, <SL is the change in palaeo-sea level relative to the present-day sea level, ρ_m, ρ_s, and ρ_w are the densities of mantle, sediments and water, respectively.

6.1.3 Heat flow

The thermal history in a sedimentary basin relies on the heat flow from the mantle and radiogenic heat produced in the crust (Lachenbruch, 1970). Allen and Allen (1990) stated that geothermal evolution is controlled by the basal heat flow history of the basin, physical properties of the lithosphere, and heat generation from radioactive sources within the sediments and regional water flow. The increase in heat flow during rifting is related to the lithospheric thinning, which influences heat entering the basin from the asthenosphere. The heat transfer modes in sedimentary rocks are conduction related to lithology, porosity and nature of pore fluids, and convection related to compaction-driven flow, gravity-driven flow and anomalous heat intrusion. In this study a one-dimensional model is used where the heat flow is transferred by vertical conduction and lateral influence is ignored. The boundary conditions of the thermal data are provided in Table 6-1. Both rift heat flow and constant heat flow models can be evaluated by comparing the measured maturity data with the calculated maturity curves.

In the BasinMod 1D software, two basic assumptions for heat flow histories can be adopted: (1) steady state, a constant heat flow over time, and (2) non-steady state, a variable heat flow over time such as a rift heat flow history.

Steady state heat flow was calculated using a heat flow/thermal conductivity model:

$$Heat\ flow = k\frac{dT}{dz}, \tag{6-3}$$

where k is thermal conductivity; T is temperature (^{o}K); z is depth (m).

Transient heat flow was calculated using the transient diffusion equation and Heat transfer is assumed to be by vertical conduction using the equation:

$$\frac{d}{dz}\left[k\frac{dT}{dz}+Q\right]=c\frac{dT}{dt}, \tag{6-4}$$

where T is temperature (^{o}K); k is thermal conductivity; c is heat capacity; t is time.

The BasinMod 1D provides a modified Jarvis and McKenzie (1980) algorithm to calculate rift heat flow.

$$F(t)=\frac{kT_1}{z}\left\{1+\pi\sum_{n=1}^{\infty}nb_n(-1)^{n+1}\times\exp\left[-n^2\pi^2(t-\Delta t)\frac{k}{a^2}\right]\right\}, \tag{6-5}$$

$$b_n=\frac{2}{n}\frac{(-1)^{n+1}}{n}\left(\frac{\beta}{n\pi}\sin\frac{n\pi}{\beta}\right), \tag{6-6}$$

where $F(t)$ is heat flow at surface at time t; t is time of rifting; k is thermal conductivity; kT_1/z is heat flow prior to rifting, based on present day heat flow; a is thickness of lithosphere, fixed at 125 km.

A $\aleph$ factor is required for the calculation of rifting heat flow in the BasinMod 1D, which is defined as:

$\aleph$ = initial lithospheric thickness / lithospheric thickness immediately after stretching

Table 6-1 Some present-day thermal parameters of 14 wells for 1D thermal modelling in the Northern Carnarvon Basin

Well Name	Geothermal Gradient ($^oC/100m$)	Seabed or Surface Temperature (^oC)	Heat Flow (mW/m^2)	Water Depth (m)	Subdivision
Jurabi-1	3.50	23	52.1	60	Exmouth Sub-basin
Zeewulf-1	3.80	4.5	59.6	1194	
Anchor-1	3.30	24	53.6	18	Barrow Sub-basin
Bambra-2	3.25	24	56.0	26	
Barrow-1	3.25	25	57.5	0	
Barrow Deep-1	3.25	25	57.5	0	
Bowers-1	3.40	21	55.3	133	
Madeleine-1	3.00	23	48.2	69	Dampier Sub-basin
Rosemary-1	3.00	21	47.5	65	
Depuch-1	3.00	21	49.4	143	Beagle Sub-basin
North Gorgon-1	3.60	20	57.1	215	Rankin Platform
North Rankin-1	2.90	21	53.5	122	
Investigator-1	3.40	5.5	56.8	841	Exmouth Plateau
Jupiter-1	3.20	5	54.3	960	

The rift heat flow model, which entails a higher heat flow episode during the rift phase and an exponential reduction during the post-rift phase (McKenzie, 1978), has been introduced as a fundamental consideration for the relationship between thermal history and tectonic evolution. The study by Allen and Allen (1990) indicates that the heat flow in an active rift (syn-rift) is about 63 to 110 mW/m^2 with an average heat flow value of 80 mW/m^2, and in a thermally subsiding rift (post-rift) is about 37 to 66 mW/m^2 with an average value of 50 mW/m^2. Lysak (1992) investigated a relationship between heat flow variations and structural positions in active continental rift systems, indicating that the highest heat flow distributes along subsiding grabens, active fault zones and around volcanic centres, while heat flow on rift shoulders is generally lower than in the axial graben system.

6.1.4 Temperature and thermal maturity

Temperature was calculated using the transient heat flow model. Time and depth steps of 1 Ma and 100 m respectively were used. The method to calculate

temperature takes into account the thermal conductivity plus the heat capacity of the lithologies in the model, giving a more accurate heat-flow profile.

The BasinMod 1D provides a method, together with default values of kinetic parameters, for the calculation of vitrinite maturation, using the chemical-kinetic model of vitrinite reflectance (Sweeney and Burnham, 1990). Vitrinite reflectance is a function of temperature and time, as described by the Arrhenius equation, which shows that the reaction rate of vitrinite maturation increases exponentially with temperature and linearly with time. The method allows the calculation of R_o values, ranging between 0.3 and 4.5 %, so as to compare with the measured maturity data and calibrate heat flow histories.

6.2 Data sets

Fourteen wells (Table 6-1 and Fig. 6-1) in various tectonic subdivisions of the Northern Carnarvon Basin were selected on the basis of available data for thermal modelling using BasinMod 1D (version 7.06, Platte River Associates, Inc.). The input data used for this modelling was collected from open files, such as well-completion reports from the Department of Minerals and Energy of Western Australia. The initial porosity, matrix density, matrix thermal conductivity and matrix heat capacity were adopted from the default values in BasinMod 1D. In addition, conventional and side-wall core samples in Bambra-2 were analyzed for Rock-Eval pyrolysis.

6.2.1 Stratigraphic data and porosity-depth relationship

The stratigraphic data include the present thickness of stratigraphic intervals, lithology, and absolute age. The formation thickness is based on well-completion reports and well-log information. The undifferentiated formations within the Cainozoic were defined using the interpreted seismic data by the AGSO. Five lithologies (sandstone, siltstone, shale/claystone, limestone and coal) were used and the average content of each lithology was calculated as a percentage of mixed lithologies in a single formation. Absolute ages were obtained from the stratigraphic

table and the micropaleontological analysis of well-completion reports. The geological time scale is referenced in Labutis (1994) and Polomka et al. (1999).

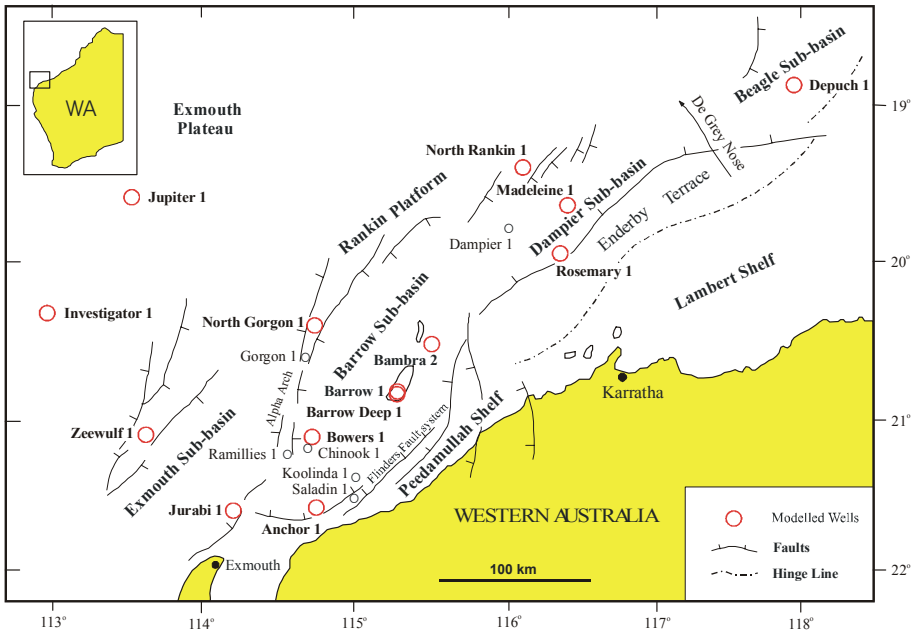

Fig. 6-1 A map shows the locations of the modelled wells and the tectonic subdivisions in the Northern Carnarvon Basin (after Woodside Offshore Petroleum, 1988; Scott, 1992).

The porosity-depth relationship for the backstripping of compacted stratigraphic thicknesses by Falvey and Middleton (1981), used in BasinMod 1D, is employed to model burial histories. The relationship was developed in the offshore Perth Basin, which also contains shallow carbonates similar to the Northern Carnarvon Basin.

6.2.2 Geothermal parameters

The present geothermal parameters include formation temperature, seabed temperature, thermal conductivity, heat capacity and heat flow. Present-day formation temperature can be estimated from drill stem test (DST) temperature, and the extrapolated bottom hole temperature (BHT-bottom hole temperature) using Horner plot correction. Where there was not sufficient data to correct the BHT using a Horner plot, BHT was corrected by adding 10 % of the raw BHT value. The current seabed temperature was based on the studies by Pickard and Emery (1982)

and Horstman (1988). Combining the formation temperature with seabed temperature allowed geothermal gradient to be calculated (Table 6-1). In the BasinMod 1D software, the default values of matrix thermal conductivity and matrix heat capacity were used (Table 6-2) and were calculated using the algorithms for temperature correction. The Deming and Chapman (1989) method was used to calculate fluid conductivity. Present-day heat flow was calculated using formation and seafloor temperatures with the steady-state heat flow model in BasinMod 1D (Table 6-1).

Table 6-2 Default matrix thermal conductivity and matrix heat capacity in the BasinMod 1D

Lithology	Matrix Thermal Conductivity ($W \exists m^{-1} \exists K^{-1}$) (Default)	Matrix Heat Capacity ($kJ \exists m^{-3} \exists K^{-1}$) (Default)
Sandstone	4.4	2800
Siltstone	2	2650
Shale	1.5	2100
Limestone	2.9	2600
Dolomite	4.8	2600
Coal	0.3	950

6.2.3 Thermal maturity

Multiple thermal maturity indicators, including vitrinite reflectance (R_o), equivalent vitrinite reflectance (Eq VR) and Rock-Eval T_{max}, have been used in an attempt to overcome problems with limited data sets and to use them in combination in the assessment of thermal maturity in this study.

The vitrinite reflectance values in dispersed organic matter are mean random vitrinite reflectance in oil (R_o %). The mean maximum reflectance values are not systematically different from the mean random reflectance in the dispersed organic matter (Kaiko and Tingate, 1996). Conversion of the maximum reflectance to random values can use an established relationship, $R_o = R_{max}/1.061$, by Hoover and Davis (1980).

The equivalent vitrinite reflectance (Eq VR) values, using the fluorescence alteration of multiple macerals (FAMM) technique, are believed to be equivalent to

unsuppressed vitrinite reflectance and calibrated in units of "mean random vitrinite reflectance". They range from about 0.45 to 1.20 % (Wilkins et al., 1992a, 1992b, 1995), and were analyzed by CSIRO Petroleum. The Eq VR data in four wells have been used for the studies of thermal and maturity modelling (Table 6-3).

The reliability of Rock-Eval T_{max} data was investigated in this basin. It was found that the problems that alter the Rock-Eval S_2 peak which in turn affect T_{max} data in assessment of thermal maturity include (1) contamination by drilling mud additives, (2) suppression due to HI > 150, (3) recycled organic matter, and (4) caved material. The abnormal Rock-Eval T_{max} data from a maturity trend of an individual well could be identified, and should be ignored when they are significantly affected by these problems. The suppression of T_{max} values due to HI > 150 could be corrected for type III kerogen based on the study of Snowdon (1995). The REESA (Rock-Eval Expert System Analysis) Rules in BasinMod 1D can be used for filtering Rock-Eval data.

Table 6-3 Eq VR data in four wells used in this study

Barrow-1		**Bowers-1**			**Depuch-1**			**Jupiter-1**	
Depth (m)	Eq VR (%)	Depth (m)	Sample Type	Eq VR (%)	Depth (m)	Sample Type	Eq VR (%)	Depth (m)	Eq VR (%)
1261	0.50	2000-2100	Cuttings	0.63	2215-2225	Cuttings	0.6	2753	0.50
1679	0.53	2545-2555	Cuttings	0.77	2530-2540	Cuttings	0.64	3013	0.49
1808	0.62	2850-2860	Cuttings	0.89	2850-2860	Cuttings	0.61	3178	0.58
1981	0.68	2955-2960	Cuttings	0.91	3160-3170	Cuttings	0.67	3328	0.59
2039	0.78	3060-3065	Cuttings	0.90	3420-3430	Cuttings	0.64	3593	0.62
2371	0.80	3550	Cuttings	0.92	3860-3870	Cuttings	0.72	3903	0.82
2597	0.86	3676.5	Cuttings	1.15	4015-4025	Cuttings	0.76	4248	0.74
2835	0.98	3750-3760	Cuttings	1.18	4125-4135	Cuttings	0.80	4397	1.14
		3915-3925	Cuttings	1.20	4200-4210	Cuttings	0.80	4533	1.00
					4290-4300	Cuttings	0.83	4838	1.14

The Eq VR values were measured by CSIRO Petroleum.

6.2.4 Eroded thickness

The erosional thickness is important for burial, thermal and maturity modelling. However, there are no available well-log data for estimating erosional thicknesses. Seismic data can be used to make a rough correlation, and estimate thicknesses at the main unconformity. Based on AGSO's seismic interpretation, the seismic reflections show obvious erosional phenomena at the unconformity between the Triassic or Jurassic and Cretaceous sequences on the Rankin Platform. The missing section of the Lower Jurassic was estimated to be from several hundred meters up to one thousand meters thick (Barber, 1982). The Triassic erosional thickness ranges from zero to more than one thousand meters. Therefore, the total erosional thickness during the rifting until breakup on the Rankin Platform ranges from several hundred meters to more than two thousand meters. Some of the Lower Jurassic rocks may have been eroded on the structural highs of the Exmouth Plateau during the Middle Jurassic. In addition, where strata are absent and there is no evidence of erosion from seismic data, it has been treated as periods of non-deposition.

6.2.5 Palaeobathymetry and sea-level variations

Palaeobathymetry may affect thermal modelling owing to the variation of palaeoseafloor temperatures. Kaiko and Tait (2001) used seismic data to study the palaeo-water depths of the Late Jurassic to Cainozoic for some individual wells of the Northern Carnarvon Basin. These palaeo-water depth data were used for 1D modelling and were also used to evaluate water-sediment interface temperatures for the wells selected in this study. The palaeobathymetric values in the Triassic and Early-Middle Jurassic were estimated using lithology and palynofacies analysis in the well completion reports, and a study by Bradshaw et al. (1988). These were about 5 to 20 metres in the Middle-Late Triassic, 20 to 50 metres in the Early Jurassic, and 50 to 350 metres in the Middle-Late Jurassic. Similar deep water conditions persisted over most of the study area until the Tertiary, when prograding carbonate sediments again produced a shallow shelf environment.

The long-term eustatic curves of the Mesozoic-Cenozoic by Haq et al. (1987) were adopted for changes of relative sea-level through time.

CHAPTER 7 ONE-DIMENSIONAL HEAT FLOW AND THERMAL MATURITY MODELLING

7.1 Introduction

The heat flow history of a basin is calculated by establishing an agreement between a calculated (or modelled) maturity curve and the equivalent observed maturity parameter (such as vitrinite reflectance, or Rock-Eval T_{max}). Then, this calculated heat flow history can be used to predict the thermal maturity of source rocks and the timing of hydrocarbon generation. The calculated, or modelled, thermal maturity parameters are usually derived from models that use (1) empirically-based temperature and time integrals (e.g. Waples, 1980; Middleton, 1982), (2) the Arrhenius-reaction approach (e.g. Lerche et al., 1984; Wood, 1988), or (3) multiple Arrhenius-reaction models, which attempt to simulate the chemical reactions which produce maturation (e.g. Larter, 1988; Sweeney and Burnham, 1990). Temperature is the most sensitive parameter in thermal maturity and hydrocarbon generation, and Tissot et al. (1987) consider that reconstruction of temperature history is essential when evaluating petroleum prospects. Formation temperature depends upon heat flow, thermal conductivity, burial depth and the water-sediment interface or surface temperature.

Vitrinite reflectance is the most widely used indicator of thermal maturity (e.g. Waples, 1985; Tissot and Welte, 1984; Allen and Allen, 1990; Hunt, 1996). Wilkins et al. (1992a) pointed out that two major causes of the anomalously low vitrinite reflectance for some North West Shelf wells are: (1) the suppression of vitrinite reflectance through marine influence; (2) the difficulty of identifying the vitrinite population in dispersed organic matter. Marine influence resulting in lower R_o values were proposed by Wilkins et al. (1992a), Hunt (1996), Kaiko and Tingate (1996) and Gurba and Ward (1998). Samuelsson and Middleton (1998) stressed that the vitrinite reflectance suppression in this basin has led to an underestimation of the true level of thermal maturity. As a major thermal maturity indicator, these problems with vitrinite reflectance make it difficult to estimate the thermal history in many wells of this basin. Researches have used alternative thermal parameters and R_o

correction for attempting to overcome the problems associated with the anomalously low R_o in studies of the basin's thermal history and the thermal evolution of source rocks. Alexander, Marzi and Kagi (1990) applied molecular markers as thermal indicators for modelling the palaeoheatflow of the Jupiter-1 well in the basin. Wilkins, Russell and Ellacott (1994) evaluated thermal maturity of five Northern Carnarvon Basin wells using equivalent vitrinite reflectance (Eq VR) data, which is analysed by the technique of the fluorescence alteration of multiple macerals (FAMM). Kaiko and Tingate (1996) used the spore coloration combined with R_o and FAMM data for assessment of thermal maturity in the Barrow and Dampier Sub-basins. Samuelsson and Middleton (1998) corrected vitrinite reflectance values based on the method of Lo (1993) for reconstruction of heat flow histories in seven wells of the basin.

Studies of palaeoheat flow in rift-related basins indicate that high palaeoheat flow is commonly associated with rifting and seafloor spreading (Mello and Karner, 1996; Zhou and Littke, 1999), and the reconstruction of thermal history from vitrinite reflectance is a function of the tectonic history in a sedimentary basin (e.g. Middleton, 1982; Allen and Allen, 1990). Based on theoretical and empirical studies (McKenzie, 1978; Barber, 1982; Hellinger and Sclater, 1983; Middleton and Hunt, 1989; Driscoll and Karner, 1998; Tindale et al., 1998; Polomka et al., 1999), the evolution of the Northern Carnarvon Basin during the Jurassic is commonly accepted to be comprised of two major phases: (1) rapid subsidence and faulting, and (2) thermal subsidence.

However, direct evidence for estimating past heat flow from palaeotemperatures (derived from vitrinite reflectance, Rock-Eval T_{max}, or similar parameters) in most Barrow and Dampier Sub-basin wells may have disappeared since the palaeotemperatures experienced during the rifting phase may have been equalled, or exceeded, by those associated during burial in later sag-phase sedimentation (Kaiko and Tingate, 1996). Nielsen (1996) proposed that organic maturity indicators tend to remember only the maximum temperature encountered, and when organic matter in the present era experiences the maximum geotemperature, maturity indicators are less sensitive to thermal reconstruction.

The Northern Carnarvon Basin is the richest hydrocarbon province in Australia (Kopsen, 1994). About 50 gas/condensate and oil fields, associated with the postulated Triassic and Jurassic source rocks, have been discovered (Vincent and Tilbury, 1988; Lawry and Carter, 1992; le Poidevin and Lowden, 1994; Baillie and Jacobson, 1997). The thermal history models for the study region have been proposed by (1) Swift et al. (1988), who proposed maximum heat flows of about 77 to 80 mW/m^2 in the Jupiter-1 well and about 105 to 110 mW/m^2 in the Dampier-1 well, (2) Alexander et al. (1990), who modelled maximum heat flow with possible ranges of 70 to 75 mW/m^2 between 140 Ma and 240 Ma in the Jupiter-1 well, (3) Wilkins et al. (1994), who modelled palaeoheat flows for the Gorgon-1 and Chinook-1 wells, (4) Kaiko and Tingate (1996), who studied the present-day heat flows and thermal histories modelling using constant heat flows in the Barrow and Dampier Sub-basins, and (5) Samuelsson and Middleton (1998), who modelled maximum palaeoheat flows of about 65 to 95 mW/m^2, between 170 Ma and 250 Ma. However, their models are not associated with the algorithm for rifting heat flow history of Jarvis and McKenzie (1980).

The aims of this chapter are (1) to investigate the applicability of the classical McKenzie- model (McKenzie, 1978; Jarvis and McKenzie, 1980) for rifting thermal history to the study area, (2) to propose a R_o-T_{max} relationship and use T_{max} data for the evaluation of thermal maturity compared with other maturity parameters of R_o and Eq VR, and (3) to present detailed thermal modelling of individual wells based on the correlation between T_{max} and R_o.

7.2 Data used in the study

Eleven wells (Table 7-1) from various subdivisions of the Northern Carnarvon Basin (Fig. 7-1) were selected on the basis of suitability for thermal modelling. The input data have been discussed in Chapter 6. The initial porosity, matrix density, matrix thermal conductivity and matrix heat capacity were adopted from the default values in BasinMod 1D.

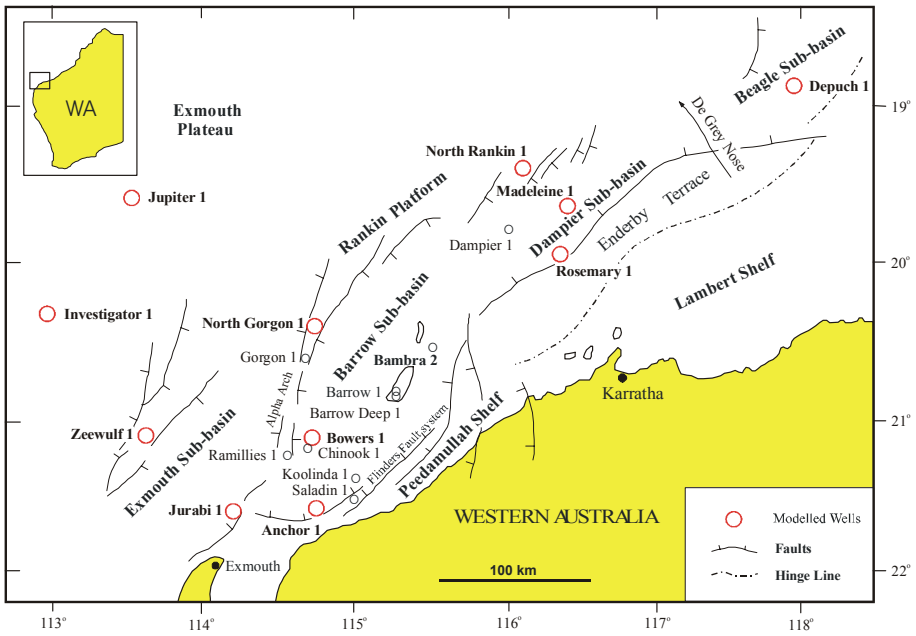

Fig. 7-1 A map showing well locations for the thermal modelling and tectonic subdivisions in the Northern Carnarvon Basin (after Woodside Offshore Petroleum, 1988; Scott, 1992).

Table 7-1 The eleven wells for thermal modelling in the Northern Carnarvon Basin

Subdivision	**Well**
Exmouth Sub-basin	Jurabi-1, Zeewulf-1
Barrow Sub-basin	Anchor-1, Bowers-1
Dampier Sub-basin	Madeleine-1, Rosemary-1
Beagle Sub-basin	Depuch-1
Rankin Platform	North Gorgon-1, North Rankin-1
Exmouth Plateau	Investigator-1, Jupiter-1

7.3 Relationship between vitrinite reflectance (R_o) and Rock-Eval T_{max}

Figure 7-2 shows a comparison of T_{max} from Rock-Eval pyrolysis versus vitrinite reflectance within the Middle-Upper Triassic (Mungaroo Formation) and Jurassic source rocks in wells of the Northern Carnarvon Basin. The Rock-Eval T_{max} and vitrinite reflectance data plotted in Fig. 7-2 are listed in Table 7-2. The data indicate

that the organic matter for the Mungaroo Formation is related to type III kerogen (Fig. 7-3). The depositional environment of the Mungaroo Formation is fluvio-deltaic with an abundance of terrestrial plants (Barber, 1982; Cook et al., 1985), and for this reason suppression of vitrinite reflectance is not expected (Wilkins et al., 1994). It is proposed that the data in Fig. 7-2 represent a reasonable correlation for T_{max} in organic matter on the North West Shelf versus vitrinite reflectance. This correlation is only marginally different from the published correlation for the generalized behavior of T_{max} versus R_o of Tissot and Welte (1984).

The values of T_{max} and R_o (measured by Robertson Research, 1986 and AGIP, 1993) in the Jurassic rocks from the Anchor-1 well are plotted in Fig. 7-2. These data indicate that the relationship between T_{max} and R_o is consistent with that plotted for the Mungaroo Formation, and thus these T_{max} and R_o data are not contaminated or exhibit significant vitrinite reflectance suppression. Furthermore, it is important to note that the organic matter for the data in Anchor-1 is related to type III kerogen (Fig. 3-7). Also, T_{max} and R_o values with type III kerogen for the Lower Jurassic source rocks in the Bowers-1 well (measured by Robertson Research and Analab) are consistent with the relationship between T_{max} and R_o plotted in Figure 7-2.

In a supporting study, T_{max}, with values ranging from 484 ^oC to 490 ^oC, was measured from a conventional core in the Middle Jurassic at 4274 to 4283 metres in the Bambra-2 (measured by Australian Mineral Development Laboratories, Amdel, in 1983 and Geological Survey of Canada, 2000, see Table 4-1). These T_{max} values correspond to R_o values of 1.5-1.8 % based on the relationships between T_{max} and R_o provided by Teichmüller and Durand (1983), Espitalié et al. (1984) and Tissot et al. (1987). Corroborating this correlation, the measured vitrinite reflectance from "verified" vitrinite particles within this core fall in a range from about 1.2 to 2.0 % (measured by L.W. Gurba of University of New South Wales, 2000). These data could correlate with the R_o measurement of 1.7 % by Cook and Kanstler (1980) at the depth of 4290 metres in the Barrow Deep-1 well. The observed T_{max} = 484 ^oC and 490 ^oC and R_o = 1.7 % (being representative of the above cited T_{max} and R_o data) for the conventional core samples in the Bambra-2 well are shown in Fig. 7-2.

Table 7-2 R_o and Rock-Eval pyrolysis data for five wells in the Northern Carnarvon Basin

Depth (m)	R_o (%)	T_{max} (°C)	S_1	S_2	S_3	TOC (wt.%)	HI	OI	PI	Sam.	Well
1800		431	0.10	0.68					0.13	CC	
1881-1896	0.55	431	0.19	1.47	1.37	1.44	102.00	95.14	0.11	CT	
1988-2003	0.61	432	0.13	1.70	1.21	1.42	119.70	85.21	0.07	CT	
2226-2241	0.67	434	0.43	2.30	1.66	1.65	139.30	100.60	0.16	CT	
2393-2409	0.64	433	0.23	1.30	1.49	1.24	104.80	120.10	0.15	CT	Anchor-1
2546-2561	0.68	434	0.24	1.40	1.61	1.72	81.40	93.60	0.15	CT	(Jurassic)
2686-2701	0.65	437	0.33	1.46	1.22	1.65	88.48	73.94	0.18	CT	
2754		438	0.23	0.73					0.24	CC	
2851-2866	0.76	439	0.19	1.18	1.28	1.63	72.39	78.53	0.14	CT	
3030-3046	0.83	442	0.09	0.48	0.84	1.16	41.38	72.41	0.16	CT	
4274	1.74	484	0.11	0.34	0.10	0.74	46	14	0.25	CC	Bambra-2
4283	1.74	490	0.13	0.39	0.03	0.97	40	3	0.24	CC	(Jurassic)
3735-3750	1.27	459	0.38	1.19	1.94	1.70	70.00	114.00	0.24	CT	Bowers-1
3840-3855	1.31	459	0.28	1.12	1.19	2.12	53.00	56.00	0.20	CT	(Jurassic)
3900-3915	1.43	468	0.38	1.43	2.02	2.80	51.00	72.00	0.21	CT	
3985-4000	1.43	474	0.34	2.10	5.79	4.67	45.00	124.00	0.14	CT	
4000-4005	1.38	468	0.21	1.27	3.61	2.49	51.00	145.00	0.14	CT	
4000-4015	1.56	467	0.32	1.15	1.64	2.21	52.00	74.00	0.22	CT	Bowers-1
4100-4105	1.56	482									(Triassic)
4200-4205	1.66	477	0.17	0.89	1.52	1.85	48.00	82.00	0.16	CT	
4295-4300	1.80	479									
4295-4300	1.87	487	2.00	7.33	1.78	10.07	72.00	17.00	0.21	CT	
3050	0.49	430	0.49	5.15	1.2	5.01	102.70	23.95	0.09	CT	
3190	0.57	428	1.04	13.5	1.92	3.51	146.40	20.77	0.07	CT	
3615	0.63	437	5.03	77.1	5.49	35.9	214.60	15.29	0.06	CT	
3910	0.83	438	3.11	34.3	1.95	18.0	190.30	10.83	0.08	CT	Jupiter-1
4220	0.77	439	0.32	3.35	1.37	2.90	115.00	47.00	0.09	CT	(Triassic)
4455	0.86	440	0.94	5.22	0.92	4.23	123.40	21.74	0.15	CT	
4750	1.33	454	2.48	22.4	0.91	13.3	168.60	6.84	0.10	CT	
4865	1.36	460	3.13	26.6	1.22	13.7	194.40	8.91	0.11	CT	
3500-3525	1.00	442	0.95	1.01	1.54	1.41	71.00	109.00	0.48	CT	
3650-3675	1.00	445	0.84	1.93	1.03	2.20	87.00	46.00	0.30	CT	
3750-3775	1.07	447	0.97	2.98	1.19	2.95	101.00	40.00	0.25	CT	North
3875-3900	1.07	446	0.39	0.65	0.70	1.05	61.00	66.00	0.38	CT	Gorgon-1
4100-4125	1.18	449	0.51	0.77	0.59	1.22	63.00	48.00	0.40	CT	(Triassic)
4285-4290	1.18	453	0.38	0.90	0.63	1.27	70.00	49.00	0.30	CT	
4385-4390	1.29	455	0.15	0.25	0.26	0.56	44.00	46.00	0.38	CT	
4490-4500	1.39	463	0.21	0.33	0.22	0.78	42.00	28.00	0.39	CT	

* Rock-Eval data were collected from the well-completion reports and the reports prepared by Robertson Research Australia Pty. Ltd., 1986.

T_{max}: Temperature of the top of S_2 peak; S_1: Free hydrocarbons (mg HC/g rock); S_2: Pyrolysable hydrocarbons (mg HC/g rock); S_3: CO_2 from pyrolysis (mg CO_2/g rock); TOC: Total organic carbon (wt. %); HI: Hydrogen index (S_2 % 100/TOC); OI: Oxygen index (S_3 % 100/TOC); PI: Production index (S_1/S_1+S_2). Sam.: Sample. CC: Conventional core; CT: Cuttings.

The Jurassic organic matter in the studied wells consists mainly of type III kerogen (Figures 3-6 to 3-9). The Jurassic organic matter in the Depuch-1 well is related to the coal-bearing strata and type III kerogen with HI ranging from about 40 to 389. The relationship between R_o versus T_{max} (Fig. 7-2), as an average conversion trend of two maturity data sets, has been used to convert T_{max} data into R_o values in the BasinMod 1D software mainly for the Mungaroo Formation and Jurassic sequence in the selected wells.

7.4 Modelling of tectonic subsidence and sedimentation rates

The tectonic subsidence (water-loaded subsidence) can be obtained after the removal of the sediment-loaded subsidence and after corrections of the palaeo-water depth (the data provided by Dr. Alex Kaiko) and palaeosea level variations through time. Subsidence analysis can help in the understanding of the histories of the syn-rift (Jurassic and earliest Cretaceous) and post-rift (Cretaceous and Cainozoic). Figure 7-4 shows the tectonic subsidence curves in the Bambra-2 and Barrow Deep-1 wells calculated by applying the equation of Steckler and Watts (1978) in the BasinMod 1D software. These curves exhibit two principal phases of subsidence in accordance with the rift tectonic regime, which generally agree with previous regional studies (e.g. Barber, 1982; Exon and Colwell, 1994; Müller et al., 1998; Polomka et al., 1999). These results indicate that rapid subsidence and corresponding high sedimentation rates took place during the rift-extensional period, and thermal subsidence with lower sedimentation rates occurred during the post-rift period. During the rift phase, the sedimentation rates ranged from about 80 m/Ma to 200 m/Ma. During the post-rift phase, sedimentation rates ranged from less than 10 m/Ma to 50 m/Ma. However, the sedimentation rates in the Cretaceous were 10 to 50 m/Ma, while the rates in the Cainozoic ranged from less than 10 to 20 m/Ma.

7.5 Modelling of heat flow and thermal maturity

7.5.1 Thermal modelling for 2 wells in the Exmouth Sub-basin

7.5.1.1 Jurabi-1 thermal modelling

The Jurabi-1 well is located on the southwestern flank of the Muiron Anticline in the eastern Exmouth Sub-basin (Fig. 7-1). The boundary between the Upper Jurassic strata and Muderong Shale is the main unconformity. Barrow Group is absent at the well site, and the group is thought to have been eroded during the breakup in the Valanginian, when a thickness of several hundred meters was eroded. This is based on seismic and sonic log data. Nevertheless, there are 1063 metres of Cretaceous-Cenozoic sedimentary rocks in this well. Three formation temperatures were determined from BHTs using Horner plots. The current heat flow of 52.1 mW/m^2 is calculated from the formation temperatures with a seafloor temperature of 23 ^oC.

The maturity profiles in this well with R_o (measured by A.C. Cook, 1982) from side-wall cores and T_{max} data from cuttings samples (measured by PGA Consultants, 1992 and Geotech, 1995) are shown in Fig. 7-5A. It can be seen that three of the four R_o values are in the Murat Siltstone, Brigadier and Mungaroo Formations, one is an anomalously low value in the Athol Formation, and all the T_{max} data are in the Middle and Upper Jurassic sequence. It should be noted that some T_{max} values, between 1535 and 2400 metres with HI ranging from 168 to 314, are likely to be suppressed about 1-3 ^oC, according to the study of Snowdon (1995). Also, the T_{max} data from 1305 to 1470 metres are possibly related to recycled organic matter. Thus, T_{max} is not as reliable as non-anomalous vitrinite reflectance, as a maturity indicator, in this well.

The thermal modelling, using the current heat flow (projected back into the past), does not give a match between the observed maturity profile and calculated maturity curve (Fig. 7-5A, curve 2). A good fit to the maturity data, however, was achieved from a rift heat flow model, with 600 metres of erosion thickness and exponentially decreasing heat flow to the present (Fig. 7-5A, curve 1 and Fig. 7-5B). The modelled maturity curve links the T_{max} data in the Dingo Claystone and Athol Formation with the R_o data in the Lower Jurassic and Upper Triassic (Fig. 7-5A). The proposed syn-rift phase in this sub-basin started at 190 Ma and terminated at 136 Ma. The maximum heat flow of about 67 mW/m^2 is 29 % greater than the current heat flow. Figure 7-6 shows the histories of burial, temperature and thermal maturity in the Jurabi-1 well with the rift-related heat flow history. It is obvious that the model produces the maximum temperature during the syn-rift phase due to an

increase in rift heat flow, recorded by the maturity indicator in the Mungaroo Formation and the Jurassic sequences.

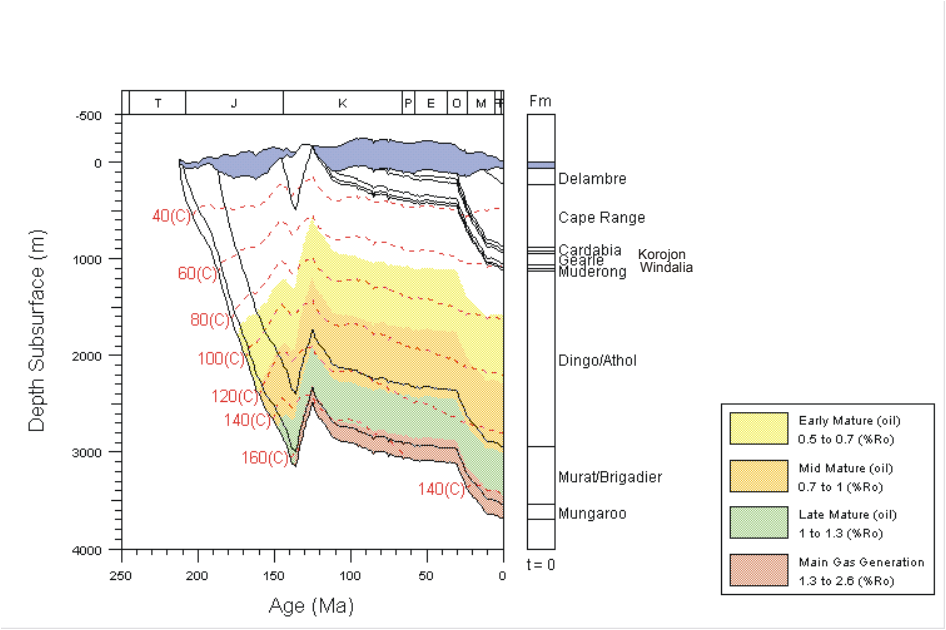

Fig. 7-6 The modelled geohistory and histories of temperature and maturity using the rift-related heat flow history for the Jurabi-1 well.

7.5.1.2 Zeewulf-1 thermal modelling

Zeewulf-1 well was drilled on a structural high in the western margin of the Exmouth Sub-basin in a water depth of 1194 metres. There is only 5 metres of Upper Jurassic rocks and a lack of Lower-Middle Jurassic and top Triassic rocks in this well. The uplift and erosion on the structure could occur during rifting until about 150 Ma. Therefore, the main unconformity is the contact between the Upper Triassic sequence and the Upper Jurassic rocks. It is likely that the Lower Jurassic and the top of the Upper Triassic were eroded during the rifting. The erosional thickness could be about 1000 metres or more. The sedimentary rocks overlying the Upper Triassic are 1887 metres thick. Two formation temperatures are Horner-plot type temperatures. The calculated current heat flow is 59.6 mW/m^2 (seabed temperature = 4.5 ^oC). Most vitrinite reflectance data (measured by A.C. Cook, 1979) are from side-wall cores, which can be modelled well by the current heat flow and seabed temperature (Fig. 7-7). Figure 7-8 gives the geohistory, temperature and

maturity histories in this well. The model indicates that the organic matter in the Mungaroo Formation experienced decreasing temperatures at the place of uplift and erosion associated with the Jurassic extension. The secondary maturity increase is due to later burial during the post-rift phase.

7.5.2 Thermal modelling for 2 wells in the Barrow Sub-basin

7.5.2.1 Anchor-1 thermal modelling

Anchor-1 well was drilled in the southern margin of the Barrow Sub-basin. In this case, six formation temperatures are corrected from the BHTs (raw BHTs + 10%). A current heat flow of 53.6 mW/m^2 is estimated, with a seabed temperature of 24 ^oC. The vitrinite reflectance values (measured by Robertson Research Australia Pty. Ltd.) and the T_{max} data (measured by Robertson Research Australia Pty. Ltd., BHP and AGIP) are shown in Fig. 7-9. Both R_o and T_{max} data can be matched with the present heat flow and seabed temperature. This modelled result suggests that both R_o and T_{max} values can be used to evaluate the thermal maturity trend in this well and also suggests that the organic matter in the well site is at maximum temperature at present (Fig. 7-9). Figure 7-10 indicates a basically continued burial and thermal effect histories in this well.

7.5.2.2 Bowers-1 thermal modelling

The Bowers-1 well was drilled on a faulted anticlinal structure on the eastern flank of the Alpha Arch in the Barrow Sub-basin (Fig. 7-1). The well contains a thin Jurassic sequence, but there is no palynological evidence to indicate that Middle-Upper Jurassic strata are absent. In this case, two formation temperatures were derived from Horner-plot corrections and the seafloor temperature is 21 ^oC. The calculated current heat flow is 55.3 mW/m. The vitrinite reflectance values (measured by Robertson Research Australia Pty. Ltd. and Keiraville Konsultants, 1989), T_{max} data (measured by Robertson Research Australia Pty. Ltd. and Analab, 1982) and Eq VR values (CSIRO Petroleum) are plotted in Fig. 7-11A. It can be seen that the R_o data from Triassic rocks, obtained from different laboratories,

unanimously support high thermal maturity, which is also consistent with the T_{max} data. Most R_o data (measured by Keiraville Konsultants, 1989) in the Jurassic to Cretaceous formations are too low to be modelled even by a constant present-day heat flow. The best match, between the measured non-anomalous maturity data (T_{max} and R_o) and the calculated maturity curve, was obtained from a rift heat flow model. The model assumes that the syn-rift phase began at 190 Ma and ended at 136 Ma, which is when the maximum rift heat flow of 105 mW/m^2 occurred (Figure 7-11B). The modelled maximum heat flow is 88 % higher than the present-day heat flow. Although the modelled maximum heat flow is anomalously high, we have no reason to suspect the validity of the vitrinite reflectance data from the Triassic-aged sediments of this well. Thus, we conclude that the palaeoheat flow in this region may be abnormally high. The modelled geohistory and thermal effect history, corresponding to the thermal model, are shown in Fig. 7-12.

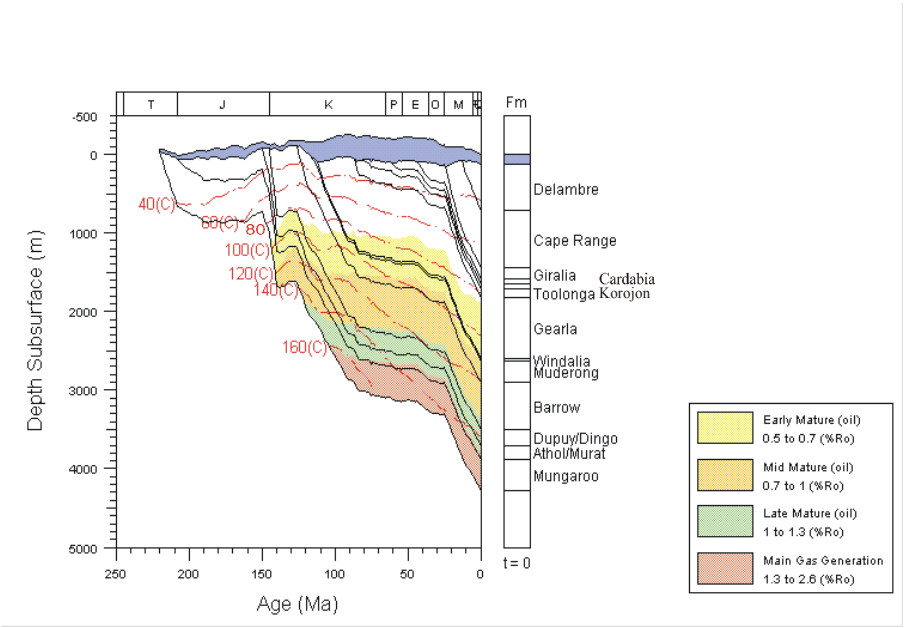

Fig. 7-12 The calculated geohistory and thermal effect history using the rift-related heat flow history for the Bowers-1 well.

7.5.3 Thermal modelling for 3 wells in the Dampier and Beagle Sub-basins

7.5.3.1 Rosemary-1 thermal modelling

The Dampier Sub-basin is a rift graben between the Beagle Sub-basin on the north and the Barrow Sub-basin on the south. It is bounded on the west by the Rankin Platform and on the east by the Lambert Shelf. The geological history of the basin has been studied by a number of workers (e.g. Crostella and Chaney, 1978; Kopsen and McGann, 1985; Veenstra, 1985; Vincent and Tilbury, 1988; Barber, 1994; Hill, 1994; Miller and Smith, 1996). Rosemary-1 was drilled on a faulted structure on the Rosemary Fault System along the east flank of the sub-basin. In the acceptable Rock-Eval data, the values of hydrogen index in the Jurassic organic-matter generally range from about 80 to 191, with the T_{max} values ranging from 432 ^{o}C to 442 ^{o}C, related to type III kerogen. The formation temperatures were corrected from BHTs (raw BHTs + 10%). A current heat flow is calculated to be 47.5 mW/m^2 with a seabed temperature of 21 ^{o}C. The two sets of measured reflectance data (CSIRO and Robertson Research Australia Pty. Ltd.) are significantly lower than the modelled maturity trend, which is based on the present-day heat flow and seabed temperature (Fig. 7-13). The modelled maturity curve, on the basis of these corrected formation temperatures, is consistent with the T_{max} data, which may represent a lower limit maturity trend. Figure 7-14 shows the modelled histories of burial, temperature and maturity for this well.

7.5.3.2 Madeleine-1 thermal modelling

The Madeleine-1 well was drilled in the Dampier Sub-basin (Fig. 7-1). In this case, the formation temperatures are corrected from the measured well temperatures (BHT + 10 %). A current heat flow of 48.2 mW/m^2 (seafloor temperature = 23 ^{o}C) is estimated. The two sets of vitrinite reflectance data (measured by Robertson Research Australia Pty. Ltd. and Woodside Petroleum) from core and cutting samples fall significantly lower than the calculated maturity curve for the constant current heat flow model (Fig. 7-15A).

T_{max} data (measured by Robertson Research Australia Pty. Ltd. and Woodside Petroleum) from both core and cutting samples can be used to evaluate the thermal maturity trend in this well (Figure 7-15A). The T_{max} data with S_1 □ 1 used for the thermal modelling was examined using the REESA Rules. The constant current heat flow model provides a good match to the relatively reliable T_{max} data. The fact that the present-day heat flow model can match the present maturity indicator suggests that the thermal effect due to present-day burial has exceeded any thermal effect that may have been imprinted on the sedimentary rocks during the syn-rift phase as noted by Kaiko and Tingate (1996). To fit the modelled maturity trend, a rift-related heat flow can be calculated with varying water-sediments interface temperature due to palaeoseawater depth changes that contain uncertainties. The rift heat flow has a peak heat flow value about 63 mW/m^2 at about 155 Ma. Figures 7-16 to 7-18 show the difference between the thermal histories and hydrocarbon generation effects using the constant heat flow with the present seabed temperature and the rift heat flow with varying seabed temperatures. The rift-related heat flow history may be more reasonable for predicting histories of thermal maturity and hydrocarbon generation according to the rift tectonic setting of this basin.

7.5.3.3 Depuch-1 thermal modelling

The Depuch-1 well was drilled on the northern flank of the main depocentre in the Beagle Sub-basin. The sub-basin is situated at the northernmost of the elongate rift grabens and is separated from the Dampier Sub-basin by the De Grey Nose (Figure 7-1). Three formation temperatures were obtained from corrected BHTs (raw BHT + 10 %). The measured maturity profiles with R_o (measured by Robertson Research and Keiraville Konsultants), Eq VR (CSIRO Petroleum) and T_{max} data (Robertson Research) are shown in Fig. 7-19.

It should be also noted that some T_{max} values are likely to be suppressed by about 1 to 4 ^oC, due to HI > 150 to 389 in coal-related samples, and the observed vitrinite reflectance values in the Jurassic rocks may be suppressed by about 0.1 to 0.3 %. The corrected T_{max} data can be matched (Fig. 7-19) by the maturity model generated from the assumption of a constant current heat flow, which was calculated to be 49.4

mW/m^2 (seabed temperature = 21 ^oC). The modelled result suggests that the maturity level, about 0.6-1.0 % R_o in the Jurassic sequence of this well, is less sensitive to rifting heat flow modelling and that the Jurassic source rocks in this location experienced relatively low temperature increases during the earlier syn-rift phase. The fact that the present-day heat flow model and seabed temperature can match these maturity data further suggests that the sedimentary sequence is currently experiencing its maximum temperature. The modelled geohistory and thermal effect are shown in Fig. 7-20.

7.5.4 Thermal modelling for 2 wells on the Rankin Platform

7.5.4.1 North Gorgon-1 thermal modelling

The North Gorgon-1 well was drilled in the northern part of the Gorgon structure of the southern part of the Rankin Platform (Fig. 7-1), a relatively high structure, which forms the western boundary of the Barrow-Dampier Sub-basins. The Gorgon structure is a series of northeast-southwest trending, en-echelon horst blocks of the Rankin Platform. The horst blocks consist of Triassic rocks. During the Early-Middle Jurassic, the structure underwent uplift and erosion associated with the syn-rift phase. Hellinger and Sclater (1983) proposed that extension and subsidence within the rift phase is generally accompanied by uplift and erosion of the rift shoulders. Structural models by Stein (1994) show that some parts of the Rankin Platform have undergone in excess of 1.5 kilometres of rift-related uplift. Based on missing successions in the well data and interpreted seismic lines from the AGSO, the Lower Jurassic and the upper part of the Mungaroo Formation are missing and the erosional thickness is estimated to be 1500 to 2000 metres. Formation temperatures are based on DST temperatures. The maturity profiles, with R_o data (measured by Keiraville Konsultants) and T_{max} data (measured by Amdel) in Fig. 7-21, indicate that there is no obvious break at the boundary between the Mungaroo Formation and Barrow Group. The measured maturity data can be matched well by the model, which assumes a constant current heat flow of 57.1 mW/m^2 (seafloor temperature = 20 ^oC), irrespective of a missing section of Triassic and Lower Jurassic from 0 to 3200 metres. It is considered that the Rankin Platform as a western rift shoulder underwent a period of temperature decrease during the rift-associated uplift and erosion. This case illustrates that the graben shoulder has

possibly experienced a higher thermal effect, associated with the burial during the Cretaceous and Cainozoic, than in the syn-rift phase. In fact, it is most likely that the platform was undergoing a period of uplift and erosional cooling during the syn-rift phase. Additionally, the distribution of the highest heat flow during the rifting is commonly along the rift grabens rather than on a rift shoulder (Lysak, 1992). Figure 7-22 shows the modelled histories of burial and temperature in this well. This indicates that the maximum burial depth before the uplift and erosion is about 3040 m and the temperature is about 125 ^{o}C, and the present-day burial depth is about 4470 m and the temperature is about 165 ^{o}C.

7.5.4.2 North Rankin-1 thermal modelling

The North Rankin-1 well was drilled in the northern part of the Rankin Platform, adjacent to the Dampier Sub-basin to the east. The well penetrated the sedimentary section of the Upper Triassic to the Quaternary with the eroded section of the upper part of the Upper Triassic to the Lower Jurassic. There is a lack of the Middle-Upper Jurassic sequences and the Barrow Group at this well site. A major unconformity is the contact between the Upper Triassic sequence and the Winning Group (Valanginian to Cenomanian). A probable erosional thickness ranges from about 1500 m to 2000 m during the rifting of the continental breakup. The post-rift sequence of the Cretaceous-Cainozoic is 2535 m. Four formation temperatures were collected from the DST data and one corrected BHT (raw BHT + 10 %) at 1703 m. The maturity profiles with vitrinite reflectance data and T_{max} data (Robertson Research) in the Upper Triassic are shown in Fig. 7-23A. The measured maturity data can be modelled by the current heat flow of 53.5 mW/m^2 (seabed temperature = 21 ^{o}C) regardless of a missing section of Triassic and Lower Jurassic rocks from 0 to 2000 metres thick. Based on this model, the calculated R_o values prior to the rift-associated uplift and erosion may be 0.46-0.64 % for the top and bottom of the Mungaroo Formation and it underwent further maturation with a R_o increment of about 0.1 % from about 30 Ma due to the post-rift reburial (Fig. 7-23B). Its burial and thermal effect histories are shown in Fig. 7-24.

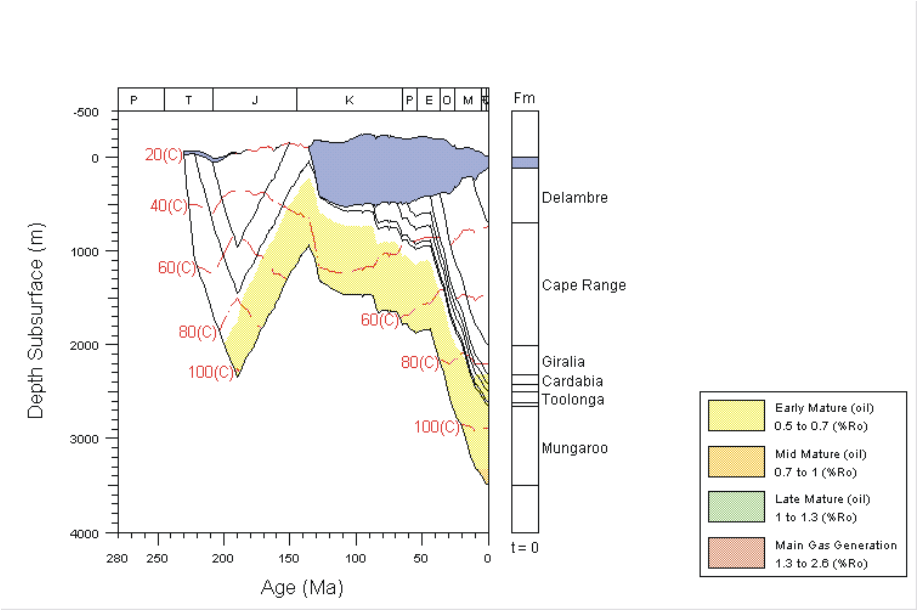

Fig. 7-24 The modelled geohistory and thermal effect using the current heat flow and seafloor temperature for the North Rankin-1 well.

7.5.5 Thermal modelling for 2 wells on the Exmouth Plateau

7.5.5.1 Investigator-1 thermal modelling

The Investigator-1 well was drilled in the southern Exmouth Plateau. The depositional and tectonic evolution of the Exmouth Plateau have been discussed by many authors (e.g. Barber, 1982, 1988; Exon and Colwell, 1994; Tindale et al., 1998). Based on the palynological analyses in the well-completion report, there is a condensed Jurassic interval (188 m) and a thick succession of the Barrow Group (1619 m). The Lower-Middle Jurassic interval is probably not completely represented, and is only 44 m thick. The formation temperatures are based on one Horner-plot-corrected temperature of 97.2 ^{o}C at 3592 m, and two corrected BHTs (raw BHT + 10 %). The maturity profiles with vitrinite reflectance (measured by A. C. Cook, 1979) and the T_{max} data (measured by BHP, 1993) are shown in Fig. 7-25A. There is an obvious break in the R_o profile at about 3000 m, and there are no T_{max} data in the Barrow Group. As a result of the breakup in the Valanginian, the unconformity is comprised of a contact between the Barrow Group and the

Muderong Shale (Tindale et al., 1998). The two segments of the R_o profile are unlikely to be caused by a discontinuous thermal effect between the Jurassic sequence and the Barrow Group due to a possible erosional period during the Middle Jurassic. The model, based on extrapolation of the current heat flow of 56.8 mW/m^2 (seafloor temperature = 5.5 ^oC) back in time, is inconsistent with the measured R_o values (Fig. 7-25A). A rift palaeoheat flow scenario is shown in Fig. 7-25B, and the modelled result is also shown in Fig. 7-25A. The rift thermal model matches the measured R_o and T_{max} profiles in the Triassic and Jurassic, but observed values are lower in the Barrow Group interval. This suggests that the measured R_o values in the Barrow Group should be inferred to be suppressed or incorrect. The syn-rift phase is assumed to commence in the earliest Jurassic (208 Ma) and continue to breakup (136 Ma). The modelled maximum heat flow, which subsequently decayed exponentially to the present-day value, was determined to be 78 mW/m^2, and was 37 % higher than the present heat flow of 56.8 mW/m^2. Figure 7-26 shows the geohistory and the modelled histories of temperature and thermal maturity using the rift-related heat flow history.

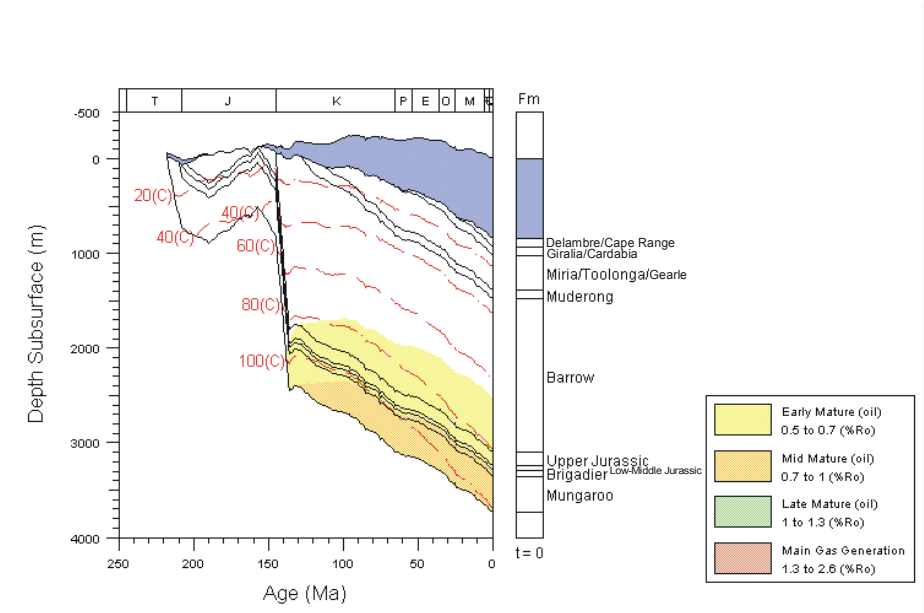

Fig. 7-26 The modelled geohistory and histories of temperature and thermal maturity using the rift-related heat flow history for the Investigator-1 well. The erosional thickness of 300 m was used during the Middle Jurassic.

7.5.5.2 Jupiter-1 thermal modelling

The Jupiter-1 well was drilled on an upthrown block of a fault half-graben on the central Exmouth Plateau. The well has a condensed Upper Jurassic interval of 15 m from the Callovian to the Tithonian. The Lower-Middle Jurassic sequence and Barrow Group are absent. The three profiles of the measured maturity data include vitrinite reflectance (measured by A. C. Cook, 1979, 1985 and AMDEL, 1996), Eq VR (CSIRO Petroleum) and T_{max} data (measured by Geotech, 1996) within the Mungaroo Formation of the Middle-Upper Triassic (Fig. 7-27A). The formation temperatures are all Horner-plot-corrected BHTs. It is difficult to get a fit between the observed maturity data and calculated (modelled) maturity curve, based on the present heat flow of 54.3 mW/m^2 (seabed temperature = 5 ^oC) in this well. A good fit between the observed and calculated maturity for this well is obtained using the rift heat flow model (Fig. 7-27B). The peak thermal influence during rifting on this well location is considered to be from 208 Ma to 155 Ma. The modelled maximum value of the rift palaeoheat flow was about 72 mW/m^2, which exponentially decreased to the present value during the post-rift phase. The peak heat flow value is about 33 % more than the present heat flow. Figure 7-28 is the geohistory, and thermal history associated with the rift-related heat flow.

7.6 Summary

Possible errors in the modelled palaeoheat flow may be related to the conceptual model for the present study, and also to input data, such as: (1) a single thermal event during syn-rifting, (2) the assumption of only vertical thermal conduction, and (3) uncertainties of the input data, such as thermal maturity, matrix thermal conductivity, formation temperature, palaeoseafloor or surface temperature, erosional thickness and hiatus time. These factors should be taken into consideration when evaluating the modelled results.

Heat flow modelling indicates that the measured thermal maturity data in some wells are consistent with rift heat flow models (Jarvis and McKenzie, 1980) associated with the Jurassic to earliest Cretaceous rifting in the sub-basins (190-136

Ma), the southern Exmouth Plateau (208-136 Ma) and central Exmouth Plateau (208-155 Ma). In the sub-basins, the modelled maximum rift heat flow is 67 mW/m^2 in Jurabi-1, which appears to be typical in the Barrow Sub-basin. However, the palaeoheat flow was found to be 105 mW/m^2 in Bowers-1. On the Exmouth Plateau, the modelled highest rift heat flow is 72 mW/m^2 in Jupiter-1, and 78 mW/m^2 in Investigator-1. This study may indicate that there is a relatively high heat flow during the syn-rift phase in the Exmouth, Barrow and Dampier Sub-basins. This thermal modelling suggests that it is necessary to use the rift heat flow model for predicting the history of thermal maturity and the timing of hydrocarbon generation of the Triassic and Jurassic source rocks along the depocentres of the Exmouth, Barrow and Dampier Sub-basins.

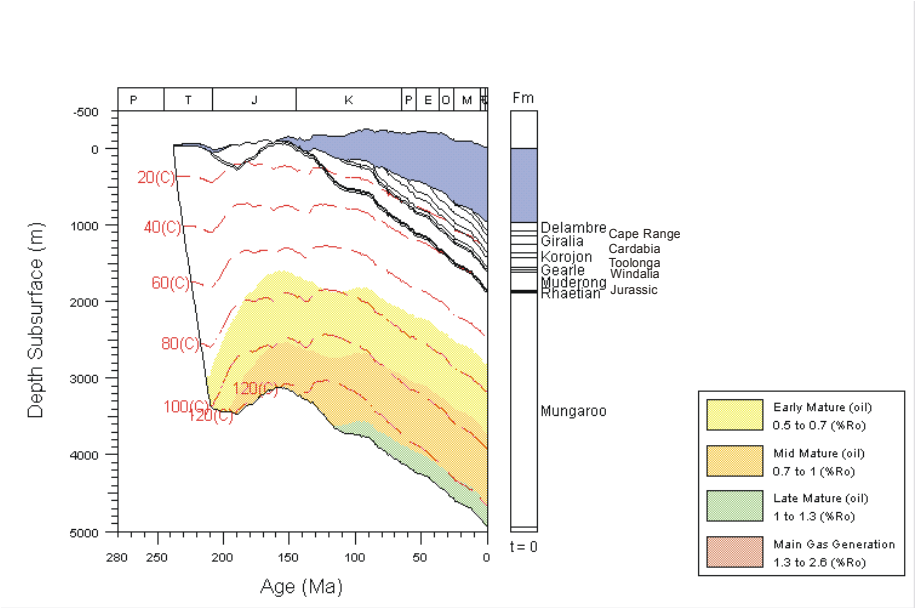

Fig. 7-28 The modelled geohistory and histories of temperature and thermal maturity using the rift-related heat flow history for the Jupiter-1 well.

It was found that the major problems influencing the reliability of T_{max} data for the assessment of thermal maturity were (1) contamination by drilling-mud additives in both cuttings and side wall cores (Chapter 4), and (2) suppression due to HI > 150, although natural bitumen, recycled organic matter and cavings may also present problems. In general, the reliable T_{max} data are consistent with the non-anomalous

(non-suppressed) R_o data and some Eq VR data, which plot according to the proposed R_o-T_{max} relationship (Fig. 7-2) for the basin. The relationship has been extensively tested with many wells in this study. This study indicates that reliable T_{max} data are important, and useful, to evaluate thermal maturity, especially where other maturity data are unavailable. The study shows the correlation developed between T_{max} and R_o in the detailed thermal modelling of individual wells and also indicates that a good, reliable correlation between T_{max} and R_o may go towards overcoming the problems associated with the anomalously low vitrinite reflectance. However, the proposed relationship of R_o to T_{max} is preliminary, and more study is needed to improve this correlation. It should be noted that the relationship between R_o and T_{max}, used in this study, may result in !3-10 % error for the calculated vitrinite reflectance.

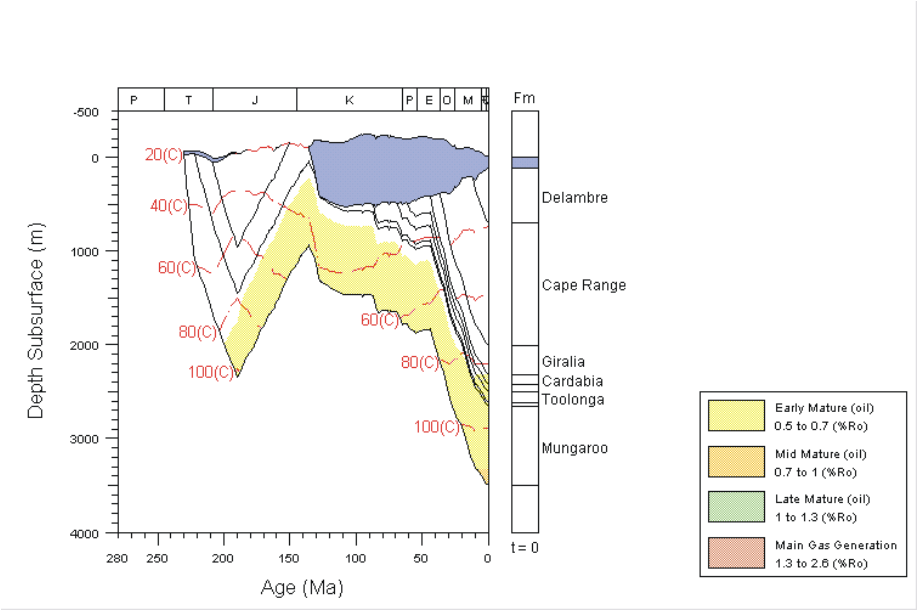

Fig. 7-24 The modelled geohistory and thermal effect using the current heat flow and seafloor temperature for the North Rankin-1 well.

7.5.5 Thermal modelling for 2 wells on the Exmouth Plateau

7.5.5.1 Investigator-1 thermal modelling

The Investigator-1 well was drilled in the southern Exmouth Plateau. The depositional and tectonic evolution of the Exmouth Plateau have been discussed by many authors (e.g. Barber, 1982, 1988; Exon and Colwell, 1994; Tindale et al., 1998). Based on the palynological analyses in the well-completion report, there is a condensed Jurassic interval (188 m) and a thick succession of the Barrow Group (1619 m). The Lower-Middle Jurassic interval is probably not completely represented, and is only 44 m thick. The formation temperatures are based on one Horner-plot-corrected temperature of 97.2 ^{o}C at 3592 m, and two corrected BHTs (raw BHT + 10 %). The maturity profiles with vitrinite reflectance (measured by A. C. Cook, 1979) and the T_{max} data (measured by BHP, 1993) are shown in Fig. 7-25A. There is an obvious break in the R_o profile at about 3000 m, and there are no T_{max} data in the Barrow Group. As a result of the breakup in the Valanginian, the unconformity is comprised of a contact between the Barrow Group and the

Muderong Shale (Tindale et al., 1998). The two segments of the R_o profile are unlikely to be caused by a discontinuous thermal effect between the Jurassic sequence and the Barrow Group due to a possible erosional period during the Middle Jurassic. The model, based on extrapolation of the current heat flow of 56.8 mW/m^2 (seafloor temperature = 5.5 ^oC) back in time, is inconsistent with the measured R_o values (Fig. 7-25A). A rift palaeoheat flow scenario is shown in Fig. 7-25B, and the modelled result is also shown in Fig. 7-25A. The rift thermal model matches the measured R_o and T_{max} profiles in the Triassic and Jurassic, but observed values are lower in the Barrow Group interval. This suggests that the measured R_o values in the Barrow Group should be inferred to be suppressed or incorrect. The syn-rift phase is assumed to commence in the earliest Jurassic (208 Ma) and continue to breakup (136 Ma). The modelled maximum heat flow, which subsequently decayed exponentially to the present-day value, was determined to be 78 mW/m^2, and was 37 % higher than the present heat flow of 56.8 mW/m^2. Figure 7-26 shows the geohistory and the modelled histories of temperature and thermal maturity using the rift-related heat flow history.

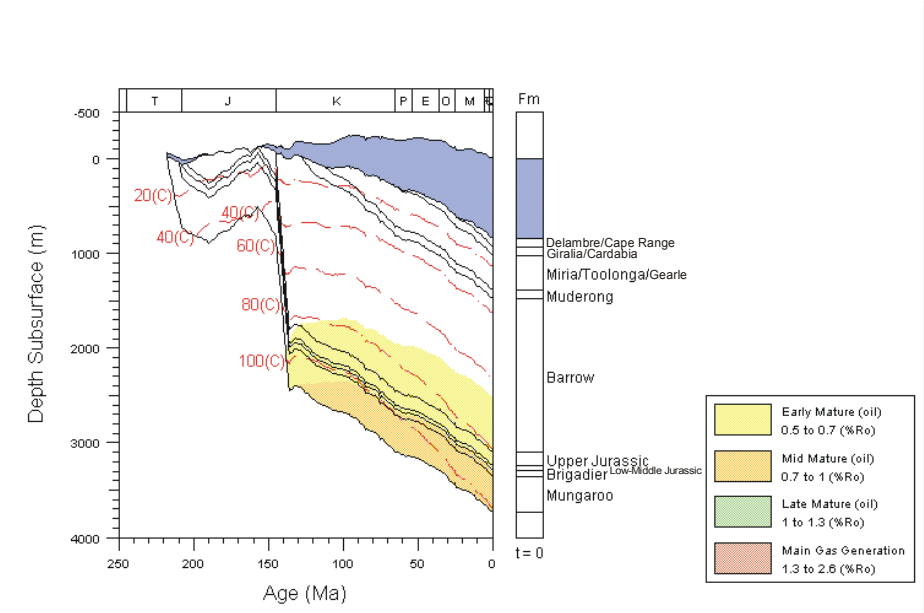

Fig. 7-26 The modelled geohistory and histories of temperature and thermal maturity using the rift-related heat flow history for the Investigator-1 well. The erosional thickness of 300 m was used during the Middle Jurassic.

7.5.5.2 Jupiter-1 thermal modelling

The Jupiter-1 well was drilled on an upthrown block of a fault half-graben on the central Exmouth Plateau. The well has a condensed Upper Jurassic interval of 15 m from the Callovian to the Tithonian. The Lower-Middle Jurassic sequence and Barrow Group are absent. The three profiles of the measured maturity data include vitrinite reflectance (measured by A. C. Cook, 1979, 1985 and AMDEL, 1996), Eq VR (CSIRO Petroleum) and T_{max} data (measured by Geotech, 1996) within the Mungaroo Formation of the Middle-Upper Triassic (Fig. 7-27A). The formation temperatures are all Horner-plot-corrected BHTs. It is difficult to get a fit between the observed maturity data and calculated (modelled) maturity curve, based on the present heat flow of 54.3 mW/m^2 (seabed temperature = 5 ^oC) in this well. A good fit between the observed and calculated maturity for this well is obtained using the rift heat flow model (Fig. 7-27B). The peak thermal influence during rifting on this well location is considered to be from 208 Ma to 155 Ma. The modelled maximum value of the rift palaeoheat flow was about 72 mW/m^2, which exponentially decreased to the present value during the post-rift phase. The peak heat flow value is about 33 % more than the present heat flow. Figure 7-28 is the geohistory, and thermal history associated with the rift-related heat flow.

7.6 Summary

Possible errors in the modelled palaeoheat flow may be related to the conceptual model for the present study, and also to input data, such as: (1) a single thermal event during syn-rifting, (2) the assumption of only vertical thermal conduction, and (3) uncertainties of the input data, such as thermal maturity, matrix thermal conductivity, formation temperature, palaeoseafloor or surface temperature, erosional thickness and hiatus time. These factors should be taken into consideration when evaluating the modelled results.

Heat flow modelling indicates that the measured thermal maturity data in some wells are consistent with rift heat flow models (Jarvis and McKenzie, 1980) associated with the Jurassic to earliest Cretaceous rifting in the sub-basins (190-136

Ma), the southern Exmouth Plateau (208-136 Ma) and central Exmouth Plateau (208-155 Ma). In the sub-basins, the modelled maximum rift heat flow is 67 mW/m^2 in Jurabi-1, which appears to be typical in the Barrow Sub-basin. However, the palaeoheat flow was found to be 105 mW/m^2 in Bowers-1. On the Exmouth Plateau, the modelled highest rift heat flow is 72 mW/m^2 in Jupiter-1, and 78 mW/m^2 in Investigator-1. This study may indicate that there is a relatively high heat flow during the syn-rift phase in the Exmouth, Barrow and Dampier Sub-basins. This thermal modelling suggests that it is necessary to use the rift heat flow model for predicting the history of thermal maturity and the timing of hydrocarbon generation of the Triassic and Jurassic source rocks along the depocentres of the Exmouth, Barrow and Dampier Sub-basins.

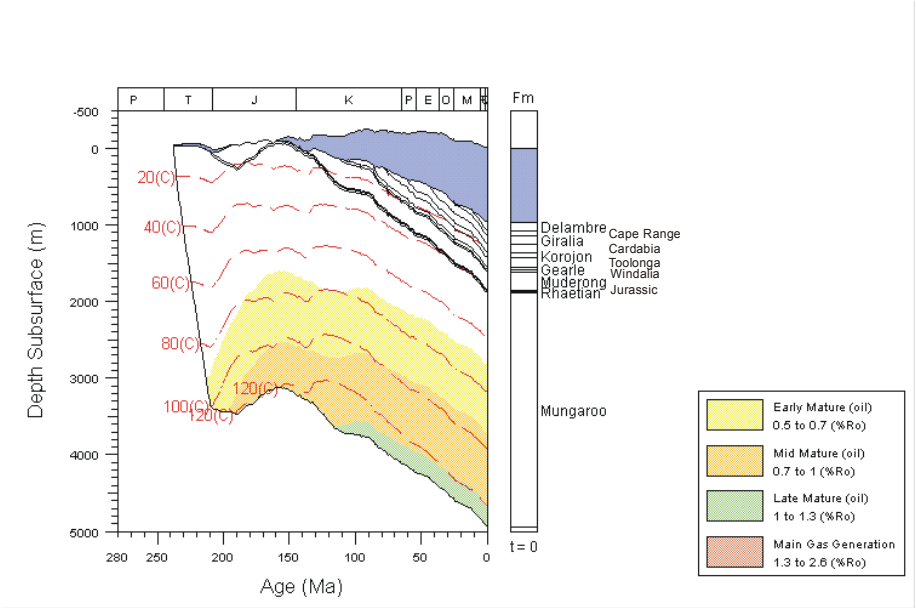

Fig. 7-28 The modelled geohistory and histories of temperature and thermal maturity using the rift-related heat flow history for the Jupiter-1 well.

It was found that the major problems influencing the reliability of T_{max} data for the assessment of thermal maturity were (1) contamination by drilling-mud additives in both cuttings and side wall cores (Chapter 4), and (2) suppression due to HI > 150, although natural bitumen, recycled organic matter and cavings may also present problems. In general, the reliable T_{max} data are consistent with the non-anomalous

(non-suppressed) R_o data and some Eq VR data, which plot according to the proposed R_o-T_{max} relationship (Fig. 7-2) for the basin. The relationship has been extensively tested with many wells in this study. This study indicates that reliable T_{max} data are important, and useful, to evaluate thermal maturity, especially where other maturity data are unavailable. The study shows the correlation developed between T_{max} and R_o in the detailed thermal modelling of individual wells and also indicates that a good, reliable correlation between T_{max} and R_o may go towards overcoming the problems associated with the anomalously low vitrinite reflectance. However, the proposed relationship of R_o to T_{max} is preliminary, and more study is needed to improve this correlation. It should be noted that the relationship between R_o and T_{max}, used in this study, may result in !3-10 % error for the calculated vitrinite reflectance.

CHAPTER 8 THERMAL MATURITY AND THERMAL MODELLING WITHIN THE OVERPRESSURED JURASSIC ROCKS IN THE BARROW AND BAMBRA WELLS

8.1 Introduction

Overpressure is common in many sedimentary basins worldwide (e.g. Bigelow, 1994b; Swarbrick and Osborne, 1998). Disequilibrium compaction and fluid volume expansion during gas generation are considered to be the major contributors to large magnitude overpressure (e.g. Swarbrick and Osborne, 1998). Hunt (1990) has noted that much of the world's oil and gas has been generated from source rocks in deep (>3000 m) overpressured fluid compartments, and the fluid thermal expansion and hydrocarbon generation result in overpressure within sealed compartments of sedimentary basins. McTavish (1998) has also pointed out that the abnormal profiles of organic matter maturation in overpressured sequence, which express the retardation of maturation, are a worldwide phenomenon.

Vitrinite reflectance (R_o) is the most widely used maturity indicator in petroleum exploration (e.g. Tissot and Welte, 1984; Allen and Allen, 1990; Hunt, 1996). A common interpretation for unexpectedly low R_o is vitrinite-reflectance suppression, which occurs when measurement is made on (1) liptinite-rich organic matter, and (2) a perhydrous vitrinite population (e.g. Hutton and Cook, 1980; Price and Barker, 1985; Raymond and Murchison, 1991), or (3) vitrinite deposited under marine influence (e.g. Wilkins et al., 1992a; Hunt, 1996; Gurba and Ward, 1998). In overpressured systems, an alternative explanation for anomalously low vitrinite reflectance values is due to overpressure retardation of organic matter maturation (McTavish, 1978; Hao et al., 1995; McTavish, 1998; Carr, 1999). McTavish (1978) described possible pressure retardation of vitrinite reflectance in some North Sea wells, and Hao et al. (1995) found that overpressure has significantly retarded organic matter maturation and petroleum generation from the LD3011 well in the Yinggehai Basin, South China Sea. In contrast, Hunt (1979; 1996) emphasized that vitrinite maturation is not significantly affected by pressure, only by temperature. Tissot and Welte (1984) pointed out that the influence of pressure is probably

subordinate to that of temperature on the basis of geological studies and experimental work. Furthermore, Allen and Allen (1990) stated that pressure is a negligible factor in thermal maturity. These authors stressed that the most important factor in thermal maturity is temperature, with pressure being relatively unimportant in hydrocarbon generation. Similarly, Khorasani and Michelsen (1994) demonstrated that the effect of overpressure in shales has no important influence on the observed relationship between temperature and vitrinite reflectance.

The unusually steep vitrinite reflectance profiles, mainly in the Jurassic and the Lower Cretaceous formations in the Northern Carnarvon Basin, North West Shelf of Australia, have been studied by various authors (e.g. Wilkins et al., 1992a; Kaiko and Tingate, 1996; Samuelsson and Middleton, 1998). Wilkins et al. (1992a) proposed that the two main sources of error in the vitrinite reflectance data for some North West Shelf wells are the suppression of vitrinite reflectance with marine influence and/or inaccurate identification of vitrinite in dispersed organic matter. They also indicated that some North West Shelf wells show a surprisingly small increase in vitrinite reflectance with increasing depth that is impossible to fit with thermal maturity modelling.

McTavish (1998) maintained that apparently abnormal maturity profiles in source rocks found in overpressured sequences are widespread in the world, including other unpublished examples from the North West Shelf of Australia. With regard to the Australian North West Shelf, and in the Barrow Sub-basin of the Northern Carnarvon Basin specifically, the deeper part of some anomalous vitrinite reflectance profiles is associated with high overpressure (e.g. Kopsen and McGann, 1985; Wilkins et al., 1992a; Swarbrick and Hillis, 1999). Kopsen and McGann (1985) described present-day thermal maturities of the Barrow and Bambra wells below expected values with the apparent vitrinite under-maturity occurring within the highly overpressured Jurassic sequence. Wilkins et al. (1992a) pointed out that the lower part of the Jurassic sequence in Barrow Deep-1 is strongly overpressured, but considered that the overpressure effect on vitrinite reflectance was likely to be small. Swarbrick and Hillis (1999) suggested that the vitrinite reflectance data from the North West Shelf basins should be used with caution where overpressuring is significant. They further suggested that the retardation of maturation was largely

responsible for delayed petroleum-trap charging, which was at variance with the charge time predicted by some basin modelling exercises. It is clear from the above that there is an unsolved problem: are the anomalously low vitrinite reflectance profiles in the overpressured Jurassic sequence of the Barrow Sub-basin due to overpressure-related retardation of thermal maturity? This topic is believed to merit further attention. This chapter aims to improve an understanding of whether the overpressure has a determinable influence on thermal maturity and petroleum generation in two separate case studies using measured maturity data and thermal modelling in the overpressured Jurassic section in the Barrow and Bambra wells. The wells for the case studies are (1) the Barrow-1/Barrow Deep-1 wells, and (2) the Bambra-1/Bambra-2 wells (Fig. 6-1).

8.2 Thermal maturity

The thermal maturity data used in this study include R_o, equivalent vitrinite reflectance (Eq VR) and Rock Eval T_{max}. The R_o data in three wells and Eq VR in Barrow-1 are listed in Table 8-1. It can be seen that the majority of measured vitrinite reflectance values in these three wells are unexpectedly low compared with Eq VR and Rock-Eval T_{max} data. Rock-Eval T_{max} data for Bambra-2, Barrow Deep-1 and Barrow-1 are listed in Table 4-1, Tables 8-2 and 8-3, respectively. Figures 8-1 and 8-2 show that the Jurassic section is highly overpressured in these wells and the Rock-Eval T_{max} data generally increase with increasing depth. It should be noted that the T_{max} data used in Bambra-2 are the acceptable and normal values in Table 4-1. However, it is uncertain whether the thermal maturity has been retarded in the overpressured zone. It needs to be further studied, combined with more maturity parameters and thermal modelling.

The molecular parameters of thermal maturity from gas chromatography (GC) and gas chromatography-mass spectrometry (GC-MS) analyses of saturated hydrocarbon fractions from paraffinic crude oils and rocks in the Barrow and Bambra areas are given in Table 8-4. Volkman et al. (1983) demonstrated that these crude oils in the Barrow Sub-basin had a source in the Upper Jurassic Dingo Claystone formation. The distributions of *n*-alkane hydrocarbons from GC analyses on the extracts of the

conventional core samples (4274.2 m and 4282.9 m) show quite high levels of thermal maturity (Fig. 4-2, A and B). Peters and Moldowan (1993) and Hunt (1996) recommend that the ratios of C_{29} 20S/(20S+20R) and C_{29} ββ/(ββ+αα) steranes can be used as maturity indicators with maturity ranges, compared with vitrinite reflectance, between < 0.4-0.8 % and < 0.4-0.9 % R_o respectively. As can be expected on the basis of Peters and Moldowan (1993) and Hunt (1996), the traditionally used biomarker maturity parameters based on steranes for the source rock samples at 3610 m, 4274 m and 4283 m (A and B; Table 8-4) in the overpressured zone have all reached their equilibrium values. The steadily decreasing pristane/*n*-C_{17} and phytane/*n*-C_{18} ratios in rocks (C and D; Table 8-4) with burial depth indicate that the thermal maturity of the source rocks in the overpressured interval increases with increasing depth (temperature). This organic geochemical evidence indicates that the organic matter in the source rocks of the observed overpressured interval in the Barrow and Bambra areas has experienced moderate to high levels of thermal maturation and that a detectable maturation retardation has not been observed from the sedimentary organic matter in the overpressured system.

8.3 Data sets for thermal maturity modelling

Key input data for the modelling comprise the present thickness of the stratigraphic interval, lithology (Table 8-5), absolute age, measured formation temperatures (Table 8-6), thermal maturities and palaeobathymetries based on the data from Dr. Alex Kaiko (personal communication). The porosity-depth relationship for backstripping established by Falvey and Middleton (1981) was adopted for the modelling of burial histories. In the study areas of the selected wells, there is no significant erosion (Ellis et al., 1999) to influence the maturity modelling, although uplift may have occurred during the Tertiary (Densley et al., 2000). Hiatuses have been treated as periods of non-deposition. Some present-day geothermal parameters are shown in Table 6-1. Formation temperatures used in this thermal modelling are listed in Table 8-6.

Table 8-1 Measured vitrinite reflectance for three wells and Eq VR values for the Barrow-1 well in the Barrow Sub-basin

Barrow-1				Barrow Deep-1				Bambra-2	
Depth (m)	[b]R_o (%)	Depth (m)	[c]Eq VR (%)	Depth (m)	[d]R_o (1) (%)	Depth (m)	[e]R_o (2) (%)	Depth (m)	[a]R_o (%)
1013	0.36	1261	0.5	2934	0.63	3053	0.78	2616	0.53
1166	0.37	1679	0.53	3025	0.61	3354	1.00	2624	0.51
1288	0.38	1808	0.62	3208	0.63	3656	0.98	2734	0.45
1349	0.42	1981	0.68	3300	0.76	3960	1.00	2815	0.51
1641	0.44	2039	0.78	3391	0.73	3964	1.68	2955	0.51
1982	0.48 C	2371	0.80	3513	0.86	4290	1.70	3056.4	0.49
2222	0.48 C	2597	0.86	3604	0.93	4650	2.17	3250	0.47
2294	0.50	2835	0.98	3787	0.89			3560	0.53
2402	0.62 Cs			4336	1.17			3671	0.57
2416	0.52			4427	1.10			3890	0.84
2597	0.51 C			4610	1.14			4447	0.97
2835	0.56 C								
2835	0.73 Cs								
2903	0.56								

a: R_o data all from side-wall cores in Bambra-2 were measured by Australian Mineral Development Laboratories (Amdel) (1983).

b: R_o data in Barrow-1 were measured by Robertson Research Australia Pty. Ltd. (1964). C: Core sample. Cs: Core samples, the R_o was measured by Cook and Kanstler (1980).

c: Eq VR data in Barrow-1 were measured by CSIRO Petroleum (1992).

d: R_o (1) data in Barrow Deep-1 were measured by Robertson Research Australia Pty. Ltd. (1979).

e: R_o (2) data in Barrow Deep-1 were measured by Cook and Kanstler (1980).

Table 8-2 Rock-Eval pyrolysis data for the cuttings samples in the Barrow Deep-1 well in the Barrow Sub-basin

Depth (m)	**T_{max} (^oC)**	**S_1**	**S_2**	**S_3**	**TOC (wt. %)**	**HI**	**OI**	**PI**
2941-2956	440		0.9048	0.8700	1.74	52	50	
2941-2956	443		1.4616	1.3440	1.68	87	80	
3002-3017	445 ?	0.1265	0.5060	1.9780	2.30	22	86	0.2
3048-3063	447	0.3073	2.7664	1.3286	1.82	152	73	0.1
3216-3231	451 ?	0.5101	1.1904	0.9176	2.48	48	37	0.3
3505-3520	459		0.3875	0.8835	1.55	25	57	
3932-3947	462	0.2923	2.6314	0.4014	2.23	118	18	0.1

Note: Rock-Eval data were collected from the report prepared by Robertson Research Australia Pty. Ltd., 1986.

T_{max}: Temperature of the top of S_2 peak; S_1: Free hydrocarbons (mg HC/g rock); S_2: Pyrolysable hydrocarbons (mg HC/g rock); S_3: CO_2 from pyrolysis (mg CO_2/g rock); TOC: Total organic carbon (wt. %); HI: Hydrogen index (S_2 % 100/TOC); OI: Oxygen index (S_3 % 100/TOC); PI: Production index (S_1/S_1+S_2).

Table 8-3 Rock-Eval pyrolysis data for the cuttings and core samples in the Barrow-1 well in the Barrow Sub-basin

Depth (m)	**T_{max} (^{o}C)**	**S_1**	**S_2**	**S_3**	**TOC (wt. %)**	**HI**	**OI**	**PI**	**Type of Sample**
1484-1500	428		1.6642	1.0676	3.14	53	34		Cuttings
1484-1500	434		1.3797	0.9417	2.19	63	43		Cuttings
1808	437	0.1280	1.1520	0.5184	1.44	80	36	0.1	Core
1942-1957	436		0.9322	0.8374	1.58	59	53		Cuttings
2222	437	0.2598	1.0395	0.8085	1.65	63	49	0.2	Core
2286-2301	437		1.0065	0.8784	1.83	55	48		Cuttings
2301-2316	440	0.2176	2.8910	0.3920	2.45	118	16	0.1	Cuttings
2423-2438	435		0.6032	0.7592	1.04	58	73		Cuttings
2499-2515	435		0.5978	1.2566	1.22	49	103		Cuttings
2515-2530	440		1.8240	0.5320	1.90	96	28		Cuttings
2597	440	0.3832	1.5330	0.6510	2.10	73	31	0.2	Core
2667-2682	439		0.7503	0.3843	1.83	41	21		Cuttings
2758-2774	444		1.3213	0.9593	1.81	73	53		Cuttings
2804-2819	439		2.3998	0.4732	1.69	142	28		Cuttings
2804-2819	440	0.2064	2.3739	0.2895	1.93	123	15	0.1	Cuttings
2835	441	0.1200	1.0800	0.6048	1.44	75	42	0.1	Core
2865-2880	443		0.2680	0.6120	1.80	126	34		Cuttings
2880-2896	444	0.1332	1.3468	0.8806	2.59	52	34	0.1	Cuttings
2911-2926	441	0.5557	2.2230	0.6270	1.90	117	33	0.2	Cuttings
2972-2981	450	0.5628	2.2512	0.4020	2.01	112	20	0.2	Cuttings
2972-2981	444	0.1272	1.1450	0.8244	2.29	50	36	0.1	Cuttings

* Rock-Eval data were collected from the report prepared by Robertson Research Australia Pty. Ltd., 1986.

T_{max}: Temperature of the top of S_2 peak; S_1: Free hydrocarbons (mg HC/g rock); S_2: Pyrolysable hydrocarbons (mg HC/g rock); S_3: CO_2 from pyrolysis (mg CO_2/g rock); TOC: Total organic carbon (wt. %); HI: Hydrogen index (S_2 % 100/TOC); OI: Oxygen index (S_3 % 100/TOC); PI: Production index (S_1/S_1+S_2).

Table 8-4 Molecular parameters of thermal maturity for rocks in the Barrow and Bambra areas

Well	Sample	Depth (m)	Formation	A	B	C	D	R_o [e] (%)	Pressure
Bambra-2[a]	Oil	2032-2033.5	Barrow	0.55	0.49	0.29	0.13		
Bambra-1[a]	Oil	2053.25	Barrow	0.53	0.52	0.30	0.12		
Barrow[b]	Oil	1890	Dupuy	0.50	0.43	0.21	0.08		
Barrow[b]	Oil	2010	Dupuy	0.52	0.48	0.19	0.07		
Bambra-1[a]	Oil	3640.5	Dingo	0.59	0.53	0.30	0.15		
Barrow-1[a]	Core 10	1036 (ST)	Barrow	0.21	0.25	1.30	0.64	0.45	Normal
Barrow-1[a]	Core 34	2402 (ST)	Dingo	0.45	0.38	0.39	0.23	0.70	Normal
Bambra-1[b]	Core	2715.5 (CS)	Dupuy	0.41	0.32	0.58	0.26	0.80	Normal
Barrow-1[a]	Core 37	2835 (CS)	Dingo	0.54	0.39	0.40	0.22	0.90	Overpressure
Bambra-1[b]	Cuttings	3610 (CS)	Dingo	0.53	0.54	0.41	0.18	1.23	Overpressure
Bambra-2[c]	Core	4274 (CS)	Athol	0.53	0.54	0.22 [b]	0.13 [b]	1.70	Overpressure
Bambra-2[d]	Core	4283 (CS)	Athol	0.53	0.53	0.27	0.12	1.70	Overpressure

ST: Siltstone; CS: Claystone

A: C_{29} 20S/(20S+20R) steranes

B: C_{29} ββ/(ββ+αα) steranes

C: Pristane / *n*-heptadecane (*n*-C_{17})

D: Phytane / *n*-octadecane (*n*-C_{18})

a: Data were taken from Volkman et al. (1983).

b: Data were collected from the well-completion reports.

c: GC-MS analysis was carried out at the Curtin University of Technology, Perth, Australia (2001).

d: GC-MS analysis was carried out at the Geological Survey of Canada, Calgary (2001).

e: R_o (%) values were predicted by thermal maturity modelling.

Table 8-5 The percentages of four lithologies for various formations of the two selected wells in the Barrow Sub-basin

Formation	Bambra-2				Barrow Deep-1			
	Sands. (%)	Silts. (%)	Clays. (%)	Limes. (%)	Sands. (%)	Silts. (%)	Clays. (%)	Limes. (%)
Delambre	0	0	0	100				
Cape Range	0	0	0	100	0	0	0	100
Giralia	0	10	10	80	0	13	8	79
Cardabia	0	0	5	95	0	0	5	95
Toolonga	10	0	30	60	0	0	40	60
Gearle	5	45	45	5	0	60	26	14
Windalia	0	30	65	5	35	60	5	0
Muderong	8	37	50	5	15	16	66	3
Barrow	80	5	10	5	72	21	5	2
Dupuy	45	25	27	3	39	57	3	1
Dingo	23	25	51	1	16	34	49	1
Athol	10	30	59	1	2	18	78	2

Sands.: Sandstone; Silts.: Siltstone; Clays.: Claystone; Limes.: Limestone

Table 8-6 Formation temperatures for the Bambra-2 and Barrow Deep-1 wells in the Barrow Sub-basin

Bambra-2			Barrow Deep-1		
Depth (m)	Formation Temperature (^oC)	Description	Depth (m)	Formation Temperature (^oC)	Description
2423	102.5	Horner Plot	3247	134	Production Test
3085	113	Horner Plot	3332	137	Production Test
3672	135	Horner Plot	3431	139	Production Test
4050	158.5	Horner Plot	3447	132	DST
4477	170	Horner Plot	3467	143	DST
4584	175	Horner Plot	4153	161	Horner Plot

8.4 Thermal maturity modelling

Palaeotemperatures were calculated using the transient-heat-flow model with a constant heat-flow history (calculated current heat flow) and seabed/surface temperature through time, because the palaeotemperatures in this region experienced during the rifting phase may have been equalled, or exceeded, by those associated during the later sag-phase sedimentation (Kaiko and Tingate, 1996; Nielsen, 1996). Palaeotemperatures were also calculated using a rift-related heat flow model and varying seabed/surface temperature over geological time. The rift-related heat flow history was calculated based on the modified Jarvis and McKenzie (1980) algorithm in the BasinMod 1D. The method of temperature calculation takes into account the thermal conductivity plus the heat capacity of the lithologies in this model. The kinetics of vitrinite maturation is a function of temperature and time. R_o curves were calculated using the chemical kinetic model of vitrinite reflectance (Sweeney and Burnham, 1990) in the BasinMod 1D.

8.4.1 Barrow-1 thermal modelling

Figure 8-3 shows the modelled maturity curves and temperature line in Barrow-1, which correspond to the upper part of Barrow Deep-1. The formation temperatures, calculated current heat flow and surface temperature are based on the values from Barrow Deep-1 (Tables 6-1 and 8-6). The modelled temperature line is consistent with the corrected BHTs (raw BHT + 10 %) in this well. The modelled result indicates that the measured R_o data (Table 8-1) are much lower than the calculated maturity curves. Nevertheless, both Eq VR data and T_{max} data measured from core and cutting samples can be matched using the current heat flow (surface temperature = 25 ^oC) (Fig. 8-3). According to the fluid pressure profile in Fig. 8-1, sedimentary rocks shallower than 2650 m are normally pressured, and 2650 m to a total depth of 2970 m is the pressure transition zone in this well. This result indicates that the measured R_o is probably suppressed and suggests that the anomalously steep vitrinite reflectance profile should not be related to the pore fluid pressure. Fig. 8-4 shows the modelled geohistory and histories of temperature and thermal maturity using the constant heat flow and surface temperature histories for this well.

8.4.2 Barrow Deep-1 thermal modelling

Figure 8-5 shows that the modelled maturity curve was obtained from the constant current heat-flow history as in the Barrow-1 modelling (Tables 6-1 and 8-6). The measured maturity data, which indicates two sets of vitrinite reflectance values (Table 8-1) and T_{max} data, are from the overpressured Jurassic source section. The R_o (1) data were measured by Robertson Research Australia Pty. Ltd. (1979) (open-file data) and the R_o (2) data by Cook and Kantsler (1980). Both R_o datasets are generally lower than the modelled maturity curves. However, the anomalously low R_o values are inconsistent with low maturity and are not supported by Rock-Eval data.

The predicted maturity curve obtained from the present-day heat flow and surface temperature (Fig. 8-5) is consistent with the T_{max} data, and the measured R_o (2) data for the three deepest values of Cook and Kantsler (1980). After a comparison of the three deepest R_o (2) values and the reliable T_{max} values with the good-fit maturity curve, it is found that there is also no reliable evidence to support overpressure influence on the thermal maturity in the highly overpressured Jurassic section. Also, the Jurassic source rocks between 3150-4550 m have experienced moderate to over maturity consistent with the predicted maturity (R_o: 1.05-2.2 %) between 3150-4550 m with small to very little remaining hydrocarbon generation potential (most of hydrogen indices range from < 10 to 50, while TOC range from 1 % to 2.5%) in the overpressured sequence, whereas the three hydrogen indices between 60 to 110 at about 3900-4170 m are thought to be due to some contribution of solid bitumen (5 % of solid bitumen content at 4145 m) based on the organic petrographic analysis of Teerman (1994) (Fig. 8-1). This case study indicates that the anomalously low R_o data, measured by Robertson Research Australia Pty. Ltd. and Cook and Kantsler (1980), are not significantly affected by the overpressuring. It should be noted that casing point control and careful sample scrutiny confirm that cavings are not responsible for the anomalously low R_o values (Fig. 8-1). Figure 8-6 shows the modelled histories of burial and thermal effect using the constant thermal condition for this well. Figure 8-7 shows the calculated cumulative oil and gas generation from the Dingo Claystone and Athol Formation with the constant heat flow and surface in this well.

Additionally, a good-fit between the valid maturity data (T_{max} data and R_o values) and the calculated maturity curve was also obtained from a rift heat flow model (Fig. 8-8). Figure 8-9 shows the modelled histories of burial, temperature and thermal maturity. Figure 8-10A indicates the rifting heat flow model used in this modelling, which has a maximum heat flow of about 67 mW/m^2 during the syn-rift phase and varying seabed temperature (or surface temperature). Figures 8-10B and 8-10C indicate the cumulative oil and gas generation from the Dingo Claystone and Athol Formation using the rift heat flow history for this well. It should be noted that the modelled results indicate the difference of the histories of temperature, maturity and hydrocarbon generation using different thermal models (Figures 8-6, 8-7, 8-9 and 8-10).

8.4.3 Bambra-2 thermal modelling

Good quality T_{max} data (acceptable and normal T_{max} data in Table 4-1 and Fig. 8-2) from conventional core and SWC samples were used for thermal maturity modelling in this well. Figure 8-11 shows the correlation between the modelled maturity curve and the observed R_o and T_{max} data in this well. The current heat flow of 56 mW/m^2 was estimated from the formation temperatures (Horner-plot-corrected BHTs) and seafloor temperature (24 C^o). The model produces the predicted temperature line and the maturity curve approximately fits to both the measured formation temperatures and T_{max} data. The measured vitrinite reflectance values, all from side-wall cores, are much lower than the modelled maturity pattern and T_{max} data trend. This suggests that the observed R_o data are anomalously low and probably suppressed in agreement with Kaiko and Tingate (1996). It is possible that the true maturity trend in the Jurassic rocks may be better indicated by the T_{max} values from core samples.

These are corroborated by measurements of vitrinite reflectance on a Bambra-2 conventional core at 4274-4283 m, which range between about 1.2 % and 2.0 % R_o (measured by Dr L.W. Gurba at the University of New South Wales, Australia). Six T_{max} values of 484-490 ^oC (Table 4-1), measured from the conventional core and extracted SWC samples at 4225-4301 m, correspond to R_o values of about 1.5-1.8 % (Tissot and Welte, 1994). The modelled R_o at 4280 m in Bambra-2 is 1.6-1.8 %. The

n-alkane distributions, from GC analyses on saturated hydrocarbon fractions of the conventional core extracts (A and B; Fig. 4-1), represent a high mature organic matter and suggest that this source rock is within a wet gas and condensate generating stage, which fits well with the T_{max} values from the conventional core. Therefore, the predicted R_o values of about 1.7 % could be the true maturity level for the conventional core.

In conjunction with the reliable pyrolysis data, biomarker maturity, *n*-alkane distributions and kinetic modelling of thermal maturity, the T_{max} values are believed to represent the true trend of thermal maturity in this well. This strongly suggests that the anomalously low vitrinite reflectance need not necessarily be a function of overpressure in the Jurassic shaley sequence.

Hunt (1996) pointed out that high geothermal gradients in overpressured shales are attributed to the low thermal conductivity of such shales that seem to act as heat insulators causing temperature increase, and this can enhance hydrocarbon generation. High porosity in the undercompacted zone yields a lower bulk thermal conductivity, and this increases the geothermal gradient. Sensitive analysis for low thermal conductivity in the overpressured Jurassic shaley sequence was carried out in this modelling, but it should be noted that this parameter does not influence the conclusions of this paper.

Figures 8-12 and 8-13 show the calculated geohistory, temperature and maturity histories, and the cumulative hydrocarbon generation from the Dingo Claystone and Athol Formation obtained using the constant heat flow and seafloor temperature.

In addition, the good T_{max} values from Bambra-2 can be also matched by the rift-related heat flow history (Fig. 8-14). Figure 8-15 displays the calculated geohistory, histories of temperature and maturity. Figure 8-16A shows the rifting heat flow history which exhibits the rift heat flow increase during 190-136 Ma with the maximum value of 68 mW/m^2 at 136 Ma and exponentially decreases in the post-rift phase. Figures 8-16B and 8-16C show the cumulative hydrocarbon generation from the Dingo Claystone and Athol Formation obtained from the rifting heat-flow

models. The histories of thermal effect and hydrocarbon generation obtained from the two heat flow models (constant and rift) are different.

8.5 Discussion

Some controversy surrounds the retardation of hydrocarbon generation in overpressured zones. Cecil et al. (1977) and Carr (1999) considered that overpressure can retard thermal maturity and hydrocarbon generation because the generated light component is unable to escape, or there is insufficient space for the generated hydrocarbons in the overpressured system. Cecil et al. (1977) pointed out that the overpressured zone behaves as a closed thermodynamic system, thus the expulsion of light hydrocarbons is retarded and organic metamorphism is inhibited. Hao et al. (1995) and Osborne and Swarbrick (1997) considered that hydrocarbon generation, and cracking to gas, may be self-limiting in a sealed system because pressure buildup may retard further organic metamorphism. In contrast, Hunt (1990) proposed that the generation and migration of oil and gas in sealed overpressured systems, plus thermal expansion of pore fluids causes fracturing of pressure seals during periods of basin sinking, and are associated with the episodic process of seal breakout and resealing cycles. In an overpressured system, fluid flow is limited, but not totally restricted by low-permeability rocks (e.g. Bredehoeft et al., 1994). Overpressures caused by hydrocarbon generation can form microfractures, which can act as migration pathways, based on geological observation of the petroleum expulsion phenomena (e.g. Düppenbecker et al., 1991; Márquez and Mountjoy, 1996). Many authors also attribute overpressure development in sedimentary basins to petroleum generation, and fluid-volume expansion during oil and gas generation and thermal cracking of crude oil to gas within a sealed compartment (e.g. Spencer, 1987; Hunt, 1990; Düppenbecker et al., 1991; Bredehoeft et al., 1994; Luo and Vasseur, 1996; Márquez and Mountjoy, 1996; Swarbrick and Osborne, 1998).

The observation of thin-sections of the claystone from the conventional core at 4274-4283 m in Bambra-2 indicates that the Jurassic source rocks contain bitumen. Teerman (1994) presented data indicating less than 5 % to 5 % bitumen in the organic matter of the Upper Jurassic samples, based on the study of visual compositions of kerogen. Perhaps lower than expected vitrinite reflectance is related

to solid bitumen to some extent, as suggested by Lo (1992). Similarly, anomalously low T_{max} values may also be influenced by an increase in heavy bitumen content in overpressured source rocks because these generated heavy hydrocarbons are not expelled efficiently. Vandenbroucke et al. (1983) showed that the T_{max} values measured on kerogen in the high pressure zone of the Handil field, Mahakam Delta, Indonesia, are significantly lower than the values measured on the coal samples because the organic matter contains abundant pyrobitumens. This process involves the migration of lighter hydrocarbons leaving behind heavy oil that, being unable to be expelled, is cracked to gas and pyrobitumens owing to thermal effects in the overpressured compartments (Hunt, 1990). Clememtz (1979) and Kruge (1983) pointed out that solid bitumen and heavy bitumen can affect the S_2 peak resulting in abnormal T_{max} values, but that these problems could be overcome by solvent extraction prior to pyrolysis, and the subsequent evaluation of S_2 after solvent extraction. Hunt (1996) stated that asphaltites, pyrobitumens and some resinites are not soluble in conventional organic solvents and that microscopic studies can assist in recognizing insoluble bitumen interference. The valid Rock-Eval T_{max} data used in this study have been carefully analyzed and examined (see Chapter 4).

As described in Chapter 4, the anomalously low vitrinite reflectance values in some samples of the Bambra-2 well appear to be also related to the difficulty of distinguishing vitrinite and inertinite macerals due to the very small size of the organic particles and quite high maturity (Dr. Lila W. Gurba, personal communication). Table 8-7 contains the examples that show this problem probably results in an inaccurate identification of vitrinite and inertinite in the two samples in Bambra-2. Thus, the inertinite reflectance range in Table 8-7 should be the range of vitrinite reflectance and inertinite reflectance.

In combination with the accumulation of hydrocarbons, oil-source geochemical correlations in the sub-basin (Volkman, et al., 1983) and the studies of thermal maturity, thermal modelling and modelled hydrocarbon generation (Figures 8-3 to 8-16), the occurrence of overpressure in the two studied cases suggests the existence of a dynamic overpressured sealed compartment in the Jurassic source section, where hydrocarbon generation, especially gas generation, is likely to be the significant mechanism for generating overpressure. In summary, for the Barrow

Deep-1 well, the Jurassic overpressured zone occurs at 2642-4642 m (true vertical depth) and temperatures of 113-175 ^{o}C, with fluid pressures of about 40-80 MPa and R_o 0.8-2.2 %. In the Bambra-2 well, the Jurassic overpressured zone occurs at 2874-4490 m (true vertical depth) and temperatures of 119-170 ^{o}C, with fluid pressures of about 40-80 MPa and R_o 0.85-1.9 %.

Table 8-7 Examples for the difficulty of distinguishing vitrinite and inertinite in the samples of Bambra-2

Depth (m)	**Type of Sample**	**Inertinite Reflectance Range (%)**	**N**	**Description**
4278.38	Core	1.44-2.72	30	Inertinite common, exinite rare, no vitrinite
4282	Core	1.26-2.82	37	Inertinite common, *vitrinite sparse, exinite rare

Note: The data were taken from the well-completion report.

N: Number of the measured grains.

* No measurements of vitrinite reflectance from the well-completion report.

Possible errors in the predicted maturity may be incurred from (1) the proposed thermal models and (2) uncertainty in the measured maturity values. However, these errors are slight, and do not impact significantly on the purpose and conclusion of this paper. Major differences do occur between the anomalously low maturity values and the "true" values which have not been suppressed or contaminated. If the anomalously low maturity data are ignored, there is no evidence for overpressure-related retardation of thermal maturity. Using the well-known thermal and chemical-kinetic model in the BasinMod software, the two fields of study in the sub-basin demonstrate that the true maturity profiles need not be significantly related to overpressure retardation within the sealed system. Although laboratory retardation of maturation and hydrocarbon generation, due to high pressure, has been observed (e.g. Sajgó et al., 1986; Price and Wenger, 1992; Hill et al., 1994; Dalla Torre et al,

1997), the overpressure effect on thermal maturity is negligible within the studied cases in the Barrow Sub-basin, North West Shelf of Australia. Although the datasets in this study are limited, these results indicate that overpressure retardation is not a global phenomenon, at least. To determine the true origins of geology and geochemistry for abnormal maturity profiles in geologically overpressured conditions, it is recommended that more field studies be carried out.

8.6 Summary

In the wells examined, the anomalously low T_{max} and R_o values do not appear to be significantly related to overpressure effects. The anomalous T_{max} values are mainly caused by contamination by drilling-mud additives. This study supports previous studies that the two major causes of abnormal R_o values are (1) the suppression of vitrinite reflectance through marine influence, and (2) misidentification of vitrinite macerals.

Thermal maturity described by the biomarker parameters and *n*-alkane distributions from GC-MS and GC analyses of the saturate fractions suggest that the organic matter in the Jurassic overpressured source rocks is not associated with a maturation anomaly. Thermal maturity modelling indicates that the temperature-time-related kinetic model can provide a match between good maturity data (R_o, T_{max} and Eq VR) and the calculated maturity curves in the Jurassic highly overpressured system. This study indicates that the true thermal maturity (R_o 0.8-2.2 %) of the observed Jurassic source rocks is not detectably influenced by the observed overpressure (fluid pressure about 40-80 MPa at 3000-4600 m). In conclusion, these field cases indicate that the overpressure is, therefore, an unimportant factor in the thermal maturity and hydrocarbon generation in this area.

In addition, both the current heat flow history (steady state) and the rift heat-flow model (no-steady state) can provide a match between the valid maturity data and the predicted maturity curves at present, but the thermal effect histories are clearly different.

Part IV

Two-dimensional Models, Deep Overpressure Modelling and Pressure Behaviour Modelling

CHAPTER 9 TWO-DIMENSIONAL MODELS AND DATA REQUIREMENTS FOR DEEP OVERPRESSURE MODELLING

9.1 BasinMod 2D

Overpressure reconstruction with two-dimensional modelling was performed using the BasinMod 2D software package (version 4.61). It was developed by Platte River Associates, Inc. and its theoretical background is explained in the BasinMod 2D reference manual (Platte River Associates, Inc., 1998b). The BasinMod uses the finite difference method in its numerical solution of the governing equations for the calculation of pressure, temperature and fluid flow. The governing equations include pressure, heat conduction and convection, and three-phase fluid migration. The model takes into consideration the contributions of compaction, temperature (water thermal expansion), hydrocarbon generation and quartz cementation to overpressure generation and maintenance. However, this model does not take lateral compressive forces into account.

9.1.1 Governing equations in the BasinMod 2D

The governing equation of pressure is:

$$\gamma \frac{\partial}{\partial x}\left(\frac{k_x \rho}{\mu}\frac{\partial P}{\partial x}\right)+\frac{\partial}{\partial \xi}\left(\frac{k_z \rho}{\mu \gamma}\frac{\partial P}{\partial \xi}\right)=\rho\frac{\partial e}{\partial t}+e\left(\frac{\partial \rho}{\partial T}\frac{\partial T}{\partial t}+\frac{\partial \rho}{\partial P}\frac{\partial P}{\partial t}\right), \tag{9-1}$$

$$\gamma=\frac{1}{1-e},\quad e=\frac{\varphi}{1-\varphi},\quad \frac{\partial e}{\partial t}=\frac{1}{(1-\varphi)^2}\frac{\partial \varphi}{\partial t},\quad \alpha=\frac{1}{\rho}\frac{\partial \rho}{\partial T},\quad \beta=\frac{1}{\rho}\frac{\partial \rho}{\partial P},$$

where ξ is rock matrix thickness; subscript x refers to x-direction and subscript z refers to z-direction; φ is porosity; P is the pore fluid pressure; T is temperature; t is time; k is permeability; ⑧ is density; ③ is viscosity.

The governing equation of temperature is:

$$\left(\frac{\partial H_r}{\partial T}\frac{\partial H_f}{\partial T}\right)\frac{\partial T}{\partial t}=\frac{\partial}{\partial x}\left(K_x\frac{\partial T}{\partial x}\right)+\frac{\partial}{\partial z}\left(K_z\frac{\partial T}{\partial z}\right)$$
$$-\frac{\rho_w c k_x}{\mu}\left(\frac{\partial P_x}{\partial x}\right)\frac{\partial T}{\partial x}-\frac{\rho_w c k_z}{\mu}\left(\frac{\partial P_z}{\partial z}+gz\frac{\partial \rho}{\partial z}\right)\frac{\partial T}{\partial z}+Q_H\,, \tag{9-2}$$

The left-hand side of equation (9-2) is:

$$\left(\frac{\partial H_r}{\partial T}\frac{\partial H_f}{\partial T}\right)\frac{\partial T}{\partial t}=\left(\rho_w\cdot c\cdot e+\rho_s c_s\right)\frac{1}{\Delta t}\left(T^{n+1}-T^n\right),\quad e=\frac{\varphi}{1-\varphi}, \tag{9-3}$$

where H is enthalpy; subscript r refers to rock matrix; subscript f refers to fluid; subscript w refers to water; subscript s refers to solid; subscript x refers to x-direction; subscript z refers to z-direction; superscript n+1 refers to the current time step; superscript n refers to the previous time step; φ is porosity; P is excess pressure; T is temperature; t is time; K is thermal conductivity; ⑧ is density; c is thermal capacity; k is permeability; ③ is viscosity; g is gravitational constant; Q_H is internal heat sources (not used in the model).

The equation of the three phases referring to water, oil and gas for migration are:

$$\frac{\partial}{\partial t}\left(\rho_f\cdot e\cdot S_f\right)=\gamma\frac{\partial}{\partial x}\left(\frac{k_x k_f \rho_f}{\mu_f}\frac{\partial P_f}{\partial x}\right)+\frac{\partial}{\partial \xi}\left(\frac{k_z k_f \rho_f}{\gamma\mu_f}\frac{\partial P_f}{\partial \xi}\right)+q_f\,, \tag{9-4}$$

$$S_w+S_o+S_g=1.0, \tag{9-5}$$

where subscript f refers to fluids of water (w), oil (o) and gas (g); P is pore fluid pressure; ⑧ is fluid density; e is void ratio (❸/1-❸); ❸ is porosity; S is saturation of fluid; ∞ is grain size; ③ is viscosity; ⑤ is rock matrix thickness; q is source term; k_x, k_z is absolute permeability in the x and z directions, respectively; k_f is relative permeabilities of water, oil and gas, respectively.

Some constant values for modelling in BasinMod 2D are listed in Table 9-1.

Table 9-1 Important constants applied in BasinMod 2D

Symbol	Constant	Unit	Value
α_o	Oil Expansibility	$^oC^{-1}$	1.0×10^{-3}
β_o	Oil Compressibility	Pa^{-1}	6.0×10^{-10}
α_w	Water Expansibility	$^oC^{-1}$	5.0×10^{-4}
β_w	Water Compressibility	Pa^{-1}	4.3×10^{-10}
μ_o	Oil Viscosity	Pa∃S	2.9991×10^{-4}
μ_w	Water Viscosity	Pa∃S	5.0960×10^{-4}
μ_g	Gas Viscosity	Pa∃S	1.5000×10^{-4}
ρ_k	Kerogen Density	$kg∃m^{-3}$	1800
ρ_o	Oil Density at Surface	$kg∃m^{-3}$	850
ρ_g	Gas Density at Surface	$kg∃m^{-3}$	0.7
C_o	Oil Heat Capacity	$J∃kg^{-1}∃K^{-1}$	1047
C_w	Water Heat Capacity	$J∃kg^{-1}∃K^{-1}$	4187
C_r	Rock Heat Capacity	$J∃kg^{-1}∃K^{-1}$	840
R	Universal Gas Constant	$J∃mol^{-1}∃K^{-1}$	8.319

9.1.2 The models used in BasinMod 2D

The subsidence and burial histories are a fundamental part of 2D modelling. Sediment compaction modelling provides a framework for subsequent thermal, hydrocarbon generation and fluid migration modelling. It is a dynamic model and a comprehensive calculation with interrelationship of physical and chemical variables.

Three options of the porosity-depth relationships in BasinMod 2D, by Sclater and Christie (1980), Falvey and Middleton (1981), and Baldwin and Butler (1985), can be chosen for backstripping. The porosity-depth relationship by Falvey and Middleton (1981) is employed to model burial history and calculate basin subsidence. The relationship is established based on the offshore Perth Basin with shallow carbonates similar to the Northern Carnarvon Basin.

Two options can be selected for the permeability reduction process. One is the power function developed by Hubbert (1940) and Lerche (1990). The other is the modified Kozeny-Carman equation developed by Ungerer et al. (1990).

These kinetic models for hydrocarbon generation modelling in BasinMod 2D are described through multiple parallel reactions governed by first-order kinetics and the Arrhenius law (Tissot et al., 1987; Espitalié et al., 1988; Burnham, 1989). The kinetic model used in this study for hydrocarbon generation modelling is the well-accepted model by Burnham (1989). The chemical kinetic model of Sweeney and Burnham (1990) was used to calculate vitrinite maturation.

The volumetric changes during the degradation of solid kerogen into oil, gas and residue may cause an increase in pore pressure. The pressure increment due to generation pressures contributed by the generated oil and gas can be calculated based on the equations of Lerche (1990) in this model. Thus, the pore pressure regime related to hydrocarbon generation can be investigated.

Two options of oil and gas expulsion models can be selected for hydrocarbon primary migration. One is the saturation expulsion model (Mackenzie and Quigley, 1988; Cooles et al., 1986). The other is the pressure-controlled expulsion model (Düppenbecker et al., 1991). Three phases refer to oil, gas and water.

Porosity loss due to quartz cementation during burial can be calculated in BasinMod 2D software using the kinetic model of Walderhaug (1996). This function was used to model the porosity loss in the top pressure-sealing zone in the Barrow Sub-basin.

The models and parameters used in BasinMod 2D, such as porosity-depth relationship, lithologic properties, kinetic parameters of hydrocarbon generation, compaction equations, models for temperature calculation, expulsion, fault, migration and algorithms for calibration parameters, can be selected or modified by users. The petroleum geological processes modelled by BasinMod 2D are dynamic and interactive in chronological order. Subsidence, burial, compaction, temperature, pore pressure evolution, multiple-phase fluid flow, organic-matter maturity, hydrocarbon generation, expulsion and migration can be calculated by the model.

9.2 Depth conversion for cross-sections and two-dimensional geological models

9.2.1 Depth conversion for cross-sections

Three seismic lines, the A-B line in the Barrow Sub-basin, 110/11 in the Exmouth Sub-basin and 101R/09 in the Dampier Sub-basin (Fig. 9-1), were selected for 2D overpressure modelling. The directions of these three lines are almost at right angles to the direction of the structural trends within the sub-basins. The 110/11 and 101R/09 seismic lines were interpreted by AGSO. The A-B line has been interpreted based on three wells along the line and two interpreted intersecting seismic lines, 101R/02 and 136/20 (Fig. 9-1).

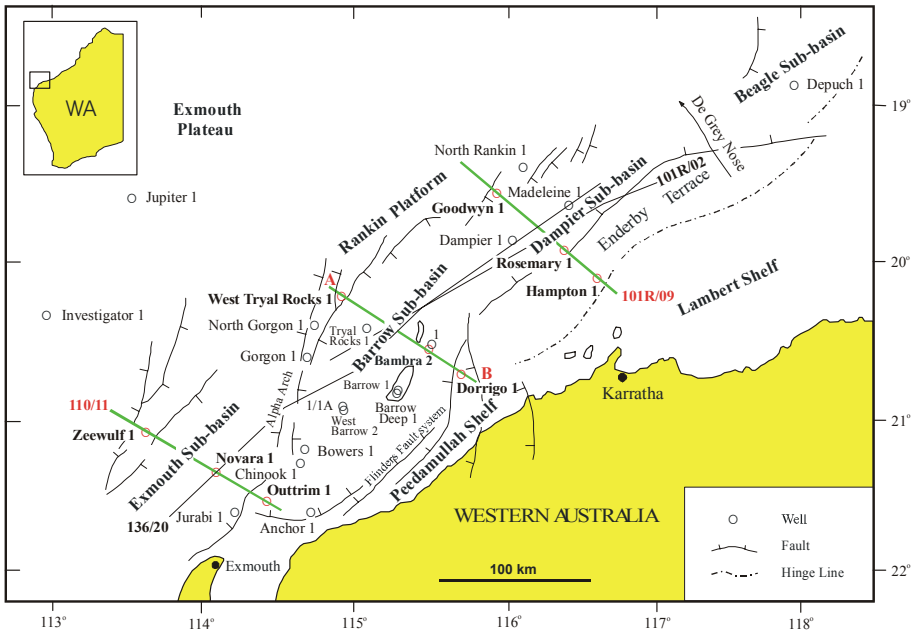

Fig. 9-1 A map showing sub-basins and locations of the modelled cross-sections and wells in the Northern Carnarvon Basin (after Woodside Offshore Petroleum, 1998; Scott, 1992).

The seismic line conversions to depth cross-sections have been made using relationships between time and depth, which can be calculated from velocity data.

Velocity surveys in wells are used to determine average velocity as a function of depth, but they are not deep enough for time-depth conversion if time (two way time) is greater than 2.5 seconds. Stacking velocities for 110/11 and 101R/09 lines from AGSO have been used to calculate time-depth curves for depth conversion. The root-mean-square velocity data (rmsv) for the A-B line have been used to produce time-depth relationships. The relationship of time-depth can be calculated from interval velocity, which is the average velocity over some interval of travel path. Interval velocity is often calculated from rmsv using the Dix equation (Dix, 1955), given below:

$$V_i = \left[\frac{V_r^2 t_n - V_{r-1}^2 t_{n-1}}{t_n - t_{n-1}} \right]^{\frac{1}{2}}, \tag{9-6}$$

where V_i is the interval velocities (m/s); V_r is the rmsv (m/s); t_n is the zero-offset arrival time corresponding to the *nth* reflection.

Stacking velocity is a function of reflection travel-time. Root-mean-square velocity can be calculated from stacking velocity after corrections. Dip correction is necessary for stacking velocity to rmsv. Thus, dip correction of stacking velocity was carried out under the assumption that reflectors are on a parallel incline.

$$V_1 = V_s \left(1 + \frac{V_s^2 tg^2 \theta}{4} \right)^{-\frac{1}{2}}, \tag{9-7}$$

$$V_r = V_s \left(1 - \frac{V_r^2 \times tg^2 \theta}{4} \right)^{\frac{1}{2}}, \tag{9-8}$$

where V_1 is the rmsv (m/s) in the first layer; V_r is the rmsv (m/s); V_s is the stacking velocities (m/s); θ is the dip of the interface from the observed $<t_0$ and <x, tg θ = $<t_0$ / <x.

The time-depth curves were calculated from rmsv using the Dix equation and a spline interpolation method with an interpolated interval of 0.05 s as shown in Figures 9-2 to 9-4. It can be seen that the seismic-velocity-derived time-depth relationships correlated well with those from velocity surveys in nearby wells along the three seismic lines. The errors of the converted depth using seismic velocity data are less than 5 % in shallow parts compared with the well data. Thus, seismic velocity data have been used for the time-depth conversion for these seismic lines. However, more errors may occur in the time-depth conversion of deep parts using the seismic-derived time-depth relationships.

9.2.2 Two-dimensional geological models

In the Barrow Sub-basin, the stratigraphy of the A-B depth-converted cross-section is divided into 8 events and lithology units (Fig. 9-5). Along the A-B cross-section, three wells, West Tryal Rocks-1, Bambra-2 and Dorrigo-1, have been selected to provide geological data. The well data from Tryal Rocks-1 has been also referred to in building the 2D geological model. In the Exmouth Sub-basin, the interpreted 110/11 seismic line is shown in Appendix 2. The stratigraphy of the 110/11 depth-converted cross-section is divided into 11 events and different lithology mixes (Fig. 9-6). The geological data from three wells, Zeewulf-1, Novara-1 and Outtrim-1 along the 110/11 cross-section have been used to set up the 2D geological model. In the Dampier Sub-basin, the interpreted 101R/09 seismic line is shown in Appendix 3. The stratigraphy of the 101R/09 depth-converted cross-section is also divided into 11 events and lithology units (Fig. 9-7). Along the 101R/09 cross-section, the geological data were derived from three wells, Goodwyn-7, Rosemary-1 and Hampton-1 for the 2D geological model.

The fault distribution and the geometry of these depth cross-sections were interpreted from seismic data and information from wells. In fact, many geological events are too complex to model quantitatively. In order to construct models, they must not only be acceptable geologically, but also be suitable for numerical procedures. Simplification of the model is necessary but over-simplification of seismic and geological information needs to be avoided. Many simplifications in

these models need to be made, for instance, the over-occurrence of faults on cross-sections and the changes of lithology and organic matter along the cross-sections were simplified. It should be emphasized that the 2D model studied here is geologically simple in terms of fluid flow and pressure dynamics. The geological conceptual model and the observed data play key roles for choosing a number of parameters in the modelling.

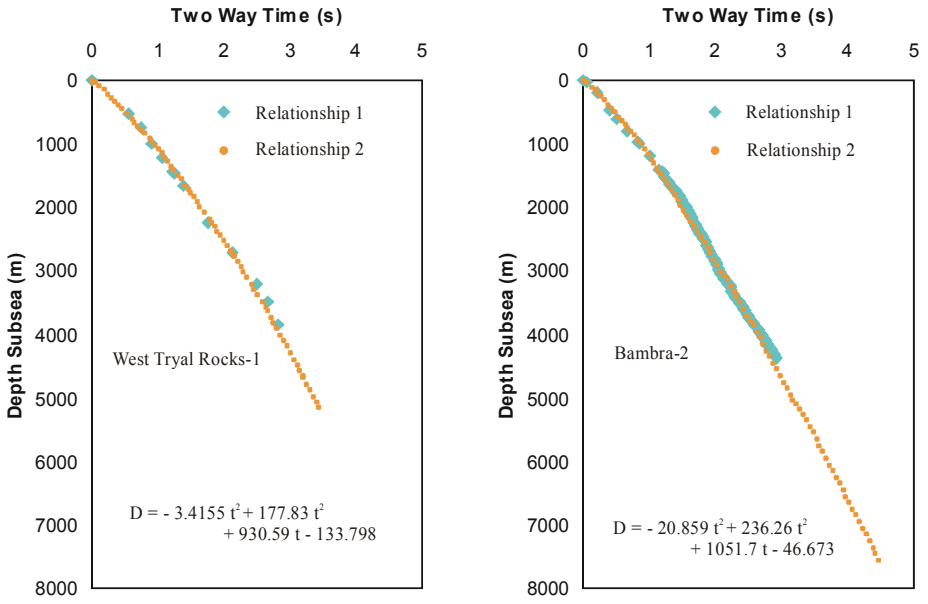

Fig. 9-4 Correlation between two time-depth relationships from well velocity surveys and seismic velocity data at approximate locations of the West Tryal Rocks-1 and Bambra-2 wells along the AB seismic line in the Barrow Sub-basin. Relationship 1: The time-depth relationship from well velocity surveys; Relationship 2: The time-depth relationship from seismic velocity data.

9.3 Porosity and permeability

The porosity for shales is mainly a function of compaction. The compaction of shales normally increases with increasing depth due to the increase in load. Therefore, under normal compaction, the porosity of shales decreases and the bulk density of shales increases with increasing depth. However, when the shale contains

50 % silt, the compaction is a complex process with chemical compaction (e.g. Chapman, 1994). The compaction of sandstones is more complex because it is the result of both mechanical and chemical processes (e.g. Lundegard, 1991; Ramm, 1992). Normal relationships between porosity and depth describe the process of mechanical compaction and are important for burial reconstruction. The permeability is a critical control on the evolution of abnormal pressure. For clastic sediments, permeability is frequently treated as a function of porosity (e.g. Ungerer et al., 1990; Lerche, 1990). Based on the study of Deming (1994), the minimum permeability needed for a geological unit (100 m to 1000 m) to act as a pressure seal over a time interval of about 1-100 Ma is in the range 10^{-21}-10^{-24} m^2.

Figure 9-8 shows 83 measured porosity values from claystone and silty claystone from 10 wells versus present-day depth. In general, the porosity ranges from 2 % to 5 % at a depth of about 3000 m. The calculated permeability values, using the modified Kozeny-Carman equation by Ungerer et al. (1990), are < 10^{-19} m. The normally compacted claystones can be described using an exponential form of the porosity (❸) and depth (D) relationship $\varphi = \varphi_0 \exp(-cD)$ (❸$_0$ is initial porosity; c is a coefficient that explains the rate at which the exponential decrease in porosity takes place with depth.). Based on the measured porosities of claystone and silty claystone in Fig. 9-8, the calculated coefficient is in range of 0.0007-0.0008 and the initial porosity is about 56 %. Figure 9-8 also shows the measured 235 porosity values from siltstones versus depth in 21 wells of the Northern Carnarvon Basin.

Ranges, and average values, of porosity and permeability from 12 wells for sandstones are shown in Table 9-2. The average values of porosity and permeability in sandstones generally decrease with burial depth. The porosity values, from 1479 sandstone samples in 45 wells of the Northern Carnarvon Basin, against depth were plotted in Fig. 9-8, which may represent a trend of porosity decrease in sandstones. The trend may not only be controlled by mechanical compaction, but also by chemical compaction involving cementation and dissolution. In general, the permeability values in sandstones are not □ 10^{-21} m^2, which is required for a rock layer to act as a pressure seal (Deming, 1994).

The measured porosity values from 100 limestone and dolomite samples versus present-day depth are also shown in Fig. 9-8.

Figure 9-9 shows the 167 coupled values of horizontal permeability (HP) and vertical permeability (VP) in sandstones from 9 wells. In ten sandstone samples, HP is equal to VP and in 20 samples is less than VP, while horizontal permeabilities in 137 sandstone samples are greater than vertical permeabilities. The ratio of VP/HP in 137 samples ranges from 0.1 to 0.9, the average value of the ratio being 0.5. In BasinMod 2D, the permeability anisotropy (the ratio of vertical permeability to horizontal permeability) is 0.4 for sandstones, 0.2 for siltstones and shales, and 0.5 for limestones.

Table 9-2 Porosity and permeability in sandstones from 12 wells in the Northern Carnarvon Basin

Formation	**Depth (m)**	**Porosity (%)**		**Permeability (md, 10^{-15} m^2)**	
		Range	Average	Range	Average
Muderong Shale	617-1254	19.4-33.4	25.95 (36)	0.01-28	1.49 (36)
Birdrong Sandstone	799-822	2.4-30	17.63 (19)	0.01-5161	1011 (19)
Barrow Group	919-2413	0.7-36.5	20.55 (123)	0.01-9656	865.78 (120)
	3063-3673	2.8-17.3	10.43 (31)	0.02-108	7.12 (31)
Dupuy Formation	1246-2729	4.2-32.7	18.11 (188)	0.01-315	36.7 (237)
Dingo, Athol, Murat	2919-3193	7-19	13.76 (20)	<0.01-0.13	0.025 (20)
Mungaroo Formation	1903-4235	3-26	15.07 (100)	<0.01-1680	151.55 (116)

Note: The numbers inside brackets are the number of measurements of porosity and permeability.
Dingo: Dingo Claystone; Athol: Athol Formation; Murat: Murat Siltstone.
The data of porosity and permeability were collected from well completion reports.

9.4 Boundary conditions and data requirements

9.4.1 Boundary conditions

The bottom boundary in BasinMod 2D can be defined by users from three different boundary conditions, a closed boundary, an open boundary and a fractionally open

boundary. In 2D modelling, the bottom boundary is usually assumed as a closed boundary because it generally represents tightly compacted sedimentary rocks. These rocks have limited fluid movement and a large uncertainty. Thus, in this 2D modelling, the bottom boundary is assumed to be a closed boundary. The lateral boundary can be chosen by users from three situations, a constant flow condition, a closed boundary and an open boundary. The constant flow condition is assumed for left and right side boundaries in the modelling. For temperature calculation, the transient heat flow model was used with constant heat flows. The seabed temperature is based on the water-sediment interface temperature data in the BasinMod 1D. There is no heat transfer through the lateral boundaries.

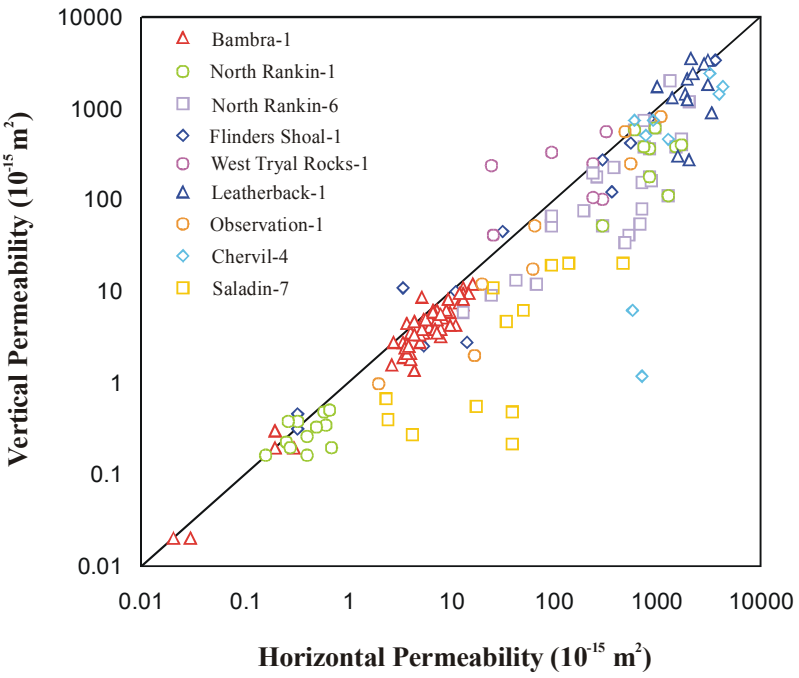

Fig. 9-9 The relationship between the measured vertical permeability and horizontal permeability values in the Northern Carnarvon Basin.

9.4.2 Data requirements

Input data for the modelling include:

(1) Depth cross-section (horizons, unconformities, hiatuses and faults).

(2) Stratigraphy and lithology.

(3) Heat flows and seabed temperatures.

(4) Kerogen type and total organic carbon (TOC, %).
(5) Palaeo-seawater depths
(6) Erosional thickness.

The measured data from an individual well, including thermal maturity, formation temperature, fluid pressure, mud weight, porosity and permeability, were used to correlate with the modelled results at the well points along the cross-section in order to calibrate and optimize parameters and to produce acceptable calculations.

Two numerical methods of finite difference and finite element are used in the BasinMod 2D software. The modelling requires the software operator to set time (Δt), lateral distance (x-distance) (Δx) and vertical-depth distance (Δz) increments. These increments are increased to allow more rapid computation, or decreased to obtain greater accuracy (albeit longer computation time). The cell divisions are based on the size of time step and the number of lateral cells which may affect the stability and precision of the calculation and resolution of the modelled compaction, fluid flow, thermal results and excess pressures. More precise results can be obtained through the use of a smaller time step. The examination, using time steps of 0.5, 1, and 2 Ma, and distance increments of 0.5 and 1 km, indicates that the time step of 1 Ma in the Jurassic section and 2 Ma in the other formations is satisfactory, and the lateral distance interval of 1 km is reasonable for the stability and precision of the calculated results. For our modelling, Δt was chosen to be 1Ma and 2 Ma, and Δx was selected to be 1 km for cell divisions. Vertical distance increments (Δz) were calculated from time increments and sedimentation rates. These values were also chosen to permit reasonable computation times on a Pentium-III, 800 MHz personal computer.

9.4.3 Date sets

The ages of stratigraphic events

The absolute age of a stratigraphic event is based on the stratigraphic table and the palaeontological analysis in the wells along the two-dimensional models. Both

isochronous and time-transgressive events concerning horizons and unconformities were handled in the BasinMod 2D. The geological time scale is referenced to the publications of Labutis (1994) and Polomka et al. (1999).

Lithologies

Lithologic mixes for stratigraphic events are calculated from the selected wells along cross-sections. The thicknesses of four main lithologies (sandstone, siltstone, shale/claystone and limestone) of each stratigraphic event from well information and the average content of each lithology are calculated as a percentage for mixed lithologies in a single stratigraphic event. There is no relevant data for explaining reservoir layers and fluid flow conduits in these studied 2D regional geological models.

Total organic carbon and kerogen type

Based on our statistics of 1030 measured TOC (%) values in shales, average values and ranges of total organic carbon content are 1.3 % and 0.5-3.0 % in the Barrow Group, 1.7 % and 0.5-5.0 % in the Dupuy Formation, Dingo Claystone and Athol Formation, 2.1 % and 0.5-6.0 % in the Murat Siltstone, 2.2 % and 0.5-14.0 % in the Mungaroo Formation. Type III kerogen was used in the Barrow Group, the Jurassic source rocks and the Mungaroo Formation.

Thermal parameters

Steady-state heat flow (constant heat flow) values and seabed temperatures, the default values of matrix thermal conductivity and matrix heat capacity in BasinMod 2D, as in BasinMod 1D, were used in the 2D modelling.

Palaeobathymetry

Palaeobathymetry is a necessary parameter for the reconstruction of subsidence history. Hardenbol et al. (1981), Joy (1992), and Emery and Myers (1996) provided methods, using seismic data, to determine palaeo-water depths. Seismic profiles

sometimes provide good information about the relative bathymetries. Palaeo-water depths can be estimated from coastal onlaps, shelf breaks, lithology, eroded and non-deposition areas with some calibrated calculation. Kaiko and Tait (2000) studied the post-rift tectonic subsidence and the palaeo-water depth using seismic data for some wells in the Northern Carnarvon Basin. Because of a lack of good data concerning palaeobathymetric values in the Triassic and Jurassic sequences, the lithology and palynofacies analysis in the wells and the studies of the environment and palaeogeography by Bint and Helby (1988) and Bradshaw et al. (1988) were used to evaluate the palaeo-water depths. These were about 2-50 m during the Middle-Late Triassic, 20-50 m during the Early Jurassic, 50-350 m during the Middle-Late Jurassic, 200-400 m during the Cretaceous and 20-300 m in the Cenozoic.

Erosional events

A large uplift and erosion event took place on the Rankin Platform and the structural highs during the syn-rift phase associated with the breakup of Gondwana. The erosional effects are clearly visible on the seismic lines. Generally, the sedimentary rocks of the Murat Siltstone (Lower Jurassic) and the upper part of the Mungaroo Formation (Upper Triassic) were eroded during the late Early Jurassic to the breakup time. It is estimated that the eroded thicknesses were from several hundred meters to two thousand meters on the Rankin Platform. Uplift and erosion also occurred on the eastern flank of the basin. Possibly several hundred meters and up to one thousand meters of the Barrow group (Earliest Cretaceous) and the Dingo Claystone (Upper Jurassic) were eroded during the breakup time. The erosional thicknesses during the Cretaceous and the Cenozoic seem to be small from the selected seismic lines.

CHAPTER 10 TWO-DIMENSIONAL DEEP OVERPRESSURE MODELLING AND PRESSURE BEHAVIOUR MODELLING

10.1 Introduction

Overpressure is encountered in the formations of Jurassic age and the Barrow Group (of the earliest Cretaceous age) in some wells within the Northern Carnarvon Basin (Zaunbrecher, 1994). Overpressure influences many fluid-related aspects of petroleum geology, including diagenesis and reservoir quality (e.g. Burley, 1993). The processes of migration and accumulation of oil and gas are strongly influenced by overpressured systems (e.g. England et al., 1987; Hunt, 1990). It also constitutes a hazard in drilling wells and directly impacts on drilling costs and the safety of petroleum exploration (Tingate et al., 2001).

The mechanisms proposed for increasing fluid pressure (pore fluid pressure) in sedimentary basins include (1) rapid loading causing compaction disequilibrium that is common in fine-grained rocks (e.g. Chapman, 1972; Magara, 1978; Swarbrick, 1995; Hunt, 1996), (2) aquathermal expansion and thermal expansion of fluids (e.g. Barker, 1972; Bradley, 1975; Plumley, 1980; Miller and Luk, 1993; Hunt, 1990; Alnes and Lilburn, 1998), (3) hydrocarbon generation (e.g. Timko and Fertl, 1971; Law and Dickinson, 1985; Spencer, 1987; Düppenbecker et al., 1991) and oil-to-gas cracking (e.g. Chaney, 1950; Barker, 1990; Luo and Vasseur, 1996), (4) compression of lateral tectonic stress (e.g. Berry, 1973), (5) smectite to illite transformation and clay dehydration (Powers, 1967; Burst, 1969; Schmidt, 1973), (6) osmosis in shales (Marine and Fritz, 1981), and (7) effect of gas buoyancy in sealed units (Swarbrick, 1995). Generating overpressures from the latter three mechanisms are considered to be small in most cases (Swarbrick, 1995). The contribution of horizontal compression to overpressure generation is considered to be minor in passive continental margin basins (Swarbrick and Osborne, 1998). Luo and Vasseur (1996) demonstrated that oil generation is unimportant for overpressure generation if the organic matter content of rocks is less than 5 %, while gas generation and oil-to-gas cracking are significant contributions to overpressure. Lou and Vasseur (1992) suggested that in practical geopressure studies, the pressuring effect of aquathermal factor could be neglected. Swarbrick and Hillis (1999)

presented data showing thermal expansion of fluid during burial to be a relatively minor mechanism for overpressure development.

Swarbrick and Osborne (1998) reviewed various overpressure mechanisms indicated in the literature and proposed that the major mechanisms for large magnitude overpressure, in most extensional sedimentary basins, are compaction disequilibrium due to rapid loading in fine-grained sequences, and fluid volume expansion during gas generation. Recently, Yardley and Swarbrick (2000) used 2D models to show that disequilibrium compaction-generated overpressure can significantly enhance the excess pressure (the difference between fluid pressure and hydrostatic pressure) at structural highs by the lateral transfer of fluids from deep overpressured parts of a basin along laterally extensive inclined aquifers, both in recently deposited reservoirs and in old structures.

In support of the compaction disequilibrium mechanism, Gretener and Bloch (1992) noted that there were two types of overpressure development in sedimentary basins: (1) compaction disequilibrium, in which there is unrestricted lateral flow and restricted vertical flow, and (2) sealed compartments, in which there is both restricted lateral and vertical flow. Mann and Mackenzie (1990) presented an argument that compaction disequilibrium was the dominant mechanism for observed fluid overpressure in the Gulf of Mexico and the North Sea, based on an empirical relationship between overpressure gradient, permeability and deposition rate. Luo and Vasseur (1992) also presented an argument that the excess pressure is so great that it cannot be explained by compaction alone in some areas, such as the United States Gulf of Coast. Despite the arguments for compaction disequilibrium (generally undercompaction) being the cause of overpressure in many basins, a significant corpus of evidence has also been gathered that may suggest otherwise. Bradley (1975) and Swarbrick (1995) suggest that excess pressure will dissipate once burial slows to a rate at which fluid loss matches the addition of overburden stress. Hermanrud et al. (1998) demonstrated that high fluid overpressures in the thick shale-prone Upper Jurassic and Lower Cretaceous sequences on Haltenbanken (offshore mid-Norway) have not significantly contributed to high porosity in overpressured zones. The conclusion of the Hermanrud et al. (1998) and Teige et al. (1999) studies is that there is no abnormally high porosity (and, thus,

undercompaction) on Haltenbanken in the North Sea, but rather the sonic and resistivity wireline logs are responding to the present day fluid overpressure. Hunt et al. (1998) stated that fine-grained quartz and carbonates stop compacting at porosities around 3 %, whereas shales containing minerals with large surface areas, such as smectite and illite, stop compacting at porosities around 10 %. More recently, Lee and Deming (2002) studied the overpressure in the Anadarko Basin, southwestern Oklahoma. They proposed that the overpressure can not be explained by compaction disequilibrium and that the best explanations are gas generation and gas capillary seals.

Barker (1972) noted that the high-pressure zones should be effectively isolated from their surroundings. Bradley (1975) considered that the abnormal pressured system must be completely enclosed by seals on all sides. Hunt (1990) pointed out that to maintain overpressure through geological time requires seals that are almost completely impermeable or a continuous pressure recharge must occur during basin sinking. Hunt (1990), Powley (1990), Bradley and Powley (1994), and Ortoleva (1994) proposed that the pressure fluid compartments are characterized by an effective seal, in three-dimensions. The efficiency of low-permeability units, fine-grained rocks, may be enhanced by diagenetic cements (Hunt, 1990; Swarbrick, 1995). Deming (1994) demonstrated that the permeability needed for a geological layer to act as a pressure seal is in the range 10^{-21}-10^{-24} m^2. To maintain overpressure in sedimentary basins over geological time, highly effective pressure seals, such as low-permeability rocks and lateral fault sealing, are required to be capable of preventing fluid expulsion from sealed compartments.

The Northern Carnarvon Basin is a hydrocarbon-rich overpressured basin. Petroleum generation is believed to be mainly associated with the Jurassic organic-rich, clay-rich section which is highly overpressured. Previous authors have proposed various origins for the generation of the fluid overpressure in the Northern Carnarvon Basin which principally include (1) hydrocarbon generation (Horstman 1988) or gas generation (Zaunbrecher 1994), and (2) compaction disequilibrium (Swarbrick & Hillis 1999; Bekele et al. 2001; Tingate et al. 2001). However, Swarbrick and Hillis (1999) suggested that the generation of a large volume of gas could be a secondary source of overpressure as well. Bekele et al. (2001) also

proposed that organic maturation has a contribution of approximately 15 percent to the maximum pressure anomaly in the Barrow Sub-basin, based on 2D numerical basin modelling. Horstman (1988) maintained that hydrocarbon generation is the most important mechanism within source rocks, based on a comparison of the depth of the oil window and the top of the overpressured zone. Zaunbrecher (1994) considered that gas generation and accumulation are the likely origin for the overpressure in reservoirs sealed by overpressured clays.

Clearly, both the hydrocarbon generation and disequilibrium compaction mechanisms have been most commonly proposed by various authors to be the dominant genesis of the observed overpressures for the Jurassic clay-rich and some Cretaceous sequences in the Northern Carnarvon Basin. With reference to previous work, the following questions concerning the deep overpressured system in the sub-basins are still of great interest to the study of overpressure modelling: (1) What is the effect of the top pressure seal for maintaining the deep overpressure in the sub-basins? (2) What does the evolution of the deep overpressured system look like in the sub-basins? (3) What are the processes and major mechanisms of the generation and maintenance of the deep overpressured system in the sub-basins? and (4) What is the pressure behaviour within low-permeability (10^{-18}-10^{-22} m^2) environments? The aim of this chapter to propose possible answers for these questions based on results from (1) studies of deep overpressure, formation compaction and pressure seal in Chapter 5 and this Chapter, and (2) overpressure modelling using BasinMod 2D software and approximation of pressure behaviour modelling within low-permeability conditions based on a well-known diffusion equation.

Two-dimensional modelling was performed using the BasinMod 2D package (version 4.61) to reconstruct the evolutions of porosity and permeability, formation of pressure seal with compaction and cementation, generation and preservation of the deep overpressure on the studied cross-sections in the Barrow, Exmouth and Dampier Sub-basins. It should be noted that the 2D modelling should be perceived to give a qualitative overview for the overpressure history rather than strict quantitative results. Three 1D models were developed to investigate the low-permeability conditions required to maintain overpressure and to determine the dissipation time of the observed deep overpressure in the Bambra locality of the

Barrow Sub-basin. This modelling was based on a well-known diffusion approximation for pressure behaviour in porous media.

10.2 Two-dimensional overpressure modelling in the Barrow Sub-basin

The length of the AB cross-section (Fig. 9-5) in the Barrow Sub-basin for the 2D modelling is 120 km and its maximum depth is about 10700 m. The cross-section has been divided into 22,537 cells with time intervals of 1-2 Ma and x-distance intervals of 1 km. Top pressure seal of the deep overpressured system in this geological model was designed with 300-500 m thickness and was modelled with quartz cementation.

10.2.1 Correlation between the predicted values and the observed data

10.2.1.1 Data from Bambra-2 for correlation

Figure 10-1A shows modelled porosity and permeability curves, and some measured porosity and permeability values at the Bambra-2 well site along the cross-section in the Barrow Sub-basin (x-distance of 90,000 m on Fig. 9-5). The porosity curve matches the observed claystone porosity values of 4.9-6.6 % from a conventional core at 4274-4283 m. The measured permeability values for this core at 4274-4283 m are generally □ 10^{-17} m^2 (data from the well completion report), which are basically consistent with the calculated values of about 10^{-18}-10^{-19} m^2 in the overpressured Middle Jurassic. Figure 10-1B shows that the modelled fluid pressure and excess pressure curves at present basically fit with the mud weight pressures and RFT pressures from Bambra-1. The modelled maximum excess pressure is about 35.6 MPa at a depth of 4600 m within the Athol Formation. Figure 10-1C shows the calculated temperature and vitrinite reflectance curves at present and the measured formation temperatures and thermal maturity values. The formation temperatures from Bambra-2 are the extrapolated bottom hole temperatures using the Horner-plot. The observed thermal maturity values were derived from a 1D modelled maturity trend obtained from Rock-Eval T_{max} data in Bambra-2, which can be modelled using the present-day seabed temperatures and constant heat flow values in the range of 43-46 mW/m^2 along the cross-section.

10.2.1.2 Data from West Tryal Rocks-1 for correlation

Figure 10-2A shows the modelled fluid pressure and the RFT pressures and mud weights at the West Tryal Rocks-1 well site along the cross-section (x-distance of 7600 m on Fig. 9-5). Figure 10-2B also shows the modelled temperature and maturity curves and the measured formation temperatures and thermal maturity values at this well site. There are two estimated formation temperatures, one (146.7 ^{o}C at 3866 m) is the extrapolated bottom hole temperature using the Horner-plot and the other is the corrected bottom hole temperature by adding 10 % of the raw temperature (120 ^{o}C at 3433 m). The measured maturity values are the 1D modelled maturity trend using the real Rock-Eval T_{max} data in West Tryal Rocks-1 which can be well matched using the constant heat flow values in the range of 43-46 mW/m^2 and current seabed temperatures along the cross-section.

10.2.2 Results of the BasinMod 2D modelling

10.2.2.1 Sedimentation rates

Based on the calculated sedimentation rates in the sub-basin, the burial history can be divided into three periods. Rapid loading occurred during the Jurassic and Earliest Cretaceous (136 Ma) with sedimentation rates of about 80-180 m/Ma in the graben. The sedimentation rates were about 40-60 m/Ma during the Early Cretaceous to the early Late Cretaceous (136-90 Ma) and about 10-20 m/Ma during the Late Cretaceous and Cainozoic.

10.2.2.2 Porosity and permeability

A number of the modelled chronological evolution profiles of porosity and permeability at x-distances of 50,000 m were selected (Fig. 10-3; approximately mid-basin, see Fig. 9-5 for the location). The various ages for the profiles of porosity and permeability are 160 Ma, 145 Ma, 136 Ma, 120 Ma, 90 Ma, 65 Ma, 24 Ma and present-day. Based on the modelled porosity, the permeability history was calculated using the modified Kozeny-Carman equation (Ungerer et al., 1990) in BasinMod 2D. Figure 10-3 indicates porosity and permeability histories:

1. At 160 Ma and 145 Ma (Fig. 10-3-1 A and B), the rapid sedimentation and compaction resulted in a porosity value of much less than 1 % and very low-permeability of about 10^{-24} m^2 at the bottom of the Jurassic section. This modelling indicates that a rock layer about 150 m thick with permeability of about 10^{-24} m^2 was formed in the Jurassic bottom section of the central sub-basin since about 140 Ma. Then this rock layer became thicker as a nearly closed boundary in the modelling.

2. At 136 Ma, 120 Ma and 90 Ma (Fig. 10-3-1 C and D, and Fig. 10-3-2 E), rapid compaction occurred at the top part of the Jurassic section resulting in the porosity decreasing from about 20 % to about 5.0 % and the vertical permeability decreasing from about 10^{-17} m^2 to 10^{-19} m^2, whereas the maximum porosities in the middle of the undercompacted zone were about 13-22 %.

3. At 65 Ma and 24 Ma (Fig. 10-3-2 F and G), the vertical permeability values at the top of the Jurassic rocks were about 10^{-20}-10^{-21} m^2, and the maximum porosity values in the middle of the Jurassic ranged from 8 % to 11 %.

4. At present (Fig. 10-3-2 H), the vertical permeability for the top pressure seal is 10^{-20}-10^{-22} m^2 and for the bottom pressure seal is 10^{-24} m^2, and the maximum porosity in the middle Jurassic section is about 7 %.

Figures 10-4 and 10-5 give the modelled distributions of porosities and vertical permeabilities at 145 Ma, 120 Ma, 65 Ma and present-day for the cross-section. The modelled results indicate that the maximum porosities in the middle of the Jurassic section remain 6-11 % at 65 Ma and 4-8 % at present. The distribution of the present-day vertical permeability (Fig. 10-5 D) shows two abnormally low permeability zones (1) at a relatively shallow depth of about 3000 m to 3500 m with permeabilities of about 10^{-20}-10^{-22} m^2, and (2) in a deep region near the base of the Jurassic (6000 m - 9000 m) with permeability of about 10^{-24} m^2 within the sub-basin. From these models, one could possibly propose the existence of a pressure cell, based on the identification of upper and lower permeability seals for the cell. The top pressure seal could be interpreted to be coincident with the upper low permeability zone (3000 - 3500 m), and the cell may be confined by lateral

closed faults and a deeper zone, which appears to be associated with the base of the Jurassic sediments (6000-9000 m).

10.2.2.3 Fluid pressure

Eight representative profiles of excess pressure were selected to demonstrate the modelled chronological results for the following geological times: the end of the Middle Jurassic (160 Ma), the end of the Late Jurassic (145 Ma), the early period of the Early Cretaceous (136 Ma), the middle of the Early Cretaceous (120 Ma), the early period of the Late cretaceous (90 Ma), the end of the Late Cretaceous (65 Ma), the end of the Oligocene (24 Ma) and present-day (Fig. 10-6). Figure 10-6-1 (A and B) shows that the Jurassic overpressure was developed during the deposition of claystone and siltstone-dominated Jurassic and the Lowest Cretaceous sequences with the maximum excess pressures of about 35 MPa and 65 MPa at 160 Ma and 145 Ma respectively in the Jurassic succession. The buildup of the high fluid pressure was modelled, which may be related to rapid sedimentation rates in Jurassic fine-grained sediments. These excess pressure profiles show that the significant upward compaction-driven water flow was indicated by the water flow direction, and that overpressure was also released along fault conduits. Figure 10-6-1 (C and D) and Figure 10-6-2 (E) show that the maximum excess pressures were about 80 MPa, 83 MPa and 90 MPa at 136 Ma, 120 Ma and 90 Ma, respectively, in the Jurassic section. The Jurassic overpressured system may be recharged in terms of the current modelling package, owing to compaction disequilibrium during the deposition of the Upper Jurassic and Lower Cretaceous indicated by the porosity history (Fig. 10-3). The direction of water flow was obviously controlled by the permeability increase from deeper to shallower. Figure 10-6-2 (F, G and H) shows the overpressure evolution in the Tertiary and Quaternary. The modelling shows that the deep overpressured system has been sealed from at least Cainozoic because the upward and lateral water flow has been significantly weakened, which could suggest that a top pressure seal, and lateral closed faults, were becoming more effective through time to maintain the overpressure. This isolation condition seems to be an important control for maintaining the deep overpressure based on the BasinMod 2D modelling.

10.2.2.4 General discussion

There is an absence of observed data from the deep overpressured section at depths greater than 4650 m. The calculated deep overpressure below 5000 m using the BasinMod 2D modelling may not be valid.

A significant error for the overpressure distribution may be related to fault distribution in the depocentre of the sub-basin because faults, as conduits allow pore fluid flow. A possible error may be also derived from the steady-state thermal model for thermal expansion of pore fluids and hydrocarbon generation, but it was discovered to be minor in the BasinMod 2D modelled results, based on the sensitivity analysis using various temperatures. The porosity is more sensitive to the overpressure modelling because the permeability calculation is based on it.

The fact that this top pressure seal was designed to be independent of formation boundaries but modelled results show a close correlation between pressure seal and location and stratigraphy is particularly interesting. The influence of the top pressure seal was examined for the deep overpressured system. The results indicate that there are various distributions of the overpressure predicted for two distinct models with, and without, the designed top pressure seal, and that these are unlikely to match measured pressure data without the top pressure seal. As the result of cementation, the modelled porosity in the interpreted top pressure seal was calculated to be 1.5-4.5 % and the calculated permeability values ranged from 10^{-20} m^2 to 10^{-22} m^2 at present (Fig. 10-4 D and Fig. 10-5 D). This suggests that quartz cementation is a significant factor in forming the low-permeability rocks in the depth interval of the interpreted top pressure seal of the sub basin.

Temperature increase results in pore fluid expansion that produces overpressure. The contribution of thermal expansion of pore fluids to overpressure has been calculated in this cross-section using the BasinMod 2D. It is about 5-10 % of the maximum excess pressures. The generated pressure owing to hydrocarbon generation has been observed in the processes of the two-dimensional overpressure modelling. However, the calculated generation pressure, using the model of the

volumetric change in BasinMod 2D, is smaller (less than 2 MPa) irrespective of TOC values from 1 % to 6 %.

10.3 Two-dimensional overpressure modelling in the Exmouth Sub-basin

The length and present-day depth of the 110/11 cross-section (see Fig. 9-6 for the cross-section) in the Exmouth Sub-basin are 150 km and about 12800 m, respectively. It has been divided into 34,397 cells with time intervals of 2 Ma and x-distance intervals of 1 km. Many normal faults in the seismic cross-section were interpreted (Appendix 2). However, only crucial normal faults have been set up on the geological 2D model and were modelled throughout geological time. It should be noted that occurrences of many small-scale normal faults within the Barrow Group and Upper Jurassic section have been ignored because it is impossible to model too many small-scale faults using the numerical model. However, this may influence the modelled distribution of the deep overpressure to some extent.

10.3.1 Correlation between the calculated values and the observed data

10.3.1.1 Fluid pressure correlation

Figure 10-7 shows the three pressure profiles of the modelled and measured fluid pressures at the well sites of Zeewulf-1, Novara-1 and Outtrim-1 along the 110/11 cross-section in the Exmouth Sub-basin. Unfortunately, all three wells along the cross-section have not been drilled into the deep overpressured zone. These modelled results are consistent with the observed data which indicate that the shallower part (depth < 2800-3000 m) of the cross-section is a normal pressure system. However, a deep overpressured system has been observed in the Jurabi-1 well at depths greater than 2900 m (Fig. 5-4), mentioned in Chapter 5.

10.3.1.2 Temperature and maturity correlation

Figure 10-8 indicates the modelled temperature lines and maturity trends, and the observed formation temperatures and thermal maturity values at the well sites of

Zeewulf-1, Novara-1 and Outtrim-1 along the 110/11 cross-section. The formation temperature values in the three wells are shown in Table 10-1. The steady-state heat flows of 52-54 mW/m^2 and constant seafloor temperatures can match well with both the measured formation temperatures and vitrinite reflectance values. It is geologically reasonable that this organic matter in the formations in the three wells experienced thermal effects only during the post-rift phase.

Table 10-1 Measured formation temperatures from three wells in the Exmouth Sub-basin

Well	Depth (m) (K.B.)	Formation Temperature (^oC)	Type of Temperature
Zeewulf-1	2860	68	Horner-plot
	3485	93.3	Horner-plot
Novara-1	1151	48.8	Horner-plot
	1342	55.6	Horner-plot
	2754	101.6	Horner-plot
Outtrim-1	1726	86	Horner-plot

10.3.2 Results of the BasinMod 2D modelling

10.3.2.1 Sedimentation rates

The burial history of this sub-basin can be divided into two periods based on calculated sedimentation rates. Rapid loading occurred during the Jurassic and Earliest Cretaceous (136 Ma) with sedimentation rates of about 80-180 m/Ma in the depocentre. The slow sedimentation rates are about 10-30 m/Ma from 135 Ma (Early Cretaceous) to the Cainozoic.

10.3.2.2 Porosity and permeability

A series of chronological profiles of porosity and permeability along the 110/11 cross-section was plotted in Figures 10-9 and 10-10. The ages for the profiles of porosity and permeability are 160 Ma, 145 Ma, 136 Ma, 120 Ma, 90 Ma, 65 Ma, 24 Ma and present-day. The porosity evolution was modelled, and, thus, based on the modelled porosity, permeability values were calculated using the modified Kozeny-Carman equation (Ungerer et al. 1990) in BasinMod 2D. Figures 10-9 and 10-10 show the evolution process of porosity and permeability:

1. At 160 Ma, 145 Ma and 136 Ma (Figures 10-9-1 A, B and C; 10-10-1 A, B and C), the bottom of the Jurassic section underwent rapid compaction leading to the occurrence of very low porosity and permeability zones with the lowest permeability values about 10^{-24} m^2, which actually formed a impermeable bottom boundary of the Jurassic in the depocentre of the sub-basin since about 138 Ma. It can be seen that strong compacted zones occurred along the major faults, which indicated that pore water rapidly migrated along the fault planes during the rifting burial and fault activity. It is obvious that porosities of about 10-45 % remained in the middle-upper part of the Jurassic sequence.

2. At 120 Ma, 90 Ma and 65 Ma (Figures 10-9-1 D; 10-9-2 E and F; 10-10-1 D; 10-10-2 E and F), porosity slowly decreased in the Jurassic section due to slow overburden loading during this period. Pore water release along fault conduits tended to cease. The estimated porosities of 7-10 % remained in the middle of the Upper Jurassic sequence, while the Middle-Lower Jurassic rocks were highly compacted.

3. At 24 Ma and present-day (Figures 10-9-2 G and H; 10-10-2 G and H), the porosity values in the Upper Jurassic section in the central sub-basin ranged from approximately 2 % to 7 %. The vertical permeability was about 10^{-20} m^2 at the top of the Upper Jurassic rocks and about 10^{-23}-10^{-25} m^2 in the Lower-Middle Jurassic rocks. It can be seen that the lateral fault sealing resulted in many separated cells in the deep overpressured system of the Jurassic section.

10.3.2.3 Fluid pressure

The calculated eight profiles of chronological excess pressure have been chosen to show the modelled deep overpressure evolution for the following geological times: the end of the Middle Jurassic (160 Ma), the end of the Late Jurassic (145 Ma), the early period of the Early Cretaceous (136 Ma), the middle of the Early Cretaceous (120 Ma), the early period of the Late Cretaceous (90 Ma), the end of the Late Cretaceous (65 Ma), the end of the Oligocene (24 Ma) and present-day (Fig. 10-11). Figure 10-11-1 (A, B and C) shows that the Jurassic overpressure was developed during the deposition of the Jurassic and the Lowest Cretaceous sequences (Barrow

Group). The maximum excess pressures were calculated to be about 35 MPa, 83 MPa and 103 MPa at 160 Ma, 145 Ma and 136 Ma, respectively in the Lower Jurassic succession. It seems that the rapid sedimentation rates in the fine-grained sediments during the rift phase were a significant cause of overpressure generation. From these excess pressure profiles, the migration of water was dominated by upward water flow as indicated by water flow direction and the lateral flow of water was presented on the cross-section. Pore water flow and overpressure emission from the Jurassic rocks along fault planes were significant events during the period. Figures 10-11-1 (D) and 10-11-2 (E) show that the upward emission of overpressure and water flow along the major normal faults from the Jurassic sequence were gradually weakened as faults closed during the time interval. The maximum excess pressures were modelled to be 85 MPa (120 Ma) and 62 MPa (90 Ma) in the Jurassic section. Figure 10-11-2 (F, G and H) shows the overpressure evolution during the Cainozoic. The modelled results indicate that the upward water flow and overpressure release from the Jurassic overpressured system appeared to be slow. It should be noted that the compaction effect for the deep overpressure should not be a significant source because most of the porosity has been lost through compaction and small porosities of 2-7 % remained in the well-compacted fine-grained Jurassic source rocks and very slow deposition from 64 Ma to present-day. However, the discharge of the modelled overpressure from the Jurassic overpressured compartments was slow and the maximum excess pressures were 53 MPa at 64 Ma and 45 MPa at present-day. The approximate 10 % of the total excess pressures were calculated to be caused by fluid thermal expansion and generated pressure. Perhaps, the deep overpressured system was significantly maintained by sealed conditions since the Cainozoic from the BasinMod 2D modelling.

10.4 Two-dimensional overpressure modelling in the Dampier Sub-basin

The length of the 101R/09 cross-section in the Dampier Sub-basin for the modelling is about 135 km and the interpreted maximum depth of the cross-section is about 11000 m. The cross-section was divided into 29,765 cells with time intervals of 2

Ma and x-distance intervals of 1 km. The critical normal faults were designed on the geological 2D model and were modelled over geological time.

10.4.1 Correlation between the calculated values and the observed data

10.4.1.1 Fluid pressure correlation

Figure 10-12 shows correlation between the modelled pressure lines and measured fluid pressures at the three well sites of Goodwyn-7, Rosemary-1 and Hampton-1 along the 101R/09 cross-section in the Dampier Sub-basin. These three wells were drilled either on the shoulders of the rift graben or on its flank (Fig. 9-7). Therefore, these wells have shown generally normal pressures in the Jurassic rocks (absence of the Jurassic formations in Goodwyn-7). The overpressure within the Jurassic section in this sub-basin was observed in Dampier-1. The slightly overpressured zone in this well occurs at a depth of about 2900 m (Fig. 5-5), mentioned in Chapter 5.

10.4.1.2 Temperature and maturity correlation

Figure 10-13 shows the calculated temperature and maturity, and the observed formation temperatures and maturity values at the well sites of Goodwyn-7, Rosemary-1 and Hampton-1 along the 101R/09 cross-section. All formation temperatures in the three wells are the corrected BHTs by adding 10 % of the raw BHTs (Table 10-2). The constant heat flows of 40-43 mW/m^2 and seafloor temperatures can match with both the measured formation temperatures in the three wells and the maturity data in Rosemary-1 and Hampton-1 (absence of maturity data in Goodwyn-7). The observed maturity data were obtained from 1D modelled maturity trends using the Rock-Eval T_{max} data in Rosemary-1 and Hampton-1.

10.4.2 Results of the BasinMod 2D modelling

10.4.2.1 Sedimentation rates

Based on the calculated sedimentation rates along the cross-section, rapid deposition occurred during the Jurassic period and the depositional rates were about 100-250

m/Ma in the depocentre of the sub-basin. The sedimentation rates in the Cretaceous ranged from 10 m/Ma to 80 m/Ma. During the Cainozoic, relatively rapid loading occurred from an x-distance of 0 km to 80 km on the cross-section with sedimentation rates of about 40-80 m/Ma, while slow sedimentation occurred from an x-distance of 80 km to 135 km on the cross-section with the depositional rates of about 10-20 m/Ma.

Table 10-2 Measured BHTs from three wells in the Dampier Sub-basin

Well	Depth (m) (K.B.)	BHT (^{o}C)	Raw BHT + 10 % (^{o}C)
Goodwyn-7	1819	63	69.3
	3445	102	112.2
Rosemary-1	1802	62.78	69.1
	1864	65.56	72.1
	2924	98.33	108.2
	3272	108.89	119.8
	3905	125.56	138.1
Hampton-1	1194	53	58.3
	2556	83	91.3

10.4.2.2 Porosity and permeability

A series of chronological profiles of the modelled porosity and permeability on the 101R/09 cross-section was plotted in Figures 10-14 and 10-15. The ages for these profiles are also 160 Ma, 145 Ma, 136 Ma 120 Ma, 90 Ma, 65 Ma, 24 Ma and present-day. The porosity evolution was modelled referring to the parameters from the Barrow Sub-basin due to the lack of measured data. The permeability profiles were calculated using the modified Kozeny-Carman equation (Ungerer et al. 1990) in the BasinMod 2D. The features of porosity and permeability evolution are shown in Figures 10-14 and 10-15:

1. At 160 Ma, 145 Ma and 136 Ma (Figures 10-14-1 A, B and C; 10-15-1 A, B and C), several hundred meters of the bottom of the Jurassic rocks experienced quick compaction and release of pore fluids in the depocentre of the sub-basin. It can be seen that modelled porosities of about 15-20 % remained in the Middle-Lower Jurassic sequence and porosities of 20-40 % were in the Upper Jurassic section at 136 Ma.

2. At 120 Ma, 90 Ma and 65 Ma (Figures 10-14-1 D; 10-14-2 E and F; 10-15-1 D; 10-15-2 E and F), with the deposition of the Cretaceous, the Jurassic rocks were gradually compacted causing porosity to decrease through the period. The maximum porosity value in the Jurassic section of the depocentre fell from about 15 % at 120 Ma to about 8 % at 65 Ma.

3. At 24 Ma and present-day (Figures 10-14-2 G and H; 10-15-2 G and H), the maximum porosity value was about 7 % at 24 Ma and 6 % at present-day in the Jurassic source rocks of the central sub-basin. The vertical permeability was about 10^{-19} m^2 at the top of the Upper Jurassic section and about 10^{-24} m^2 at the bottom of the Lower-Middle Jurassic section. It can be seen that the vertical permeability values in the rocks along faults in the central sub-basin were about 10^{-24} m^2. Therefore, from this modelling, the bottom of the Jurassic rocks and the fault rocks actually formed impermeable boundaries for the Jurassic source section in the centre of the sub-basin.

10.4.2.3 Fluid pressure

Eight profiles of the modelled excess pressure have been selected to explain the modelled deep overpressure history for the following geological times: the end of the Middle Jurassic (160 Ma), the end of the Late Jurassic (145 Ma), the early period of the Early Cretaceous (136 Ma), the middle of the Early Cretaceous (120 Ma), the early period of the Late Cretaceous (90 Ma), the end of the Late Cretaceous (65 Ma), the end of the Oligocene (24 Ma) and present-day (Fig. 10-16). Figure 10-16-1 (A and B) shows that the Jurassic overpressure was developed mainly in the Lower-Middle Jurassic section during the deposition of the Jurassic rocks. The maximum excess pressures were about 40 MPa at 160 Ma and 65 MPa at 145 Ma. The lower part of the Jurassic section was overpressured in the central sub-basin. The dominant direction of water flow was upward. Figure 10-16-1 (C and D) shows that the deep overpressure was maintained in the Lower-Middle Jurassic rocks with the highest excess pressure of about 68 MPa. Upward water flow continued through this period. Figure 10-16-2 (E and F) shows the distribution of deep overpressure in the Jurassic was similar to that at 136-120 Ma. However, upward water flow significantly weakened during this time. Figure 10-16-2 (G and H) indicates that the overpressure

in the lower part of the Upper Jurassic from the left boundary to about middle of the cross-section was enhanced, which may be due to the deposition of the Cainozoic. Upward water flow occurred significantly in the Cainozoic sequence.

10.5 Pressure behaviour modelling

It seems that the variable of permeability is not sensitive to the deep overpressure calculation in the 2D overpressure modelling if the permeabilites are less than 10^{-19}-10^{-20} m^2. Based on presently available stratigraphic, petrographical and petrophysical data, a pressure seal may exist within the sub-basins. However, questions remain as to whether the present-day maintained overpressure is caused by compaction disequilibrium in the geological past, and whether permeabilities of 10^{-19}-10^{-22} m^{-2} (10^{-4}-10^{-7} md) for a pressure seal are sufficiently low to preserve the overpressure for tens of millions of years. A simple 1D model was used in the hope of estimating how rapidly pressure dissipates. It should be noted that dissipation of excess pressure is different in the 2D and 1D processes, in spite of fluid expulsion from overpressured shaly sections being dominantly vertical. However, with 2D, an extra dimension is added to permit dissipation (rather than just vertically), and the dissipation may be even more rapid. Thus, the deductions below may be strengthened. Therefore, the simple theoretical considerations below provide important information about overpressure longevity.

Fundamental questions posed by the computer-based basin modelling are (1) the persistence of an overpressure cell over time, (2) the importance of compaction disequilibrium as a cause of maintained overpressure, and (3) the importance of hydrocarbon generation as a cause of maintained overpressure. Such questions may be resolved by the application of some simple mathematically tractable models. This section describes these simple models and their results.

The theory of pressure modelling has been fully dealt with by Bear (1972) and Sahimi (1995), amongst others. It has been long recognised that diffusion approximation of pressure behaviour (Bear, 1972, pp. 408-409; Cossé, 1993, p. 134) by using exact tractable mathematical solutions is a relatively simple way to solve

pressure problems. One can thus circumvent the necessity of using time, and distance increments, which in turn may have compromised the accuracy of the modelling.

These mathematical solutions can be used to determine the dissipation time of the overpressure observed in the pressure-depth profiles of Figures 5-1 to 5-7, assuming that compaction disequilibrium and hydrocarbon generation do not maintain the overpressure. The specifically selected area is the Bambra locality in the Barrow Sub-basin, where subsidence and deposition has been particularly slow over the past 50 Ma, and compaction disequilibrium cannot be a major mechanism for maintaining overpressure. It is also assumed that the overpressured region is 3000 m thick (Fig. 10-17), and represents the Type-3 behaviour of Tingate et al. (2001, fig. 9, p. 582), which is consistent with the BasinMod 2D models in Fig. 10-6.

For the present modelling, it is assumed that there is an overpressured zone at some depth below the surface. Hydrostatic pressure is maintained to the top of this zone, and is also maintained below the zone. Initially, there is an excess pressure of ΔP throughout the zone, which has a thickness H. Figure 10-17 shows this initial model, and subsequent pressure-depth decay profiles for various times, as calculated by the equation below. For the above model conditions, the diffusion-behaviour equation for excess pressure (as a function of time and depth), P_{ex}, has been well approximated by Carslaw and Jaeger (1959, p. 96):

$$P_{ex} = \Delta P(4/\pi) \exp[-\beta\pi^2 t/H^2]\sin[\pi z/H] \quad , \qquad (10\text{-}1)$$

where ΔP is the initial excess pressure of the zone, β is a diffusivity parameter (units of m^2/s), t is time in seconds, H is the thickness of the overpressured zone in metres, and z is depth in the overpressured zone in metres. The parameter β is defined as $k/\phi\mu c$, where k is permeability, ϕ is porosity, μ is viscosity and c is compressibility of fluid.

Three models have been computed:

(1) where the porosity and the permeability of the overpressured zone are 1 % and 10^{-22} m^2 (10^{-7} md), respectively (Fig. 10-17),

(2) where the porosity and the permeability of the overpressured zone are 5 % and 10^{-20} m^2 (10^{-5} md), respectively (Fig. 10-18), and

(3) where the porosity and the permeability of the overpressured zone are 5 % and 10^{-18} m^2 (10^{-3} md), respectively (Fig. 10-19).

The compressibility is assumed to be 5 x 10^{-10} Pa^{-1}, and the viscosity is assumed to be 0.001 Pa∃S, which are both close to that of water. The thickness of the overpressured zone is taken to be 3000 m.

When interpreting these results, it must be remembered that the model is designed to show the amount of excess pressure remaining in the Bambra locality, if the presently observed overpressure were to decay. Thus, the model in Fig. 10-17 suggests that some small amount of initial excess pressure would remain after 2 million years of dissipation, and that a half amount of excess pressure would be lost after 1 million years, if the permeability of the overpressured zone were predominantly 10^{-22} m^2 (10^{-7} md). The model in Fig. 10-18 suggests that the overpressure would be almost dissipated after 100,000 years, if the permeability of the zone were 10^{-20} m^2 (10^{-5} md). The model in Fig. 10-19 suggests that after only 1000 years most of the excess pressure has dissipated from a 3000 m thick overpressure zone with the average permeability of 10^{-18} m^2 (10^{-3} md).

10.6 Discussion

10.6.1 Pressure seal

Deming (1994) discussed three factors (time, thickness and permeability) necessary to define a pressure seal in greater detail, and calculated the maximum time related to a seal layer of given thickness and permeability to confine excess pressures, using the well-known diffusion equation (Fig. 10-20). The calculated results indicate that

(1) a 800-1000-m-thick rock layer with permeability of 10^{-21} m^2 (10^{-6} md) would maintain overpressure from one million years to several million years, (2) the overpressure would be dissipated after one million years to several million years if there was a 300-500-m-thick rock layer with the permeability of 10^{-22} m^2 (10^{-7} md), and (3) a 300-500-m-thick rock layer with permeability of about 10^{-23} m^2 (10^{-8} md), or less, would maintain the overpressure from ten million years to several tens of millions of years.

The pressure seal modelling of pressure behaviour in porous media in the Bambra locality of the Barrow Sub-basin for maintaining excess pressures in the sealed environments also suggests that even in an overpressure zone of over a thousand meters thick within a very low-permeability (10^{-22} m^{-2}) area, the overpressure can be maintained only several million years at best. It implies that it is almost impossible for the observed top pressure seal in the Barrow Sub-basin to preserve the deep overpressure for tens of millions of years, without continued renewal of the overpressure.

This modelling, therefore, raises the issue of realistic average permeabilities for the Middle-Upper Jurassic shale sequence in the Barrow Sub-basin. Bruce et al. (1996) suggested that compacted clays typically have permeabilities in the 10^{-16} m^2 to 10^{-17} m^2 (10^{-1}-10^{-2} md) range. Schön (1996) also suggested from an extensive literature review that the lower limit of permeability in shale is about 10^{-20} m^2 (10^{-5} md). As mentioned above, the porosities in the top pressure seal generally range from 2 % to 5 % based on the well-log data and some measured porosity data from claystone, thus, the permeabilities possibly range from 10^{-19} m^2 (10^{-4} md) to 10^{-22} m^2 (10^{-7} md). It seems that a permeability value as low as 10^{-22} m^2 is the lower limit for a compacted, even strongly compacted shale. However, the above results of the pressure seal imply that for overpressures to be retained in a thick zone for several million years, or longer, the permeability of the zone must be significantly less than 10^{-20} m^2 (10^{-5} md) by several orders of magnitude (about, or less than, 10^{-23} m^2). It requires a porosity of less than 1 % but this very small porosity for the whole top pressure seal is very unlikely to occur.

From the physio-chemical point of view, the difficulty for hydrocarbon expulsion from source rocks may depend on its saturation and wettability in the pore media. Firstly, it is more difficult for oil and gas migration to occur from a well-compacted shale if water saturation is high, as the hydrocarbon relative permeabilities will be very low. Secondly, the capillary pressure for oil and gas migration will be high if there are water-wet source rocks. The low hydrocarbon relative permeabilities at a top pressure seal, which is water-wet, may be quite efficient in preventing oil and gas being expelled from the deep overpressured source rocks. It has been, however, proposed that the wettability in source shales is different from reservoirs. There may be a possibility of variable hydrocarbon-wettability in various parts of the source section, for example, a distribution of bitumen within the pore centre network of a shale (Barker, 1980), or specific wetting paths (Ungerer et al., 1990) with relatively high hydrocarbon saturation and relative permeabilities. To maintain the overpressure, a seal is still required, or, at least, the release of overpressure through the seal should be slower than generating overpressure. Although the occurrence of deep overpressure suggests the existence of a relatively effective pressure seal, it is very unlikely that the seal is a unique factor for maintaining the deep overpressure for up to several millions of years or so. The results using BasinMod 2D, therefore, may have significantly overstated the effect of the seal conditions for maintaining overpressure. Thus, it is suggested that continuous oil and gas generation, and thermal expansion with continuous pressure recharge over the past tens of millions of years is required to maintain the deep overpressure.

10.6.2 Possible major mechanisms for the deep overpressure

It seems that the practical top pressure seal is unlikely to maintain overpressure for more than several million years without a continued pressure recharge. There is no evidence that smectite to illite transformation has a determined role on the observed deep overpressure in the study area. These pose the consideration of two commonly proposed mechanisms of the observed overpressure (1) compaction disequilibrium, and (2) hydrocarbon generation.

10.6.2.1 Compaction disequilibrium

Compaction disequilibrium is common in fine-grained rocks with high sedimentation rates which are usually overpressured (Swarbrick, 1995). These rates in fine-grained rocks during the Jurassic may cause overpressure in the sub-basins due to compaction disequilibrium. However, deep overpressure is very likely to dissipate in several million years unless the permeability of the top pressure seal is about 10^{-23} m^2 (10^{-8} md), or less, which is very unlikely to occur. Since the Cainozoic, it seems that compaction disequilibrium has been an unlikely significant source of overpressure in the well-compacted Jurassic source rocks, if very low rates of subsidence and deposition occurred over the past tens of millions of years, as mentioned above.

Many researchers assume the relationship between fluid pressure and effective stress of Terzaghi (1923):

$$P_{fl} = P_{ob} - \sigma_{eff} \ , \qquad (10\text{-}2)$$

where P_{fl} is fluid pressure, P_{ob} is overburden pressure, σ_{eff} is effective stress. This relationship is based on laboratory experiments under surface conditions.

The assumption supposes that fluid pressure increases as effective stress decreases, as is often suggested to occur during undercompaction (anomalous high porosities) of shales. Terzaghi's principle has been widely used to evaluate fluid pressure from well logs. However, Hermanrud et al. (1998) have questioned the application of the Terzaghi relationship (with respect to porosities derived from the sonic and resistivity log) on the basis of their study of porosities in overpressured shales in the Haltenbanken.

In the present study (see also Chapter 5), the core-, neutron- and density-derived porosities in shales of the deep overpressured system are significantly lower than the sonic- and resistivity-derived porosities, which is consistent with the findings of Hermanrud et al. (1998). For example, the measured shale porosities range from 4.9-6.6 % at 4274-4283 m in Bambra-2, but sonic-log derived porosities are 13-18 % (high sonic transit times of 279-295 ③s/m) at the same depths in Bambra-2 (Fig. 5-3). Density logs in Bambra-1, West Barrow-1/1A and Jurabi-1 in the deep

overpressured system do not exhibit any porosity anomaly (Figures 5-2, 5-4 and 5-6). These suggest that the sonic-log and resistivity-log data may not be consistent with abnormally high porosities expected in the overpressured source rocks. In turn, this suggests that the present day deep overpressure is not associated with a significant porosity anomaly due to compaction disequilibrium in the fine-grained rocks. The maintenance of the overpressure in the Jurassic source rocks to the present-day, therefore, requires that a mechanism other than compaction disequilibrium be sought to explain the deep overpressures in the sub-basins.

10.6.2.2 Hydrocarbon generation

On the basis of this study, one has to consider that the major causes for pressure recharge to maintain the deep overpressures are hydrocarbon generation in the Cainozoic after the thick Jurassic shales and siltstones had been compacted and most of the porosity in the Jurassic sequence had been lost through compaction. In fact, the deep overpressured system in the Barrow Sub-basin, interpreted by the sonic-log, resistivity-log and the measured pressure data, is in agreement with the observed zone of organic maturity of 0.8-2.0 % R_o (vitrinite reflectance) and an increased volume of gas-generating organic matter. The boundary between the pressure transition zone and the overpressured compartment (bottom of top pressure seal) is consistent with a maturity of about 1 % R_o. R_o at the top of the deep overpressured zone is about 1 % in Dampier-1 of the Dampier Sub-basin and also about 1 % in Jurabi-1 of the Exmouth Sub-basin. This may be why the deep overpressured zone frequently appears to have a planar top in a basin. The depth of the planar top seems to be associated with the upper part of the hydrocarbon generation zone with the thermal maturity range of about 0.8-1 %. It is proposed that if an effective pressure seal exists it can only maintain the overpressure for several million years at best, while continuous hydrocarbon generation, especially gas generation and thermal expansion, for a pressure recharge over the past several tens of millions of years is very likely to be the major cause of maintenance of the deep overpressure. As hydrocarbon generation and charge in the Jurassic source rocks is believed to have occurred since the Cainozoic, it is not inconceivable that an overpressure regime has been maintained since that time.

10.7 Summary

This study and modelling has shown several possible ways of interpreting the observed abnormal fluid pressures in the sub-basins. The BasinMod 2D basin modelling has suggested a maintained pressure cell in the Jurassic sequence since the Cainozoic. This modelling may inadvertently support some unrealistic petrophysical parameters, and computational assumptions. Nevertheless, the modelled overpressure distribution at present-day is fairly consistent with the observed data. The pressure seal that appears to be present in the Barrow Sub-basin clearly suggests that the observed overpressure can be only maintained by the top pressure seal for several million years at best, unless extremely low permeabilities (10^{-23} m^2 or less) occur for a thousand meters in the Jurassic shaley sequences of the sub-basins.

The modelled results using the BasinMod 2D software suggest the following observations:

(1) The rapid sedimentation rates in fine-grained rocks during the basin subsidence of the Jurassic, resulting in compaction disequilibrium, are likely to be a mechanism for generating overpressure.

(2) The pressure seal, including top and bottom low-permeability rocks and lateral sealed faults, is one of the major controls on the deep overpressured compartments in the Jurassic shaley sequence since the Cainozoic.

(3) Quartz cementation may be a significant factor in forming a low-permeability rock layer for a top pressure seal.

(4) Thermal expansion of pore fluids makes a 5-10 % contribution to the maximum excess pressure in the studied case, and the generated pressure of hydrocarbon generation makes a less than 2 % contribution to the maximum excess pressure in the sub-basins.

(5) Additionally, the modelled heat flow values required to match the measured maturity data and formation temperatures, at the selected well sites along three cross-sections using BasinMod 2D, are significantly lower than the calculated current heat flows in these wells using BasinMod 1D. The calculated heat flows in these wells using the BasinMod 1D modelling are 10 % to 20 % higher than those from the BasinMod 2D modelling at these well sites along the cross-sections (Table 10-3).

Table 10-3 The heat flow values required for fitting the measured maturity data from the 1D BasinMod modelling and the BasinMod 2D modelling in three sub-basins

Well Name	**1D Heat Flow (mW/m^2)**	**2D Heat Flow (mW/m^2)**	**Surface Temperature (^oC)**	**Water Depth (m)**
Bambra-2	56.0	43-46	24	26
West Tryal Rocks-1	54.3	**Barrow**	21	138
Outtrim-1	60.4		22	91
Novara-1	52.8	52-54	17	372
Zeewulf-1	59.7	**Exmouth**	4.5	1194
Goodwyn-7	48.0		21	134
Hampton-1	43.9	40-43	23	53
Rosemary-1	47.5	**Dampier**	23	65

Further modelling studies of pressure behaviour and formation compaction also suggest:

(1) The permeability values of 10^{-19} m^2 to 10^{-22} m^2 in situ may be not sufficient for required permeabilities of about 10^{-23} m^2, or less, to maintain the deep overpressured regime in the Jurassic section over a time span of several tens of millions of years.

(2) Compaction disequilibrium may not be a significant source to charge and maintain the deep overpressures since the Cainozoic.

(3) There is the strong possibility of the validity of the hypothesis proposed by Horstman (1988) and Zaunbrecher (1994) that a maintained deep overpressure regime in the sub-basins is the product of continued hydrocarbon generation, especially gas generation and thermal expansion, and subsequent further maturation, which entails oil to gas cracking. The sealed conditions of low-permeability to retain the deep overpressure are still required.

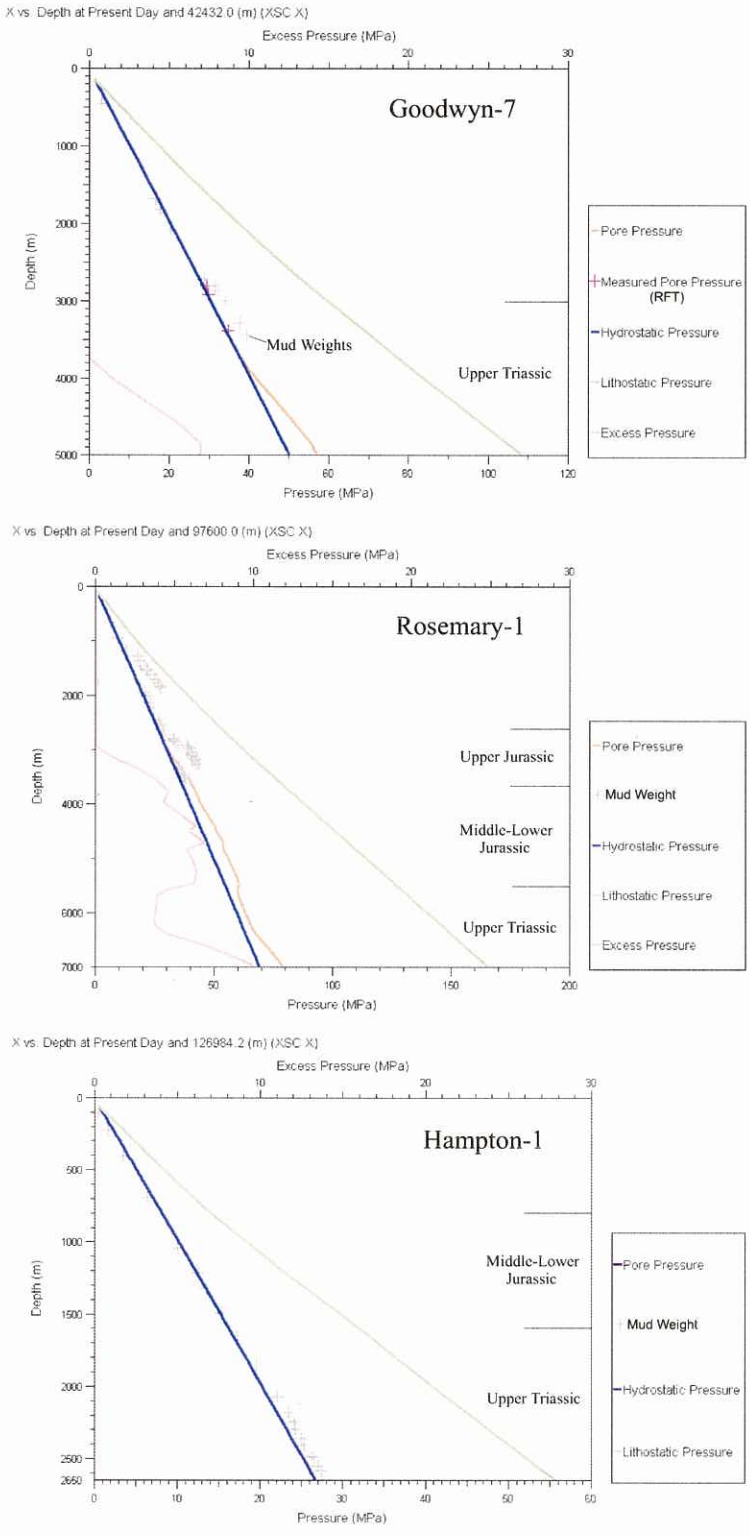

Fig. 10-12 Correlation between the modelled fluid pressures and the measured fluid pressures, including RFT pressures and mud weight pressures, at the three well sites of Goodwyn-7, Rosemary-1 and Hampton-1along the 101R/09 cross-section in the Dampier Sub-basin.

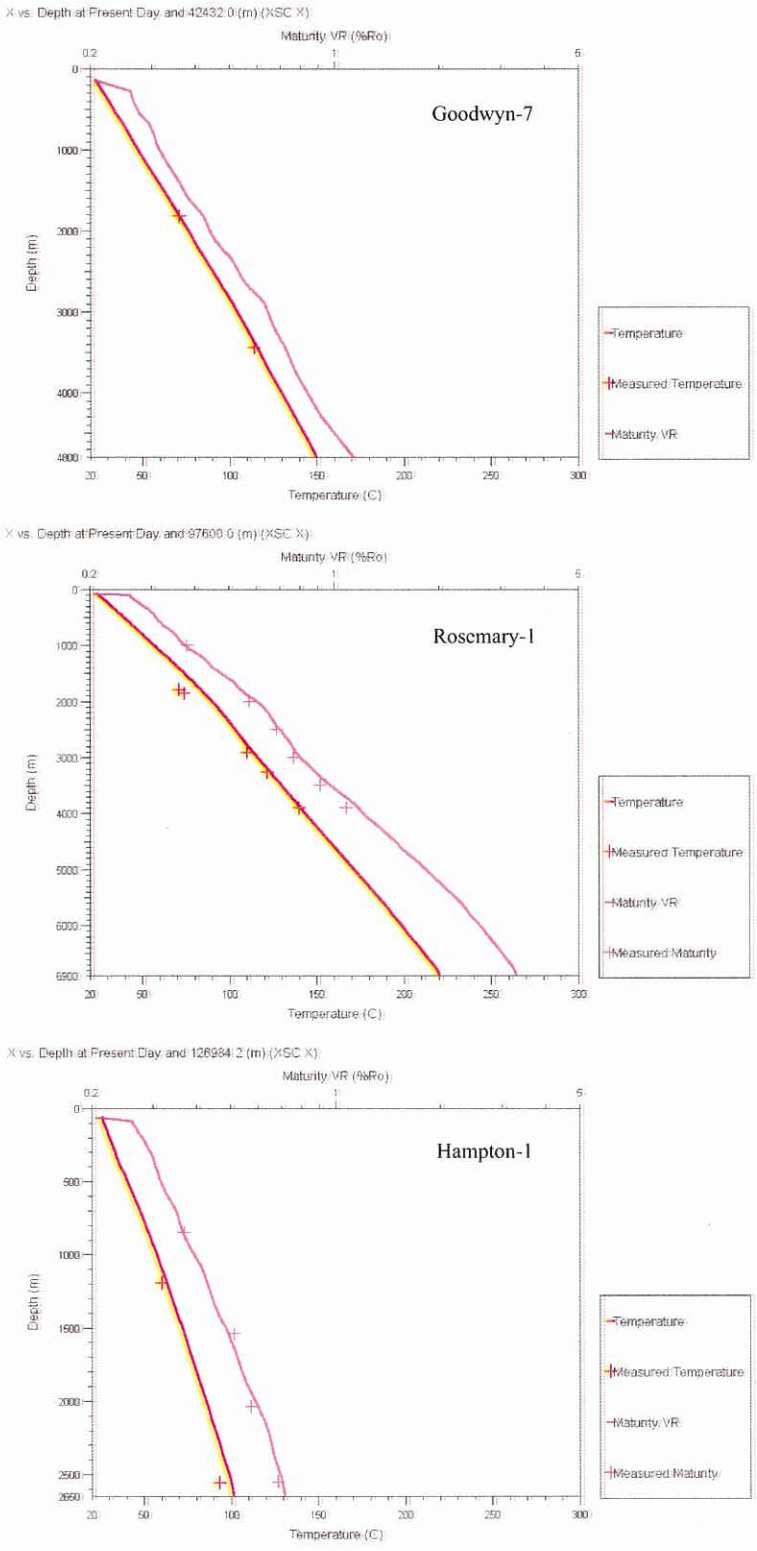

Fig. 10-13 Correlations between the modelled temperature and maturity curves and the observed formation temperatures and thermal maturity data at the well sites of Goodwyn-7, Rosemary-1 and Hampton-1 along the 101R/09 cross-section in the Dampier Sub-basin.

m/Ma in the depocentre of the sub-basin. The sedimentation rates in the Cretaceous ranged from 10 m/Ma to 80 m/Ma. During the Cainozoic time, relatively rapid loading occurred from an x-distance of 0 km to 80 km on the cross-section with sedimentation rates of about 40-80 m/Ma, while slow sedimentation occurred from an x-distance of 80 km to 135 km on the cross-section with the depositional rates of about 10-20 m/Ma.

Table 10-2 Measured BHTs from three wells in the Dampier Sub-basin

Well	Depth (m) (K.B.)	BHT (^{o}C)	Raw BHT + 10 % (^{o}C)
Goodwyn-7	1819	63	69.3
	3445	102	112.2
Rosemary-1	1802	62.78	69.1
	1864	65.56	72.1
	2924	98.33	108.2
	3272	108.89	119.8
	3905	125.56	138.1
Hampton-1	1194	53	58.3
	2556	83	91.3

10.4.2.2 Porosity and permeability

A series of chronological profiles of the modelled porosity and permeability on the 101R/09 cross-section was plotted in Figures 10-14 and 10-15. The ages for these profiles are also 160 Ma, 145 Ma, 136 Ma 120 Ma, 90 Ma, 65 Ma, 24 Ma and present-day. The porosity evolution was modelled referring to the parameters from the Barrow Sub-basin due to the lack of measured data. The permeability profiles were calculated using the modified Kozeny-Carman equation (Ungerer et al. 1990) in the BasinMod 2D. The features of porosity and permeability evolution are shown in Figures 10-14 and 10-15:

1. At 160 Ma, 145 Ma and 136 Ma (Figures 10-14-1 A, B and C; 10-15-1 A, B and C), several hundred meters of the bottom of the Jurassic rocks experienced quick compaction and released of pore fluids in the depocentre of the sub-basin. It can be seen that the modelled porosities of about 15-20 % remained in the Middle-Lower Jurassic sequence and the porosities of 20-40 % were in the Upper Jurassic section at 136 Ma.

2. At 120 Ma, 90 Ma and 65 Ma (Figures 10-14-1 D; 10-14-2 E and F; 10-15-1 D; 10-15-2 E and F), with the deposition of the Cretaceous, the Jurassic rocks were gradually compacted causing porosity to decrease through the period. The maximum porosity value in the Jurassic section of the depocentre fell from about 15 % at 120 Ma to about 8 % at 65 Ma.

3. At 24 Ma and present-day (Figures 10-14-2 G and H; 10-15-2 G and H), the maximum porosity value was about 7 % at 24 Ma and 6 % at present-day in the Jurassic source rocks of the central sub-basin. The vertical permeability was about 10^{-19} m^2 at the top of the Upper Jurassic section and about 10^{-24} m^2 at the bottom of the Lower-Middle Jurassic section. It can be seen that the vertical permeability values in the rocks along faults in the central sub-basin were about 10^{-24} m^2. Therefore, from this modelling, the bottom of the Jurassic rocks and the fault rocks actually formed impermeable boundaries for the Jurassic source section in the centre of the sub-basin.

10.4.2.3 Fluid pressure

Eight profiles of the modelled excess pressure have been selected to explain the modelled deep overpressure history for the following geological times: the end of the Middle Jurassic (160 Ma), the end of the Late Jurassic (145 Ma), the early period of the Early Cretaceous (136 Ma), the middle of the Early Cretaceous (120 Ma), the early period of the Late Cretaceous (90 Ma), the end of the Late Cretaceous (65 Ma), the end of the Oligocene (24 Ma) and present-day (Fig. 10-16). Figure 10-16-1 (A and B) shows that the Jurassic overpressure was developed mainly in the Lower-Middle Jurassic section during the deposition of the Jurassic rocks. The maximum excess pressures were about 40 MPa at 160 Ma and 65 MPa at 145 Ma. The lower part of the Jurassic section was overpressured in the central sub-basin. The dominant direction of water flow was upward. Figure 10-16-1 (C and D) shows that the deep overpressure was maintained in the Lower-Middle Jurassic rocks with the highest excess pressure of about 68 MPa. Upward water flow continued through this period. Figure 10-16-2 (E and F) shows the distribution of deep overpressure in the Jurassic was similar to that at 136-120 Ma. However, upward water flow significantly weakened during this time. Figure 10-16-2 (G and H) indicates that the overpressure

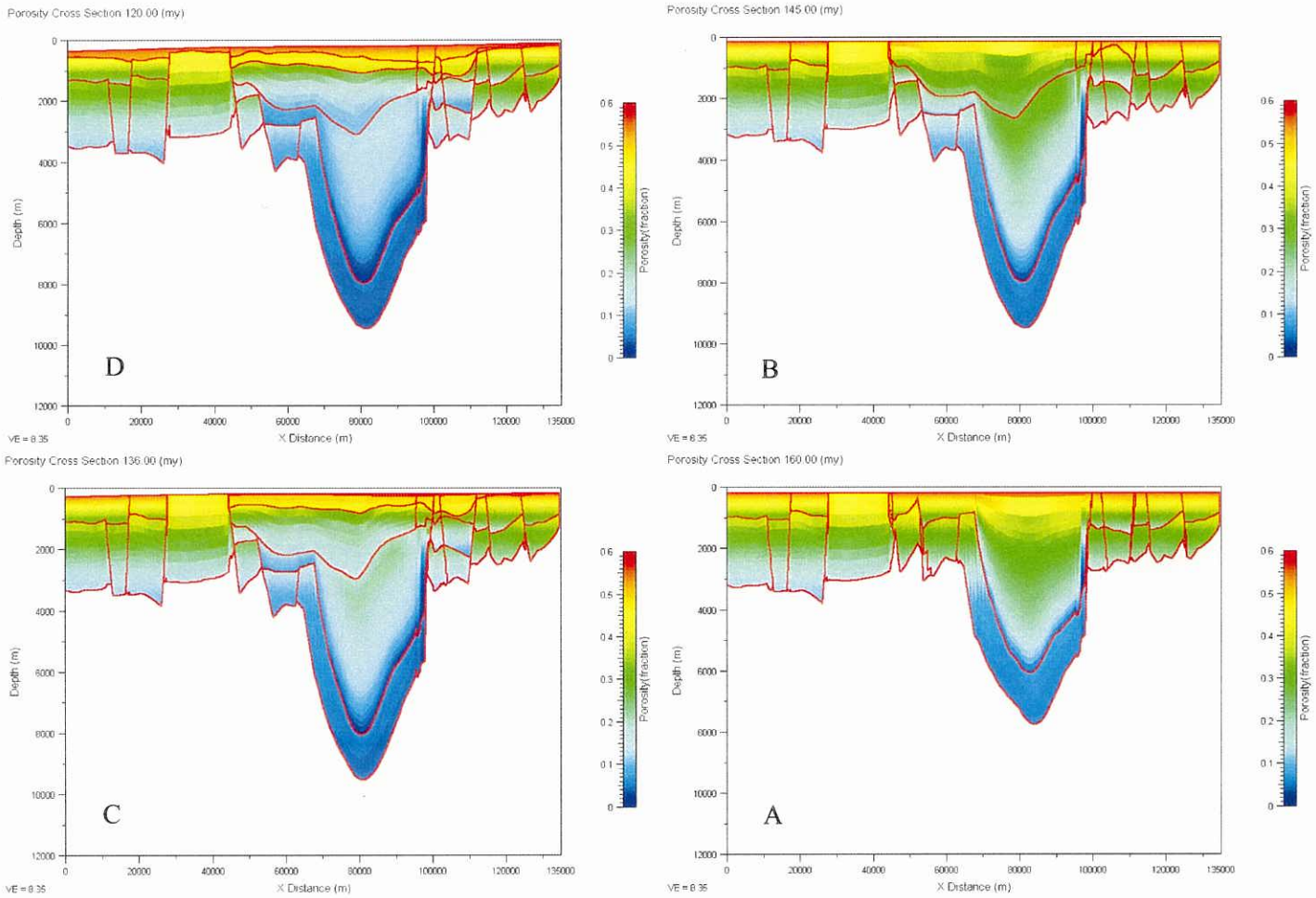

Fig. 10-14-1 Four modelled profiles of porosity evolution at 160 Ma (A), 145 Ma (B), 136 Ma (C) and 120 Ma (D) for the 101R/09 cross-section in the Dampier Sub-basin.

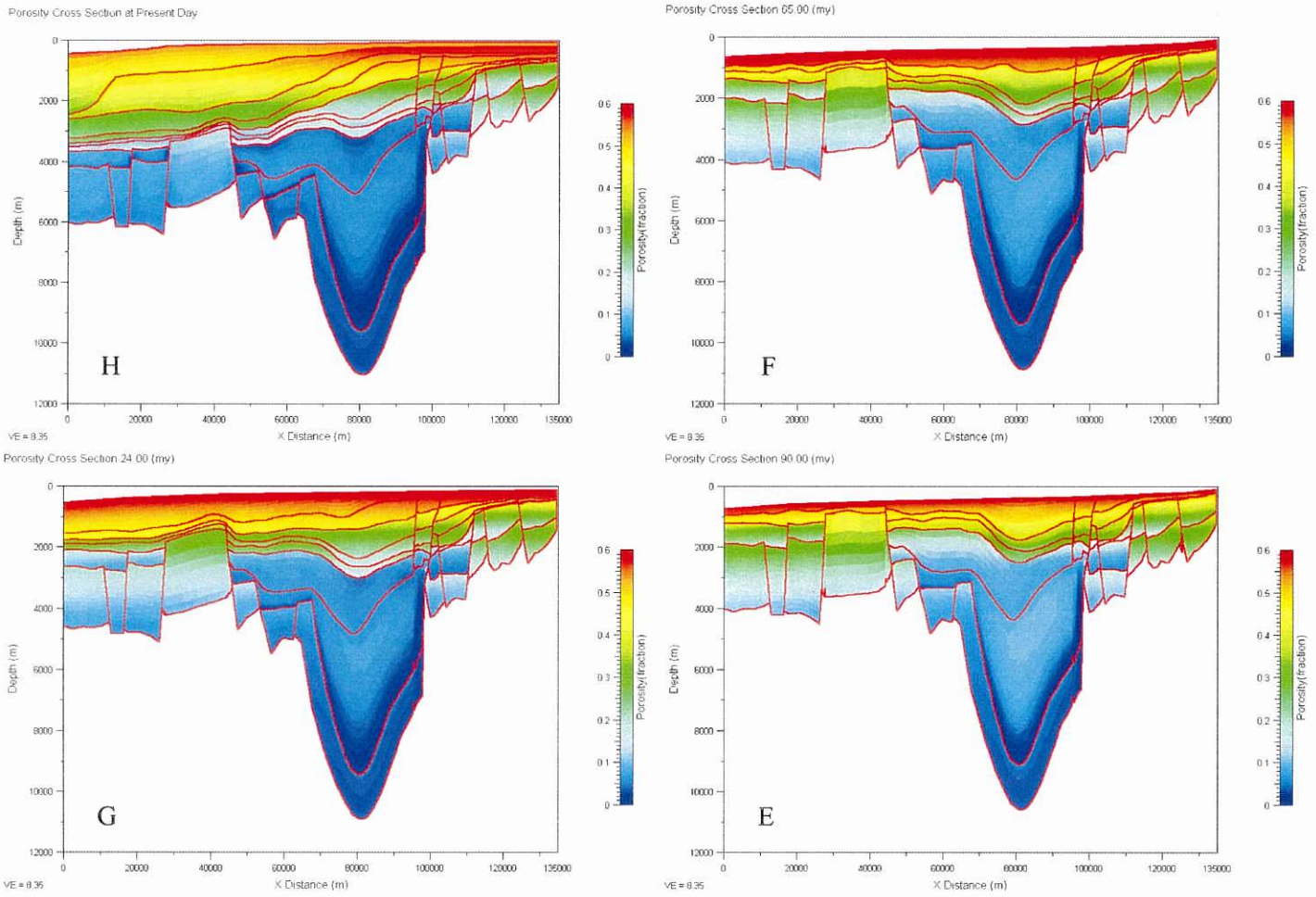

Fig. 10-14-2 Four modelled profiles of porosity evolution at 90 Ma (E), 65 Ma (F), 24 Ma (G) and 0 Ma (H) for the 101R/09 cross-section in the Dampier Sub-basin.

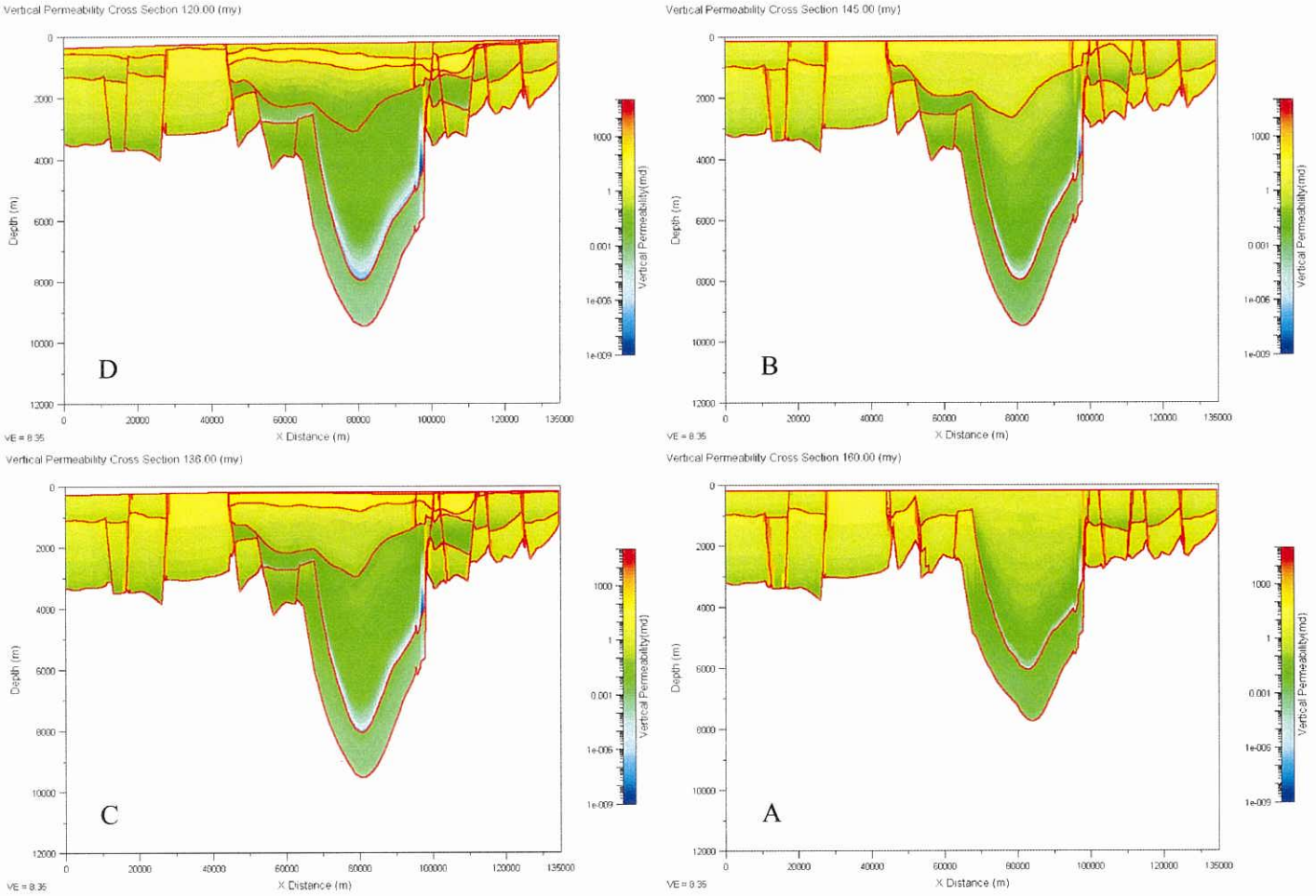

Fig. 10-15-1 Four modelled profiles of vertical permeability evolution at 160 Ma (A), 145 Ma (B), 136 Ma (C) and 120 Ma (D) for the 101R/09 cross-section in the Dampier Sub-basin.

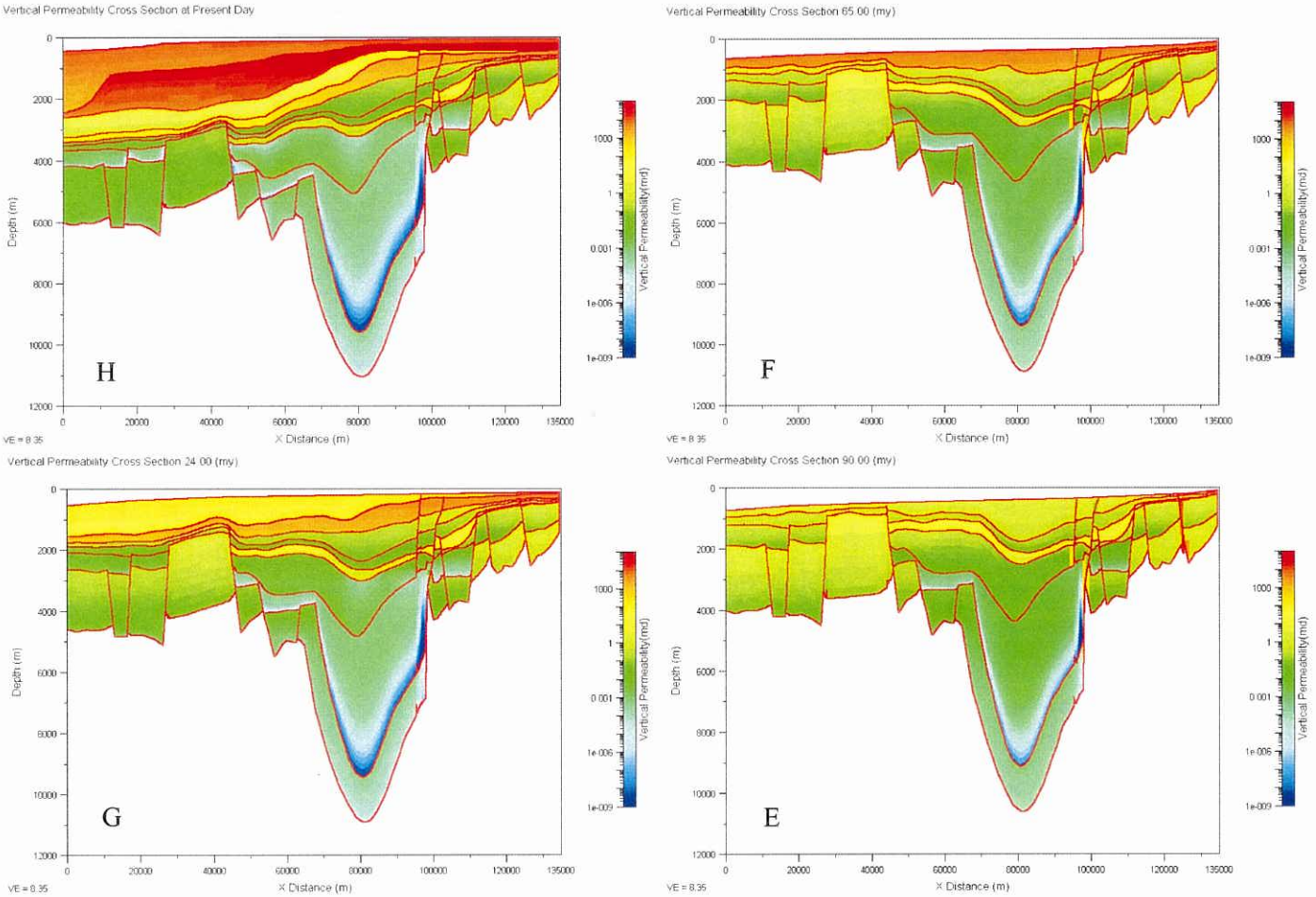

Fig. 10-15-2 Four modelled profiles of vertical permeability evolution at 90 Ma (E), 65 Ma (F), 24 Ma (G) and 0 Ma (H) for the 101R/09 cross-section in the Dampier Sub-basin.

in the lower part of the Upper Jurassic from the left boundary to about middle of the cross-section was enhanced, which may be due to the deposition of the Cainozoic. Upward water flow occurred significantly in the Cainozoic sequence.

10.5 Pressure behaviour modelling

It seems that the variable of permeability is not sensitive to the deep overpressure calculation in the 2D overpressure modelling if the permeabilites are less than 10^{-19}-10^{-20} m^2. Based on presently available stratigraphic, petrographical and petrophysical data, the existence of a pressure seal may exist within the sub-basins. However, questions remain as to whether the present-day maintained overpressure is caused by compaction disequilibrium in the geological past, and whether permeabilities of 10^{-19}-10^{-22} m^{-2} (10^{-4}-10^{-7} md) for a pressure seal are sufficiently low to preserve the overpressure for tens of millions of years. A simple 1D model was used in the hope of estimating how rapidly pressure dissipates. It should be noted that dissipation of excess pressure varies 2D and 1D processes, in spite of fluid expulsion from overpressured shaly sections being dominantly vertical. However, with 2D, an extra dimension is added to permit dissipation (rather than just vertically), and the dissipation may be even more rapid. Thus, the deductions below may be strengthened. Therefore, the simple theoretical considerations below provide important information about overpressure longevity.

Fundamental questions posed by the computer-based basin modelling are (1) the persistence of an overpressure cell over time, (2) the importance of compaction disequilibrium as a cause of maintained overpressure, and (3) the importance of hydrocarbon generation as a cause of maintained overpressure. Such questions may be resolved by the application of some simple mathematically tractable models. This section describes these simple models and their results.

The theory of pressure modelling has been fully dealt with by Bear (1972) and Sahimi (1995), amongst others. It has been long recognised that diffusion approximation of pressure behaviour (Bear, 1972, pp. 408-409; Cossé, 1993, p. 134) by using exact tractable mathematical solutions is a relatively simple way to solve

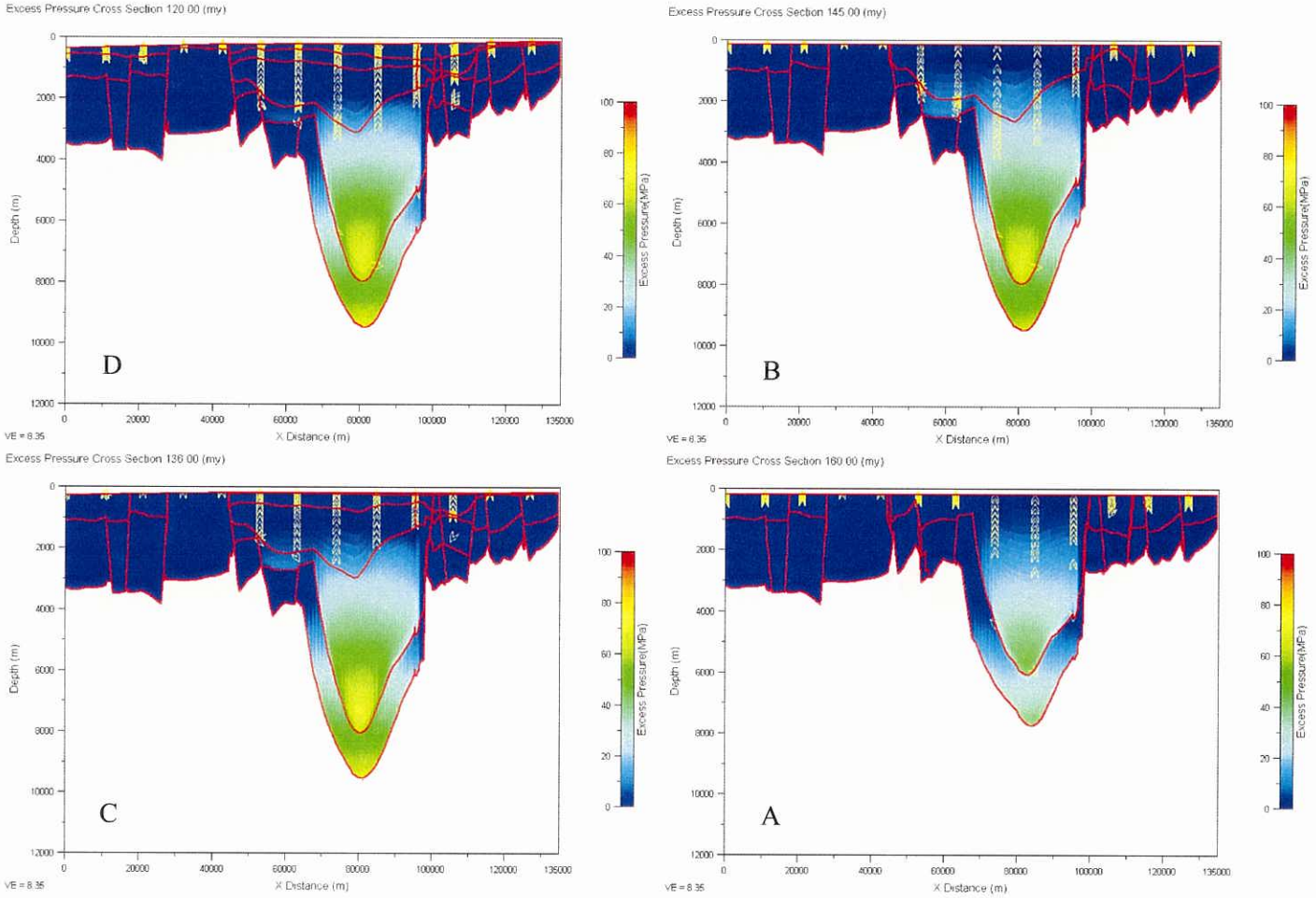

Fig. 10-16-1 Four modelled profiles of the excess pressure at 160 Ma (A), 145 Ma (B), 136 Ma (C) and 120 Ma (D) for the deep overpressure evolution along the 101R/09 cross-section in the Dampier Sub-basin. Arrows show water flow direction.

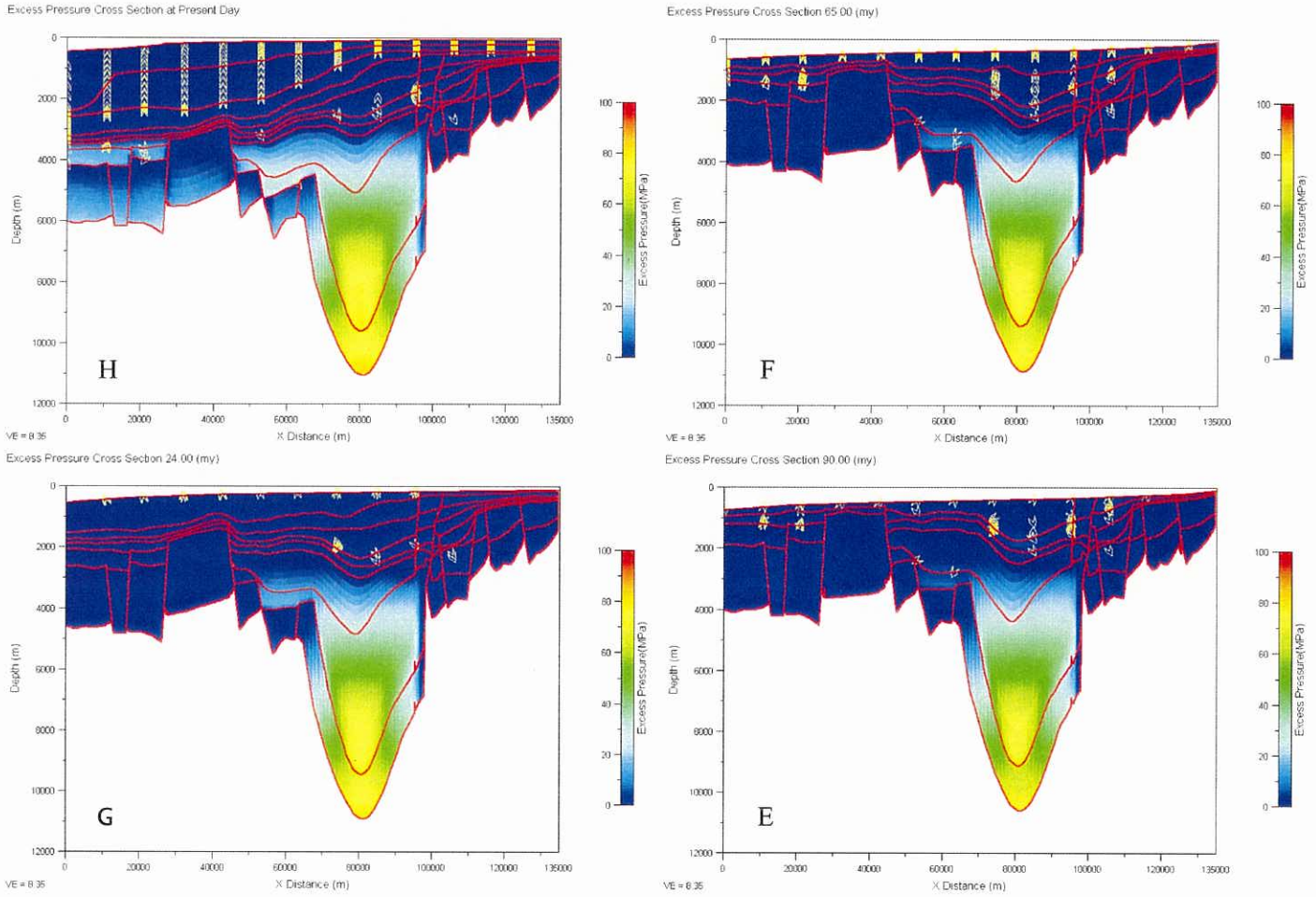

Fig. 10-16-2 Four modelled profiles of the excess pressure at 90 Ma (E), 65 Ma (F), 24 Ma (G) and 0 Ma (H) for the deep overpressure evolution along the 101R/09 cross-section in the Dampier Sub-basin. Arrows show water flow direction.

pressure problems. One can thus circumvent the necessity of using time, and distance increments, which in turn may have compromised the accuracy of the modelling.

The following problem relevant to the present-day overpressured zones of the Barrow Sub-basin was posed. These mathematical solutions to determine the dissipation time of the overpressure observed in the pressure-depth profiles of Figures 5-1 to 5-7, assuming that compaction disequilibrium and hydrocarbon generation do not maintain the overpressure. The specifically selected area is the Bambra locality, where subsidence and deposition has been particularly slow over the past 50 Ma, and compaction disequilibrium cannot be a major mechanism for maintaining overpressure. It is also assumed that the overpressured region is 3000 m thick (Fig. 10-17), and represents the Type-3 behaviour of Tingate et al. (2001, fig. 9, p. 582), which is consistent with the BasinMod 2D models in Fig. 10-6.

For the present modelling, it is assumed that there is an overpressured zone at some depth below the surface. Hydrostatic pressure is maintained to the top of this zone, and is also maintained below the zone. Initially within the zone, there is an excess pressure of ΔP throughout the zone, which has a thickness H. Figure 10-17 shows this initial model, and subsequent pressure-depth decay profiles for various times, as calculated by the equation below. For the above model conditions, the diffusion-behaviour equation for excess pressure (as a function of time and depth), P_{ex}, has been well-approximated by Carslaw and Jaeger (1959, p. 96):

$$P_{ex} = \Delta P(4/\pi)\, exp[-\beta\pi^2 t/H^2] sin[\pi z/H] \quad , \qquad (10\text{-}1)$$

where ΔP is the initial excess pressure of the zone, β is a diffusivity parameter (units of m^2/s), t is time in seconds, H is the thickness of the overpressured zone in metres, and z is depth in the overpressured zone in metres. The parameter β is defined as $k/\phi\mu c$, where k is permeability, ϕ is porosity, μ is viscosity and c is compressibility of fluid.

Three models have been computed:

(1) where the porosity and the permeability of the overpressured zone are 1 % and 10^{-22} m^2 (10^{-7} md), respectively (Fig. 10-17),

(2) where the porosity and the permeability of the overpressured zone are 5 % and 10^{-20} m^2 (10^{-5} md), respectively (Fig. 10-18), and

(3) where the porosity and the permeability of the overpressured zone are 5 % and 10^{-18} m^2 (10^{-3} md), respectively (Fig. 10-19).

The compressibility is assumed to be 5 x 10^{-10} Pa^{-1}, and the viscosity is assumed to be 0.001 Pa∃S, which are both close to that of water. The thickness of the overpressured zone is taken to be 3000 m.

When interpreting these results, it must be remembered that the model is designed to show the amount of excess pressure remaining in the Bambra locality, if the presently observed overpressure were to decay. Thus, the model in Fig. 10-17 suggests that some small amount of initial excess pressure would remain after 2 million years of dissipation, and that a half amount of excess pressure would be lost after 1 million years, if the permeability of the overpressured zone were predominantly 10^{-22} m^2 (10^{-7} md). The model in Fig. 10-18 suggests that the overpressure would be almost dissipated after 100,000 years, if the permeability of the zone were 10^{-20} m^2 (10^{-5} md). The model in Fig. 10-19 suggests that after only 1000 years most of the excess pressure has dissipated from a 3000 m thick overpressure zone with the average permeability of 10^{-18} m^2 (10^{-3} md).

10.6 Discussion

10.6.1 Pressure seal

Deming (1994) discussed three factors (time, thickness and permeability) necessary to define a pressure seal in greater detail, and calculated the maximum time related to a seal layer of given thickness and permeability to confine excess pressures, using the well-known diffusion equation (Fig. 10-20). The calculated results indicate that

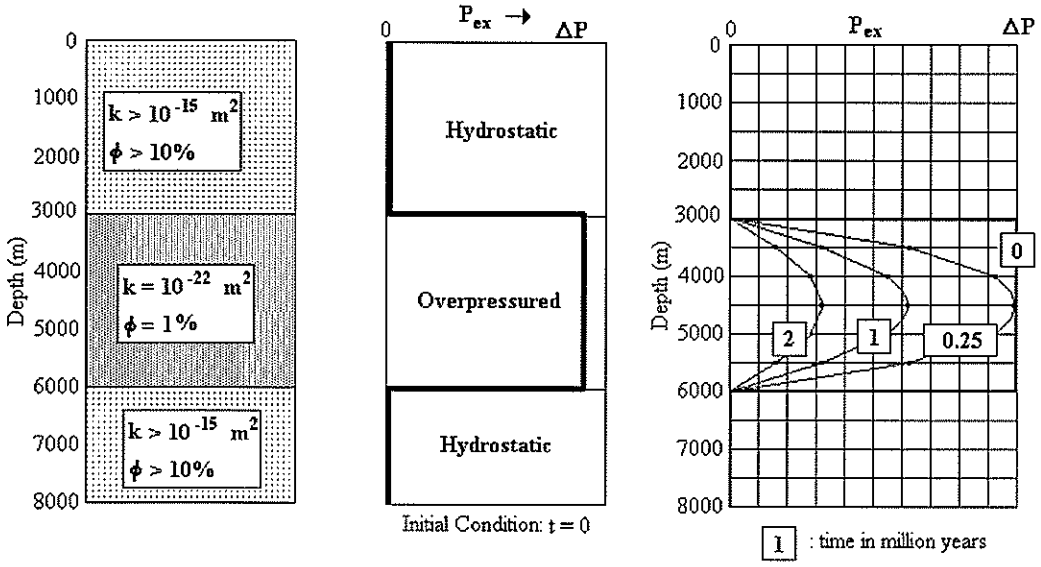

Fig. 10-17 A graph showing the conditions of the modelling based on Equation (10-1), and depth versus excess pressure (P_{ex}) for various times after initial application of the excess pressure zone ($\triangle P$) between 3000 m and 6000 m. The porosity (ϕ) and permeability (k) of the various layers used are illustrated.

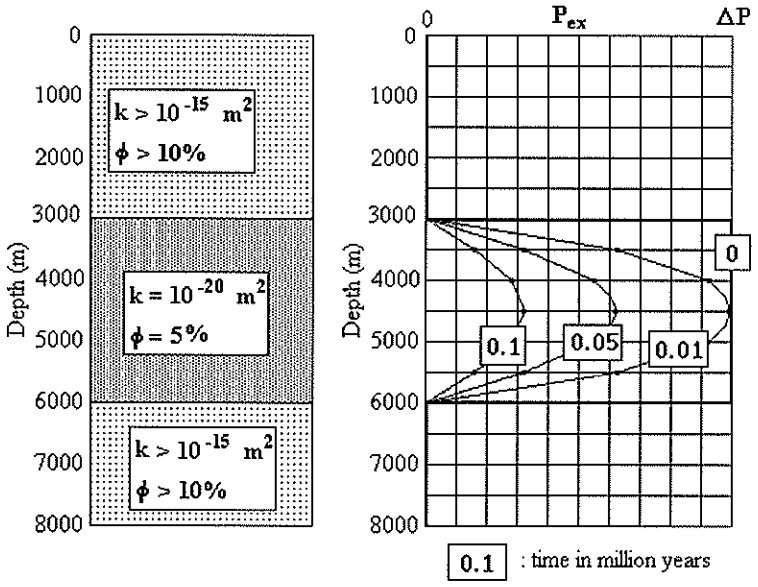

Fig. 10-18 A graph of depth versus excess pressure (P_{ex}) for various times after initial application of the excess pressure zone ($\triangle P$) between 3000 m and 6000 m. The porosity (ϕ) and permeability (k) of the various layers used are illustrated.

(1) a 800-1000-m-thick rock layer with the permeability of 10^{-21} m^2 (10^{-6} md) would maintain overpressure from one million years to several million years, (2) the overpressure would be dissipated after one million years to several million years if there was a 300-500-m-thick rock layer with the permeability of 10^{-22} m^2 (10^{-7} md), (3) a 300-500-m-thick rock layer with the permeability of about 10^{-23} m^2 (10^{-8} md)or less would maintain the overpressure from ten million years to several tens of millions of years.

The pressure seal modelling of pressure behaviour in porous media in the Bambra locality of the Barrow Sub-basin for maintaining excess pressures in the sealed environments also suggests that even in the overpressure zone of over a thousand meters thick within a very low-permeability (10^{-22} m^{-2}) area, the overpressure can be maintained only several million years at best. It implies that the observed top pressure seal in the Barrow Sub-basin is almost impossible to preserve the deep overpressure for tens of millions of years, without continued renewal of the overpressure.

This modelling, therefore, raises the issue of realistic average permeabilities for the Middle-Upper Jurassic shale sequence are in the Barrow Sub-basin. Bruce et al. (1996) suggested that compacted clays typically have permeabilities in the 10^{-16} m^2 to 10^{-17} m^2 (10^{-1}-10^{-2} md) range. Schön (1996) also suggested from an extensive literature review that the lower limit of permeability in shale is about 10^{-20} m^2 (10^{-5} md). As mentioned above, the porosities in the top pressure seal generally range from 2 % to 5 % based on the well-log data and some measured porosity data from claystone, thus, the permeabilities possibly range from 10^{-19} m^2 (10^{-4} md) to 10^{-22} m^2 (10^{-7} md). It seems that a permeability value as low as 10^{-22} m^2 is the lower limit value for a compacted, even strongly compacted shale. However, the above results of the pressure seal imply that for overpressures to be retained in a thick zone for several million years, or longer, the permeability of the zone must be significantly less than 10^{-20} m^2 (10^{-5} md) by several orders of magnitude (about, or less than, 10^{-23} m^2). It requires a porosity of less than 1 % but this very small porosity for the whole top pressure seal is very unlikely to occur.

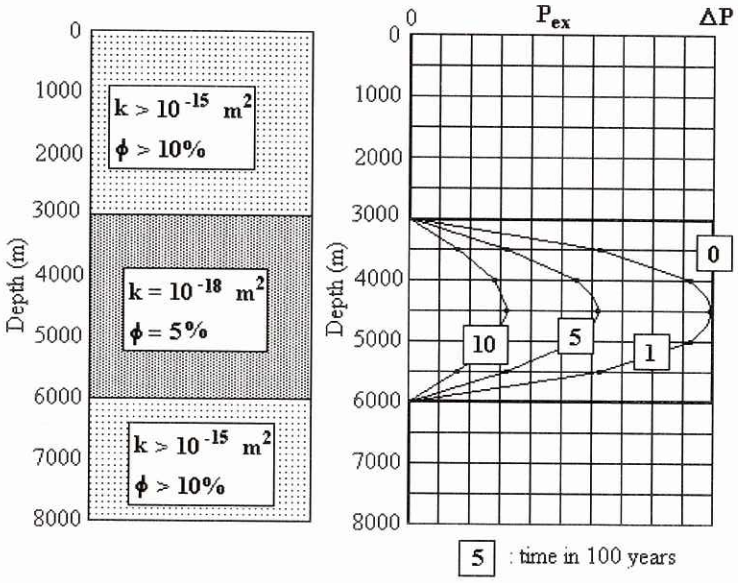

Fig. 10-19 A graph of depth versus excess pressure (P_{ex}) for various times after initial application of the excess pressure zone ($\triangle P$) between 3000 m and 6000 m. The porosity (ϕ) and permeability (k) of the various layers used are illustrated.

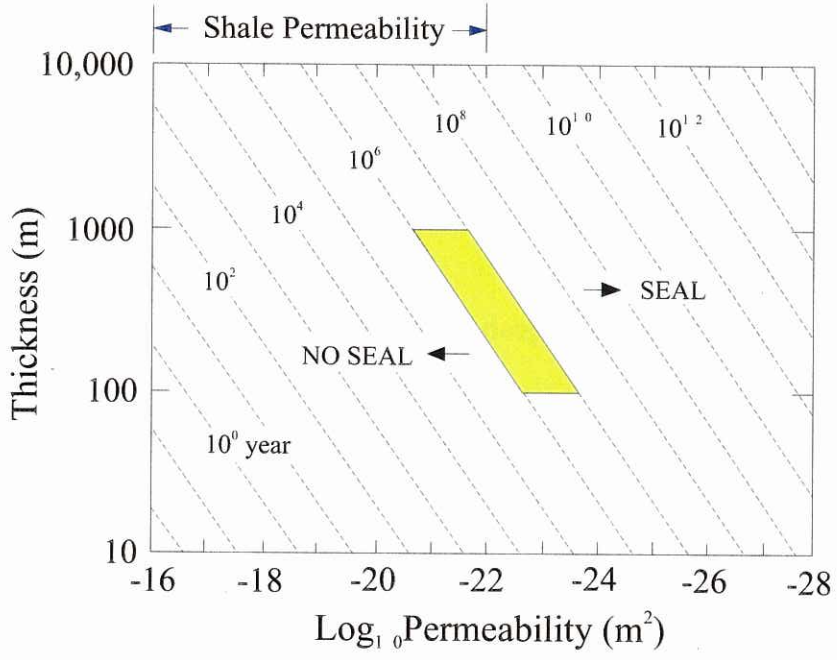

Fig. 10-20 Maximum time (in years) over which a layer of given thickness and permeability may confine excess pressures. Shaded area indicates approximate permeability required to sustain a 100-1000-m-thick seal over geologic time (Deming, 1994).

From the physio-chemical point of view, the difficulty for hydrocarbon expulsion from source rocks may depend on its saturation and wettability in the pore media. Firstly, it is more difficult for oil and gas migration to occur from a well-compacted shale if water saturation is high, as the hydrocarbon relative permeabilities will be very low. Secondly, the capillary pressure for oil and gas migration will be high if there are water-wet source rocks. The low hydrocarbon relative permeabilities at a top pressure seal, which is water-wet, may be quite efficient in preventing oil and gas being expelled from the deep overpressured source rocks. It has been, however, proposed that the wettability in source shales is different from reservoirs. There may be a possibility of variable hydrocarbon-wettability in various parts of the source section, for example, a distribution of bitumen within the pore centre network of a shale (Barker, 1980), or specific wetting paths (Ungerer et al., 1990) with relatively high hydrocarbon saturation and relative permeabilities. To maintain the overpressure, a seal is still required, or, at least, the release of overpressure through the seal should be slower than generating overpressure. Although the occurrence of deep overpressure suggests the existence of a relatively effective pressure seal, it is very unlikely that the seal is a unique factor for maintaining the deep overpressure for up to several millions of years or so. The results using the BasinMod 2D, therefore, may have significantly overstated the effect of the seal conditions for maintaining overpressure. Thus, it is suggested that continuous oil and gas generation, and thermal expansion with continuous pressure recharge over the past tens of millions of years is required to maintain the deep overpressure.

10.6.2 Possible major mechanisms for the deep overpressure

It seems that the practical top pressure seal is unlikely to maintain overpressure for more than several million years without a continued pressure recharge. This poses the consideration of two commonly proposed mechanisms of the observed overpressure (1) compaction disequilibrium, and (2) hydrocarbon generation.

10.6.2.1 Compaction disequilibrium

Compaction disequilibrium is common in fine-grained rocks with high sedimentation rates which are usually overpressured (Swarbrick, 1995). These rates

in fine-grained rocks during the Jurassic may wide cause overpressure in the sub-basins due to compaction disequilibrium. However, deep overpressure is very likely to dissipate in several million years only if the permeability of the top pressure seal is about 10^{-23} m^2 (10^{-8} md), or less, which is very unlikely to occur. Since the Cainozoic, it seems that the compaction disequilibrium has been an unlikely significant source of overpressure in the well-compacted Jurassic source rocks, if very low rates of subsidence and deposition occurred over the past tens of millions of years, as mentioned above.

Many researchers assume the relationship between fluid pressure and effective stress of Terzaghi (1923):

$$P_{fl} = P_{ob} - \mathcal{O}_{eff} \ , \qquad (10\text{-}2)$$

where P_{fl} is fluid pressure, P_{ob} is overburden pressure, $\mathcal{O}_{eff}$ is effective stress. This relationship is based on laboratory experiments under surface conditions.

The assumption supposes that fluid pressure increases as effective stress decreases, as often suggested to occur during undercompaction (anomalous high porosities) of shales. Terzaghi's principle has been widely used to evaluate fluid pressure from well logs. However, Hermanrud et al. (1998) have questioned the application of the Terzaghi relationship (with respect to porosities derived from the sonic and resistivity log) on the basis of their study of porosities in overpressured shales in the Haltenbanken.

In the present study (see also Chapter 5), the core-, neutron- and density-derived porosities in shales of the deep overpressured system are significantly lower than the sonic- and resistivity-derived porosities, which is consistent with the findings of Hermanrud et al. (1998). For example, the measured shale porosities range from 4.9-6.6 % at 4274-4283 m in Bambra-2, but sonic-log derived porosities are 13-18 % (high sonic transit times of 279-295 ③s/m) at the same depths of Bambra-2 (Fig. 5-3). Density-logs in Bambra-1, West Barrow-1/1A and Jurabi-1 in the deep overpressured system do not exhibit any porosity anomaly (Figures 5-2, 5-4 and 5-6). These suggest that the sonic-log and resistivity-log data may not be consistent

with abnormally high porosities expected in the overpressured source rocks. In turn, this suggests that the present day deep overpressure is not associated with a significant porosity anomaly due to compaction disequilibrium in the fine-grained rocks. The maintenance of the overpressure in the Jurassic source rocks to the present-day, therefore, requires that a mechanism other than compaction disequilibrium be sought to explain the deep overpressures in the sub-basins.

10.6.2.2 Hydrocarbon generation

On the basis of this study, one has to consider that the major causes for pressure recharge to maintain the deep overpressures are hydrocarbon generation in the Cainozoic after the thick Jurassic shales and siltstones had been compacted and most of the porosity in the Jurassic sequence had been lost through compaction. In fact, the deep overpressured system in the Barrow Sub-basin, interpreted by the sonic-log, resistivity-log and the measured pressure data, is in agreement with the observed zone of organic maturity of 0.8-2.0 % R_o (vitrinite reflectance) and an increased volume of gas-generating organic matter. The boundary between the pressure transition zone and the overpressured compartment (bottom of top pressure seal) is consistent with a maturity of about 1 % R_o. R_o at the top of the deep overpressured zone is about 1 % in Dampier-1 of the Dampier Sub-basin and also about 1 % in Jurabi-1 of the Exmouth Sub-basin. This may be why the deep overpressured zone frequently appears to have a planar top in a basin. The depth of the planar top seems to be associated with the upper part of the hydrocarbon generation zone with the thermal maturity range of about 0.8-1 %. It is proposed that if an effective pressure seal exists it can only maintain the overpressure for several million years at best, while continuous hydrocarbon generation, especially gas generation and thermal expansion, for a pressure recharge over the past several tens of millions of years is very likely to be the major cause of maintenance of the deep overpressure. As hydrocarbon generation and charge in the Jurassic source rocks is believed to have occurred since the Cainozoic, it is not inconceivable that an overpressure regime has been maintained since that time.

10.7 Summary

This study and modelling has shown several possible ways of interpreting the observed abnormal fluid pressures in the sub-basins. The BasinMod 2D basin modelling has suggested a maintained pressure cell in the Jurassic sequence since the Cainozoic. This modelling may inadvertently support some unrealistic petrophysical parameters, and computational assumptions. Nevertheless, the modelled overpressure distribution at present-day is fairly consistent with the observed data. The pressure seal that appears to be present in the Barrow Sub-basin clearly suggests that the observed overpressure can be only maintained by the top pressure seal for several million years at best, unless extremely low permeabilities (10^{-23} m^2 or less) occur a thousand meters in the Jurassic shaley sequences of the sub-basins.

The modelled results using the BasinMod 2D software suggest the following observations:

(1) The rapid sedimentation rates in fine-grained rocks during the basin subsidence of the Jurassic, resulting in compaction disequilibrium, are likely to be a mechanism for generating overpressure.

(2) The pressure seal, including top and bottom low-permeability rocks and lateral sealed faults, is one of the major controls on the deep overpressured compartments in the Jurassic shaley sequence since the Cainozoic.

(3) Quartz cementation may be a significant factor in forming a low-permeability rock layer for a top pressure seal.

(4) Thermal expansion of pore fluids makes a 5-10 % contribution to the maximum excess pressure in the studied case, and the generated pressure of hydrocarbon generation makes a less than 2 % contribution to the maximum excess pressure in the sub-basins.

(5) Additionally, the modelled heat flow values required to match the measured maturity data and formation temperatures, at the selected well sites along three cross-sections using the BasinMod 2D, are significantly lower than the calculated current heat flows in these wells using the BasinMod 1D. The calculated heat flows in these wells using the BasinMod 1D modelling are 10 % to 20 % higher than those from the BasinMod 2D modelling at these well sites along the cross-sections (Table 10-3).

Table 10-3 The heat flow values required for fitting the measured maturity data from the 1D BasinMod modelling and the BasinMod 2D modelling in three sub-basins

Well Name	**1D Heat Flow (mW/m^2)**	**2D Heat Flow (mW/m^2)**	**Surface Temperature (^oC)**	**Water Depth (m)**
Bambra-2	56.0	43-46	24	26
West Tryal Rocks-1	54.3	**Barrow**	21	138
Outtrim-1	60.4		22	91
Novara-1	52.8	52-54	17	372
Zeewulf-1	59.7	**Exmouth**	4.5	1194
Goodwyn-7	48.0		21	134
Hampton-1	43.9	40-43	23	53
Rosemary-1	47.5	**Dampier**	23	65

Further modelling studies of pressure behaviour and formation compaction also suggest:

(1) The permeability values of 10^{-19} m^2 to 10^{-22} m^2 in situ may be not sufficient for required permeabilities of about 10^{-23} m^2, or less, to maintain the deep overpressured regime in the Jurassic section over a time span of several tens of millions of years.

(2) Compaction disequilibrium may not be a significant source to charge and maintain the deep overpressures since the Cainozoic.

(3) There is the strong possibility of the validity of the hypothesis proposed by Horstman (1988) and Zaunbrecher (1994) that a maintained deep overpressure regime in the sub-basins is the product of continued hydrocarbon generation, especially gas generation and thermal expansion, and subsequent further maturation, which entails oil to gas cracking. The sealed conditions of low-permeability to retain the deep overpressure are still required.

CONCLUSIONS AND LIMITATIONS

Conclusions

The principal aims of this study were evaluation of (1) heat flow history, (2) thermal maturity and hydrocarbon generation in the deep overpressured system, and (3) pressure seal and evolution of deep overpressure. The prime methods used were (1) geological analysis, and (2) basin modelling. Eight chapters contain the most important research work, data and viewpoints. Chapters 3, 4 and 5 explain the characteristics of organic matter, a case study of the reliability of T_{max} data, the deep overpressured system and its top pressure seal. Chapters 6 and 7 describe the 1D model, parameters and BasinMod 1D modelling for thermal history and thermal maturity. Chapter 8 contains two case studies of the thermal maturity and thermal modelling in the deep overpressured zone. Chapters 9 and 10 establish 2D geological models and choose parameters, show the results of BasinMod 2D overpressure modelling, and discuss the effect of the pressure seal and major origins to generate and maintain the deep overpressured system.

The major new findings from this study are as follows:

- Reliable T_{max} data are useful to evaluate thermal maturity and a relationship between vitrinite reflectance and Rock-Eval T_{max} is proposed.

- Some thermal maturity data are consistent with the rifting heat flow model of Jarvis and McKenzie (1980).

- No undercompaction overpressure effect on retardation of maturation can be observed in these studied wells. The deep overpressure is a result of the thermal maturity and hydrocarbon generation in this basin.

- The present day deep overpressured zone is not associated with a high porosity anomaly owing to compaction disequilibrium.

- The observed deep overpressure can not be maintained over tens of millions of years in a very low-permeability (10^{-22} m^2 or 10^{-7} md) environment.

- The major mechanism to maintain the observed deep overpressure through the last tens of millions of years is continued hydrocarbon generation, especially gas generation and thermal expansion, within sealed conditions.

The conclusions, new facts and suggestions to be drawn from this study are as follows:

1. The Jurassic and Upper Triassic formations are rich in total organic carbon on the basis of 1256 TOC values. TOC values in the Dupuy Formation, Dingo Claystone and Athol Formation of the Jurassic range from about 0.2 % to 13 % with an average value of about 1.74 %. TOC values in the Murat Siltstone of the Lower Jurassic range from about 0.4 % to 11 % with an average value of about 2.09 %. TOC values in the Mungaroo Formation of the Middle-Upper Triassic range from about 0.2 % to 36 % with an average value of about 2.19 % calculated from the TOC values of less than 15 %. TOC contents in the coal-bearing sequence of the Lower-Middle Jurassic of the Beagle Sub-basin have higher values.

2. The organic matter in the Jurassic source rocks is a mixture of terrestrial and marine input, but its bulk geochemical feature appears to be dominated by type III kerogen based on the current data. The organic matter in the Lower-Middle Jurassic contains more terrigenous material and mainly gas generating type of organic matter, while the organic matter in the Upper Jurassic may consist of more marine material and some mixed type II/III kerogen for a more oil-prone type may occur in the Barrow-Dampier Sub-basins.

3. The major problems influencing the reliability of Rock-Eval T_{max} data for the assessment of thermal maturity are (1) contamination by drilling-mud additives, and (2) suppression due to HI > 150. Carefully estimating and selecting T_{max} data are important. The reliable T_{max} data are useful to evaluate thermal maturity, especially where no other reliable measured maturity parameters are available.

4. The Jurassic sequence and some low parts of the Barrow Group are overpressured with excess pressures of about 5-29 MPa at depths of about 2900-3640 m from observations by repeat formation tests (RFTs) and drill stem tests (DSTs). The deep overpressured system (mainly in Jurassic rocks) is also coincident with increase in mud weights within the observed depth range of 2650-4650 m.

5. The Jurassic source rocks are also overpressured, corroborated by high sonic transit times and low formation resistivities in the fine-grained rocks. However, the measured claystone porosities are significantly lower than the sonic-log and resistivity-log derived porosities, and the density-log data are not in agreement with abnormal high porosities due to compaction disequilibrium in the overpressured source rocks. A possible explanation is that the sonic-log and resistivity-log also directly respond to the overpressuring in the deep overpressured fine-grained rocks of the sub-basins, which is consistent with the observation by Hermanrud et al. (1998).

6. The top pressure seal for the deep overpressured system in the Barrow Sub-basin is interpreted to be consistent with a pressure transition zone. The top pressure seal was observed to be a rock layer containing 60-80 % claystone and siltstone with 20-40 % sandstone and thin limestone. The top of the rock layer has varying depths of about 2650-3000 m with temperatures of 110-125 ^{o}C. The bottom of the rock layer has depths ranging from 3100 m to 3300 m with temperatures of 125-135 ^{o}C. The thicknesses of the rock layer range from about 300 m to 500 m. The estimated porosities of claystone in the rock layer, based on the well-log data and measured claystone porosities, are about 2-5 % and calculated permeabilities range from about 10^{-19}- 10^{-22} m^2.

7. The evidence of rifting heat flow histories, during the rift event of the Jurassic and earliest Cretaceous, was modelled using multiple thermal maturity data from 4 wells, Jurabi-1 in the Exmouth Sub-basin, Bowers-1 in the Barrow Sub-basin, and Investigator-1 and Jupiter-1 on the Exmouth Plateau. The thermal maturity data are consistent with the rifting heat flow model of Jarvis and McKenzie (1980). The maximum typical heat flow values during the rifting along the

rifting grabens (sub-basins) were determined to be 60-70 mW/m^2 with relatively higher values in the Exmouth and Barrow Sub-basins and relatively lower values in the Dampier and Beagle Sub-basins. The maximum heat flow values during the rifting on the southern and central areas of the Exmouth Plateau possibly range from 70 mW/m^2 to 80 mW/m^2.

8. During the rifting in the Jurassic and earliest Cretaceous, the Rankin Platform, as a western shoulder of grabens, underwent substantial uplift and erosion. The estimated erosional thickness may range from hundreds meters up to 2500 m. The 1D thermal modelling indicates that the Rankin Platform was experiencing a decrease of temperature during the rifting. There is no evidence that a higher rift-associated heat flow occurred on the Rankin Platform (western graben shoulder).

9. The study of thermal modelling suggests that it is more geologically reasonable to use the rift-related heat flow histories for predicting temperature, thermal maturity and hydrocarbon generation in the depocentres of the sub-basins, while the constant heat flow model (calculated current heat flow and surface or seafloor temperature) can be generally used to predict the thermal effects on the graben shoulders. The constant heat flow model can be also used to calculate the maturity and temperature histories during the post-rift phase of basin development.

10. This study propose a relationship between vitrinite reflectance and Rock-Eval T_{max} for the assessment of thermal maturity and thermal modelling. The relationship is preliminary and further study is needed to improve the correlation. The relationship between R_o and T_{max} used in the thermal study may result in ! 3-10 % error for the calculated vitrinite reflectance.

11. The true thermal maturity (R_o: 0.8-2.2 %) in the observed Jurassic overpressured source rocks of the Barrow Sub-basin is not detectably influenced by the observed overpressure (fluid pressures of about 40-80 MPa at depths of 3000-4600 m). Based on this study, overpressure retardation of organic-matter

maturation does not appear to be a global phenomenon, and the overpressure is not a significant factor in the thermal maturity and hydrocarbon generation in the study region. The temperature-time-related kinetic model can still be used to predict the thermal effects and timing of hydrocarbon generation in the deep overpressured Jurassic section in this basin.

12. Rapid loading occurred during the Jurassic and earliest Cretaceous in the central areas of the sub-basins with sedimentation rates of about 80-250 m/Ma. The sedimentation rates were 10-80 m/Ma in the Cretaceous and generally 10-30 m/Ma in Cainozoic.

13. 2D modelled porosity along selected cross-sections indicate that higher porosity was retained in the Jurassic fine-grained rocks, and movement of the pore fluids was inhibited during the rapid deposition in the Jurassic and Early Cretaceous. However, the porosities at the present-day in the observed deep overpressured Jurassic section probably range from 2 % to 7 %. The discrepancy is probably due to an inappropriate porosity algorithm used in the modelling software.

14. 2D overpressure modelling indicates that rapid sedimentation rates resulted in compaction disequilibrium in the fine-grained rocks, which is likely to be a significant mechanism of deep overpressure generation in the sub-basins during the Jurassic and Early Cretaceous. However, since the Cainozoic, the compaction disequilibrium should be much less important to maintain the deep highly overpressured system, because the Jurassic section had been well compacted and the depositional rates were very slow in most areas of the sub-basins.

15. The sealed conditions for the deep overpressured Jurassic section since the Cainozoic were modelled using the BasinMod 2D modelling. These conditions were formed by (1) laterally closed faults, (b) near impermeable rocks with permeabilities of about 10^{-23}-10^{-25} m^2 at the bottom of Jurassic, and (c) a top pressure seal with permeabilities of about 10^{-20}-10^{-22} m^2 in the Barrow Sub-basin and permeabilities in the top of the Jurassic section ranging from about 10^{-19} m^2 to 10^{-20} m^2 in the Exmouth and Dampier Sub-basins. The model-derived

permeabilities of 10^{-23}-10^{-25} m^2 for the bottom of the Jurassic section may not necessarily be suitable to represent the bottom sealed conditions of the observed present day deep overpressured system.

16. In combination with the characteristics of the top pressure seal in the Barrow Sub-basin, (a) 2D modelling for the deep overpressure, (b) the modelling for pressure behavior in low-permeability (10^{-18}-10^{-22} m^2) environments, and (c) the studies of pressure sealing by Deming (1994), one may conclude that the top pressure seal with a permeability of more than 10^{-23} m^2 (10^{-23} md) is not sufficient to maintain deep overpressure without pressure recharge over the past tens of millions of years. The permeabilities required for the top pressure seal to retain deep overpressure over geological time span are 10^{-23} m^2, or less, which are almost unlikely to occur in most natural geological circumstances.

17. The study suggests that (1) the present day overpressured zone is not associated with an anomalous high porosity due to undercompaction, (2) slower sedimentation rates and subsidence occurred since the Early Cainozoic, (3) the Jurassic source rocks were compacted and most of the porosity had been lost through compaction since the middle Tertiary, and (4) the present-day observed deep overpressure is unlikely to have been the preserved, due to a mechanism of compaction disequilibrium, in the geological past. Therefore, it seems that compaction disequilibrium is not a significant mechanism for the deep overpressured system since the Cainozoic.

18. An acceptable hypothesis for the major cause to maintain the observed deep overpressure through the last tens of millions of years is organic-matter maturation and continued hydrocarbon generation, especially gas generation and thermal expansion, as proposed by Horstman (1988), Hunt (1990) and Zaunbrecher (1994). Sealed conditions or low-permeability environments for retaining the deep overpressure are still necessary.

19. On the basis of the 2D modelled results, it appears that quartz cementation may be a significant cause in creating a low-permeability rock layer with permeabilities of 10^{-19}-10^{-22} m^2 for a top pressure seal, which may be more

effective in preventing oil and gas being expelled from the well-compacted, overpressured Jurassic source section in a short period of geological time. This may imply (1) an episodic sequence of (a) hydrocarbon generation (especially gas generation) - (b) overpressure - (c) fracture - (d) hydrocarbon migration - (e) resealing, and (2) a pressure-driven process due to high overpressure caused by continuous hydrocarbon generation, especially gas generation, in the sealed overpressured source rocks for oil and gas migration, which occurred in the geological past in this basin.

20. Based on 1D maturity modelling and the study of 2D overpressure evolution, oil and gas generation, migration and accumulation in the sub-basins since the Late Cretaceous are the most important events for an understanding and evaluation of oil and gas potential, and for petroleum exploration in this basin with deep overpressured compartments.

Limitations

The main limitations for this study are as follows:

1. Although a great deal of data have been obtained for this study, the observed data are still insufficient for detailed studies of basin history.

2. The geological models have been built with many simplifications, especially the 2D geological models, due to numerical procedures and data limitation.

3. The uncertainties of thermal parameters and fluid parameters, and claystone permeability have not been fully resolved.

4. It seems that the mathematical models in the 2D modelling are still far from satisfactory for the practical dynamic, and interaction, processes of geology and geochemistry.

REFERENCES

AGSO North West Shelf Study Group. (1994). Deep reflections on the North West Shelf: changing perceptions of basin formations. In: Purcell, P. G. and Purcell, R. R. eds., *The Sedimentary Basins of Western Australia* (pp. 63-76): Proceedings of the Petroleum Exploration Society of Australia, Perth, 1994.

Alexander, R., Kagi, R.I., Toh, E. and van Bronswijk, W. (1988). The use of aromatic hydrocarbons for assessment of thermal histories of sediments. In: Purcell, P. G. and Purcell, R. R. eds., *The North West Shelf, Australia* (pp. 559-562): Proceedings of the Petroleum Exploration Society of Australia, Perth, 1988.

Alexander, R., Marzi, R. and Kagi, R.I. (1990). A new method for assessing the thermal history of sediments: a case study from the Exmouth Plateau in Northwestern Australia. *Australian Petroleum Exploration Association Journal*, **30**, 364-372.

Allan, J. and Douglas, A.G. (1977). Variations in the content and distribution of n-alkanes in a series of Carboniferous vitrinite and sporinites of bituminous rank. *Geochim. Cosmochim. Acta*, **40**, 1223-1230.

Allen, P.A. and Allen, J.R. (1990). *Basin analysis: principles and applications* (pp. 282-283). Oxford, England: Blackwell Scientific Publications.

Alnes, J.R. and Lilburn, R.A. (1998). Mechanisms for generating overpressure in sedimentary basins: A Reevalution: Discussion. *American Association of Petroleum Geologists Bulletin*, **82**, 2266-2269.

Apthorpe, M.C. (1979). Depositional history of the Upper Cretaceous of the Northwest Shelf, based on Foraminifera. *Australian Petroleum Exploration Association Journal*, **19**, 74-89.

Asquith, G.B. and Gibson, C.R. (1983). *Basic well log analysis for geologists* (pp. 41-44). Tulsa, Oklahoma: American Association of Petroleum Geologists.

Aydin, A. (2000). Fracture, faults, and hydrocarbon entrapment, migration and flow. *Marine and Petroleum Geology*, **17**, 797-814.

Baillie, P.W. and Jacobson, E.P. (1997). Prospectivity and exploration history of the Barrow Sub-basin, Western Australia. *Australian Petroleum Production and Exploration Association Journal, **37***, 117-135.

Baldwin, B. and Butler, C.O. (1985). Compaction curves. *American Association of Petroleum Geologists Bulletin*, **69**, 622-626.

Barber, P.M. (1982). Palaeotectonic evolution and hydrocarbon genesis of the central Exmouth Plateau. *Australian Petroleum Exploration Association Journal, **23***, 131-144.

Barber, P.M. (1988). The Exmouth Plateau deep water frontier: a case history. In: Purcell, P. G. and Purcell, R. R. eds., *The North West Shelf, Australia* (pp. 173-187): Proceedings of the Petroleum Exploration Society of Australia, Perth, 1988.

Barber, P. (1994). Sequence stratigraphy and petroleum potential of Upper Jurassic-Lower Cretaceous depositional systems in the Dampier Sub-basin, North West Shelf, Australia. In: Purcell, P. G. and Purcell, R. R. eds., *The Sedimentary Basins of Western Australia* (pp. 526-542): Proceedings of the Petroleum Exploration Society of Australia, Perth, 1994.

Barker, C. (1972). Aquathermal pressuring-role of temperature in development of abnormal–pressure zones. *American Association of Petroleum Geologists Bulletin*, **56**, 2068-2071.

Barker, C. (1980). Primary migration: the importance of water-mineral-organic matter interactions in the source rock. In: Roberts, W. H. and Cordell, R. J. eds., *Problems of Petroleum Migration*: American Association of Petroleum Geologists Studies in Geology No. **10**, 19-31.

Barker, C. (1990). Calculated volume and pressure changes during the thermal cracking of oil to gas in reservoirs. *American Association of Petroleum Geologists Bulletin*, **74**, 1254-1261.

Barker, C. (1996). *Thermal modelling of petroleum generation: theory and applications*. New York; Amsterdam: Elsevier.

Bear, J. (1972). *Dynamics of fluids in porous media*. New York: Elsevier Science.

Bekele, E.B., Johnson, M.D. and Higgs, W.G. (2001). Numerical modelling of overpressure generation in the Barrow Sub-basin, Northwest Australia. *Australian Petroleum Production and Exploration Association Journal*, **41**, 595-607.

Berry, F.A.F. (1973). High fluid potential in California Coast Ranges and their tectonic significance. *American Association of Petroleum Geologists Bulletin*, **57**, 1219-1245.

Beston, N.B. (1986). Reservoir geological modelling of the North Rankin Field, Northwest Australia. *Australian Petroleum Exploration Association Journal*, **26**, 375-388.

Bigelow, E.L. (1994a). Well logging methods to detect abnormal pressure. In: Fertl, W.H., Chapman, R.E. and Hotz, R.F. eds., *Studies in abnormal pressures* (pp. 187-240). Amsterdam; New York: Elsevier Science.

Bigelow, E.L. (1994b). Global occurrences of abnormal pressures. In: Fertl, W.H., Chapman, R.E. and Hotz, R.F. eds., *Studies in abnormal pressures* (pp. 1-16). Amsterdam; New York: Elsevier Science.

Bint, A.N. and Helby, R. (1988). Upper Triassic palynofacies and environmental interpretations for the Rankin Trend, Northern Carnarvon Basin, W.A. In: Purcell P.G. and Purcell R.R. eds., *The North West Shelf, Australia* (pp. 591-598). Proceedings of the Petroleum Exploration Society of Australia, Perth, 1988.

Bjørlykke, K. and Egeberg, P.K. (1993). Quartz cementation in sedimentary basins. *American Association of Petroleum Geologists Bulletin*, **77**, 1538-1548.

Blevin, J.E., Stephenson, A.E. and West, B.G. (1994). Mesozoic structural development of the Beagle Sub-basin – implication for the petroleum potential of the Northern Carnarvon Basin. In: Purcell, P. G. and Purcell, R. R. eds., *The Sedimentary Basins of Western Australia* (pp. 479-496): Proceedings of the Petroleum Exploration Society of Australia, Perth, 1994.

Bordenave, M.L., Espitalié, J, Leplat, P., Oudin, J.L. and Vandenbroucke, M. (1993). Screening techniques for source rock evaluation. In: Bordenave, M.L. (ed), *Applied Petroleum Geochemistry* (pp. 217-278, Chapter II. 2). Paris: Editions Technip.

Boyd, R., Williamson, P. and Haq, B.U. (1993). Seismic stratigraphy and passive-margin evolution of the southern Exmouth Plateau. *Spec. Publs Int. Ass. Sediment.*, **18**, 581-603.

Bradley, J.S. (1975). Abnormal formation pressure. *American Association of Petroleum Geologists Bulletin*, **59**, 957-973.

Bradley, J.S. and Powley, D.E. (1994). Pressure compartments in sedimentary basins: a review. In: Ortoleva, P.J. ed., *Basin Compartments and Seals* (pp. 3-26): American Association of Petroleum Geologists Memoir, **61**.

Bradshaw, M.T., Yeates, A.N., Beynon, R.M., Brakel, A.T., Langford, R.P., Totterdell, J.M. and Yeung, M. (1988). Palaeogeographic evolution of the North West Shelf Region. In: Purcell P.G. and Purcell R.R. eds., *The North West Shelf, Australia* (pp. 29-54). Proceedings of the Petroleum Exploration Society of Australia, Perth, 1988.

Bredehoeft, J., Wesley, J. and Fouch, T. (1994). Simulation of the origin of fluid pressure, fracture generation, and the movement of fluids in the Uinta Basin, Utah. *American Association of Petroleum Geologists Bulletin,* **78**, 1729-1747.

Brikké, I. (1982). Geochemical interpretation of some oils and condensates from the Dampier Sub-basin of Western Australia. *Australian Petroleum Exploration Association Journal*, **22**, 179-187.

Bruce, R.H., Middleton, M.F., Holyland, P., Loewenthal, D. and Bruner, I. (1996). Modelling of petroleum formation associated with heat transfer due to hydrodynamic processes. *Petroleum Exploration Society of Australia Journal*, **24**, 6-12.

Burley, S. (1993). Models of burial diagenesis for deep exploration plays in Jurassic fault traps of the Central and Northern North Sea. In: Parker, J. ed., *Petroleum Geology of Northwest Europe* (pp. 1353-1375). London: Geological Society.

Burnham, A.K. (1989). A simple kinetic model of petroleum formation and cracking (pp. 1-11). Lawrence Livermore National Laboratory Report UCID-21665 (unpublished).

Burnham, A.K. and Sweeney, J.J. (1989). A chemical kinetic model of vitrinite maturation and reflectance. *Geochimica et Cosmochimica Acta*, **53**, 2649-2657.

Burst, J.F. (1969). Diagenesis of Gulf Coast sediments and its possible relation to petroleum migration. *American Association of Petroleum Geologists Bulletin*, **53**, 73-93.

Campbell, I.R. and Smith, D.N. (1982). Gorgon 1 - Southernmost Rankin Platform gas discovery. *Australian Petroleum Exploration Association Journal*, **22**, 102-111.

Campbell, I.R., Tait, A.M. and Reiser, R.F. (1984). Barrow Island Oilfield, revisited. *Australian Petroleum Exploration Association Journal,* **24**, 289-298.

Carr, A.D. (1999). A vitrinite reflectance kinetic model incorporating overpressure retardation. *Marine and Petroleum Geology,* **16**, 355-377.

Carslaw, H.S. and Jaeger, J.C. (1959). *Conduction of heat in solids*. Oxford at the Clarendon Press, 510 p.

Cecil, B.C., Stanton, R.W. and Robbins, E.I. (1977). Geologic factors controlling coalification and hydrocarbon maturation (abstract). *American Association of Petroleum Geologists Bulletin,* **61**, 775.

Chaney, P.E. 1950. Abnormal pressure and lost circulation. *World Oil*, **130**, 122-126.

Chapman, R.E. (1972). Clays with abnormal interstitial fluid pressures. *American Association of Petroleum Geologists Bulletin*, **56**, 790-795.

Chapman, R.E. (1994). Abnormal pore pressures: essential theory, possible causes, and sliding. In: Fertl, W.H., Chapman, R.E. and Hotz, R.F. eds., *Studies in abnormal pressures* (pp. 51-91). Amsterdam; New York: Elsevier Science.

Clementz, D.M. (1979). Effect of oil and bitumen saturation on source-rock pyrolysis. *American Association of Petroleum Geologists Bulletin,* **63**, 2227-2232.

Cockbain, A.E. (1989). The North West Shelf. *Australian Petroleum Exploration Association Journal*, **29**, 529-545.

Colwell, J.B., Röhl, U., von Rad, U. and Kristan Tollmann, E. (1994). Mesozoic sedimentary and volcaniclastic rocks dredged from the northern Exmouth Plateau and Rowley Terrace, offshore northwest Australia. *AGSO Journal of Australian Geology and Geophysics*, **15**, 11-42.

Cook, A.C. and Kantsler, A.J. (1980). The maturation history of the epicontinental basins of Western Australia. *United Nations Economic Social Commission for Asia and Pacific, CCOP/SOPAC Technical Bulletin, 3*, 171-195.

Cook, A.C., Smyth, M. and Vos, R.G. (1985). Source potential of Upper Triassic fluvio-deltaic systems of the Exmouth Plateau. *Australian Petroleum Exploration Association Journal,* **25**, 204-215.

Cooles, G.P., Mackenzie, A.S. and Quigley, T.M. (1986). Calculation of petroleum masses generated and expelled from source rocks. *Organic Geochemistry*, **10**, 235-245.

Cossé, R. (1993). *Basics of reservoir engineering, oil and gas field development techniques*. Institute Francais du Pétrole Publications, Editions Technip, 342 p.

Cranganu, C. and Deming, D. (1996). Heat flow and hydrocarbon generation in the Transylvanian Basin, Romania. *American Association of Petroleum Geologists Bulletin*, **80**, 1641-1653.

Crostella, A. and Chaney, M.A. (1978). The petroleum geology of the Outer Dampier Sub-basin. *Australian Petroleum Exploration Association Journal*, **18**, 13-22.

Crostella, A. and Barter, T. (1980). Triassic-Jurassic depositional history of the Dampier and Beagle Sub-basins, Northwest Shelf of Australia. *Australian Petroleum Exploration Association Journal*, **20**, 25-33.

Crostella, A., Iasky, R.P., Blundell, K.A., Yasin, A.R., and Ghori, K.A. (2000). Petroleum geology of the Peedamullah Shelf and Onslow Terrace, Northern Carnarvon Basin, Western Australia. Report No. 73, Geological Survey of Western Australia, 2000 (unpublished).

Daim, F.M. and Lennox, P.G. (1998). A new tectonic model for the evolution of the Northern Carnarvon Basin, Western Australia. In: Purcell, P. G. and Purcell, R. R. eds., *The Sedimentary Basins of Western Australia 2* (pp. 435-446): Proceedings of the Petroleum Exploration Society of Australia, Perth, 1998.

Dalla Torre, M., Mahlmann, R.F. and Ernst, W.G. (1997). Experimental study on the pressure dependence of vitrinite maturation. *Geochimica et Cosmochimica Acta,* **61**, 2921-2928.

Deming, D. and Chapman, D.S. (1989). Thermal histories and hydrocarbon generation: Example from Utah-Wyoming thrust belt. *American Association of Petroleum Geologists Bulletin*, **73**, 1455-1471.

Deming, D. (1994). Factors necessary to define a pressure seal. *American Association of Petroleum Geologists Bulletin*, **78**, 1005-1009.

Densley, M.R., Hillis, R.R. and Redfearn, J.E.P. (2000). Quantification of uplift in the Carnarvon Basin based on interval velocities. *Australian Journal of Earth Sciences,* **47**, 111-122.

Dickinson, G. (1953). Geological aspects of abnormal reservoir pressure in Gulf Coast Louisiana. *American Association of Petroleum Geologists Bulletin*, **37**, 410-432.

Dix, C.H. (1955). Seismic velocities from surface measurements. *Geophysics*, **20**, 68-86.

Driscoll, N.W., and Karner, G.D. (1998). Lower crustal extensional across the Northern Carnarvon Basin, Australia: Evidence for an eastward dipping detachment. *Journal of Geophysical Research*, **103**, 4975-4991.

Düppenbecker, S.J., Dohmen, L. and Welte D.H. (1991). Numerical modelling of petroleum expulsion in two areas of the Lower Saxony Basin, Northern Germany. In: England, W.A. and Fleet, A.J., eds., *Petroleum Migration* (pp. 47-64). London: The Geological Society.

Ellis, G.K., Pitchford, A. and Bruce, R.H. (1999). Barrow Island oil field. *Australian Petroleum Production and Exploration Association Journal,* **39**, 158-176.

Emery, D. and Myers, K. (1996). *Sequence stratigraphy* (pp. 11-41). Cambridge, Mass.: Blackwell Science, 1996.

England, W., Mackenzie, A., Mann, D. and Quigley, T. (1987). The movement and entrapment of petroleum fluids in the subsurface. *Journal of the Geological Society, Landon*, **144**, 327-347.

Espitalié, J., Marquis, F. and Barsony, I. (1984). Geochemical logging. In: Voorhees, K.J. ed., *Analytical pyrolysis: techniques and applications* (pp. 276-304). London: Butterworths.

Etheridge, M.A. and O'Brien, G.W. (1994). Structural and tectonic evolution of the Western Australia Margin basin system. *Petroleum Exploration Society of Australia Journal*, **34**, 45-63.

Exon, N.F. and Colwell, J.B. (1994). Geological history of the outer NorthWest Shelf of Australia: a synthesis. *AGSO Journal of Australian Geology and Geophysics*, **15**, 177-190.

Falvey, D.A. and Middleton, M.F. (1981). Passive continental margins: evidence for a prebreakup deep crustal metamorphic subsidence mechanism. *Oceanologica Acta, 1981* (pp. 103-114). Proceedings 26th International Geological Congress, Geology of Continental Margins Symposium, Paris, 7-17 July, 1981.

Falvey, D.A. and Mutter, J.C. (1981). Regional plate tectonics and the evolution of Australia's passive continental margins. *BMR (Bureau of Mineral Resources) Journal of Australian Geology and Geophysics,* **6**, 1-29.

Ghori, K.A.R. (1995). Measuring thermal conductivities improve maturation modelling in the Northern Carnarvon Basin, Western Australia. *Petroleum Exploration Society of Australia Journal*, **23**, 3-12.

Ghori, K.A.R. (1999). Silurian-Devonian Petroleum source-rock potential and thermal history, Carnarvon Basin, Western Australia. Report No. 72, 88 p. Department of Minerals and Energy, Geological Survey of Western Australia (unpublished).

Gorter, J.D. (1994). Interpretation of raw Rock-Eval Data: A cautionary tale from the Carnarvon Basin, Western Australia. A Report for Hardy Petroleum (unpublished).

Gretener, P.E. and Bloch, G. (1992). Geopressures: two distinctly different kinds of conditions. *1992 Annual Convention, Abstracts* (pp. 48-49), American Association of Petroleum Geologists.

Gurba, L.W. and Ward, C.R. (1998). Vitrinite reflectance anomalies in the high-volatile bituminous coals of the Gunnedah Basin, New South Wales, Australia. *International Journal of Coal Geology,* **36**, 111-140.

Hao, F., Sun, Y.C., Li, S.T. and Zhang, Q.M. (1995). Overpressure retardation of organic-matter maturation and petroleum generation: a case study from the Yinggehai and Qiongdongnan Basins, South China Sea. *American Association of Petroleum Geologists Bulletin,* **79**, 551-562.

Haq, B.U., Hardenbol, J. and Vail, P.R. (1987). Chronology of fluctuating sea levels since the Triassic. *Science,* **235**, 1156-1166.

Hardenbol, J., Vail, P.R. and Ferrer, J. (1981). Interpreting paleoenvironments, subsidence history and sea-level changes of passive margins from seismic and biostratigraphy. *Oceanologica Acta*, **N^{o} SP**, 33-44.

Hellinger, S. and Sclater, J. G. (1983). Some comments on two-layer extensional models for the evolution of sedimentary basins. *Journal of Geophysical Research*, **88**, 8251-8269.

Hermanrud, C., Wensaas, L., Teige, G.M.G., Nordgård Bolås, H.M., Hansen, S. and Vik, E. (1998). Shale porosities from well logs on Haltenbanken (Offshore Mid-Norway) show no influence of overpressuring. In: Law, B.E., Ulmishek, G.F. and Slavin, V.I. eds., *Abnormal pressures in hydrocarbon environments* (pp. 65-85): American Association of Petroleum Geologists Memoir, **70**.

Hill, G. (1994). The role of the pre-rift structure in the architecture of the Dampier Basin Area, North West Shelf, Australia. *Australian Petroleum Exploration Association Journal*, **34**, 603-613.

Hill, R.J., Jenden, P.D., Tang, Y.C., Teerman, S.C. and Kaplan, I.R. (1994). Influence of pressure on pyrolysis of coal. In: Mukhopadhyay P.K. and Dow W.G. eds., *Vitrinite reflectance as a maturity parameter: Application and limitations* (pp. 161-193): American Chemical Society Symposium Series 570.

Hocking, R. M., Moors, H. T., and Van De Graaff, W. J. E. (1987). Geology of the Carnarvon Basin Western Australia. *Geological Survey Western Australia Bulletin*, **133**.

Hocking, R.M. (1988). Regional Geology of the Northern Carnarvon Basin. In: Purcell P.G. and Purcell R.R. eds., *The North West Shelf, Australia* (pp. 97-114): Proceedings of the Petroleum Exploration Society of Australia, Perth, 1988.

Hocking, R., Mory, A.J. and Williams, I.R. (1994). An atlas of Neoproterozoic and Phanerozoic Basins of Western Australia. In: Purcell, P. G. and Purcell, R. R. eds., *The Sedimentary Basins of Western Australia* (pp. 21-43): Proceedings of the Petroleum Exploration Society of Australia, Perth, 1994.

Hoover, D.S. and Davis, A. (1980). The development and evaluation of an automated reflectance microscope system for the petrographic characterization of bituminous coals. Penn State Univ., U.S. Dept. Energy, Techn. Rep., FE-2030-TR23, Contract No. EX-76-C-01-2030.

Horstman, E.L. (1988). Source maturity, overpressures and production North West Shelf, Australia. In: Purcell P.G. and Purcell R.R. eds., *The North West Shelf, Australia* (pp. 529-537): Proceedings of the Petroleum Exploration Society of Australia, Perth, 1988.

Huang, W.Y. and Meinschein, W.G. (1979). Sterols as ecological indicators. *Geochimica et Cosmochimica Acta*, **43**, 739-745.

Hubbert, M.K. (1940). The theory of ground-water motion. *Journal of Geology*, **48**, 785-944.

Hubbert, M.K. (1953). Entrapment of petroleum under hydrodynamic conditions. *American Association of Petroleum Geologists Bulletin*, **37**, 1954-2026.

Hunt, J.M. (1979). *Petroleum geochemistry and geology* (pp. 332). San Francisco: W. H. Freeman.

Hunt, J.M. (1990). Generation and migration of petroleum from abnormally pressure fluid compartments. *American Association of Petroleum Geologists Bulletin,* **74**, 1-12.

Hunt, J.M., Lewan, M.D. and Hennet, R.J-C. (1991). Modeling oil generation with time-temperature index graphs based on the Arrhenius equation. *American Association of Petroleum Geologists Bulletin*, **75**, 795-807.

Hunt, J.M. (1996). *Petroleum geochemistry and geology (2nd ed.)* (pp. 291, 370, 380-388, 491-516). New York: W. H. Freeman.

Hunt, J.M., Whelan, J.K., Eglinton, L.B. and Cathles III, L.M. (1998). Relation of Shale Porosities, Gas Generation, and Compaction to Deep Overpressures in the U.S. Gulf Coast. In Law, B.E., Ulmishek, G.F. and Slavin, V.I. eds., *Abnormal Pressures in Hydrocarbon Environments* (pp. 87-104): American Association of Petroleum Geologists Memoir, **70**.

Hutton, A.C. and Cook, A.C. (1980). Influence of alginate on the reflectance of vitrinite from Joadja, NSW, and some coals and other oil shales containing alginate. *Fuel,* **59**, 711-714.

Jarvis, G.T. and McKenzie, D.P. (1980). Sedimentary basin formation with finite extension rates. *Earth Planetary Science Letters*, **48**, 42-52.

Jones, R.W. (1984). Comparison of carbonate and shale source rocks. In: James G. Palaces ed., *Petroleum geochemistry and source rock potential of carbonate rocks*, American Association of Petroleum Geologists Studies in Geology, No. 18 (pp. 163-180). Tulsa, Oklahoma 74101, U.S.A.

Joy, A.M. (1992). Estimation of Cenozoic water depths in the Western Central Graben, UK North Sea, by subsidence modelling. In: R.F.P. Hardman ed., *Exploration Britain; geological insights for the next decade* (pp. 107-125). Geological Society Special Publications No. 67, Geological Society of London. London, United Kingdom, 1992.

Kaiko, A.R. and Tingate, P.R. (1996). Suppressed vitrinite reflectance and its effect on thermal history modelling in the Barrow and Dampier Sub-basins. *Australian Petroleum Production and Exploration Association Journal,* **36**, 428-444.

Kaiko, A.R. (1998). Thermal history analysis of the Barrow and Dampier Sub-basins, North West Shelf, Western Australia (PhD thesis, University of South Australia).

Kaiko, A.R. (2000). Evidence for a rift related heating event around the Alpha Arch, Barrow Sub-basin, Western Australia (abstract, pp. 1444-1445). *AAPG international conference and exhibition, Bali, Indonesia, October 15-18, 2000.*

Kaiko, A.R. and Tait, A. M. (2001). Post-rift tectonic subsidence and palaeo-water depths in the Northern Carnarvon Basin, Western Australia. *Australian Petroleum Production and Exploration Association Journal*, **41**, 367-379.

Keep, M., Powell, C.McA. and Baillie, P.W. (1998). Neogene deformation of the North West Shelf, Australia. In: Purcell P.G. and Purcell R.R. eds., *The Sedimentary Basins of Western Australia 2* (pp. 81-91). Proceedings of the Petroleum Exploration Society of Australia, Perth, 1998.

Khorasani, G.K. and Michelsen, J.K. (1994). The effects of overpressure, lithology, chemistry and heating rate on vitrinite reflectance evolution, and its relationship with oil generation. *Australian Petroleum Exploration Association Journal,* **34**, 418-435.

Kopsen, E. and McGann, G. (1985). A review of the hydrocarbon habitat of the Eastern and Central Barrow-Dampier Sub-basin, Western Australia. *Australian Petroleum Exploration Association Journal,* **25**, 154-176.

Kopsen, E. (1994). Northern Carnarvon Basin hydrocarbon distribution and future petroleum potential. In: Purcell, P. G. and Purcell, R. R. eds., *The Sedimentary Basins of Western Australia* (pp. 127-139): Proceedings of the Petroleum Exploration Society of Australia, Perth, 1994.

Kruge, M.A. (1983). Diagenesis of Miocene Biogenic Sediments in Lost Hills Oil Field, San Joaquin Basin, California. In: Isaacs, C.M. and Garrison, R.E. eds., *Petroleum generation and occurrence in the Miocene Monterey Formation, California* (pp. 39-51). Los Angeles: The Pacific Section, Society of Economic Paleontologists and Mineralogists.

Labutis, V.R. (1994). Sequence stratigraphy and the North West Shelf of Australia. In: Purcell, P.G. and Purcell, R.R. eds., *The Sedimentary Basins of Western Australia* (pp. 159-180): Proceedings of West Australian Basins Symposium, Perth, Western Australia, 1994.

Lachenbruch, A. (1970). Crustal temperature and heat productivity: implications of the linear heat flow relation. *Journal of Geophysical Research*, **75**, 3291-3300.

Larter, S.R. (1988). Some pragmatic perspectives in source rock geochemistry. *Marine and Petroleum Geology*, **5**, 194-204.

Law, B. and Dickinson, W. (1985). Conceptual model for origin of abnormally pressured gas accumulation in low-permeability reservoirs. *American Association of Petroleum Geologists Bulletin*, **69**, 1295-1304.

Lawry, P.J. and Carter, P.A. (1992). Rivoli-1 gas discovery - Exmouth Sub-basin, Western Australia. *Australian Petroleum Exploration Association Journal*, **32**, 94-102.

le Poidevin, S.R. and Lowden, R.D. (1994). Petroleum resource of the Western Australia. In: Purcell, P. G. and Purcell, R. R. eds., *The Sedimentary Basins of Western Australia* (pp. 119-125): Proceedings of the Petroleum Exploration Society of Australia, Perth, 1994.

Lee, Y. and Deming, D. (2002). Overpressure in the Anadarko basin, southwestern Oklahoma: Static or dynamic? *American Association of Petroleum Geologists Bulletin*, **86**, 145-160.

Lerche, I., Yarzab, R.F. and Kendall, C.G.St.C. (1984). Determination of paleoheat flux from vitrinite reflectance. *American Association of Petroleum Geologists Bulletin*, **68**, 1704-1717.

Lerche, I. (1990). *Basin analysis - quantitative methods* (pp. 232-235). San Diego: Academic Press, Inc.

Lo, H.B. (1992). Identification of indigenous vitrinite for improved thermal maturity evaluation. *Organic Geochemistry,* **17**, 359-364.

Lo, H.B. (1993). Correction criteria for the suppression of vitrinite reflectance in hydrogen-rich kerogen: preliminary guideline. *Organic Geochemistry*, **20**, 653-657.

Ludden, J.N. (1992). Radiometric age determinations for basement from Sites 765 and 766, Argo Abyssal Plain and Northwestern Australia Margin. In F.M. Gradstein et al., eds., *Preceedings of the Ocean Drilling Program* (PP. 557-559). Scientific Results: College Station, Texas A and M University. ODP. v. 123.

Lundegard, P.D. (1991). Sandstone porosity loss - A "Big Picture" view of the importance of compaction. *Journal of Sedimentary Research*, **62**, 250-260.

Luo, X.R. and Vasseur, G. (1992). Contributions of compaction and aquathermal pressuring to geopressure and the influence of environmental conditions. *American Association of Petroleum Geologists Bulletin*, **76**, 1550-1559.

Luo, X.R. and Vasseur, G. (1996). Geopressuring mechanism of organic matter cracking: numerical modeling. *American Association of Petroleum Geologists Bulletin,* **80**, 856-874.

Lysak, S.V. (1992). Heat flow variations in continental rifts. *Tectonophysics*, **208**, 309-323.

Mackenzie, A.S. and Quigley, T.M. (1988). Principles of geochemical prospect appraisal. *American Association of Petroleum Geologists Bulletin*, **72**, 399-413.

Magara, K. (1978). *Compaction and fluid migration: practical petroleum geology* (pp. 47-85). Amsterdam: Elsevier Science.

Mann, D.M. and Mackenzie, A.S. (1990). Prediction of pore pressure in sedimentary basin. *Marine and Petroleum Geology*, **7**, 55-65.

Marine, I.W. and Fritz, S.J. (1981). Osmotic model to explain anomalous hydraulic heads. *Water Resources Research*, **17**, 73-82.

Márquez, X.M. and Mountjoy, E.W. (1996). Microfractures due to overpressures caused by thermal cracking in well-sealed Upper Devonian reservoirs, Deep Alberta Basin. *American Association of Petroleum Geologists Bulletin,* **80**, 570-588

McAuliffe, C.D. (1979). Oil and gas migration - chemical and physical constraints. *American Association of Petroleum Geologists Bulletin*, **63**, 761-781.

McClure, I.M., Smith, D.N., Williams, A.F., Clegg, L.J. and Ford, C.C. (1988). Oil and gas fields in the Barrow Sub-basin. In: Purcell P.G. and Purcell R.R. eds., *The North West Shelf, Australia* (pp. 371-390): Proceedings of the Petroleum Exploration Society of Australia, Perth, 1988.

McKenzie, D. (1978). Some remarks on the development of sedimentary basin. *Earth and Planetary Science Letters*, **40**, 25-32.

McTavish, R.A. (1978). Pressure retardation of vitrinite diagenesis, offshore north-west Europe. *Nature*, **271**, 648-650.

McTavish, R.A. (1998). The role of overpressure in the retardation of organic matter maturation. *Journal of Petroleum Geology,* **21**, 153-186.

Mello, U.T. and Karner, G.D. (1996). Development of sediment overpressure and its effect on thermal maturation: application to the Gulf of Mexico Basin. *American Association of Petroleum Geologists Bulletin*, **80**, 1367-1396.

Middleton, M.F. (1982). Tectonic history from vitrinite reflectance. *Geophysical Journal of the Royal astronomical Society*, **68**, 121-132.

Middleton, M.F. and Hunt, J.W. (1989). Influence of tectonics on Permian coal-rank patterns in Australia. *International Journal of Coal Geology*, **13**, 391-411.

Miller, L.R. and Smith, S.A. (1996) The development and regional significance of rift-related depositional systems in the Dampier Sub-basin. *Australian Petroleum Production and Exploration Association Journal*, **36**, 369-384.

Miller, T.W. and Luk, C.H. (1993). Contributions of compaction and aquathermal pressuring to geopressure and the influence of environmental conditions: Discussion. *American Association of Petroleum Geologists Bulletin*, **77**, 2006-2010.

Müller, R.D., Mihut, D. and Baldwin, S. (1998). A new kinematic model for the formation and evolution of the west and northwest Australian margin. In: Purcell P.G. and Purcell R.R. eds., *The Sedimentary Basins of Western Australia 2* (pp. 55-71): Proceedings of the Petroleum Exploration Society of Australia, Perth, 1998.

Nielsen, S.B. (1996). Sensitivity analysis in thermal and maturity modelling. *Marine and Petroleum Geology,* **13**, 415-425.

Ortoleva, P.J. (1994). Basin compartmentation: definitions and mechanisms. In: Ortoleva, P.J. ed., *Basin Compartments and Seals* (pp. 39-51): American Association of Petroleum Geologists Memoir, **61**.

Osborne, M.J. and Swarbrick, R.E. (1997). Mechanisms for generating overpressure in sedimentary basins: a re-evaluation. *American Association of Petroleum Geologists Bulletin,* **81**, 1023-1041.

Parry, J.C. and Smith, D.N. (1988). The Barrow and Exmouth Sub-basins. In: Purcell P.G. and Purcell R.R. eds., *The North West Shelf, Australia* (pp. 129-145): Proceedings of the Petroleum Exploration Society of Australia, Perth, 1988.

Peters, K.E. (1986). Guidelines for evaluating petroleum source rock using programmed pyrolysis. *American Association of Petroleum Geologists Bulletin,* **70**, 318-329.

Peters, K.E. and Moldowan, J.M. (1993). *The biomarker guide: interpreting molecular fossils in petroleum and ancient sediments* (pp. 220-251). Englewood Cliffs, New Jersey: Prentice Hall.

Petroleum Division of the Department of Minerals and Energy, Western Australia (1999). North West Shelf oil and gas.

Pickard, G.L. and Emery, W.J. (1982). *Physical oceanography*: an introduction (4th edition). Oxford: Pergamon Press, 249 p.

Pitchford, A., Teerman, S.C. and Clark, P.A. (1999). The use of oil fingerprinting to enhance field production on Barrow Island. *Australian Petroleum Production and Exploration Association Journal*, **39**, 408-419.

Platte River Associates, Inc. (1996). BasinMod 1D Basin Modelling System (version, 5.20) (unpublished).

Platte River Associates, Inc. (1998a). BasinMod 1D Basin Modelling System (version, 7.00) (unpublished).

Platte River Associates, Inc. (1998b). BasinMod 2D Basin Modelling System (version, 2.52) (unpublished).

Plumley, W.J. (1980). Abnormally high fluid pressure: survey of some basic principles. *American Association of Petroleum Geologists Bulletin*, **64**, 414-430.

Polomka, S.M., Bruins, J., Spanninga, G.A. and Mennie, J.P. (1999). WA-271-P, Exmouth Sub-basin - integrated prospectivity evaluation. *Australian Petroleum Production and Exploration Association Journal,* **39**, 115-127.

Powell, T.G. and McKirdy, D.M. (1972). The geochemical characterization of Australian crude oils. *Australian Petroleum Exploration Association Journal*, **12**, 125-131.

Powell, T.G. and McKirdy, D.M. (1973a). Crude oil correlations in the Perth and Carnarvon Basins. *Australian Petroleum Exploration Association Journal,* **13**, 81-85.

Powell, T.G. and McKirdy, D.M. (1973b). Relationship between ratio of pristane to phytane, crude oil composition and geological environment in Australia. *Nature Physical Science*, **243**, 37-39.

Powers, M.C. (1967). Fluid release mechanisms in compacting marine mudrocks and their importance in oil exploration. *American Association of Petroleum Geologists Bulletin*, **51**, 1240-1254.

Powley, D.E. (1990). Pressure compartments and fluid flow in basins. In: V. M. Goldschmidt conference, program and abstracts (p. 75): Geochem. Soc., United States. 1990.

Price, L.C. and Barker, C.E. (1985). Suppression of vitrinite reflectance in amorphous rich kerogen - a major unrecognized problem. *Journal of Petroleum Geology,* **8**, 59-84.

Price, L.C. and Wenger, L.M. (1992). The influence of pressure on petroleum generation and maturation as suggested by aqueous pyrolysis. *Organic Geochemistry,* **19**, 1-3, 141-159.

Purcell, P.G. and Purcell, R.R. (1994). The sedimentary basin of Western Australia: An introduction. In: P. G. and R. R. Purcell eds., *The Sedimentary Basins of*

Western Australia (pp. 3-18): Proceedings of the Petroleum Exploration Society of Australia, Perth, 1994.

Quilty, P.G. (1977). Cenozoic sedimentation cycles in Western Australia. *Geology*, **5**, 336-340.

Ramm, M. (1992). Porosity-depth trends in reservoir sandstones: off-shore Norway. *Marine and Petroleum Geology*, **9**, 553-567.

Raymond, A.C. and Murchison, D.G. (1991). Influence of exinitic macerals on the reflectance of vitrinite in Carboniferous sediments of the Midland Valley of Scotland. *Fuel,* **70**, 155-161.

Robertson Research Australia Pty. Ltd. (1986). Petroleum geology and geochemistry, North West Shelf, Australia (unpublished).

Sajgó, Cs., McEvov, J., Wolff, G.A. and Horváth, Z.A. (1986). Influence of temperature and pressure on maturation processes-I. Preliminary report. *Organic Geochemistry,* **10**, 331-337.

Sahimi, M. (1995). Flow and transport in porous media and fractured rock (482 p.). VCH Verlagsgesellcshaft mbH, Weinheim.

Samuelsson, J. and Middleton, M.F. (1998). A thermal maturation study of the Carnarvon Basin, Australia and the northern North Sea, Europe. *Exploration Geophysics, **29***, 597-604.

Schegg, R., Cornford, C. and Leu, W. (1999). Migration and accumulation of hydrocarbon in the Swiss Molass Basin: implication of a 2D basin modeling study. *Marine and Petroleum Geology*, **16**, 511-531.

Schenk, H.J., Horsfield, B., Krooss, B., Schaefer, R.G. and Schwochau, K. (1997). Kinetics of petroleum formation and cracking. In: D.H. Welte, B. Horsfield and D.R. Baker eds., *Petroleum and Basin Evolution* (pp. 233-269): Springer-Verlag Berlin: Scientific Publishing Services (P) Ltd, Madras.

Schmidt, G.W. (1973). Interstitial water composition and geochemistry of deep Gulf Coast shales and sandstones. *American Association of Petroleum Geologists Bulletin*, **57**, 321-337.

Schön, J.H. (1996). *Physical properties of rocks, fundamentals and principles of petrophysics*. New York: Elsevier Science.

Schowalter, T. (1979). Mechanics of secondary hydrocarbon migration, and entrapment. *American Association of Petroleum Geologists Bulletin*, **63**, 723-760.

Sclater, J.G. and Christie, P.A.F. (1980). Continental stretching: an explanation of the post-mid-Cretaceous subsidence of the central North Sea Basin. *Journal of Geophysical Research*, **85**, 3711-3739.

Scott, J. (1992). Accurate recognition of source rock character in the Jurassic of the North West Shelf, Western Australia. *Australian Petroleum Exploration Association Journal,* **32**, 289-299.

Scott, J. (1994). Source rocks of Western Australia - distribution, character and models. In: Purcell P. G. and Purcell R. R. eds., *The Sedimentary Basins of Western Australia* (pp. 141-155): Proceedings of the Petroleum Exploration Society of Australia, Perth, 1994.

Snowdon, L.R. (1995). Rock-Eval T_{max} suppression: documentation and amelioration. *American Association of Petroleum Geologists Bulletin,* **79**, 1337-1348.

Spencer, C.W. (1987). Hydrocarbon generation as a mechanism for overpressure in the Rocky Mountains region. *American Association of Petroleum Geologists Bulletin,* **71**, 368-388.

Stagg, M.J. and Colwell, J.B. (1994). The structure foundations of the Northern Carnarvon Basin. In: Purcell, P. G. and Purcell, R. R. eds., *The Sedimentary Basins of Western Australia* (pp. 349-364): Proceedings of the Petroleum Exploration Society of Australia, Perth, 1994.

Steckler, M.S. and Watts, A.B. (1978). Subsidence of the atlantic-type continental margin off New York. *Earth and Planetary Science Letters*, **41**, 1-13.

Stein, A. (1994). Rankin Platform, Western Australia: structural development and exploration potential. In: Purcell P. G. and Purcell R. R. eds., *The Sedimentary Basins of Western Australia* (pp. 509-523): Proceedings of the Petroleum Exploration Society of Australia, Perth, 1994.

Swarbrick, R.E. (1995). Distribution and generation of the overpressure system, Eastern Delaware Basin, Western Texas and Southern New Mexico: Discussion. *American Association of Petroleum Geologists Bulletin*, **79**, 1817-1821.

Swarbrick, R.E. and Osborne, M.J. (1998). Mechanisms that generate abnormal pressures: an overview. In: Law, B.E., Ulmishek, G.F. and Slavin, V.I. eds., *Abnormal pressures in hydrocarbon environments* (pp. 13-34): American Association of Petroleum Geologists Memoir, **70**.

Swarbrick, R.E. and Hillis, R.R. (1999). The origin and influence of overpressure with reference to the North West Shelf, Australia. *Australian Petroleum Production and Exploration Association Journal,* **39**, 64-72.

Sweeney, J.J. and Burnham, A.K. (1990). Evaluation of a simple model of vitrinite reflectance based on chemical kinetics. *American Association of Petroleum Geologists Bulletin,* **74**, 1559-1570.

Swift, M. G., Stagg, H. M. J. and Falvey, D. A. (1988). Heat flow regime and implications for oil maturation and migration in the Offshore Northern Carnarvon Basin. In: Purcell, P. G. and Purcell, R. R. eds., *The North West Shelf, Australia* (pp. 540-551): Proceedings of the Petroleum Exploration Society of Australia, Perth, 1988.

Tait, A.M. (1985). A depositional model for the Dupuy Member and the Barrow Group in the Barrow Sub-basin, Northwestern Australia. *Australian Petroleum Exploration Association Journal,* **25**, 282-290.

Teerman, S.C. (1994). Organic petrographic analysis of selected intervals in nine Barrow Sub-basin wells. Report., Approval No. S30940 (unpublished).

Teichmüller, M. and Durand, B. (1983). Fluorescence in microscopical rank studies on liptinites and vitrinites in peat and coals, and comparison with the results of the rock-Eval pyrolysis. *International Journal of Coal Geology,* **2**, 197-230.

Teige, G.M.G., Hermanrud, C., Wensaas, L., Bolas, H.M.N. (1999). The lack of relationship between overpressure and porosity in North Sea and Haltenbanken shales. *Marine and Petroleum Geology,* **16**, 321-335.

Terzaghi, K. (1923). Die berechnung der durchlässigkeitsziffer des tones as dem verlauf der hydrodynamichen spannungsercheinungen: Sitzungsgbrg. Akad. Wiss. Wien, Math. Naturwess. K1., IIa, **132** (3/4), p. 125-138.

Timko, D.J. and Fertl, W.H. (1971). Relationship between hydrocarbon accumulation and geopressure and its economic significance. *Journal of Petroleum Technology*, **22**, 923-930.

Tindale, K., Newell, N., Keall, J. and Smith, N. (1998). Structural evolution and charge history of the Exmouth Sub-basin, Northern Carnarvon Basin, Western Australia. In: Purcell P. G. and Purcell R. R. eds., *The Sedimentary Basins of Western Australia 2* (pp. 447-472). Proceedings of the Petroleum Exploration Society of Australia, Perth, 1998.

Tingate, P.R., Khaksar, A, van Ruth, P., Dewhurst, D., Raven, M., Young, H., Hillis, R. and Dodds, K. (2001). Geological controls on overpressure in the Northern Carnarvon Basin. *Australian Petroleum Production and Exploration Association Journal*, **41**, 573-593.

Tissot, B.P. and Welte D.H. (1984). *Petroleum formation and Occurrence (2nd Edn)* (pp. 223, 509-523). Berlin: Springer-Verlag.

Tissot, B.P., Pelet, R. and Ungerer, P.H. (1987). Thermal history of sedimentary basins, maturation indices, and kinetics of oil and gas generation. *American Association of Petroleum Geologists Bulletin,* **71**, 1445-1466.

Trendall, A.F. and Cockbain, A.E. (1990). Basin: Introduction. In: Geology and mineral resources of Western Australia (pp. 290-293). Geological Survey of Western Australia, Memoir, 3 (unpublished).

Ungerer, P., Burrus, J., Doligez, B., Chenet, P. Y. and Bessis, F. (1990). Basin evaluation by integrated two-dimensional modeling of heat transfer, fluid flow, hydrocarbon generation, and migration. *American Association of Petroleum Geologists Bulletin*, **76**, 309-335.

van Aarssen, B.G.K., Alexander, R. and Kagi, R.I. (1996). The origin of Barrow Sub-basin crude oils: a geochemical correlation using land-plant biomarkers. *Australian Petroleum Production and Exploration Association Journal,* **36**, 465-476.

van Aarssen, B.G.K., Bastow, T.P., Alexander, R. and Kagi, R.I. (1999). Age determination of crude oils in the Barrow Sub-basin using palaeoclimate related variations in higher plant biomarkers. *Australian Petroleum Production and Exploration Association Journal*, **39**, 399-407.

van Ruth, P., Hillis, R., Swarbrick, R and Tingate, P. (2000). Mud weights, transient pressure tests, and the distribution of overpressure in the North West Shelf, Australia. *The Petroleum Exploration Society of Australia Journal,* **28**, 59-66.

Vandenbroucke, M., Durand, B. and Oudin, J.L. (1983). Detecting migration phenomena in a geological series by means of C_1-C_{35} hydrocarbon amounts and distributions. In: Bjorøy, M. et al., eds., *Advances in Organic Geochemistry, 1981* (pp. 147-155). Chichester, England: Wiley.

Vear, A. (1998). Analysis of the Dampier Sub-basin petroleum system using integrated 2D modelling techniques. *Australian Petroleum Production and Exploration Association Journal*, **38**, 339-350.

Veenstra, E. (1985). Rift and drift in the Dampier Sub-basin, a seismic and structural interpretation. *Australian Petroleum Exploration Association Journal*, **25**, 177-189.

Veevers, J.J. and Li, Z.X. (1991). Review of seafloor spreading around Australia. I. Synthesis of the patterns of spreading. *Australian Journal of Earth Sciences*, **38**, 391-408.

Vincent, P. and Tilbury, L. (1988). Gas and oil fields of the Ranikn Trend and Northern Barrow-Dampier Sub-basin. In: Purcell, P. G. and Purcell, R. R. eds., *The North West Shelf, Australia* (pp. 341-369 Proceedings of the Petroleum Exploration Society of Australia, Perth, 1988.

Volkman, J.K., Alexander, R. and Kagi, R.I. (1983). A geochemical reconstruction of oil generation in the Barrow Sub-basin of Western Australia. *Geochimica et Cosmochimica Acta,* **47**, 2091-2105.

von Stackelberg, U., Exon, N.F., Von Rad, U., Quilty, P., Shafik, S., Beiersdorf, H., Seibertz, E. and Veevers, J.J. (1980). Geology of the Exmouth and Wallaby plateaus off northwest Australia. *Journal of Australian Geology and Geophysics*, **5**, 113-140.

Walderhaug, O. (1996). Kinetic modelling of quartz cementation and porosity loss in deeply buried sandstone reservoirs. *American Association of Petroleum Geologists Bulletin*, **80**, 731-745.

Wangen, M. (2000). Generation of overpressure by cementation of pore space in sedimentary rocks. *Geophys. J. Int.*, **143**, 608-620.

Waples, D.W. (1980). Time and temperature in petroleum formation: application of Lopatin's method to petroleum exploration. *American Association of Petroleum Geologists Bulletin*, **64**, 916-926.

Waples, D.W. (1985). *Geochemistry in Petroleum Exploration* (pp. 102, 108). Dordrecht: D. Reidel Publishing Company.

Waples, D.W., Kamata, H. and Suizu, M. (1992a). Art of Maturity modeling. Part 1: Finding a satisfactory geologic model. *American Association of Petroleum Geologists Bulletin*, **76**, 31-46.

Waples, D.W., Suizu, M. and Kamata, H. (1992b). Art of Maturity modeling. Part 2: Alternative models and sensitivity analysis. *American Association of Petroleum Geologists Bulletin*, **76**, 47-66.

Weedman, S. D., Brantley, S.L., Ryoji, S. and Poulson, S.R. (1996). Diagenesis, compaction, and fluid chemistry modelling of a sandstone near a pressure seal: Lower Tuscaloosa Formation, Gulf Coast. *American Association of Petroleum Geologists Bulletin*, **80**, 1045-1064.

Westphal, H. and Aigner, T. (1997). Seismic stratigraphy and subsidence analysis in the Barrow-Dampier Subbasin, Northwest Australia. *American Association of Petroleum Geologists Bulletin,* **81**, 1721-1749.

Wilkins, R.W.T., Wilmshurst, J.R., Hladky, G., Ellacott, M.V. and Buckingham, C.P. (1992a). The suppression of vitrinite reflectance in some North West Shelf wells: Barrow-1, Jupiter-1 and Flamingo-1. *Australian Petroleum Exploration Association Journal,* **32**, 300-312.

Wilkins, R.W.T., Wilmshurst, J.R., Russell, N.J., Hladky, G., Ellacott, M.V. and Buckingham, C. (1992b). Fluorescence alteration and suppression of vitrinite reflectance. *Organic Geochemistry*, **18**, 629-640.

Wilkins, R.W.T., Russell, N.J. and Ellacott, M.V. (1994). Fluorescence alteration and thermal maturity modelling of Carnarvon Basin wells. In: Purcell P. G. and Purcell R. R. eds., *The Sedimentary Basins of Western Australia* (pp. 415-432): Proceedings of the Petroleum Exploration Society of Australia, Perth, 1994.

Wilkins, R.W.T., Wilmshurst, J.R., Hladky, G., Ellacott, M.V. and Buckingham, C.P. (1995). Should fluorescence alteration replace vitrinite reflectance as a major tool for thermal maturity determination in oil exploration? *Organic Geochemistry,* **22**, 191-209.

Wood, D.A. (1988). Relationship between thermal maturation indices calculated using Arrhenius equations and Lopatin method: implications for petroleum exploration. *American Association of Petroleum Geologists Bulletin*, **72**, 115-134.

Woodside Offshore Petroleum (1988). A review of the petroleum geology and hydrocarbon potential of the Barrow-Dampier Sub-basin and Environs. In: Purcell P. G. and Purcell R. R. eds., *The North West Shelf, Australia* (pp. 115-128): Proceedings of the Petroleum Exploration Society of Australia, Perth, 1988.

Wulff, K.J. (1991). Upper Jurassic of the Barrow Sub-basin: Sedimentology, sequence stratigraphy and implications for reservoir development (PhD thesis, Curtin University of Technology).

Yardley, G.S. and Swarbrick, R.E. (2000). Lateral transfer: a source of additional overpressure? *Marine and Petroleum Geology*, **17**, 523-537.

Yassir, N. (1996). Overpressuring in the Dampier Sub-basin. APCRC Petroleum Confidential Report, 15 (unpublished).

Yeates, A.N., Bradshaw, M.T., Dickins, J.M., Brakel, A.T., Exon, N.F., Langford, R.P., Mulholland, S.M., Totterdell, J.M. and Yeung, M. (1987). The Westralian Superbasin, an Australian link with Tethys. In: McKenzie, K.G., ed., *Shallow Tethys 2*: Proceedings of the International Symposium on Shallow Tethys 2. Wagga Wagga, 199-213.

Zaunbrecher, M.L. (1994). Oil and gas accumulations of the Offshore Barrow and Exmouth Sub-basins - Trends in hydrocarbon habitat. In: Purcell P.G. and Purcell R.R. eds., *The Sedimentary Basins of Western Australia* (pp. 449-458). Proceedings of the Petroleum Exploration Society of Australia, Perth, 1994.

Zhou, Y.S. and Littke, R. (1999). Numerical simulation of the thermal maturation, oil generation and migration in the Songliao Basin, Northeastern China. *Marine and Petroleum Geology*, **16**, 771-792.

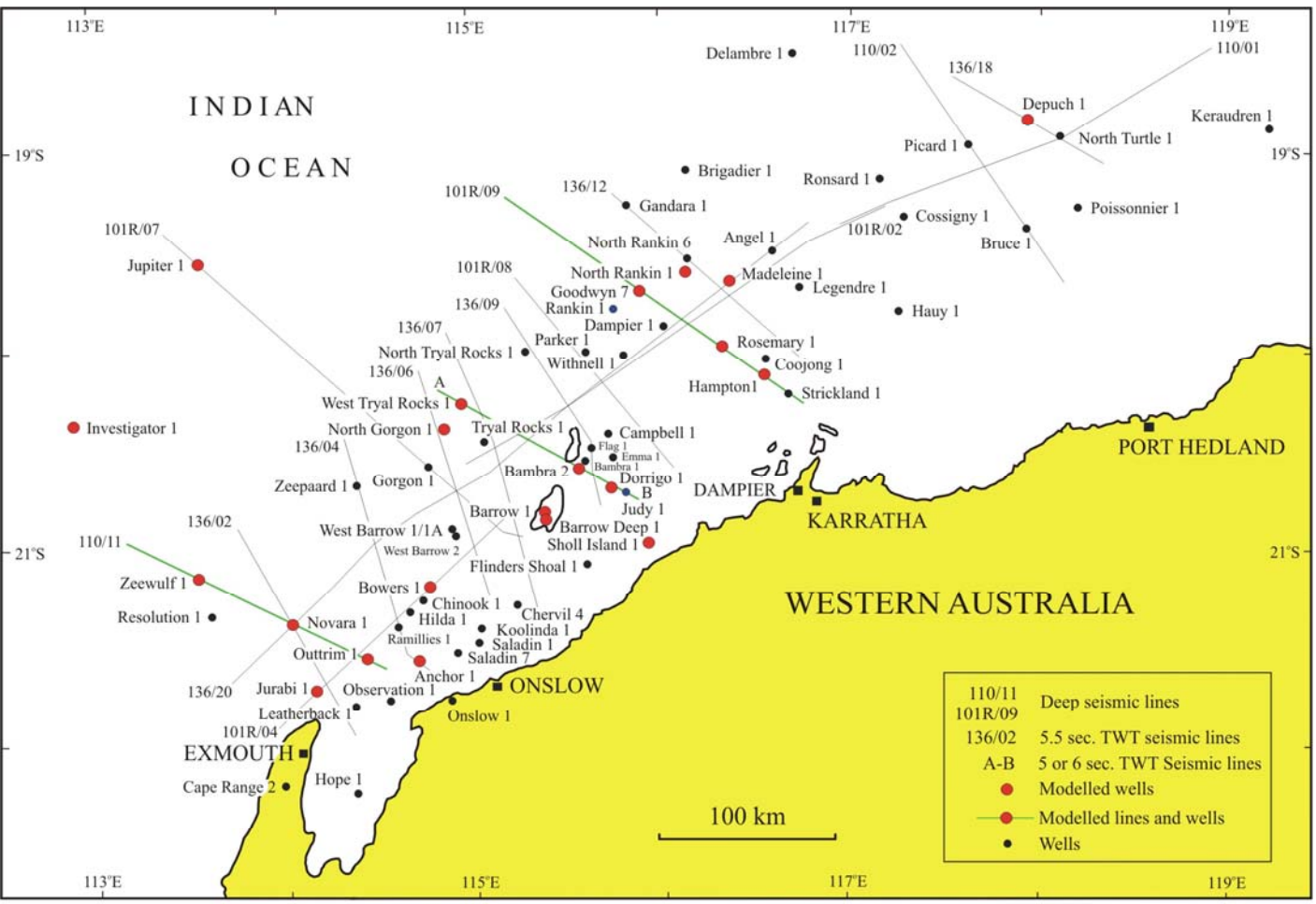

Fig. 1-3 Database of seismic lines and well locations in the Northern Carnarvon Basin.

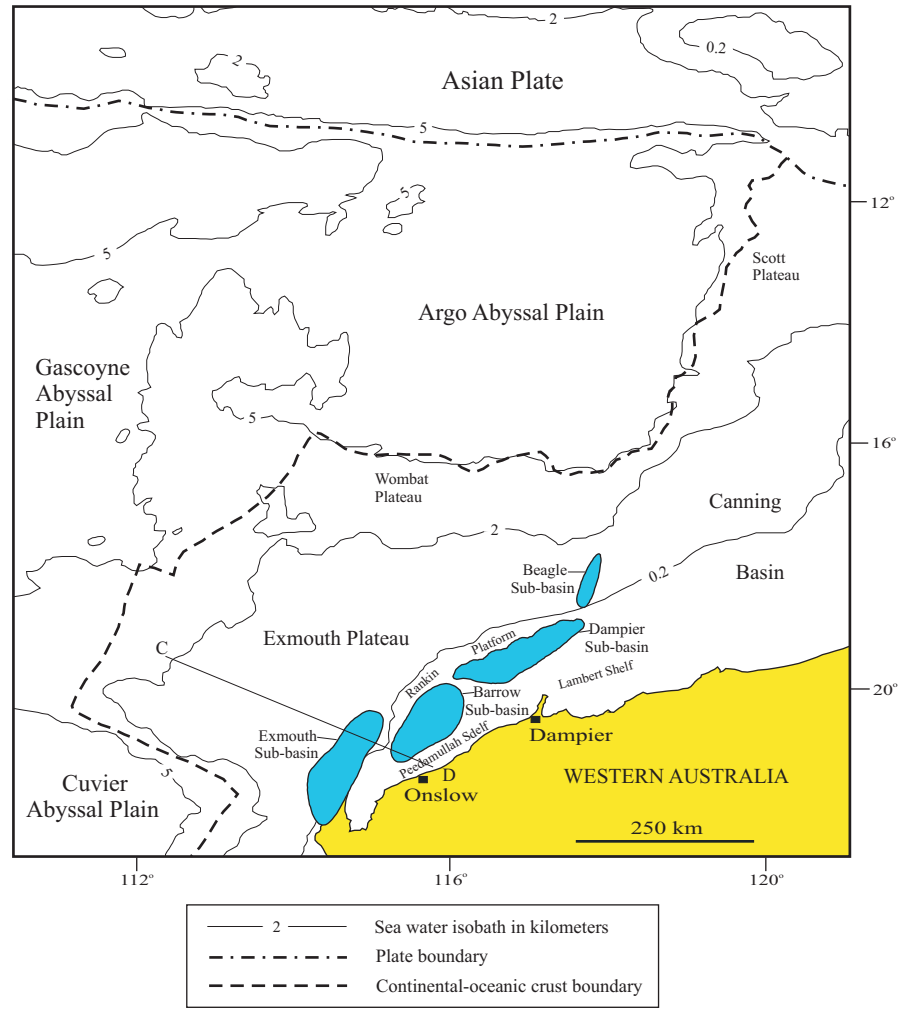

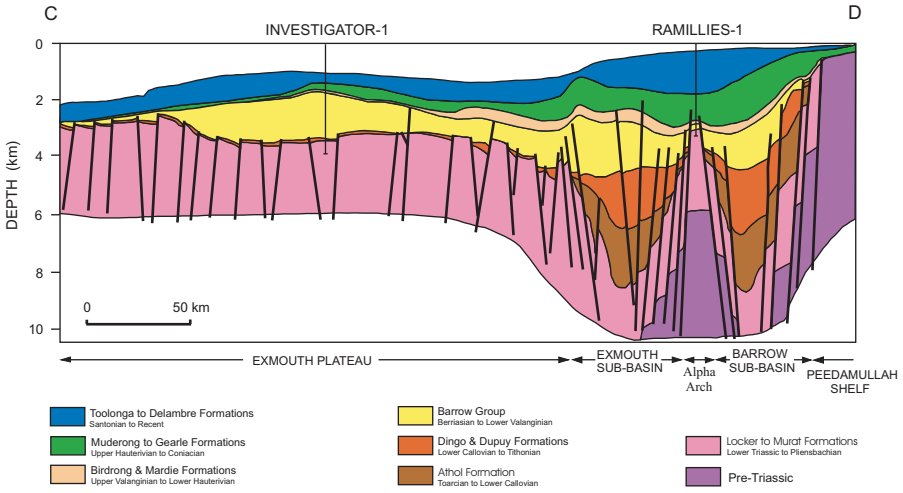

Fig. 2-2 The Exmouth, Barrow, Dampier and Beagle Sub-basins, Rankin Platform and Exmouth Plateau in the Northern Carnarvon Basin with adjacent three abyssal plains (after AGSO North West Shelf Study Group, 1994; Polomka et al.,1999). Also showing the cross-section (CD) of the Exmouth and Barrow Sub-basins, Alpha Arch and Exmouth Plateau (simplified from Tindale et al., 1998). See Fig.1-3 for well locations.

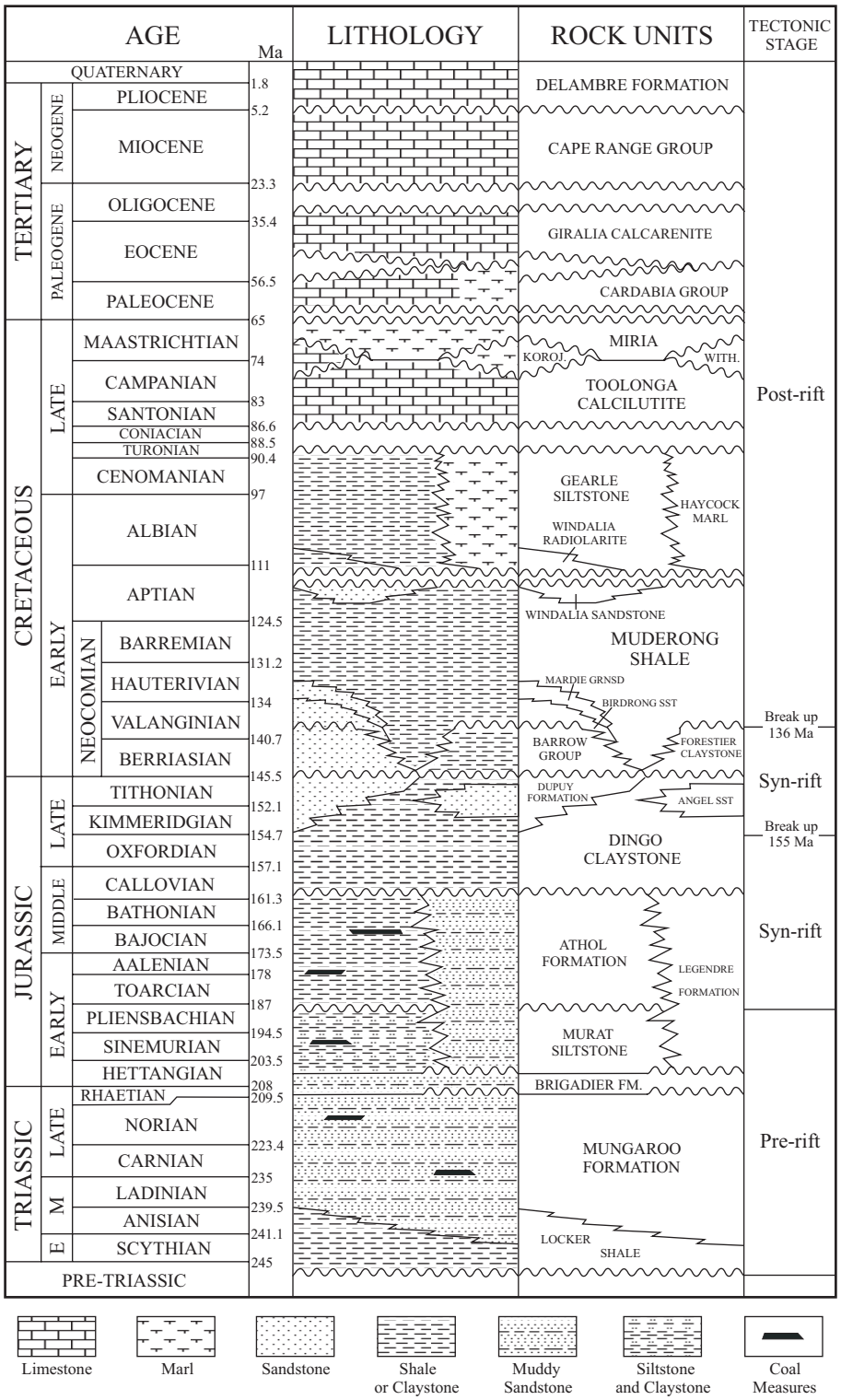

Fig. 2-3 Generalized stratigraphic column of the sub-basins in the Northern Carnarvon Basin (after Blevin et al., 1994; Labutis, 1994; Stagg and Colwell,1994; Polomka et al.,1999).

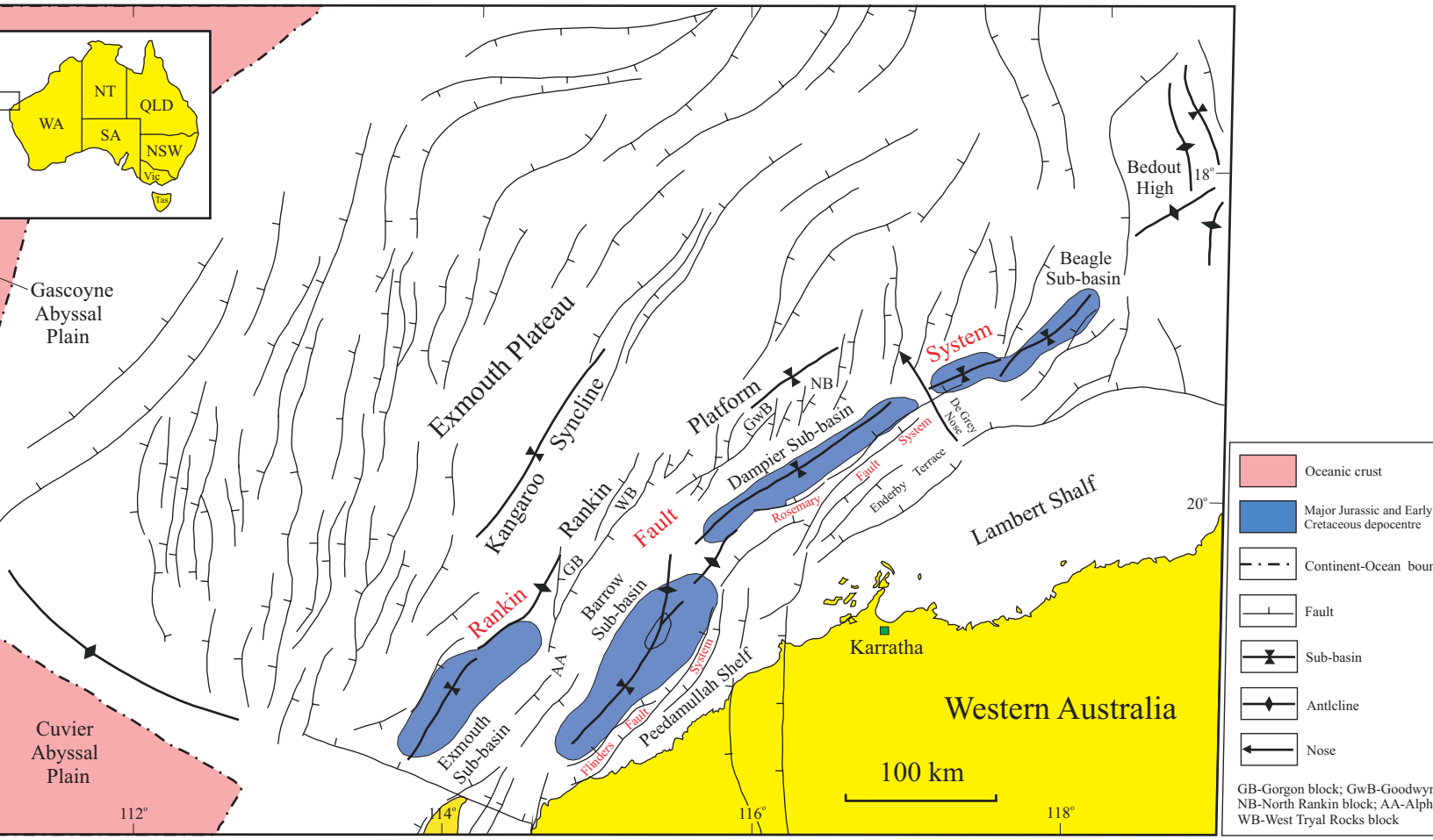

Fig. 2-4 Tectonic subdivisions, structures and faults of the North Carnarvon Basin (after Stagg and Colwell, 1994).

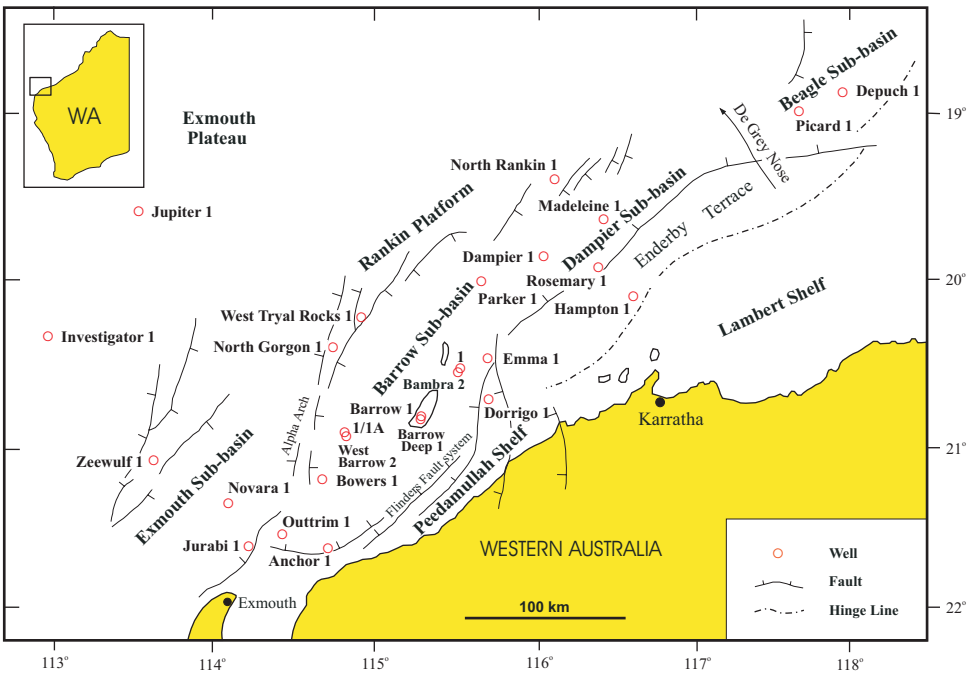

Fig. 3-1 Locations of the wells for the data sources of total organic carbon and organic matter type analyses in the Northern Carnarvon Basin (after Woodside Offshore Petroleum, 1998; Scott, 1992).

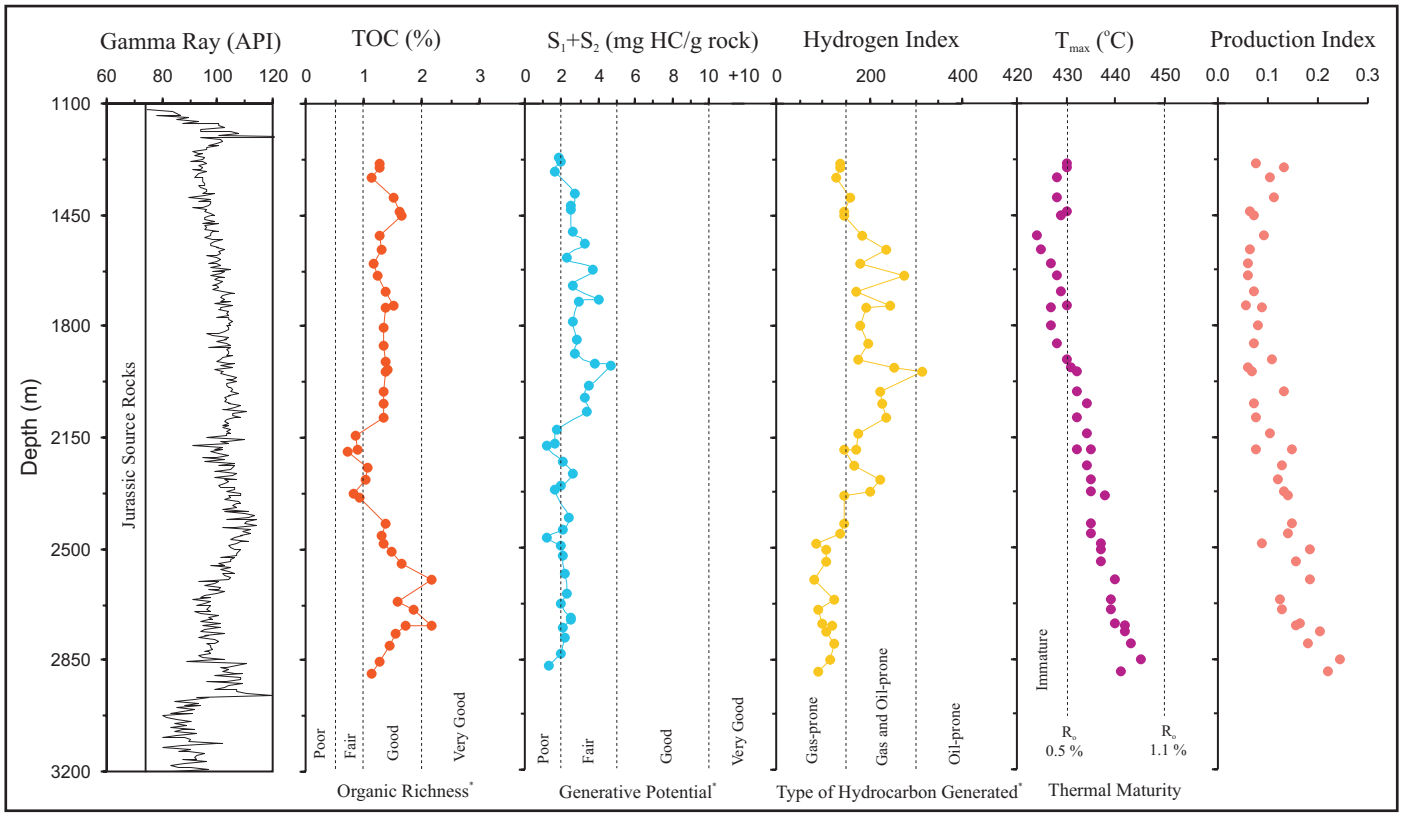

Fig. 3-11 Geochemical profiles of the Jurassic source rocks in the Jurabi-1 well of the Exmouth Sub-basin. TOC: Total organic carbon; S_1: Free hydrocarbons (mg HC/g rock); S_2: Pyrolysable hydrocarbons (mg HC/g rock); Hydrogen index: S_2*100/TOC; T_{max}: Temperature at the top of S_2 peak; Production index S_1/S_1+S_2. Type of hydrocarbon generated for immature stage.

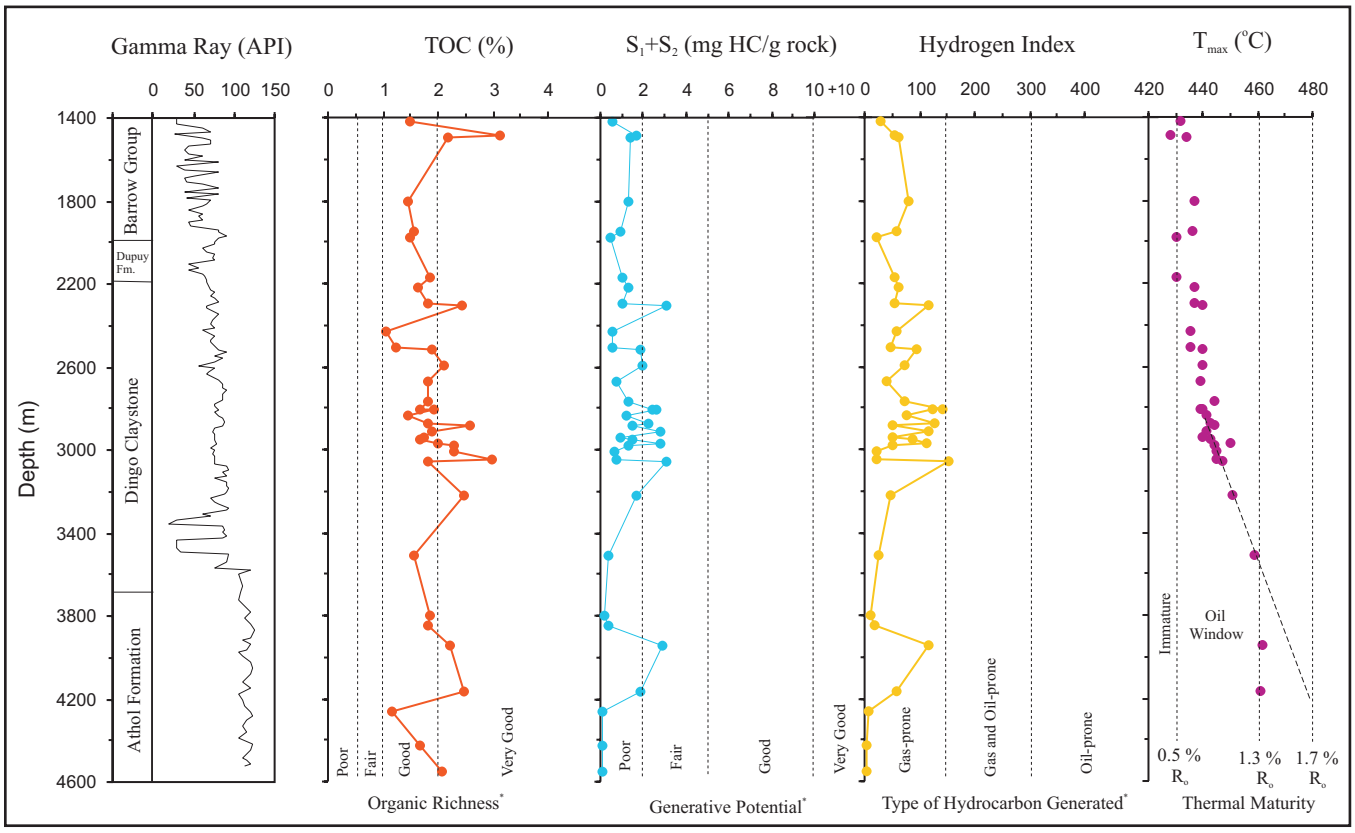

Fig. 3-12 Geochemical profiles of the Middle-Upper Jurassic and the lower part of the Barrow Group for the Barrow Deep-1 and Barrow-1 wells in the Barrow Sub-basin. TOC: Total organic carbon; S_1: Free hydrocarbons (mg HC/g rock); S_2: Pyrolysable hydrocarbons (mg HC/g rock); Hydrogen index: S_2*100/TOC; T_{max}: Temperature at the top of S_2 peak; Production index S_1/S_1+S_2. Type of hydrocarbon generated for immature stage. See Fig. 3-1 for well locations.

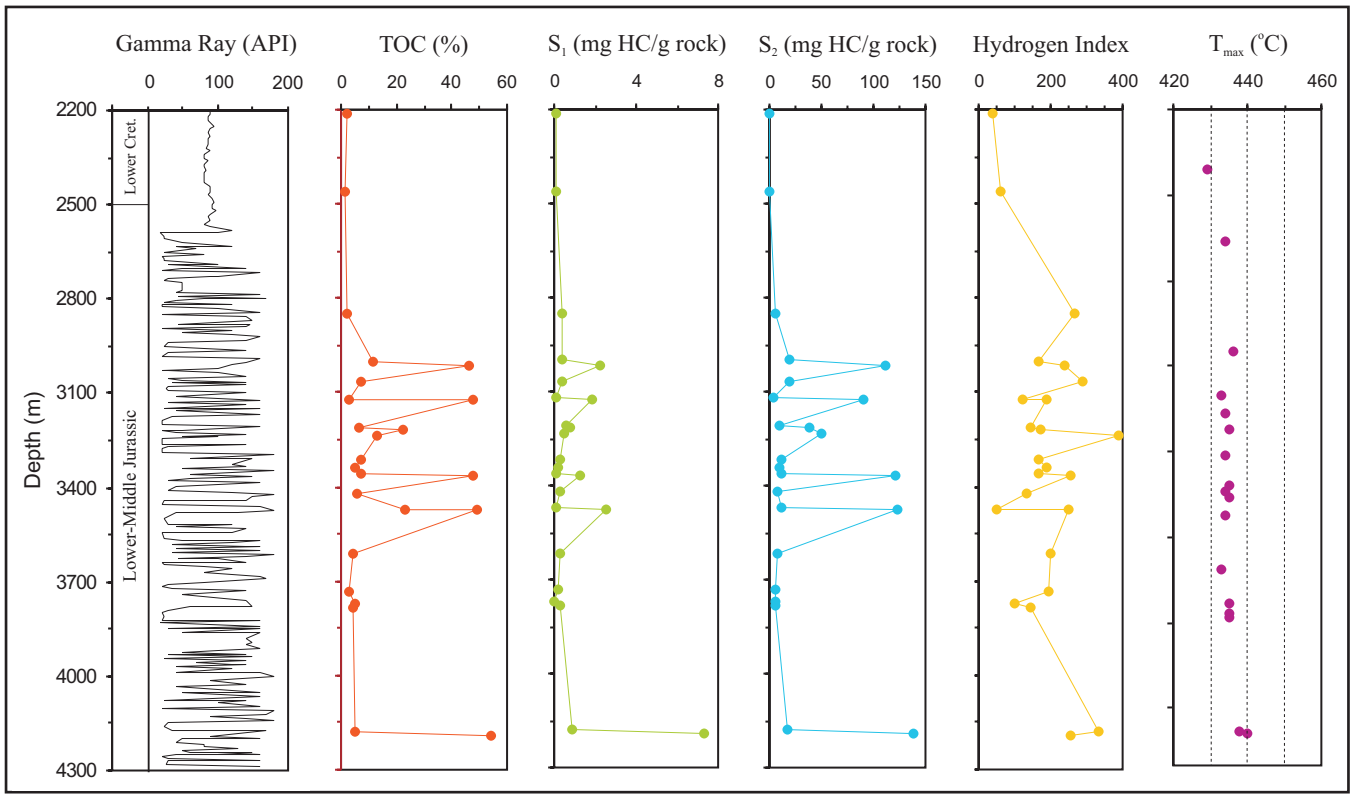

Fig. 3-13 Geochemical profiles of the Middle-Upper Jurassic and Lower Cretaceous in the Depuch-1 well of the Beagle Sub-basin. TOC: Total organic carbon; S_1: Free hydrocarbons (mg HC/g rock); S_2: Pyrolysable hydrocarbons (mg HC/g rock); Hydrogen index: S_2*100/TOC; T_{max}: Temperature at the top of S_2 peak; Production index: S_1/S_1+S_2.

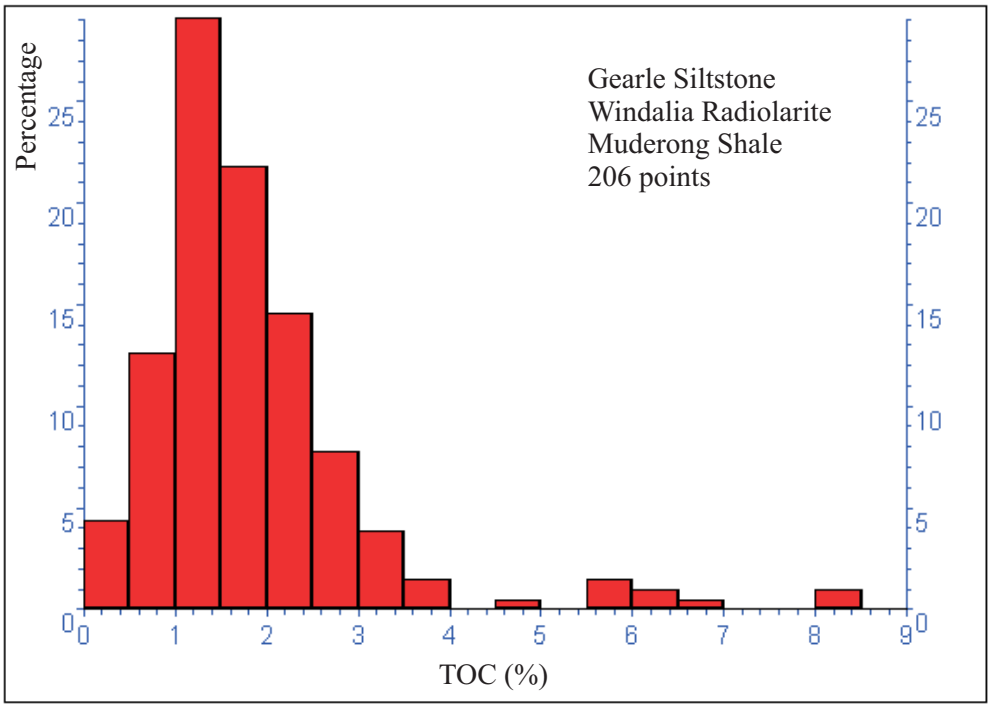

Fig. 3-2 Histogram of total organic matter for the Gearle Siltstone, Windalia Radiolarite and Muderong Shale in the Northern Carnarvon Basin.

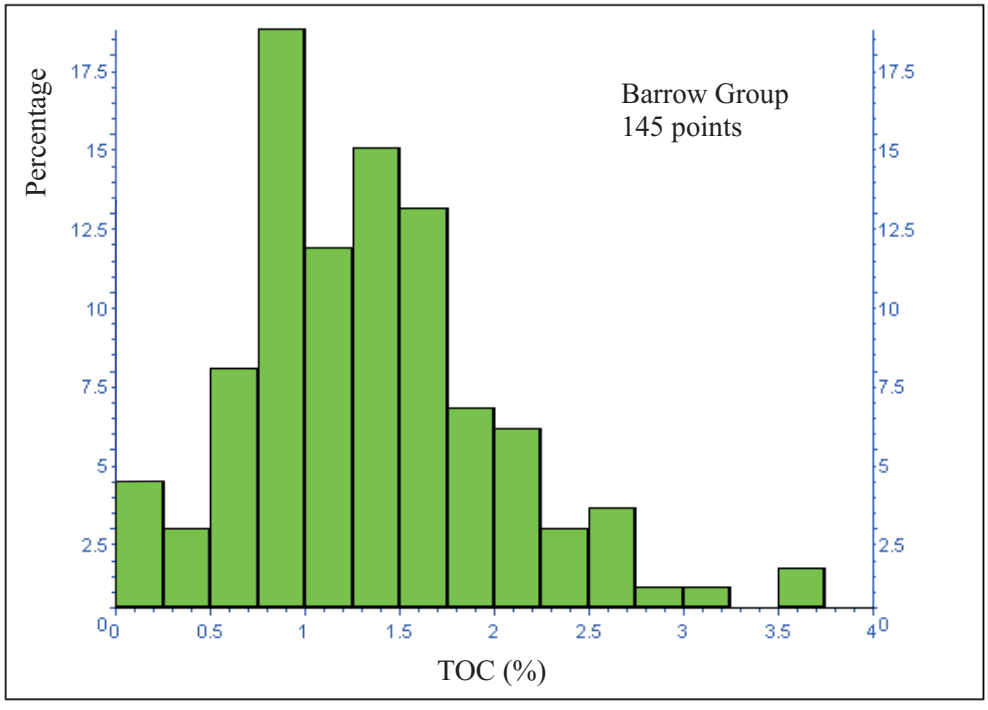

Fig. 3-3 Histogram of total organic matter for the Barrow Group in the Northern Carnarvon Basin.

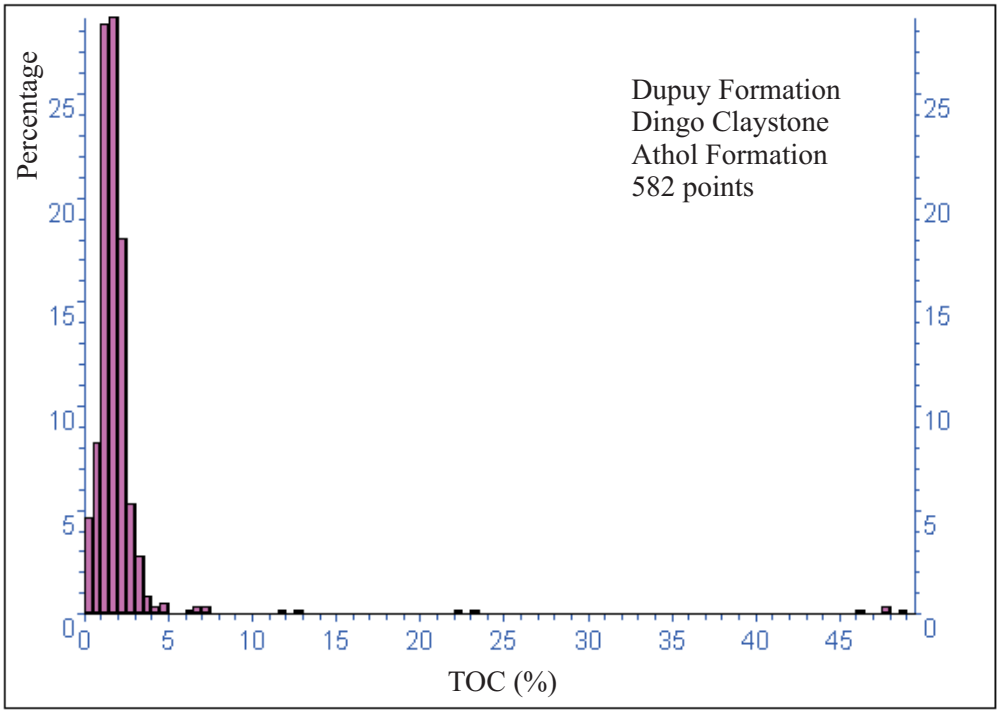

Fig. 3-4 Histogram of total organic matter for the Dupuy Formation, Dingo Claystone and Athol Formation in the Northern Carnarvon Basin.

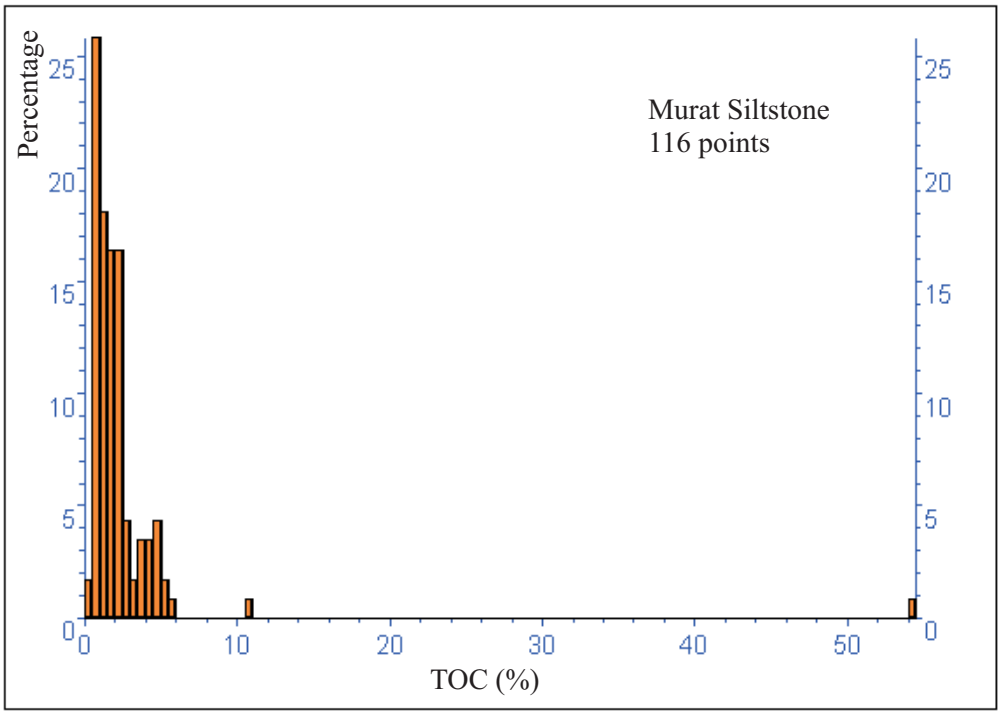

Fig. 3-5 Histogram of total organic matter for the Murat Siltstone in the Northern Carnarvon Basin.

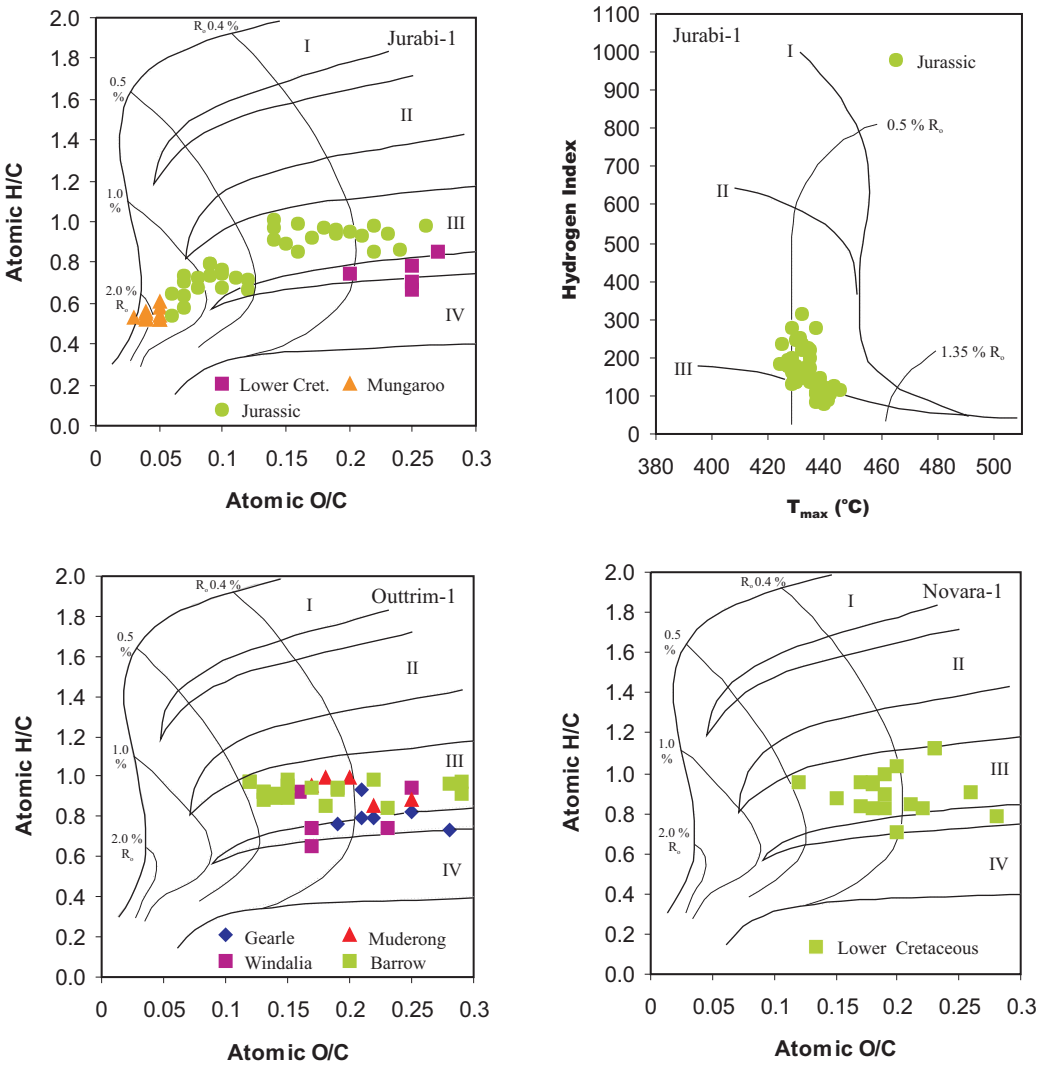

Fig. 3-7 Plots of atomic H/C versus atomic O/C and hydrogen index versus T_{max} show mainly type III organic matter for the samples from three wells within the Exmouth Sub-basin. See Fig. 3-1 for well locations.

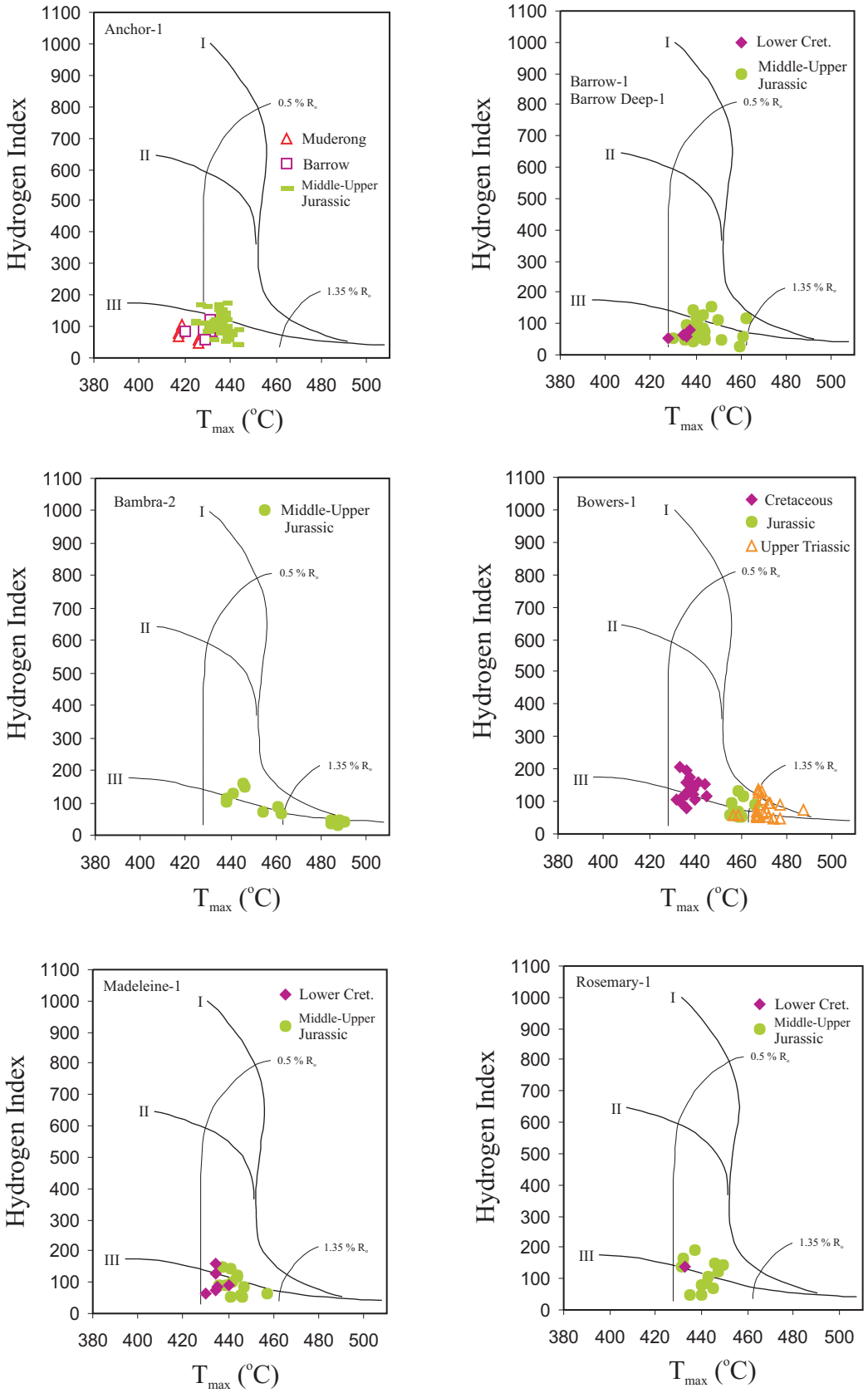

Fig. 3-8 Plots of hydrogen index versus T_{max} show kerogen type for the samples from six wells in the Barrow and Dampier Sub-basins. See Fig. 3-1 for well locations.

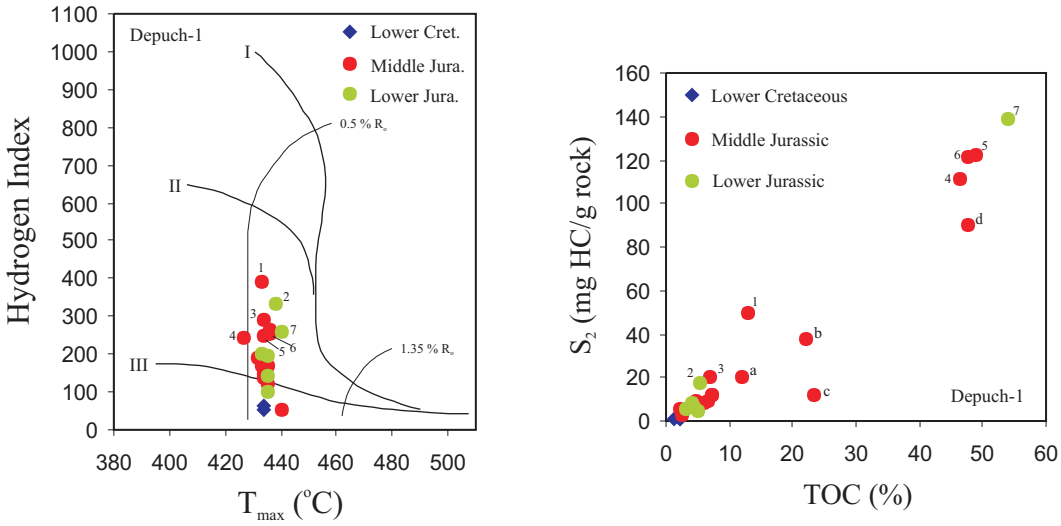

Fig. 3-9 Diagrams of HI (hydrogen index) versus T_{max} and S_2 versus TOC show the characteristics of organic matter in the samples from the Depuch-1 well of the Beagle Sub-basin. The numbers show that the samples with relatively high HI values are generally consistent with relatively high TOC or coals. a: HI=167; b: HI=171; c: HI=51; d: HI=190. See Fig. 3-1 for the well location.

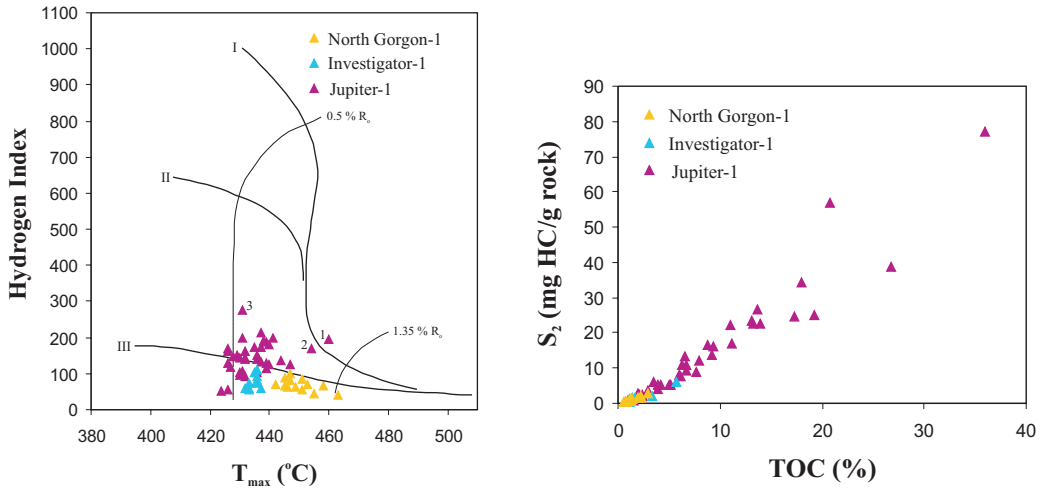

Fig. 3-10 Diagrams of HI (hydrogen index) versus T_{max} and S_2 versus TOC show the characteristics of organic matter within the Mungaroo Formation in three wells on the Rankin Platform and Exmouth Plateau. Samples with number 1, 2 and 3 are coal-bearing samples with TOC more than 10 %.1: TOC=13.7 %, HI=194.4; 2: TOC=13.3 %, HI=168.5; 3: TOC=20.7 %, HI=274.3. See Fig. 3-1 for well locations.

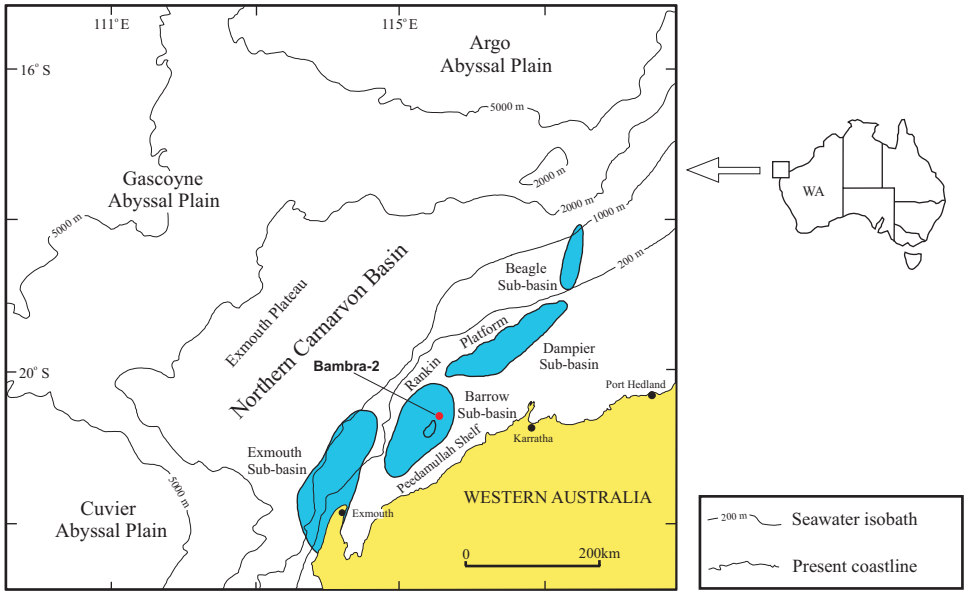

Fig. 4-1 Location of the Bambra-2 well in the Barrow Sub-basin of the Northern Carnarvon Basin.

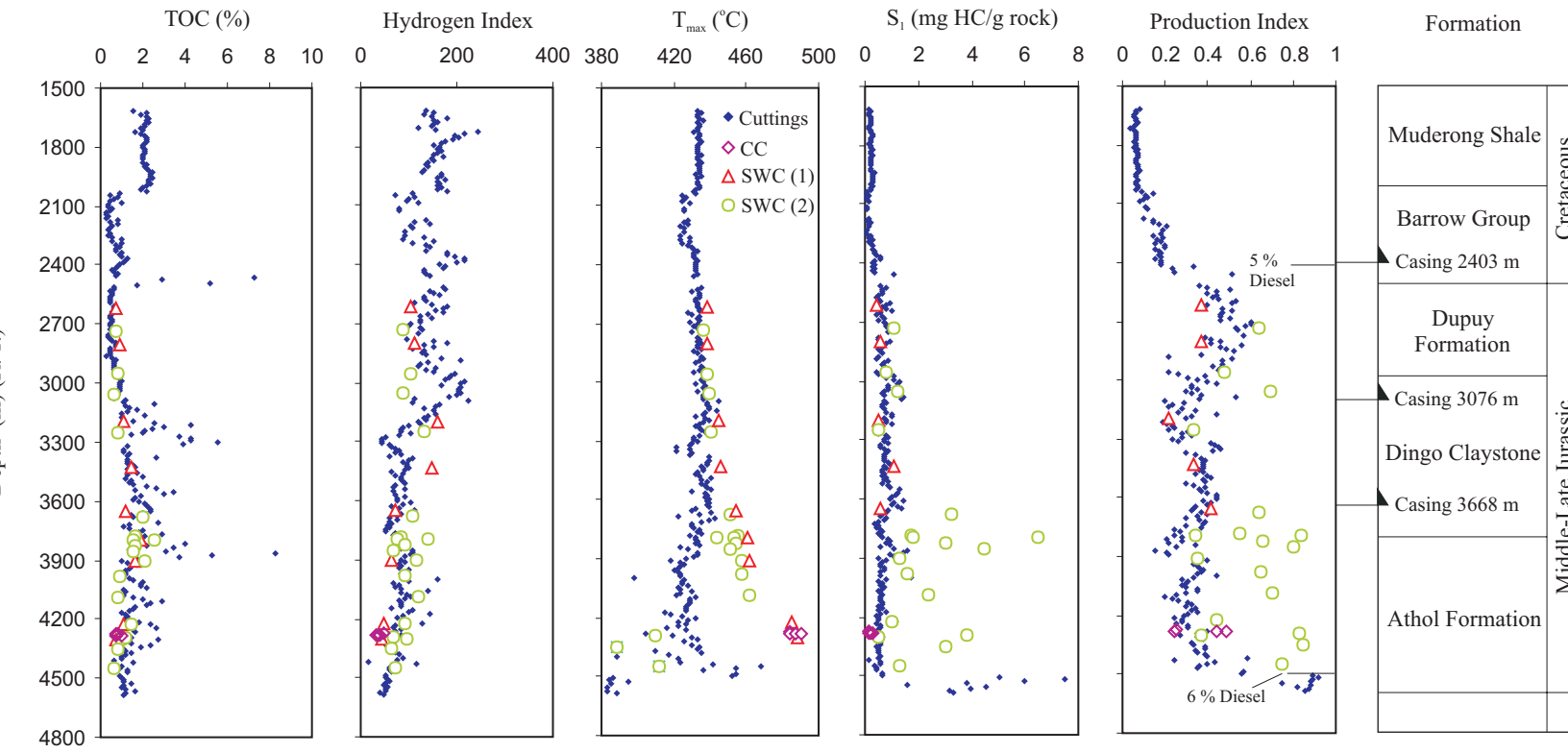

Fig. 4-1 Well profiles for total organic matter (TOC), hydrogen index (HI=S_2*100/TOC), Rock-Eval Tmax, S_1 (free hydrocarbons) and production index (PI=S_1/S_1+S_2) values versus depth for 280 cuttings samples and 27 side-wall cores and 4 conventional core samples in the Bambra-2 well. CC: Conventional core samples; SWC (1): SWC samples with normal and acceptable Tmax values; SWC (2): SWC samples with low and three abnormal T_{max} values. See Table 1 for the Rock-Eval data in the core samples.

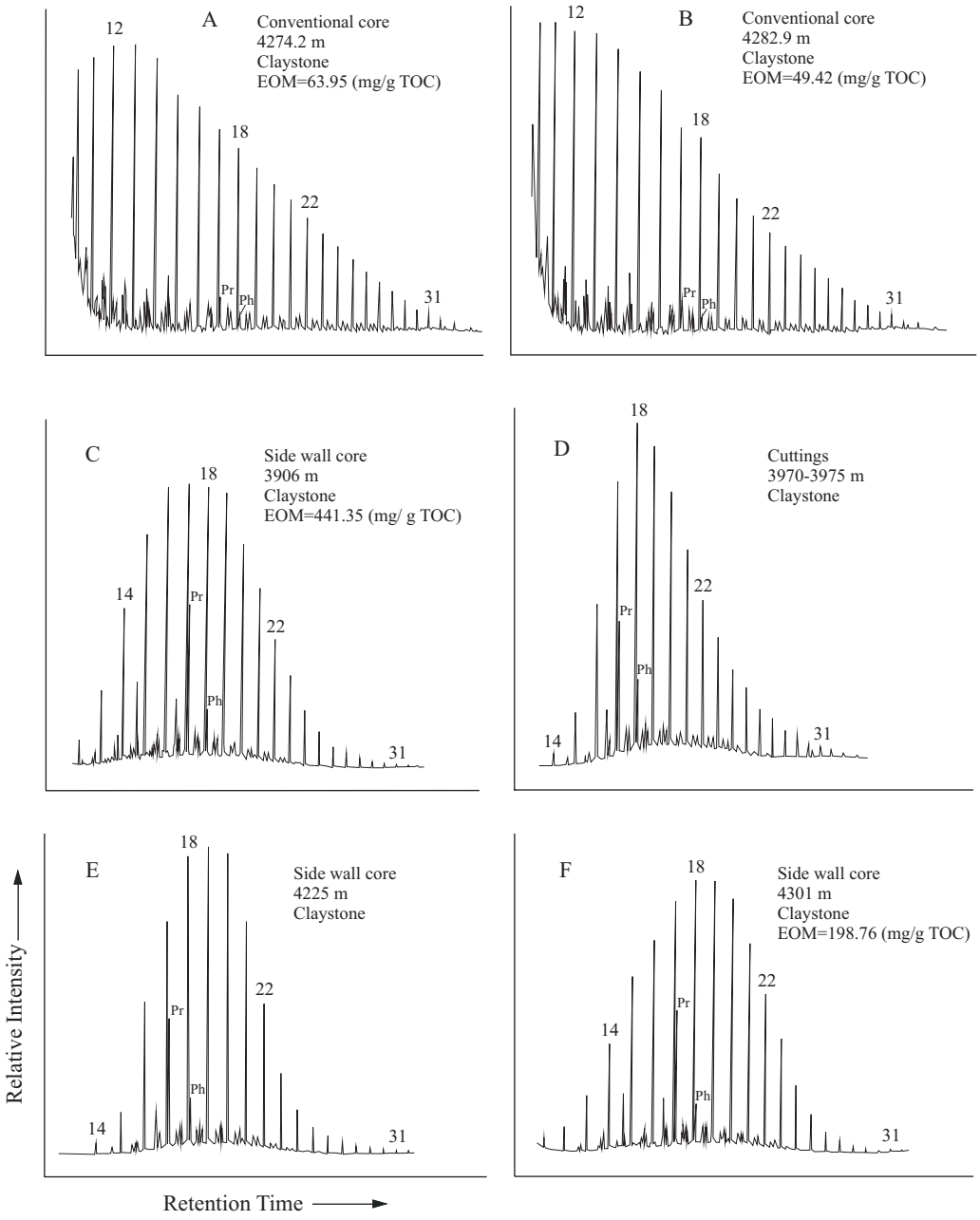

Fig. 4-2 Six examples of saturated hydrocarbon distributions from gas chromatography for two uncontaminated conventional core samples (A and B), three contaminated side-wall cores (C, E, and F) and one contaminated cuttings (D) in the Bambra-2 well.EOM: Extractable organic matter (mg/g TOC). A, B, C and F from AMDEL (1983); D and E from GSCC (2000).

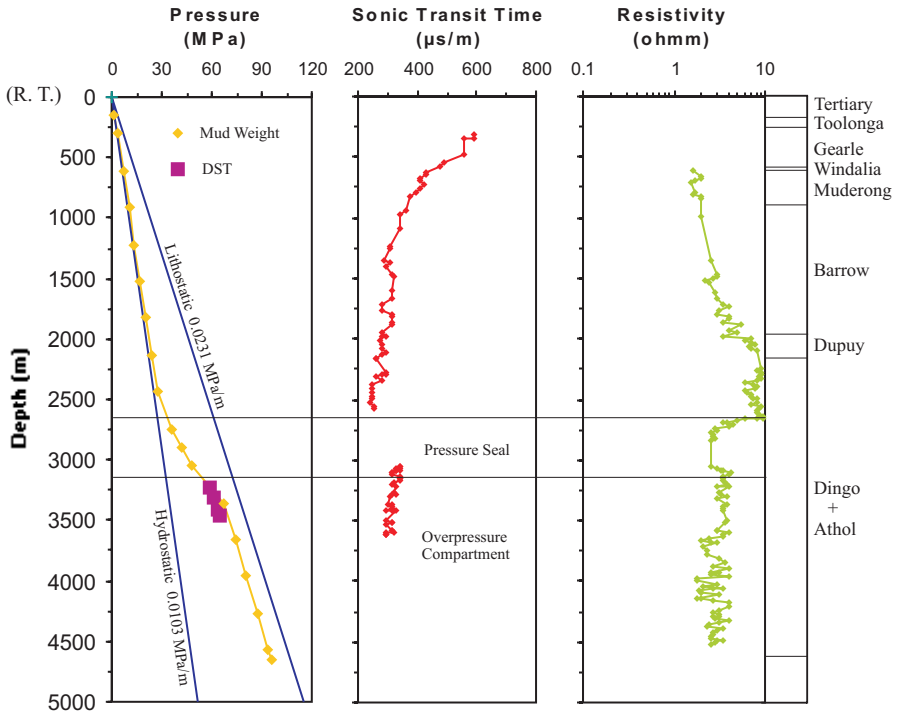

Fig. 5-1 Profiles of fluid pressure versus depth in Barrow Deep-1; sonic transit times and formation resistivities within claystone and silty claystone versus depth in Barrow Deep-1/Barrow-1. DST: Drill stem test.

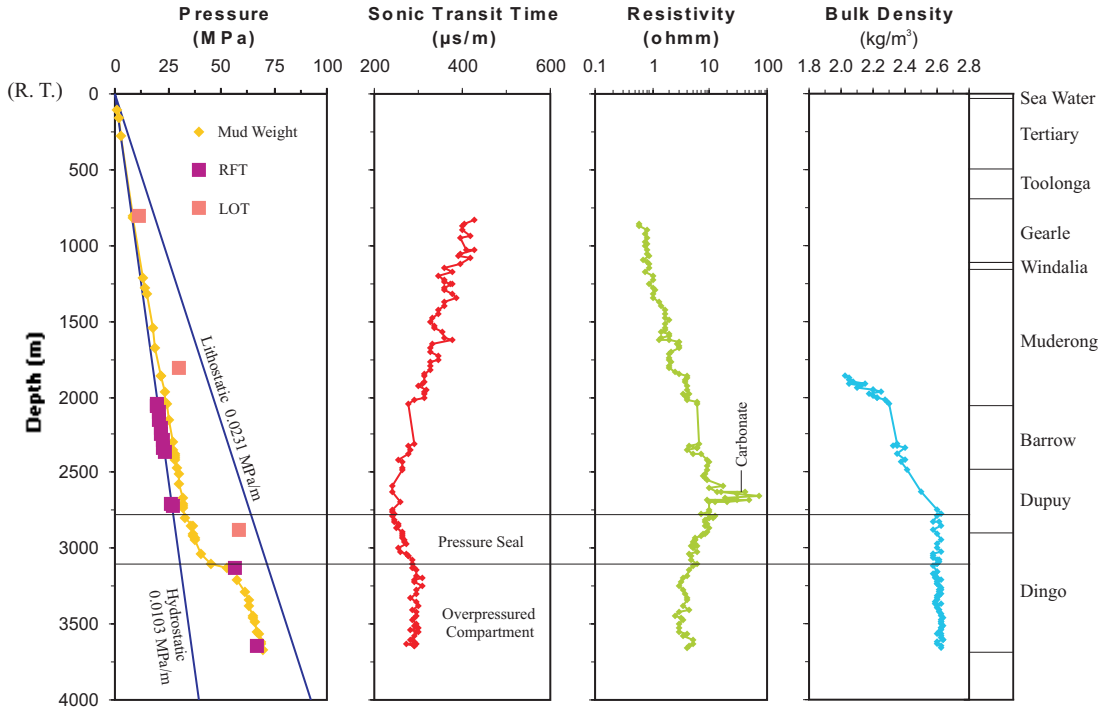

Fig. 5-2 Profiles of fluid pressure versus depth; sonic, resistivity and density log data within claystone and silty claystone versus depth in Bambra-1. RFT: Repeat formation test; LOT: Leak-off test.

WELL COMPLETION REPORTS

Angel-1 Well Completion Report (1972). Woodside Offshore Petroleum Pty. Ltd.

Anchor-1 Well Completion Report (1969). West Australian Petroleum Pty. Ltd.

Cape Range-1 Well Completion Report (1954). West Australian Petroleum Pty. Ltd.

Cape Range-2 Well Completion Report (1956). West Australian Petroleum Pty. Ltd.

Caretta-1 Well Completion Report (1991). LASMO Oil (Australia) Limited.

Chervil-1 Well Completion Report (1983). MESA Australia Ltd.

Chinook-1 Well Completion Report (1989). BHP Petroleum Pty. Ltd.

Coojong-1 Well Completion Report (1992). AMPOLEX Ltd.

Bambra-1 Well Completion Report (1983). Australian Occidental Pty. Ltd.

Bambra-2 Well Completion Report (1983). Australian Occidental Pty. Ltd.

Barrow-1 Well Completion Report (1964). West Australian Petroleum Pty. Ltd.

Barrow Deep-1 Well Completion Report (1973). West Australian Petroleum Pty. Ltd.

Bowers-1 Well Completion Report (1982). West Australian Petroleum Pty. Ltd.

Brigadier-1 Well Completion Report (1979). Woodside Offshore Petroleum Pty. Ltd.

Depuch-1 Well Completion Report (1974). Woodside Offshore Petroleum Pty. Ltd.

Dampier-1 Well Completion Report (1969). Woodside Offshore Petroleum Pty. Ltd.

Dorrigo-1 Well Completion Report (1982). Australian Occidental Pty. Ltd.

Eaglehawk-1 Well Completion Report (1972). Woodside Offshore Petroleum Pty. Ltd.

Eendracht-1 Well Completion Report (1981). ESSO Exploration and Production Australia Ltd.

Emma-1 Well Completion Report (1983). Australian Occidental Pty. Ltd.

Flag-1 Well Completion Report (1969). West Australian Petroleum Pty. Ltd.

Flinders Shoal-1 Well Completion Report (1969). West Australian Petroleum Pty. Ltd.

Gandara-1 Well Completion Report (1979). Hudbay Oil (Australia) Ltd.

Goodwyn-1 Well Completion Report (1972). Woodside Offshore Petroleum Pty. Ltd.

Goodwyn-7 Well Completion Report (1985). Woodside Offshore Petroleum Pty. Ltd.

Gorgon-1 Well Completion Report (1980). West Australian Petroleum Pty. Ltd.

Griffin-1 Well Completion Report (1990). BHP Petroleum Pty. Ltd.

Hampton-1 Well Completion Report (1974). Woodside Offshore Petroleum Pty. Ltd.

Investigator-1 Well Completion Report (1979). ESSO Exploration and Production Australia Ltd.

Judy-1 Well Completion Report (1983). Australian Occidental Pty. Ltd.

Jupiter-1 Well Completion Report (1979). Phillips Australian Petroleum Oil Company.

Jurabi-1 Well Completion Report (1982). ESSO Exploration and Production Australia Ltd.

Keraudren-1 Well Completion Report (1974). Hematite Petroleum Pty. Ltd.

Koolinda-1 Well Completion Report (1978). West Australian Petroleum Pty. Ltd.

Leatherback-1 Well Completion Report (1991). LASMO Oil (Australia) Limited.

Legendre-1 Well Completion Report (1968). Woodside Offshore Petroleum Pty. Ltd.

Madeleine-1 Well Completion Report (1969). Woodside Offshore Petroleum Pty. Ltd.

Mercury-1 Well Completion Report (1980). Phillips Australian Oil Company.

North Gorgon-1 Well Completion Report (1983). West Australian Petroleum Pty. Ltd.

North Rankin-1 Well Completion Report (1971). Woodside Offshore Petroleum Pty. Ltd.

North Tryal Rocks-1 Well Completion Report (1972). West Australian Petroleum Pty. Ltd.

Novara-1 Well Completion Report (1983). ESSO Exploration and Production Australia Ltd.

Observation-1 Well Completion Report (1968). West Australian Petroleum Pty. Ltd.

Onslow-1 Well Completion Report (1967). West Australian Petroleum Pty. Ltd.

Outtrim-1 Well Completion Report (1984). ESSO Exploration and Production Australia Ltd.

Pepper-1 Well Completion Report (1971). West Australian Petroleum Pty. Ltd.

Picard-1 Well Completion Report (1972). Woodside Offshore Petroleum Pty. Ltd.

Poissonnier-1 Well Completion Report (1974). Woodside Offshore Petroleum Pty. Ltd.

Rankin-1 Well Completion Report (1971). Woodside Offshore Petroleum Pty. Ltd.

Resolution-1 Well Completion Report (1979). ESSO Exploration and Production Australia Ltd.

Ronsard-1 Well Completion Report (1974). Woodside Offshore Petroleum Pty. Ltd.

Rosemary-1 Well Completion Report (1973). Woodside Offshore Petroleum Pty. Ltd.

Saladin-1 Well Completion Report (1985). West Australian Petroleum Pty. Ltd.

Saturn-1 Well Completion Report (1981). Phillips Australian Oil Company.

Sholl Island-1 Well Completion Report (1967). West Australian Petroleum Pty. Ltd.

Sirius-1 Well Completion Report (1981). ESSO Exploration and Production Australia Ltd.

South Chervil-1 Well Completion Report (1983). Wesminco Oil Pty. Ltd.

Spar-1 Well Completion Report (1977). West Australian Petroleum Pty. Ltd.

Strickland-1 Well Completion Report (1982). Hudbay Oil (Australia) Ltd.

Tryal Rocks-1 Well Completion Report (1971). West Australian Petroleum Pty. Ltd.

Vinck-1 Well Completion Report (1980). ESSO Exploration and Production Australia Ltd.

West Barrow-1/1A Well Completion Report (1982). Offshore Oil N.L.

West Barrow-2 Well Completion Report (1985). BHP Petroleum Pty. Ltd.

West Tryal Rocks-1 Well Completion Report (1973). West Australian Petroleum Pty. Ltd.

Wonnich-1 Well Completion Report (1996). Ampolex Limited.

Zeepaard-1 Well Completion Report (1980). ESSO Exploration and Production Australia Ltd.

Zeewulf-1 Well Completion Report (1979). ESSO Exploration and Production Australia Ltd.

Appendix 4

Horizon Legend
for 110/11 and 101R/09Seismic Lines

Sea floor

Late Miocene

Base Miocene

Mid Oligocene

Base Eocene

Base Tertiary

Turonian

Aptian

Valanginian

Base Cretaceous

Callovian

Base Jurassic / Top Triassic

Mid Triassic

Near Top Permian

Late Carboniferous (Late Namurian)

"Basement"

Appendix 5

LIST OF PUBLISHED PAPERS AND CONFERENCE PRESENTATIONS DURING THIS STUDY

Published papers

Sheng He, Mike Middleton, Alex Kaiko, Chunqing Jiang and Maowen Li, (2002). Two case studies of thermal maturity and thermal modelling in the overpressured Jurassic rocks of the Barrow Sub-basin, North West Shelf of Australia. *Marine and Petroleum Geology*, 19, 143-159.

Sheng He and Mike Middleton, (2002). Pressure seal and deep overpressure modelling in the Barrow Sub-basin, Northern Carnarvon Basin of the North West Shelf, Australia, in Keep, M. & Moss, S.J. (Eds.), 2002, *The sedimentary Basins of Western Australia 3 (pp. 531-549):* Proceedings of the Petroleum Exploration Society of Australia Symposium, Perth, WA, 2002.

S. He, M. Middleton and Z. H. Tang, (2000). Characteristics and origin of underpressure system in the Shiwu Fault Depression, south-east Songliao Basin, China. *Basin Research*, 12, 147-158.

I.D. Sills and S. He, (1999). Determination of evolved gas transfer time from a thermoanalyser to a coupled gas detection system using pyrite oxidation. *Thermochimica Acta*, 339, 125-130.

Tang Zhonghua, He Sheng and Wu Jingfu, (1999). Thermal backstripping from vitrinite reflectance profiles in comparison with an extensional model for passive continental margin basins on northern continental shelf of South China Sea. *Journal of China University of Geosciences*, 10, 251-257.

He Sheng, (1999). Relationship between paleoclimate and source rocks from molecular markers in the North Sea (abstract). *AAPG Bulletin*, 83, 1887. (the grant-in aid from the American Association of Petroleum Geologists Foundation, 1999)

Conference presentations

He-Sheng and Middleton-Mike, (2002). Pressure seal and modelling of the Jurassic overpressure in the Barrow Sub-basin, North West Shelf of Australia. *AAPG Annual Convention, Houston, Texas, March 10-13, 2002*.

He-Sheng, Middleton-Mike-F and Collins-Lindsay, (2000). Thermal history modeling in the Offshore Carnarvon Basin, North West shelf, Australia. *AAPG International Conference and Exhibition, Bali, Indonesia, October 15-18, 2000*.

He-Sheng, Middleton-Mike-F, Zhao-Kejing and Gu-Wenbin, (2000). Characters of high-sulfur lacustrine source rocks of sour-gas and heavy-oil in the Jinxian Sub-basin of the Bohaiwan Basin, China. *AAPG International Conference and Exhibition, Bali, Indonesia, October 15-18, 2000*.

He-Sheng and Middleton-Mike, (2000). Study of anomalous low vitrinite reflectance profiles in the Barrow Sub-basin, Western Australia. *15th Australian Geological Convention, Sydney, July 3rd-7th, 2000*.

He-Sheng, Middleton-Mike and Tang-Zhonghua, (1999). Hydrochemical characters and origin of underpressure system in the southeast area of Songliao Basin, China. *AAPG Annual Meeting, San Antonio, Texas, April 11-14, 1999*.

He-Sheng, Middleton-Mike and Tang-Zhonghua, (1999). A thermal backstripping model for determining the palaeo-heat flow from vitrinite reflectance profiles in South China Sea Basins. *AAPG Annual Meeting, San Antonio, Texas, April 11-14, 1999*.

Papers under review

He Sheng and Mike Middleton. Heat flow modelling and thermal maturity in the Northern Carnarvon Basin, the North West Shelf, Australia. *Marine and Petroleum Geology*.

Sheng He, Alex Kaiko, Mike Middleton and Chunqing Jiang, Assessment of Rock-Eval T_{max} data, a case study from the Bambra-2 well of the Barrow Sub-basin, Western Australia. *PESA Journal*.